MASTERARBEIT

Windenergienutzung an der Neumayer-Station III in der Antarktis

Vorgelegt am 28.01.2025

Yazen Alhaiani

1. Erstprüferin: Prof. Dr. Vera Schorbach
2. Zweitprüfer: Prof. Dr.-Eng. Torsten Birth-Reichert

HOCHSCHULE FÜR ANGEWANDTE WISSENSCHAFTEN HAMBURG
Department Maschinenbau und Produktion
Berliner Tor 21
20099 Hamburg

Zusammenfassung

Yazen Alhaiani

Thema der Masterthesis

Windenergienutzung an der Neumayer-Station III in der Antarktis

Stichworte

Windenergie, WAsP, Flugwindkraftanlagen, Antarktis, Neumayer Station III, Kalte Klimazonen, Windressourcen Analyse, Polarforschung, Ertragsberechnung, Erneuerbare Energien, Kostenanalyse, Windrichtung, Windmessungen, Windturbinen, Geländeprofil, Windgeschwindigkeit, Höhenwindkraft, Standortanalyse, Weibull-Verteilung, Wind Atlas, Orographie, Topografie, REMA, DEM.

Kurzzusammenfassung

In dieser Masterarbeit werden die Potenziale für die Einführung neuer Windenergieerzeugungssysteme an der Neumayer Station III in der Antarktis untersucht. Die Arbeit umfasst eine umfassende Recherche zu vorhandenen Windenergieprojekte in der Antarktis und eine Energieertragsberechnung für ausgewählte Wind- und Flugwindkraftanlagen. Die Auswertung des Windpotenzials erfolgt mit der Software WaSP für Windenergieanlagen und mit MATLAB für Flugwindenergieanlagen. Eine Kostenanalyse für die ausgewählte Systeme wird schließlich erstellt.

Summary

Yazen Alhaiani

Title of the paper

Wind Energy Utilization at the Neumayer Station III in Antarctica

Keywords

Wind Energy, WAsP, Airborne Wind Energy Systems, Antarctica, Neumayer Station III, Cold Climate, Wind Resource Assessment, Polar Research, Annual Energy Production, Renewable Energies, Cost Analyses, Wind Direction, Wind Measurements, Wind Turbines, Terrain, Wind Speeds, Site Assessment, Weibull-Distribution, Wind Atlas, Orography, Topography, REMA, DEM.

Abstract

In this master's thesis the potential for the implementation of new wind energy generation systems at the Neumayer Station III in Antarctica is examined. Existing wind energy projects in Antarctica are investigated. Wind energy resource assessments and annual energy production calculations for a selected wind turbine and a selected airborne wind energy system are implemented using the software WAsP and MATLAB. A cost analysis for each selected systems is created.

Masterarbeit

Windenergienutzung an der Neumayer-Station III in der Antarktis

Alfred-Wegener-Institut awi.de

Diese Masterarbeit befasst sich mit den Potentialen der Windenergienutzung an der Neumayer-Station III in der Antarktis.

Derzeit wird die Station über vier Dieselgeneratoren versorgt, von denen jeder eine elektrische Leistung von 160kW und eine thermische Leistung von 190kW zur Verfügung stellen kann. Ergänzt wird dies durch eine 30kW Kleinwindenergieanlage.

Im Rahmen der Arbeit soll die technische Machbarkeit und die Potentiale weiterer Windenergieanlagen (sowohl bodenfeste Turbinen als auch Flugwindenergieanlagen) geprüft werden.

Die Arbeit gliedert sich in folgende Schritte:

- Recherche zu derzeitigen Energieversorgungskonzepten der Neumayer III und weiterer ganzjähriger Antarktis-Stationen sowie möglicher bodenfester Kleinwindenergieanlagen und Flugwindenergieanlagen an Cold Climate Standorten
- Auswertung von Windmessdaten
- Erstellung verschiedener Szenarien für die Windstromversorgung
- Ertragssimulation
- Bewertung und Gegenüberstellung der Szenarien

Beginn: ab sofort

Kontakt:

Prof. Dr. Vera Schorbach

Acknowledgements

I would like to extend my heartfelt thanks to Prof. Dr. Vera Schorbach for the support and guidance throughout the duration of this thesis. Her expertise was pivotal in shaping the quality of this thesis and I am fortunate to have had the opportunity to work under her supervision.
I would also like to thank the second examiner of this thesis, Prof. Dr.-Eng. Torsten Birth-Reichert, for taking the time to review my work.
Finally, I would like to acknowledge the Hamburg University of Applied Sciences for providing the access to software tools and literature that contributed to the completion of this work.
To my family and friends, I owe endless gratitude for their love, patience, and unwavering belief in me. Their support and understanding, especially during the challenging moments, have been my greatest source of strength.
To all those who have contributed to this journey, directly or indirectly, I am profoundly thankful.

Contents

1 Introduction **1**

2 Literature Review **2**

2.1 Wind energy potential in Antarctica 2

2.2 Operational Aspects of Wind Energy in Antarctica 8

2.3 Active wind energy projects in Antarctica 11

2.3.1 Ross Island Wind Farm 12

2.3.2 Mawson station 12

2.3.3 Princess Elisabeth Research Station 13

2.3.4 Other small-scale wind turbine projects in Antarctica 13

2.4 The Neumayer Station III 14

2.4.1 The Meteorological Observatory Neumayer 16

2.4.2 Logistical Setup of the Neumayer Station III 17

2.5 AWES: Calculation of AEP and Simulation Tools 18

3 Fundamentals **20**

3.1 Wind Energy Resource Assessment 20

3.1.1 Characterisation of Wind Energy 20

3.1.2 The Atmospheric Boundary Layer 21

3.1.3 Effects of terrain on wind characteristics 23

3.1.4 Wind Turbine Energy Production 25

3.1.5 Wind Resource and Energy Yield Assessment Procedures 30

3.1.6 Topographical Inputs 32

3.1.7 WAsP 34

3.2 Airborne Wind Energy Systems 35

3.2.1 Energy of Pumping Cycle AWES 37

3.2.2 Annual Energy Production of Pumping Cycle AWES 42

4 Methodology **44**

4.1 Picking a Wind Energy System 44

4.1.1 Selected Wind Turbine 45

4.1.2 Selected AWES 49
4.2 Wind Resource Assessment Implementation for the selected Wind Turbine using WAsP 52
4.2.1 Wind Data Analysis 52
4.2.2 Wind Turbine Parameters 55
4.2.3 Adding Topographical Inputs 56
4.2.4 Creating the WAsP Project 61
4.3 Wind Energy Assessment Implementation: AWES 63

5 Results **66**
5.1 Wind Energy Resource Assessment: Wind Farm 66
5.2 Wind Energy Resource Assessment: AWES 73

6 Financial Analysis **75**
6.1 Wind Farm 75
6.2 AWES 77

7 Discussion **82**

8 Conclusion **84**
8.1 Outlook 85

List of Figures

2.1 World Map - Wind Flow [38] . . . 3
2.2 Formation of katabatic winds [45] . . . 3
2.3 The Antarctic continent with terrain contours in meters (a) and Mean wind streamlines over Antarctica(b) . . . 5
2.4 Map of Antarctica [64] . . . 7
2.5 Wind power density in the Antarctic in W/m² [33] . . . 7
2.6 Effect of cold microclimate on wind turbines [6] . . . 8
2.7 Icing effects on the energy harvest of wind turbines [6] . . . 9
2.8 The impact ice on the power curves [5] . . . 10
2.9 Research Stations in Antarctica [19] . . . 11
2.10 Princess Elisabeth research station Wind Farm[28] . . . 13
2.11 Neumayer Station III - Detailed Model[4] . . . 14
2.12 Neumayer Station III - Energy Supply[7] . . . 16
2.13 Measurement Site - Meteorological Observatory Neumayer [3] . . . 17
2.14 Logistical Setup and Routes of the Neumayer Station III [34] . . . 18

3.1 Power Law Exponent and Vertical Wind Profile [44] . . . 23
3.2 Determination of flat terrain [44] . . . 24
3.3 Effect of change in surface roughness [44] . . . 24
3.4 Speed, power, and turbulence effects downstream of a building [44] . . . 25
3.5 Rayleigh probability density function for different mean wind speeds. . . . 28
3.6 Example of Weibull probability density function for $\overline{U} = 6\,\mathrm{m/s}$. . . . 29
3.7 Wind Resource and Energy Yield Assessment Procedure . . . 31
3.8 Clockwise: Contours on antarctic elevation - Elevation tinted hillshade on antarctic elevation - Hillshade on antarctic elevation - AspectMap on antarctic elevation [30] . . . 33
3.9 WAsP Example Workflow . . . 35
3.10 Relevant speeds and forces around a wing for wind power generation. [58] 36
3.11 Pumping cycle AWES representation [47] . . . 37
3.12 Forces and velocities of a kite flying crosswind [42] . . . 38

4.1 Evaluation Matrix - Wind Turbines 47
4.2 SD6+ [22] 48
4.3 SD6+: Power Curve 49
4.4 Kitepower Falcon AWES [61] 50
4.5 Space Requirements Kitepower Falcon [35] 50
4.6 Cycle Power - Kitepower Faclon [35] 51
4.7 Power Curve - Kitepower Faclon [35] 51
4.8 Flowchart for MATLAB Function for processing files and extracting columns 53
4.9 WAsP Climate Analyst - Wind Direction and Wind Speeds 2016/03-2022/01 54
4.10 WAsP Climate Analyst Plot - Zoomed in to 28/01/2022 54
4.11 Original Data Snippet from 28/01/2022 55
4.12 WAsP Wind Turbine Editor 56
4.13 REMA Raster Map 57
4.14 REMA Raster Map - Edited 57
4.15 Contours Map after change of CRS 58
4.16 WAsP Map Editor 58
4.17 Cropped Map 59
4.18 Map with Roughness Lengths 60
4.19 Roughness Lengths Change Lines 60
4.20 Imported Map to WAsP 62
4.21 Final WAsP Project Overview 63
4.22 Extracted Vertical Wind Profile from Wind Data - All Altitudes and 500 Meters 64

5.1 Observed Wind Climate - Emergent and Fitted 67
5.2 Hourly Mean Wind Speeds by Month 68
5.3 Annual Maxima OWEC 69
5.4 Peak Over Threshold OWEC 69
5.5 Generated Grid Maps in WAsP 71
5.6 Power Curve: Wind Farm 73
5.7 Weibull Wind Speed Distribution - 350m 74

6.1 Representation of Inputs and Outputs of the Reference Economic Model for AWES [31] 78
6.2 Components considered in the Reference Economic Model for AWES [31] 78
6.3 Reference Economic Model for AWES: Output Results Breakdown 81

List of Tables

2.1 Overview of operating wind turbines in Antarctica [40, 41, 17, 68, 20, 55, 26, 53, 62, 54] 12
2.2 Neumayer Station III - Detailed Description[4] 15
2.3 Parameters and Instruments: Meteorological Observatory Neumayer [59] 17

4.1 Proposed Wind Turbines [48, 11, 13, 21, 22, 63, 23, 12, 39] 46
4.2 SD6+ Wind Turbine Specification [21] 48
4.3 GWC - Barometric Reference Information 61
4.4 Site Information 61
4.5 Locations of NMS-III, Measuring Site and Wind Farm 63

5.1 OWC Results 67
5.2 GWC Results for different heights 70
5.3 AEP Results 72
5.4 Results Weibull Distribution and AEP 74

6.1 Parameters, values, and descriptions for the financial analysis 77
6.2 Reference Economic Model for AWES - Input Parameters 80
6.3 Reference Economic Model for AWES - Output Parameters 81

Nomenclature

Symbol	Description
Δt	Time interval [s]
A	Airfoil area in AWES calculations [m^2]
a	Axial induction factor [-]
A	Rotor-swept area [m^2]
a.s.l.	Above sea level
AEP	Annual Energy Production
AWES	Airborne Wind Energy System
BoP	Balance of plant
BoS	Balance of system
c	Scale factor [-]
C_D	Drag coefficient [-]
C_L	Lift coefficient [-]
$C_{O\&M}$	Annual operation and maintenance costs [€]
C_p	Rotor power coefficient [-]
C_R	Aerodynamic force coefficient [-]
C_{Turbines}	Capital cost of wind turbines [€]
CapEx	Capital expenditure [€]
CF	Capacity Factor [-]
CHP	Combined heat and power

Symbol	Description
COE	Cost of energy [€]
CoVE	Cost of Variable Expenses
CRF	Capital recovery factor [-]
CRS	Coordinate reference system
DEM	Digital elevation model
$\frac{dm}{dt}$	Mass flow of air [kg/s]
$\overline{E_w}$	Total energy output of a wind turbine [kWh]
E_c	Energy produced per cycle [kWh]
E_{fuel}	Fuel energy replaced by the wind turbine [L/year]
E_T	Energy output under low-temperature conditions [MWh]
EO	Energy output under normal conditions [MWh]
EPSG	European Petroleum Survey Group
F_a	Aerodynamic force experienced by a wing
f_c	Normalised power factor [-]
$f_{c,\mu}$	Normalised Power factor [-]
$f_c^{\max}$	Maximum normalized power factor [-]
F_L	Aerodynamic lift force [N]
F_{out}	Dimensionless force factor [-]
f_{space}	Space factor for transport costs [-]
$f(t)$	Probability density function of air temperature [%]
FCR	Fixed charge rate [€]
GG	Ground generation
GWA	Global wind atlas
h	Height for wind speed calculations [m]
H	Height of an obstacle [m]

Symbol	Description
IEA	International Energy Association
IEC	International Electrotechnical Commission
IRR	Internal Rate of Return
k	Shape factor [-]
K_e	Energy pattern factor [-]
KSU	Kite steering unit
l_c	Tether length in AWES calculations [m]
LCOE	Levelized cost of energy [€/MWh]
LPoE	Levelized Profit of Energy [€/MWh]
LRoE	Levelized Revenue of Energy [€/MWh]
M_{Fuel}	Monthly fuel consumption [MT]
MGO	Marine gas oil
N	Number of hours in a year [h]
NMS-III	Neumayer Station III
NPV	Net present value [€]
OCP	Optimal control problem
OEWC	Observed extreme wind climate
OpEx	Operational expenditure [€]
OWC	Observed wind climate
P	Power [W]
p	Pressure [Pa]
$\overline{P_w}$	Average wind machine power [W]
P_{av}	Average power output [W]
P_c	Power per cycle in AWES calculations [W]
P_{Diesel}	Price of diesel [€]

Symbol	Description
$P_{\text{out}}^{\text{n}}$	Nominal power AWES [-]
P_R	Rated power [W]
P_w	Wind power density [W]
$p(U)$	Probability density function
PDF	Probability density function
POT	Peak over threshold
r	Discount rate [%]
R	Rotor radius [m]
REMA	Reference Elevation Model of Antarctica
RIX	Roughness Index [%]
RV	Research vessel
S	Annual savings [€]
SRTM	Shuttle Radar Topography Mission
T	Temperature (In wind energy calculations) [°C]
T	Tether force in AWES calculations [N]
T	Thrust force in wind turbine calculations [N]
T	Turbine's lower temperature limit (In cold temperature calculations) [°C]
t_c	Cycle duration [s]
T_{in}^{n}	Nominal tether force by reel-in [N]
$T_{\text{out}}^{\text{n}}$	Nominal tether force by reel-out [N]
$\overline{U}$	Hourly wind speeds averages [m/s]
U	Uniform wind speed [m^2]
U_0	Reference wind speed at height z_0 [m/s]
U_i	Hourly wind speed averages [m/s]

Symbol	Description
$U(z)$	Wind speed at height z [m/s]
UTM	Universal Transverse Mercator
v_a	Apparent wind speed [m/s]
$v_{k,c}$	Crosswind speed [m/s]
v_n	Nominal wind speed [m/s]
v_{out}	Reel-out speed [m/s]
$v_{\text{out,opt}}$	Optimal reel-out speed [m/s]
v_w	Wind speed [m/s]
WAsP	Wind Atlas Analysis and Application Program
WGS84	World Geodetic System 1984
WTG	Wind turbine generator
z	Height above sea level [m]
α	Power law exponent [-]
γ	Angle between the direction of the aerodynamic force and the wind direction [-]
Γ	Gamma function
γ_{in}	Dimensionless factor [-]
γ_{out}	Dimensionless factor [-]
$\eta_{\text{Generator}}$	Efficiency of diesel generator [%]
λ	Ratio of the blade tip speed to the wind speed [-]
μ	Dimensionless velocity parameter [-]
ρ	Air density [kg/m^3]
σ_U	Standard deviation of wind speeds [m/s]
Ω	Angular velocity of the rotor [m/s]

Chapter 1

Introduction

Research in the South Pole holds substantial importance and facilities a comprehensive understanding of global atmospheric and environmental issues. Currently over 90 scientific facilities are present in Antarctica encompassing a broad range of research disciplines [41]. A steady and abundant energy supply is essential for the operation of the research stations in Antarctica. The stations are highly dependent on fossil fuels for power generation and transportation. However, delivering these fuels to Antarctica is both costly and hazardous, with the risk of oil spills and fires posing significant safety threats and potential long-term environmental impacts [27]. The use of renewable energies on the other hand, provides a lot of environmental, economical and logistical advantages. This is the motivation for this thesis which aims to analyse the potential of deploying new wind energy systems for the german Neumayer Station III, which currently primarily uses diesel generators for power and heat generation [9]. An overview of currently active wind energy systems in Antarctica is made to investigate the current use of wind energy in Antarctica. Significant challenges for wind energy deployment in Antarctica will be addressed. The fundamentals of wind energy resource assessment will be presented and the current status of energy supply at the the Neumayer Station III will be handled. An objective will be set to replace a part of the current energy supply with wind energy systems. Multiple wind turbines will be evaluated and a wind turbine will be selected for the assessment. The wind energy resource assessment will be implemented using WAsP, a wind energy resource assessment software tool. The assessment will take into account critical factors including wind speeds, wind direction, and terrain data. Assessments will be extended to airborne wind energy systems (AWES) and the foundations for the calculation of energy power generation of AWES will be handled. An estimated AEP for the selected wind turbine and the selected AWES will be calculated. The economic viability of the proposed systems will be analysed to determine the feasibility of using the selected systems.

Chapter 2

Literature Review

2.1 Wind energy potential in Antarctica

The high potential of wind energy in Antarctica has been documented in multiple works [8]. 20 years after the first ever large scale wind turbine was commissioned in Antarctica at the Australian Antarctic station Mawson [16], 10 year-round stations and 3 seasonal research stations currently use wind energy for the energy supply [41]. In this section, an analysis of the atmospheric characteristics of Antarctica and the current state of wind energy projects in Antarctica will be conducted. This will include an examination of both currently operational and planned small-scale and large-scale wind turbine projects in Antarctica and the key challenges associated with the deployment and expansion of wind energy systems in Antarctica.

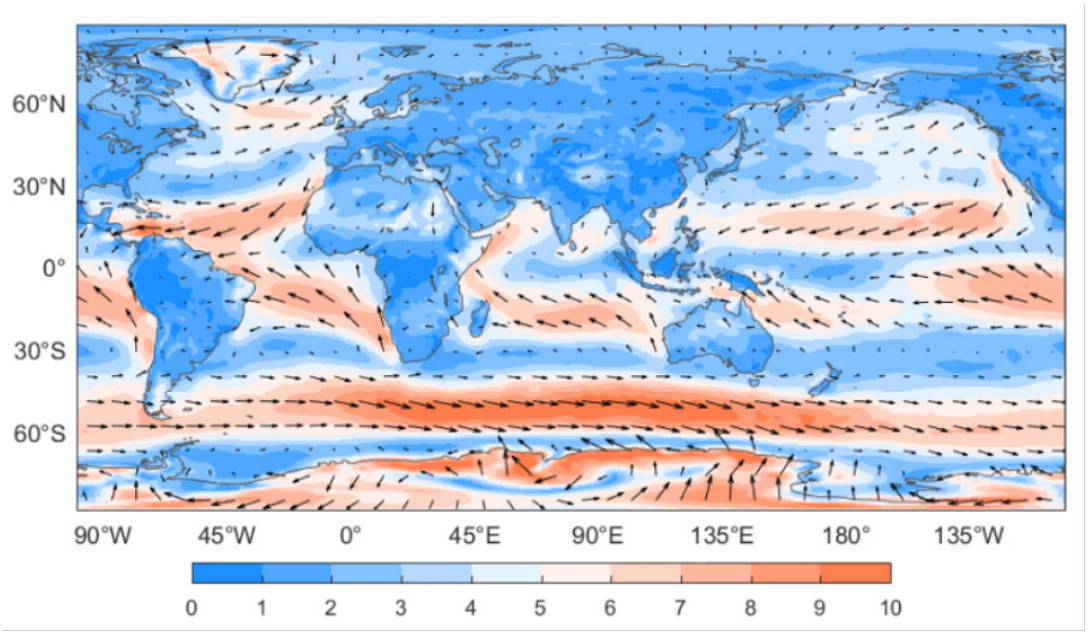

Figure 2.1: World Map - Wind Flow [38]

Geographic and meteorological factors make Antarctica the windiest continent on Earth

as shown in Figure 2.1. This is due to katabatic wind that is a result of Antarctica's interior region the Polar Plateau [51]. The Polar Plateau is a large area in East Antarctica that extends over an area with a diameter of about 1000 kilometres and has an average elevation of about 3000 meters [45]. The Polar Plateau is covered with a thick ice sheet that cools the air above it, creating a temperature inversion where the coldest, densest air is near the ground, which is usually the other way around. This dense air flows downhill from the interior to the coast as inversion winds. When these winds are funnelled through rugged ice and mountainous landforms, they become compressed and accelerate, forming fast katabatic winds [51]. The formation of katabatic winds is visualised in Figure 2.2.

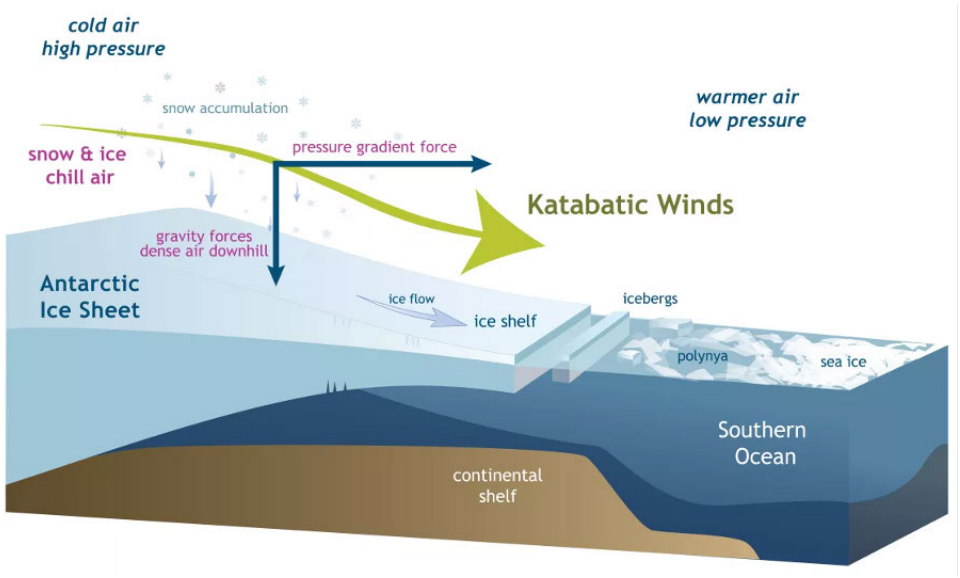

Figure 2.2: Formation of katabatic winds [45]

Due to the topographic features of Antarctica, katabatic winds have a significant effect on the continent in regards to wind speeds and the general atmosphere. These effects are more clear when the wind flow patterns in the continent are analysed with the topography of Antarctica in mind as shown in Figure 2.3(a). As an example, many of the winds at stations around the coast of East Antarctica are katabatic in origin [52]. This is shown in Figure 2.3(b) where the near-surface wind streamlines across the continent were derived from the output of a high-resolution weather-forecasting model [52]. The results indicate that a significant portion of the flow originates in the higher parts of East Antarctica and flows toward the coast, often converging [52]. The katabatic winds are most pronounced during winter, when there is no incoming solar radiation, and a large pool of cold air over the interior is formed to feed the katabatic flow [52]. Surface winds over the interior show a high directional constancy, indicating that they are dictated by the local orography. The wind speeds are closely related to the slope of the orography, with the strongest winds being measured at stations on the coastal escarpment and the weakest on the parts of the plateau with the smallest orographic gradient [52]. When the katabatic

winds in Antarctica descend from the plateau they interact with larger weather systems. Northerly winds can weaken these katabatic flows, while southerly winds can strengthen them. The Coriolis force shifts the winds left, merging them with coastal easterlies and creating a cold, anticyclonic outflow. When these winds meet high terrain, they can accumulate and form 'barrier winds' that push north due to pressure buildup [52].

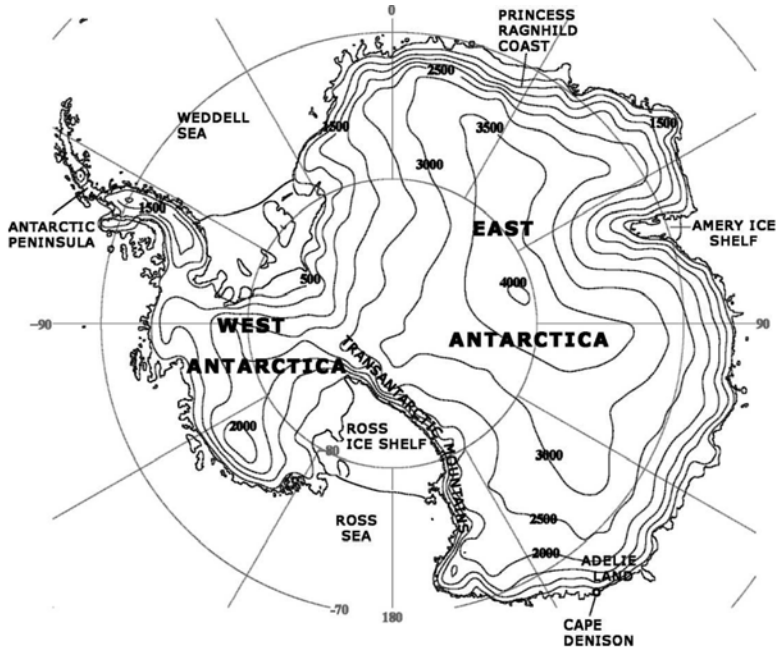

(a) [52]

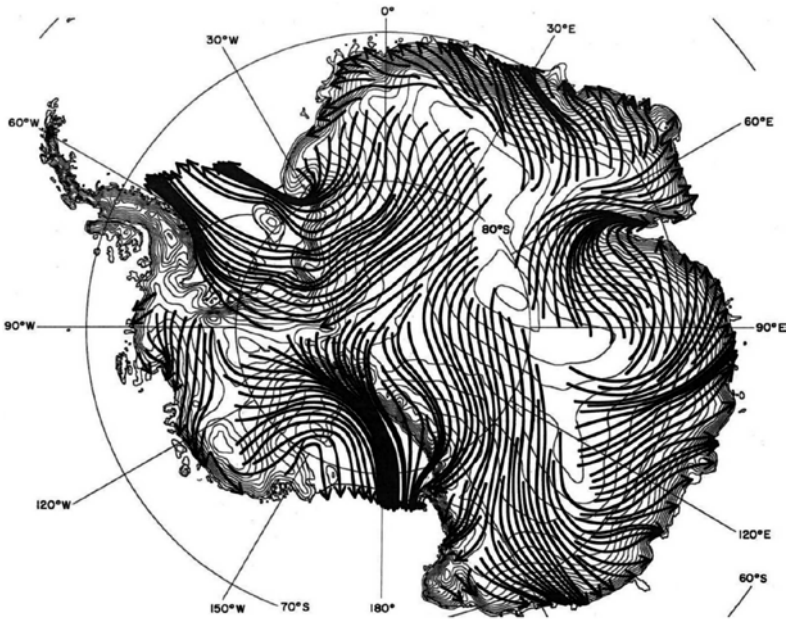

(b) [52]

Figure 2.3: The Antarctic continent with terrain contours in meters (a) and Mean wind streamlines over Antarctica(b)

Current active wind energy projects to be discussed in the next section and multiple studies show that wind energy in Antarctica exhibits characteristics generally conducive to wind energy generation. Analysing wind resources in Antarctica provides valuable insights into wind power density across the continent. A study using ERA5 reanalysis data evaluated wind energy potential and determined multi-year averages for the four seasons and annual wind power density over the past 40 years [33]. Figure 2.4 presents the study's findings on wind density. Figure 2.5 serves as a reference for understanding the geographic references presented in the study findings. The analysis revealed key patterns and variations in wind energy distribution across Antarctica. The study highlighted that Antarctic wind power density is generally optimistic. High-density areas are concentrated along the coast of East Antarctica (where the NMS-III is located), the Bellingshausen Sea, Cape Adare, and the Southern Ocean, with values exceeding 1200 W/m^2 and some sites reaching as high as 2500 W/m^2. In contrast, the South Pacific Ocean shows higher wind power density (800–1200 W/m^2) compared to other oceans. Weak wind areas, where densities fall below 100 W/m^2, are located near the Transantarctic Mountains, the Antarctic Peninsula, and the Ronne Ice Shelf. Moderate wind power density (100–300 W/m^2) is observed in central East Antarctica, the Weddell Sea, and the Ross Sea. The Southern Hemisphere's westerly belt achieves a maximum density of 1600 W/m^2, yet some Antarctic stations register densities twice as high as those in other global sea areas. Seasonal variations in wind power density further emphasise the dynamic nature of Antarctic wind resources. In spring, the distribution and values closely resemble the multi-year average, making it representative of general conditions. However, summer experiences the weakest wind power density, with maximum values along the East Antarctic coast reaching 1500 W/m^2 and most of East Antarctica registering below 100 W/m^2. In autumn, wind power density begins to intensify, with high-density areas along the East Antarctic coast exceeding the multi-year averages. Winter exhibits the strongest wind power densities, with rich zones expanding significantly and poor zones shrinking. In some regions, densities exceed 3000 W/m^2. Overall, autumn and winter emerge as the most favourable seasons for wind energy, while summer has the lowest wind power density. The observed variations in wind power density are influenced by the origins of Antarctic winds. The strong westerly circulation of the Southern Ocean exhibits minimal seasonal fluctuation, maintaining densities around 800–1000 W/m^2 throughout the year. The polar easterly winds, caused by the polar high-pressure zone, have a smaller extent and are less significant. Katabatic winds, as discussed earlier, play a critical role in shaping wind energy potential, particularly in East Antarctica. These winds are strongest in autumn and winter, driven by denser cold air in lower temperatures. Additionally, unstable weather systems, such as cyclones near the Amundsen Sea, contribute to the abundant wind energy resources in specific areas [33].

Figure 2.4: Map of Antarctica [64]

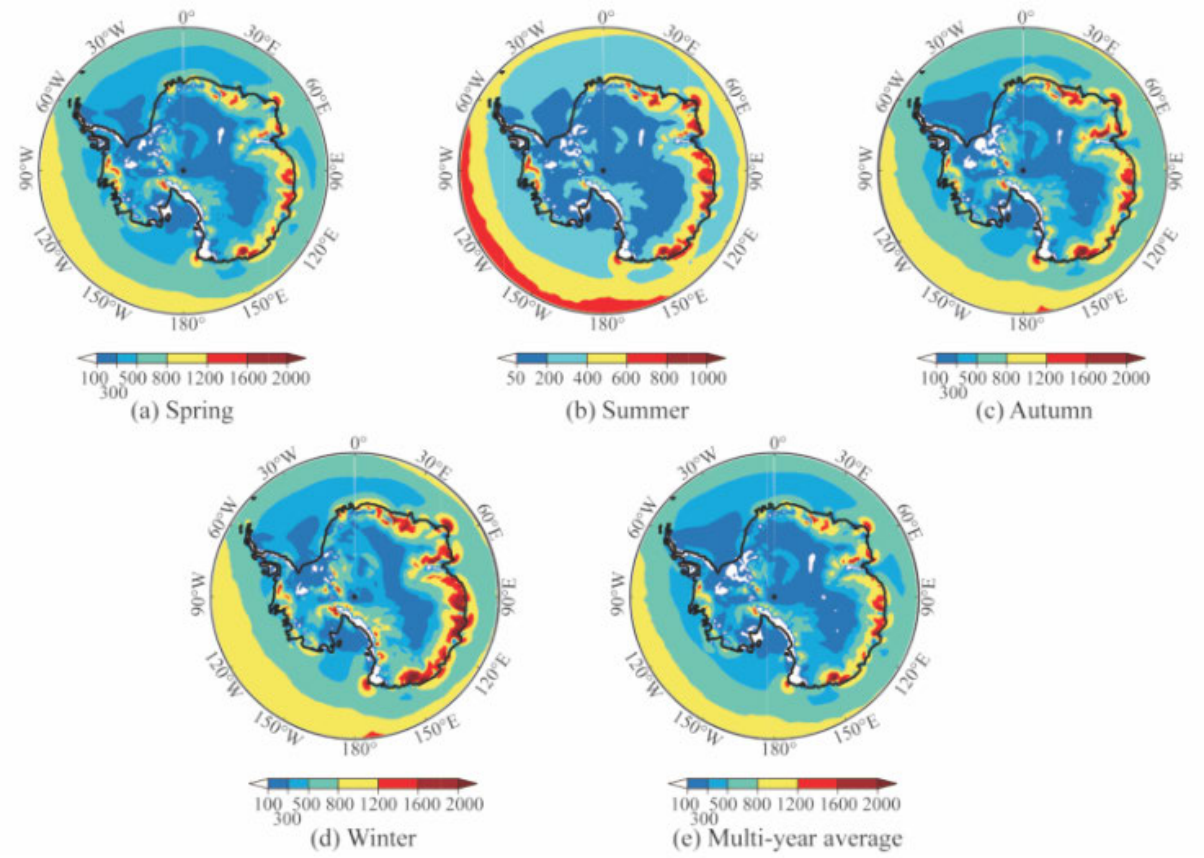

Figure 2.5: Wind power density in the Antarctic in W/m^2 [33]

In summary, westerly circulation, polar easterlies, katabatic winds, and cyclonic systems create a highly favourable environment for wind energy in Antarctica. The seasonal and spatial variations underscore the continent's vast potential, with autumn and winter standing out as the most productive seasons for harnessing wind power. Additionally, high air density at low temperatures enhances the efficiency of wind energy systems, with studies indicating up to a 20% efficiency increase at temperatures around -37 °C compared to temperate climates [15].

2.2 Operational Aspects of Wind Energy in Antarctica

Certain conditions in Antarctica, such as high-speed gusts combined with extremely low temperatures, present operational challenges for wind turbines [15]. Observations suggest that wind patterns in the interior regions of Antarctica tend to be more stable compared to coastal areas. Seasonal variability is evident, with stations like Syowa Base reporting lower wind speeds during winter, while regions such as the Brazilian Comandante Ferraz Station experience stronger winds during late winter and spring [15]. Seasonal fluctuations in wind energy potential reveal a marked reduction in generation capacity during the Antarctic summer, with peak outputs typically observed in spring and fall [15]. The operation of wind turbines In cold climates without implementing specific precautions typically results in a diminished energy yield. Figure 2.6 shows factors that affect wind turbines in cold climates.

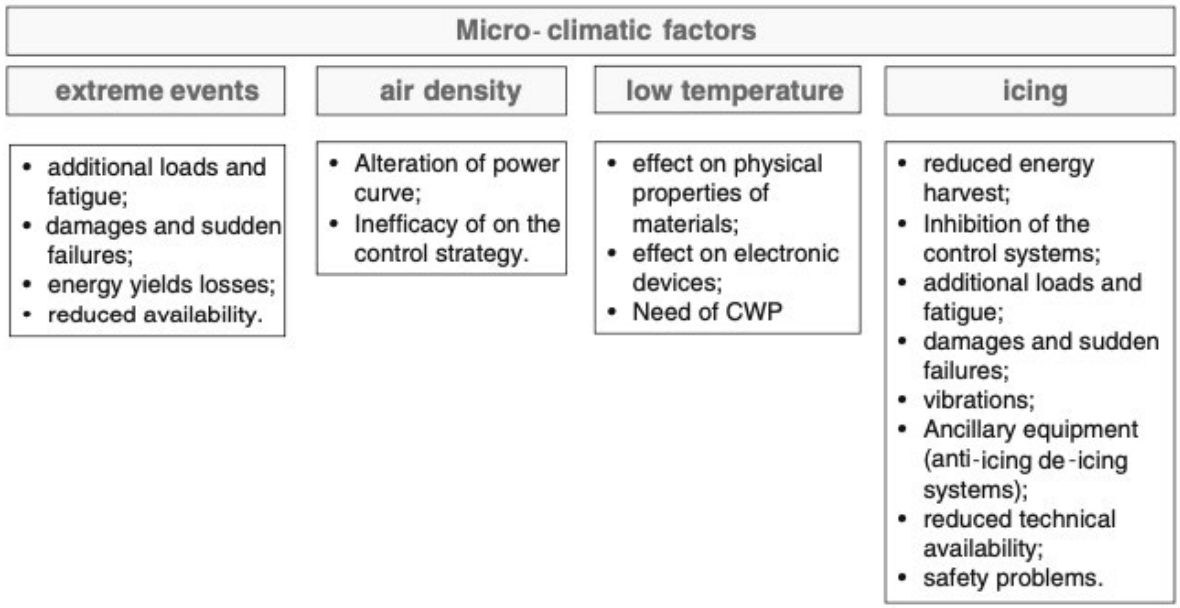

Figure 2.6: Effect of cold microclimate on wind turbines [6]

Extreme weather events impose additional loads and fatigue, leading to structural damage, sudden failures, and energy losses from precipitation events or extended turbine standstills, ultimately reducing overall availability [6]. Altered air density, influenced by low temperatures or high elevations, affects energy yield and significantly impacts control strategies. Low temperatures further influence the physical properties of materials and disrupt the normal operation of electronic components [6]. Additionally, icing introduces extra loads and fatigue, induces vibrations, decreases availability, and results in energy losses [6]. To counteract these effects, ancillary systems such as anti-icing and de-icing mechanisms are necessary [6]. Icing phenomenon can also influence the expected energy yield significantly as seen in Figure 2.7.

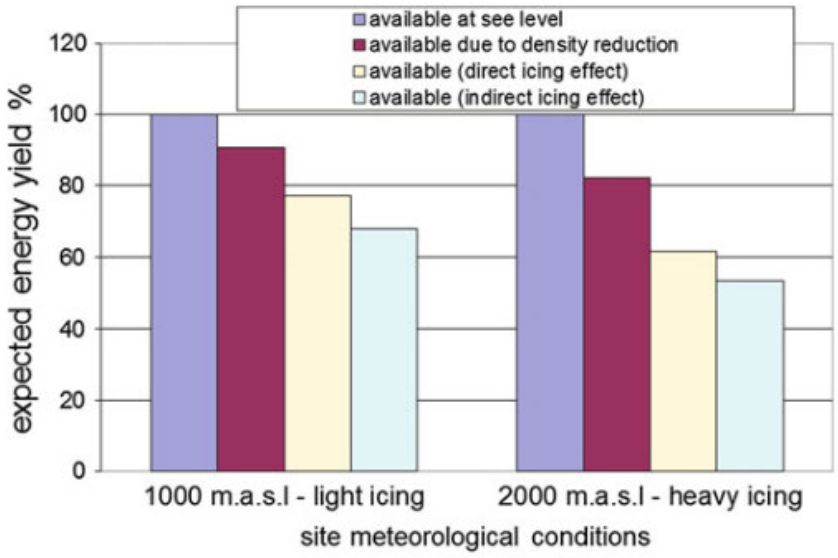

Figure 2.7: Icing effects on the energy harvest of wind turbines [6]

Icing can be understood as the combination of direct and indirect icing: Direct icing occurs when ice accumulates on the turbine structure during adverse weather conditions, whereas indirect icing refers to the residual effects of direct icing [6]. These effects affect normal operations and can lead to additional mechanical or electrical malfunctions, as well as increased power consumption by auxiliary equipment [6].
Without anti-icing or de-icing systems and heated wind sensors, icing can lead to frequent power losses, shutdowns from high vibration amplitudes, and errors in wind measurements. Even with these systems, fault-free operation under icing conditions is not always guaranteed. Indirect effects of icing include shortened turbine lifespan, safety risks from falling ice, material damage, and increased noise levels [5]. Temperatures dropping below a wind turbine's operational limit can disrupt its functionality, significantly affecting its availability. The influence of extremely low temperatures can therefore be substantial. Ice accumulation on wind turbine blades typically diminishes lift while increasing drag, leading to reduced power output and, in severe cases, complete turbine

shutdown [5]. Atmospheric icing significantly impairs rotor aerodynamic performance, as the blade's sensitivity to surface roughness and shape changes caused by ice compromises its efficiency [5]. Key factors influencing energy production losses from icing include the intensity, duration, and frequency of icing, along with the maximum ice load and ice type relative to prevailing wind conditions. Figure 2.8 shows that Stall-regulated turbines experience notable reductions in production, even after brief icing events, whereas pitch-regulated turbines are less affected, particularly under light icing conditions [5].

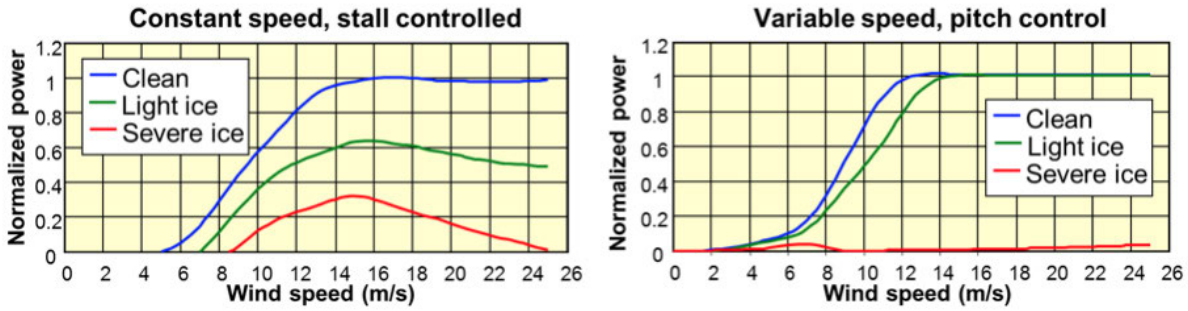

Figure 2.8: The impact ice on the power curves [5]

The impact of extremely low temperatures on energy production can be calculated using the following equation [5]:

$$E_T = EO\left(1 - \int_{-\infty}^{T} f(t)\,dt\right) \tag{2.1}$$

where E_T represents the energy output under low-temperature conditions, EO is the energy output under normal conditions, T is the turbine's lower temperature limit, and $f(t)$ is the probability density function of air temperature [5].

Operating wind turbines in Antarctica involves significant challenges, not only due to the extreme climatic conditions but also because of the logistical constraints associated with construction projects in such a remote and harsh environment. Projects must be carefully planned, with all required materials and tools delivered to the site in advance. Even minor components, such as bolts or screws, must be accounted for, as the absence of any item can halt construction until the next resupply, which often involves delays of up to a year [15]. Additionally, the availability of construction machinery poses constraints on the design and assembly of wind turbines. For instance, the type of crane accessible at the site may limit the height of the turbine or the weight of its components [15]. Furthermore, turbine parts must conform to the dimensions of the local transportation infrastructure, such as sleds, making oversized or irregularly shaped components difficult to transport over long distances across the ice [15]. These logistical and structural limitations necessitate careful consideration in both the design and execution phases of Antarctic wind energy projects.

2.3 Active wind energy projects in Antarctica

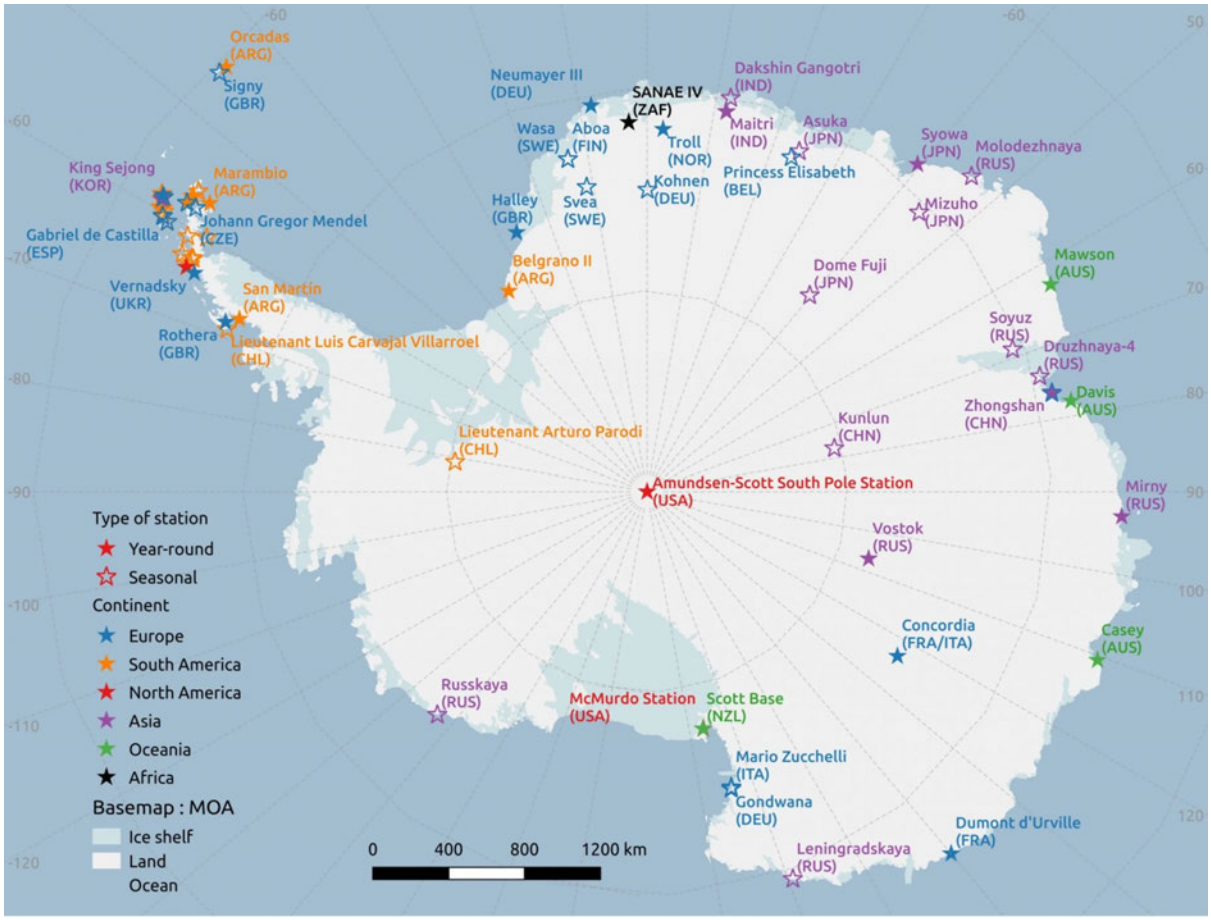

Figure 2.9: Research Stations in Antarctica [19]

Figure 2.9 shows an overview of the research stations in Antarctica. 37 of these Research Stations use renewable energies [15]. In This section, the currently used wind energy systems in Antarctica will be handled. This will give a better understanding of which wind systems research stations are using and give an insight on the technologies being used. Table 2.1 lists current research stations in Antarctica using wind turbines. Some research stations generate energy using wind farms, like the The Ross Island wind farm with three wind turbines with a power rating of 330 kW producing a combined power rating of 990 kW to deliver energy to New Zealand's Scott Base and the American McMurdo Station. The Belgian Princess Elizabeth Station uses 9 wind turbines with a power rating of 6 kW producing a combined power rating of 48 kW and the Italian research station Zucchelli uses 3 wind turbines with a 11.5 kW power rating for each wind turbine producing a combined power rating of 34.5 kW.

Facility	Country	Wind Turbine	Power Rating [kW]	Percentage
Dumont d'Urville	France	Ropatec Megastar	20	22
Mawson	Australia	The Mawson turbine	300	40
McMurdo	USA	Enercon E33/330	330	20
Mendel	Czech Republic	MG Plast AP1500	1.5	65
Neumayer III	Germany	Enercon E-10	30	5
Princess Elizabeth	Belgium	SD6	6 kW	48
Scott Base	New Zealand	Enercon E33/330	330	70
Zucchelli	Italy	Vertical Axis WT	11.5 kW	18.9
Jang Bogo	South Korea	WS-0,15	0.15 kW	-

Table 2.1: Overview of operating wind turbines in Antarctica [40, 41, 17, 68, 20, 55, 26, 53, 62, 54]

2.3.1 Ross Island Wind Farm

The Ross Island Wind Farm is the wind farm with the largest capacity in Antarctica. Three Enercon E33/330 deliver 990 KW of power for the American McMurdo Station and the New Zealand Scott Base Research Station. The Wind Farm has been fully operation since 2009 and has reduced the annual fuel consumption by approximately 463,000 litres, and greenhouse gas production by 1,242 tonnes of carbon dioxide [54]. The foundations for the wind turbines were prefabricated in New Zealand and shipped to Antarctica. The selected Enercon E33/330 Wind Turbines are direct drive, which usually have less mechanical wear and tear. This is in this case important, as the wind turbine were to be installed in a remote location [46]. The three wind turbines will be replaced as the current wind turbines will come to the end of their design life in 2030 [70]. Three new wind turbines of the type DW54X-1MW have been chosen to replace the current wind turbines. The new wind turbines will be used to reach new renewable energy goals at the stations [23] .

2.3.2 Mawson station

The Australian Mawson research station has a 300 kW Wind turbine that covers 40% of the station's energy needs. The station had two wind turbines with a capcity of 300 kW untill 2017 when one of the turbines suffered a a critical failure and is since then out of operation [17]. The wind turbine is connected to an energy management system that coordinates the electrical energy from the turbine and a diesel generator [17].

2.3.3 Princess Elisabeth Research Station

The Belgian Princess Elisabeth research station in Antarctica operates entirely on renewable energy resources and utilises a mix of wind and solar energies to power the station [41]. The station was constructed as a zero-emission station. The Princess Elisbaeth research station uses small-scale wind turbines for the electricity generation. Nine SD6 wind turbines with a capacity of 48 kW cover 40% of the station's energy needs [20, 41].

Figure 2.10: Princess Elisabeth research station Wind Farm[28]

2.3.4 Other small-scale wind turbine projects in Antarctica

The Czech Republic research station in Antarctica Mendel uses 8 1.5 kW small-scale wind turbines with a total capacity of 12 kW. This covers 65% of the stations energy needs with wind energy [41]. According to a report from the research station, the wind turbines are facing challenges like extreme mechanical disturbance of wind turbine parts when there are either high wind velocities and/or frequently changed wind velocities. The report states that the wind turbines will be replaced with new ones with new technology to reduce probability of mechanical failures [55].

The Italian research station Zucchelli uses 3 vertical axis wind turbines with a total capacity of 34.5 kW which covers around 18.9 % of the station's energy need. The wind turbines had to be integrated into the energy management system of the station. The wind turbines weren't able to produce the expected energy due to excessively high winds, which sent the turbines into protection until they shut down. The wind turbines are also

connected to a battery pack that stores the energy produced during winter [53].
The german Neumayer Station III which is the main focus of this study uses one 30 kW wind turbine that covers 5 % of the station's energy needs.

2.4 The Neumayer Station III

The Neumayer Station III in Antarctica was commissioned in 2009 and is operated by the Alfred Wegener Institute. The station was constructed on the Ekström Ice Shelf at Atka Bay, northeastern Weddell Sea and is designed as a jack-up platform above a garage [7]. This enables the station to be lifted in accordance with the annual ice accumulation that could be more than 100 cm [7]. The stations has a length of 68 m and is 24 m wide [7]. The floor space is 1,632 m^2 and spans across two primary decks housing accommodations, laboratories, and support facilities. A vehicle hall is embedded in the ice below the station. The station maintains nine permanent positions to operate its observatories year-round, with overwintering personnel staying 12 to 15 months [7]. From November to March, seasonal staff is accommodated in addition to the team, increasing the number of residents to 20-50.

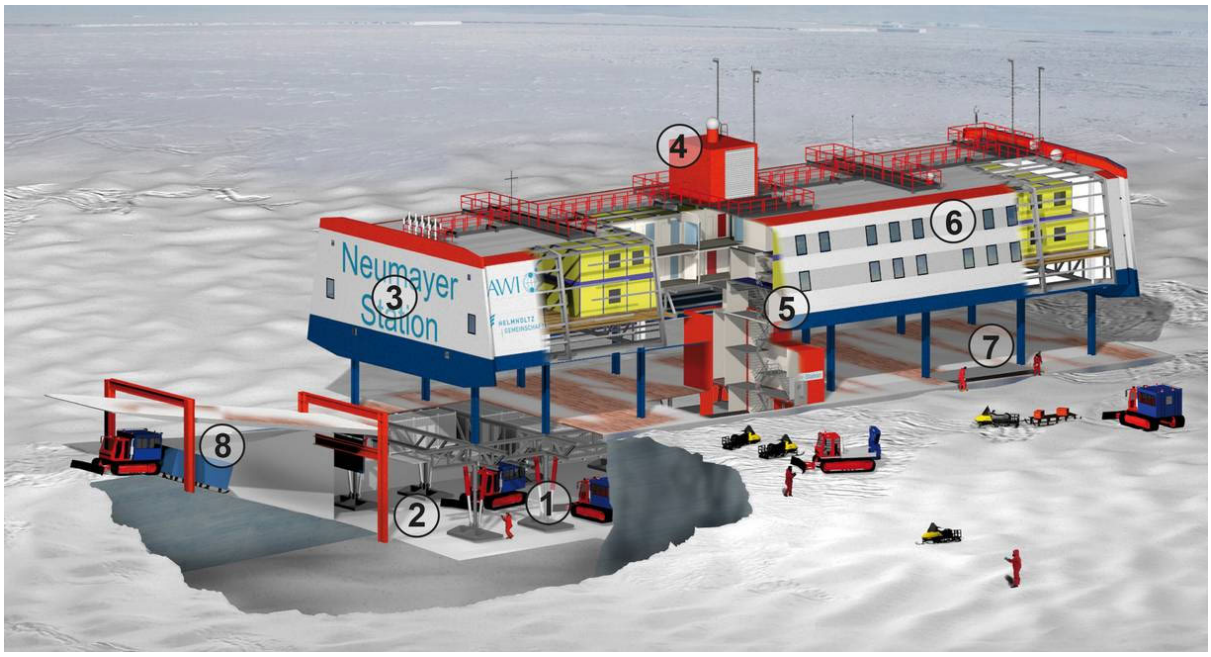

Figure 2.11: Neumayer Station III - Detailed Model[4]

#	**Description**
1	Foundation: The station's total weight of ca. 2,300 tonnes is distributed among 16 foundation plates. Hydraulic supports are used to raise the station on a regular basis, allowing it to compensate for new snowfall.
2	Garage: The garage offers ample room for the entire vehicle fleet (caterpillar trucks, Ski-Doos, etc.). Additional storage and utility rooms have been integrated into the interstitial deck.
3	Power unit: An intelligent management system regulates the station's electrical and thermal power supply.
4	Balloon-launching hall: Meteorological balloons with radiosondes can be launched from the hall on the station's roof.
5	Stairwell.
6	Living quarters and workrooms.
7	Water supply: A snowmelt supplies the station with fresh drinking water.
8	Access: Returning vehicles enter the station's garage via a ramp of pure snow with a tightly sealing lid.

Table 2.2: Neumayer Station III - Detailed Description[4]

For the energy supply, the station uses four diesel generators as combined heat and power units (CHP), to produce electricity and heat [7]. Each unit supplies 160 kW of electrical energy and 190 kW of thermal energy. Three of the four CHP Units are used for a steady supply of energy with the fourth being used as a standby. As previously stated, the station also uses one wind turbine with a capacity of 30 kW for the energy supply. The station's energy distribution system channels thermal energy for space heating, ventilation, snow melting, and hot water production. Space heating is facilitated by radiators, while CHP modules with cooling and exhaust gas exchangers contribute waste heat to condition incoming air. Drinking water is generated from melted snow, heated using waste energy from the CHP or auxiliary heater. The station's total installed heating capacity is approximately 410 kW. Given the extreme Antarctic conditions and station isolation, design priorities focus on high redundancy and secure, reliable operation of all heat and power supply systems. The annual energy demand covered with diesel for the CHP has been calculated in a feasibility study and amounts to 2645.8 MWh/a [7]. Figure 2.12 shows the current energy supply system of the NMS-III.

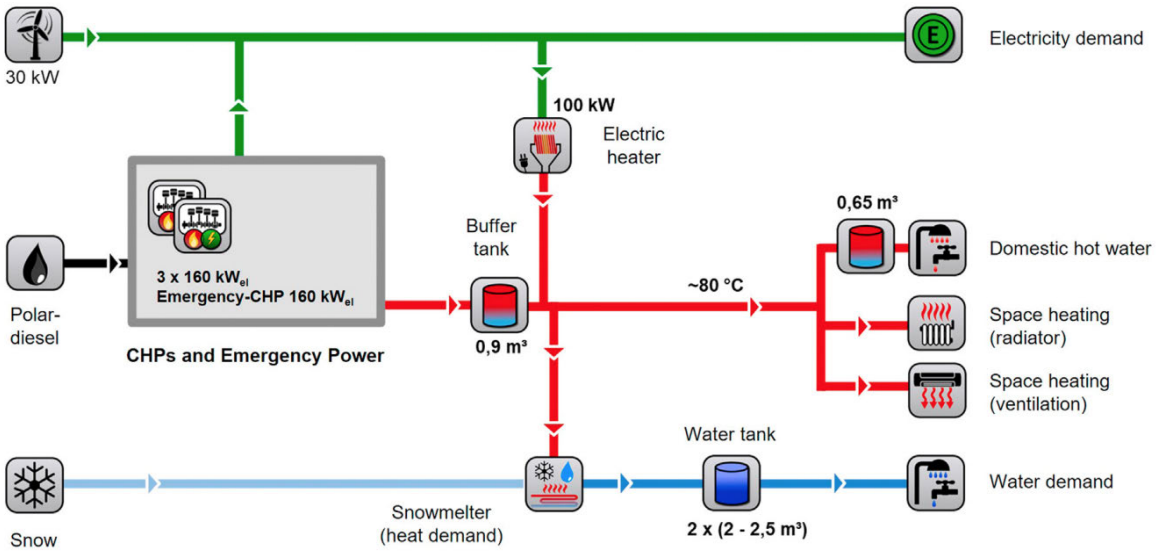

Figure 2.12: Neumayer Station III - Energy Supply[7]

2.4.1 The Meteorological Observatory Neumayer

The Meteorological Observatory Neumayer has been continuously collecting meteorological data since March 1982 [3]. The observatory is located approximately 300 meters from the main station building to minimise structural interference. The site includes a 10-meter mast equipped with sensors at both 2-meter and 10-meter levels, a central electrical cabinet, and two additional racks for radiation measurements. Due to the region's annual snow accumulation of approximately 1 meter, all cables at the site are routed above the snow surface [3]. Meteorological parameters such as temperature, humidity, wind, and air pressure are measured at this site [3]. Radiation measurements are conducted on dedicated racks or with a solar tracker. Initially, data collection intervals were set at 10 minutes, reduced to 5 minutes in March 1992, and further refined to 1-minute intervals by February 1998 [3]. The data undergoes stringent quality control processes: all measurements are reviewed daily on-site and undergo additional validation prior to publication. Any errors or impacted data is systematically excluded [3].
Data is recorded at high temporal resolutions, with readings taken every 1 to 6 seconds [3]. These readings are averaged into minutely values for global distribution and archival in the Pangaea database [59]. The instruments at the site are inspected and cleaned daily. Adverse weather conditions, such as rime, glaze, or snow, can cause measurement disruptions; however, daily inspections ensure that technical issues are promptly identified and resolved. The collected data is validated and cleaned as part of a routine maintenance process. The measurement data of the observatory will be further discussed in Chapter 4, as the data lays the groundwork for the wind assessment. The data is available as tab-delimited text files for each year [59]. The parameters and instruments used are listed in Table 2.3.

Figure 2.13: Measurement Site - Meteorological Observatory Neumayer [3]

Parameter	Unit	Instrument
DATE/TIME	YYYY-MM-DD T HH:SS	-
Sunshine duration (SSD)	min	Sunshine indicator, Kipp & Zonen, CSD 3
Air temperature at 10 m height (T10)	°C	Thermometer, Thies Clima, Ventilated Air Temperature Transmitter
Wind direction at 10 m height (DD10)	deg	Anemometer, Thies Clima, Combined Wind Transmitter
Wind speed at 10 m height (FF10)	m/s	Anemometer, Thies Clima, Combined Wind Transmitter
Air temperature at 2 m height (T2)	°C	Thermometer, Thies Clima, Ventilated Air Temperature Transmitter
Wind direction at 2 m height (DD2)	deg	Anemometer, Thies Clima, Combined Wind Transmitter
Wind speed at 2 m height (FF2)	m/s	Anemometer, Thies Clima, Combined Wind Transmitter
Humidity, relative (RH) at 2 m	%	Hygrometer, Vaisala, HMT337 in T2 housing
Humidity, relative (RH) at 2 m (redundant)	%	Hygrometer, Vaisala, HMP155 in T2 housing
Humidity, relative (RH) at 10 m	%	Hygrometer, Vaisala, HMT337 in T10 housing
Humidity, relative (RH) at 10 m (redundant)	%	Hygrometer, Vaisala, HMP155 in T10 housing
Station pressure (PoPoPoPo)	hPa	Barometer, Paroscientific, Digiquartz 6000-16B
Station pressure (PoPoPoPo, redundant)	hPa	Barometer, Vaisala, PTB330
Short-wave downward radiation (SWD OG1)	W/m^2	Pyranometer, Eppley, CM11
Short-wave downward radiation (SWD RG8)	W/m^2	Pyranometer, Eppley, CM11
Ultraviolet radiation (UV rad)	W/m^2	Total Ultraviolet Radiometer, Eppley, TUVR
Long-wave downward radiation (LWD)	W/m^2	Pyrgeometer, Kipp & Zonen, CGR4

Table 2.3: Parameters and Instruments: Meteorological Observatory Neumayer [59]

In addition to the meteorological measurements, the observatory conducts daily radiosonde launches to collect radiosonde data [60]. The latest data is recorded at a 1-second resolution. All data undergo quality control as is the case with the meteorological measurements [60]. The Vaisala RS41-SGP radiosonde is used to gather atmospheric data including air temperature, relative humidity, pressure, wind speed, and wind direction at different altitudes ranging from 0 to 3500 meters [60]. Radiosonde data will be utilised in subsequent analyses.

2.4.2 Logistical Setup of the Neumayer Station III

The logistical setup of the station involves multiple supply methods to ensure consistent operations. The primary resupply method involves the RV Polarstern, a research and supply vessel capable of navigating through ice-covered waters [2]. The vessel transports essential supplies such as food, fuel, and scientific equipment to the station. During the

Antarctic summer, the RV Polarstern transports fully loaded containers with supplies and technical equipment. These containers are unloaded at the ice shelf edge in Akta Bay and transported to the station using piste bashers.
Additionally, supply planes conduct eight to ten landings at the station during the short Antarctic summer. While these flights also carry materials, their primary purpose is to transport scientists and technicians. The typical flight route for deliveries begins in Germany (Frankfurt am Main), proceeds to Cape Town, then to the Russian station Novolazarevskaya, and finally reaches Neumayer Station. From Cape Town to Novo, the cargo is flown aboard an Ilyushin aircraft, and for the final leg from Novo to Neumayer, it is often transferred to smaller Basler planes [69]. This logistical chain is supported by specialised vehicles, which are used to distribute supplies and support field operations on the ice shelf. These vehicles are also instrumental in conducting maintenance tasks and facilitating the transport of scientific instruments [69].

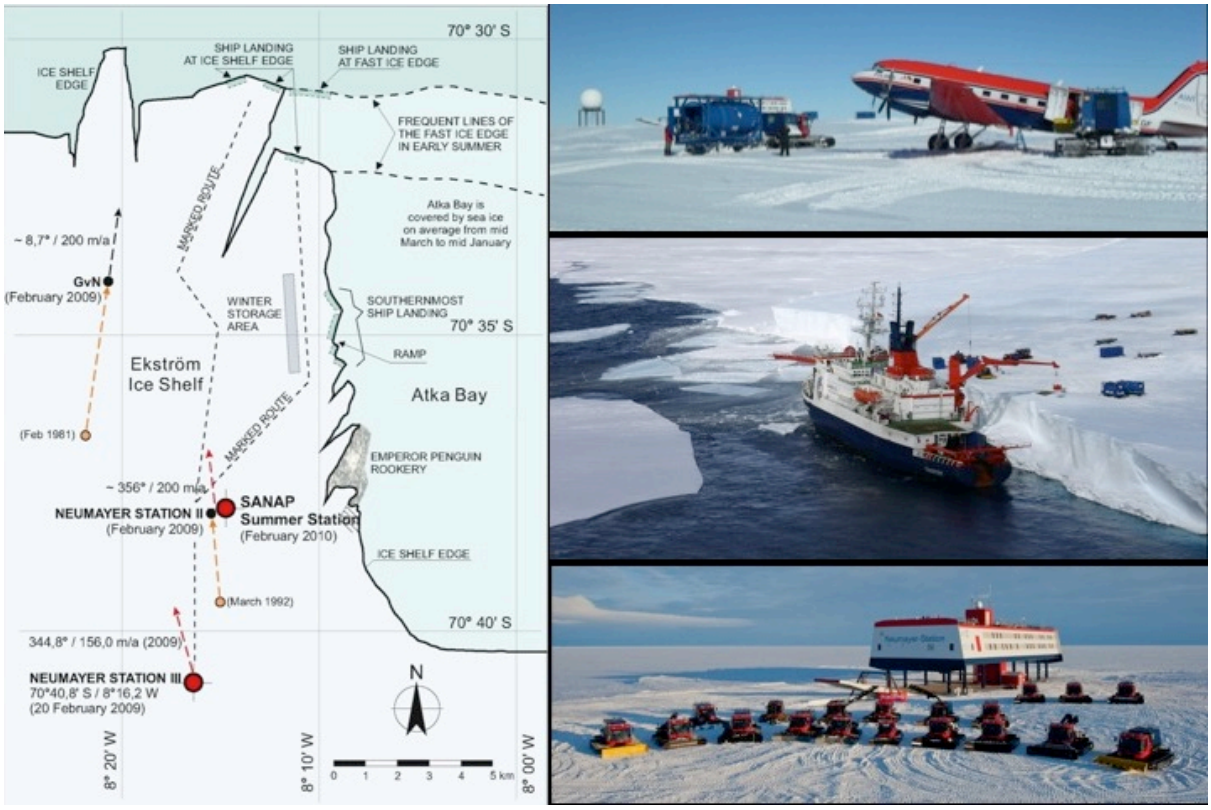

Figure 2.14: Logistical Setup and Routes of the Neumayer Station III [34]

2.5 AWES: Calculation of AEP and Simulation Tools

The fundamentals of AWES Technology will be handled in the next chapter, in this section, tools and calculation methods found in literature for the estimation of AEP for AWESs will be presented. AWESs present a unique challenge when it comes to calculating the AEP. This complexity arises from the highly dynamic nature of AWES operations,

which involve tethered kites or wings exploiting high-altitude wind currents. Unlike traditional wind turbines that rely on power curves correlating wind speed and energy output, AWES efficiency depends on flight trajectories, wind profiles, and system-specific operational parameters. The lack of standardisation in performance evaluation, coupled with the need to model high-altitude wind dynamics and tether behaviour, makes AEP estimation an intensive task. In this thesis, a simplified approach will be utilised later to calculate the AEP. However, the following methods and tools were also explored in the process of attempting to calculate the AEP. One approach is to use an optimal control problem (OCP) framework to simulate AEP for AWES[43]. By solving the OCP for large datasets of wind profiles, the study demonstrates methods to reduce computational complexity using homotopy-path-following algorithms [43]. This enables the estimation of power output at high spatial and temporal resolutions, showcasing the value of combining advanced mathematical optimisation with large-scale atmospheric datasets [43]. Another method is to use clustering algorithms to refine wind profile data for AEP estimation[57]. By using wind profiles derived from reanalysis datasets, the study generates power curves specific to different atmospheric conditions [57]. The clustering approach minimises computational burdens while maintaining accuracy, addressing the variability inherent in high-altitude wind resources [57]. Another study presents a quasi-steady approach for fixed-wing AWES[32], accounting for gravity, vertical wind shear, and hardware constraints. Their scaling models incorporate aerodynamic properties and tether dynamics, offering insights into performance optimisation for large-scale AWES [32]. By leveraging optimisation methods, the study identifies trade-offs between tether dimensions, wind speeds, and operational efficiency [32]. Through these studies, a pattern emerges where traditional methods like Lloyd's theory, which will be later discussed in detail and used for the AEP calculation, are extended with modern computational tools to address the unique dynamics of AWES. These efforts underscore the ongoing alignment of theoretical modelling and practical simulation in advancing the field of airborne wind energy. In addition to these theoretical and computational approaches, specialised software tools have been developed to simulate AWES operations. Tools like MegAWES and KiteSimulatorsjl are used to model the dynamics, control strategies, and energy output of AWES systems. However, challenges remain, particularly in integrating realistic wind profiles, system constraints, and environmental factors. A software review by industry experts highlighted the challenges associated with adopting simulation tools for AWES [24] - Numerous software packages are available for AWES, but they do not address the fundamental question of how much energy an AWES can harvest at a specific location. Nine software tools were examined and many were found to be challenging to install or are no longer maintained [24]. Some simulators overlook the influence of the ground station of an AWES or operate only at a limited number of discrete wind speeds, restricting their utility for power curve derivation [24].

Chapter 3

Fundamentals

As this thesis is focused on wind energy, a closer look into the main fundamentals of wind energy calculations is necessary. This chapter will cover the core principles of wind resource assessment for wind energy systems and incorporate a detailed overview of the methodologies used for evaluating wind characteristics and the factors that need to be addressed with it like topography, wind turbines and AWESs. The main objective is to get a better understanding of how an AEP can be calculated analytically for wind turbines or AWESs. In Addition, the methodology WAsP uses for wind energy resource assessment will be presented as the tool will be later used for the wind resource assessment.

3.1 Wind Energy Resource Assessment

Wind resource assessment is the process of estimating the wind resource or wind power potential at one or several sites, or over an area [49]. The result of wind resource assessment is therefore an estimate of the mean wind climate at a specific site. The result is usually visualised with wind direction probability distribution (wind rose), which shows the frequency distribution of wind directions at the site and sector-wise wind speed probability distribution functions, which show the frequency distributions of wind speeds at the site [49].

3.1.1 Characterisation of Wind Energy

To get a better understanding of wind assessment, it's essential to understand how an estimate of available wind power and power production via wind turbines is calculated. The equations and explanations in the next sections are based on the book titled 'Wind Energy Explained' from J. F. Manwell, J. G. McGowan and A. L. Rogers: [44]. Calculating available wind power can be done by using the continuity equation of fluid mechanics assuming The mass flow of air dm/dt through a rotor disc of area A is a function of air

density ρ with uniform air velocity U [44] and the kinetic energy equation which result in an equation for wind power per unit area: Equation 3.3.

$$\frac{dm}{dt} = \rho A U \tag{3.1}$$

$$P = \frac{1}{2}\frac{dm}{dt}U^2 = \frac{1}{2}\rho A U^3 \tag{3.2}$$

$$\frac{P}{A} = \frac{1}{2}\rho U^3 \tag{3.3}$$

If annual average wind speeds are known for certain regions, the wind power density can be calculated to assess the feasibility of wind power projects in those regions. More accurate estimates can be made if hourly averages, U_i, are available for a year [44]. Then, the average of power estimates for each hour can be determined. The average wind power density, based on hourly averages can the be calculated where $\overline{U}$ is the annual average wind speed and K_e is the energy pattern factor and N is the number of hours in a year, 8760.

$$\frac{\overline{P}}{A} = \frac{1}{2}\rho \overline{U}^3 K_e \tag{3.4}$$

$$K_e = \frac{1}{N\overline{U}^3}\sum_{i=1}^{N} U_i^3 \tag{3.5}$$

A wind speed of 5 m/s would have a Power/Area of 80 W/m^2 while a wind speed of 20 m/s has a Power/Area of 4900 W/m^2. This shows the strong correlation between wind speeds and wind power density which is highly sensitive to wind velocity, increasing with the cube of the wind speed. The wind power density is also directly proportional to the density of air and to the area swept by the rotor of a wind turbine. However, the actual power production potential of a wind turbine is influenced by the fluid mechanics of the airflow through the rotor, as well as the aerodynamics and efficiency of the rotor and generator system. In practice, even the most advanced horizontal-axis wind turbines are capable of harvesting only about 45 of the available wind power [44].

3.1.2 The Atmospheric Boundary Layer

Calculating wind energy potential using wind velocities only offers a basic estimate of wind energy production. Other factors influence the actual energy production [44]. As an example, the atmospheric boundary layer, the lowest part of the atmosphere, is directly influenced by its interaction with the earth's surface. Within this layer, parameters such as wind velocity, temperature, and humidity can change rapidly. This leads to a variation

of horizontal wind speed with height, known as the vertical wind profile or wind shear. Wind speed increases with elevation, influencing both turbine productivity and rotor blade lifespan due to cyclic loads. As demonstrated previously, the power in the wind is a function of air density. Air density ρ is a function of temperature T and pressure p both of which vary with height.
The equations for the density ρ and pressure p are given as:

$$\rho = \frac{p}{RT} = 3.4837\frac{p}{T} \tag{3.6}$$

where ρ is the air density, p is the pressure, R is the specific gas constant, and T is the temperature. The pressure p as a function of height z (height above sea level) is expressed as:

$$p = 101.29 - (0.011837)z + \left(4.793 \times 10^{-7}\right) z^2 \tag{3.7}$$

Air density can thereby be affected by altitude, temperature, and humidity. Higher altitudes, warmer temperatures, or increased humidity result in lower air density, reducing power output.
The stability of the atmospheric boundary layer plays a crucial role in shaping the characteristics of turbulence, which significantly influences wind potential. Turbulence arises from the dissipation of the wind's kinetic energy into thermal energy, creating smaller and smaller eddies. While turbulent wind may exhibit a relatively steady mean over long periods (hours), its short-term variability (minutes or less) is marked by distinct patterns rather than pure randomness. Stability in the the atmospheric boundary layer affects these turbulent features, thereby influencing wind energy potential, rotor performance, and turbine design considerations [44].
Due to the effects of turbulence wind speeds vary in time and direction. The mean wind speed increases with height, this is due to wind shear [44]. Wind shear is important for the evaluation of wind resources and the design of wind turbines as while assessing wind resources over large areas, anemometer data from various sources may need to be adjusted to a common elevation. Therefore, a model that describes how wind speed varies with altitude is essential for wind energy applications. The vertical profile of wind speed can be modelled using the power law which represents a simple model for the vertical wind speed profile.

$$U(z) = U_0 \left(\frac{z}{z_0}\right)^{\alpha} \tag{3.8}$$

Where $U(z)$ is the wind speed at height z, U_0 is the reference wind speed at height z_0, and α is the power law exponent. The value of α depends on the surface roughness of the terrain and the atmospheric conditions. When wind speeds are measured and plotted across varying heights above the ground, the result is a vertical wind shear profile. This

profile characterises how wind speed changes with altitude. The vertical wind shear profile can be affected by atmospheric stability and surface roughness. The Influence can be quantified with the power law exponent, as a higher power law exponent usually indicates greater surface roughness or stronger vertical wind shear, which can be associated with more complex terrain.

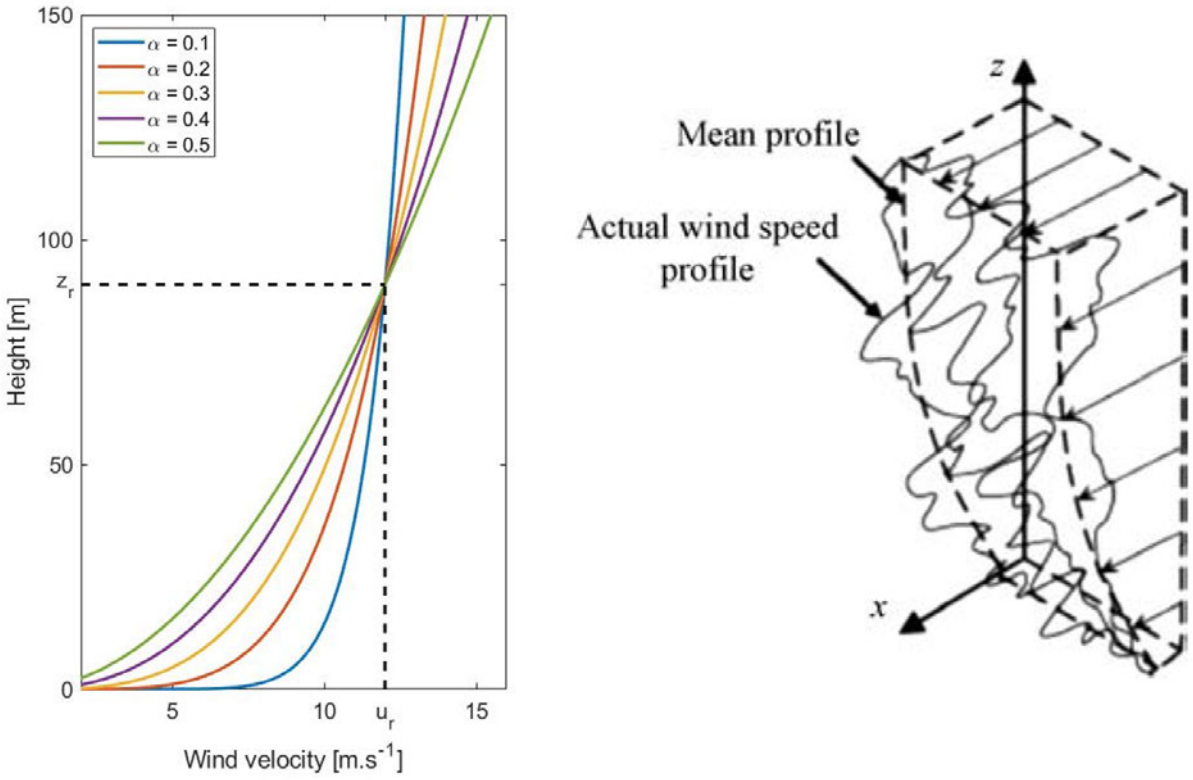

Figure 3.1: Power Law Exponent and Vertical Wind Profile [44]

3.1.3 Effects of terrain on wind characteristics

Terrain can influence wind dynamics through effects such as velocity deficits, unusual wind shear, and wind acceleration [44]. These influences can significantly affect a turbine's energy output. The vertical wind speed profile can be affected by terrain, which could lead to substantial changes in the energy production of a wind turbine as irregularities in the earth's surface alter wind flow patterns, limiting the accuracy of a predicted energy outcome. Terrain can be broadly classified into flat and non-flat terrain [44]. Flat terrain includes areas with minor irregularities, such as forests or small elevation differences, and must meet conditions such as elevation differences below 60m within an 11.5 km diameter and aspect ratios of hills below 1/50 within 4 km of the turbine site [44].

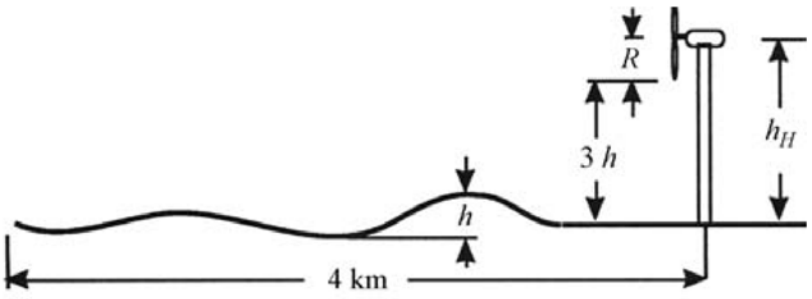

Figure 3.2: Determination of flat terrain [44]

Non-flat terrain includes large-scale features like hills, ridges, valleys, and mountainous regions, which significantly impact wind flow. Complex terrain can be further divided into isolated features or mountainous terrain, with flow complexity varying based on the scale of elevation relative to the planetary boundary layer. Wind direction is also critical in classification; for example, a hill affecting wind only 5% of the time with low speeds might still qualify as flat terrain. Flow over flat terrain with obstacles, both man-made and natural, significantly influences wind flow by creating wakes and turbulence [44].

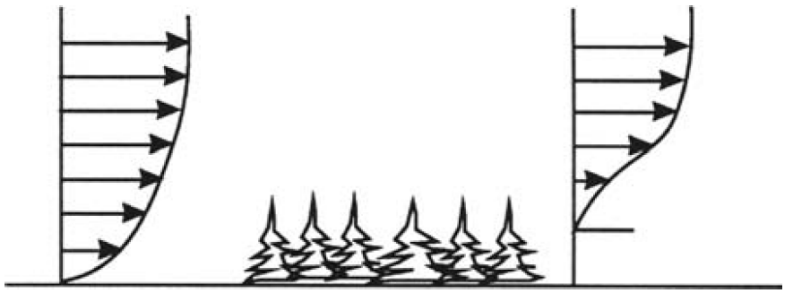

Figure 3.3: Effect of change in surface roughness [44]

For man-made obstacles, flow is often modelled as two-dimensional, with power losses and turbulence diminishing about 15 building heights downwind. Changes in surface roughness, such as transitioning from smooth to rough terrain, also alter the wind profile. In non-flat terrain, small-scale features like elevations and depressions impact wind behaviour [44].

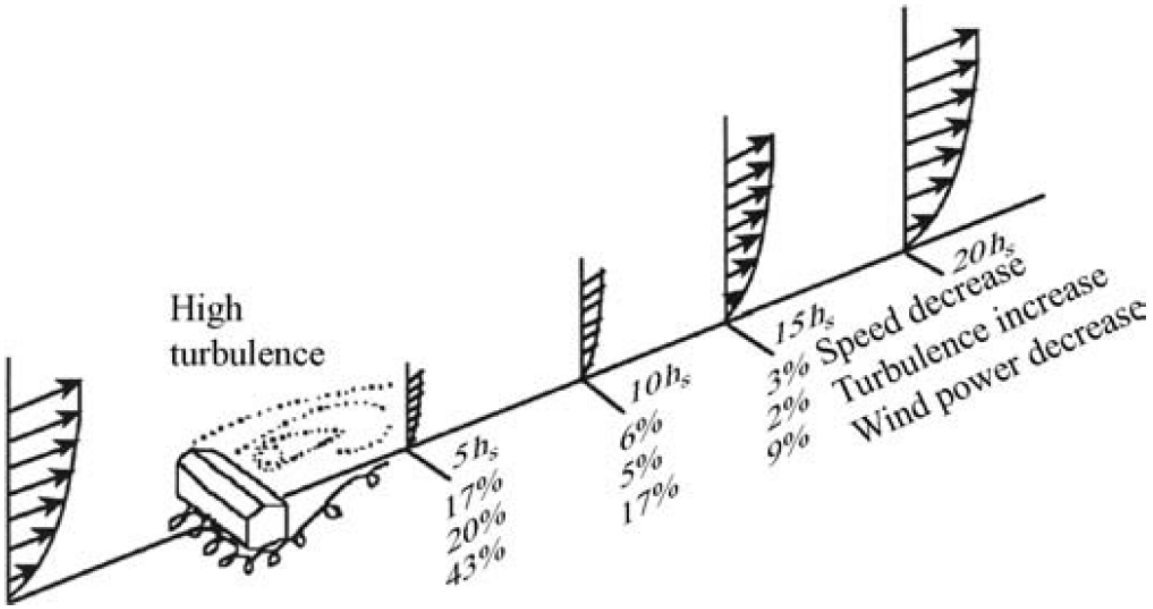

Figure 3.4: Speed, power, and turbulence effects downstream of a building [44]

3.1.4 Wind Turbine Energy Production

Now that the importance of air density, turbulence, terrain and wind speeds for wind energy resource assessment have been discussed, the energy production of a wind turbine can be explored. The determination of wind turbine energy production can be calculated using multiple methods. As the wind energy resource assessment for wind turbines in this Thesis will be implemented using the software WAsP, the methods used by WAsP will be described here. The method of bins can be used to summarise wind data and in addition the energy produced by a wind turbine. Data is firstly separated into wind speed intervals with the same size (bins). Given a series of N wind speed observations, U_i, averaged over a time interval Δt, key parameters can be derived to analyze wind energy potential. These include the long-term average wind speed ($\overline{U}$), the standard deviation of wind speeds (σ_U), the average wind power density ($\overline{P}/A$), the wind energy density per unit area (E/A), the average wind machine power ($\overline{P_w}$), and the total energy output of a wind turbine (E_w) [44].

$$\overline{U} = \frac{1}{N}\sum_{i=1}^{N} U_i \tag{3.9}$$

$$\sigma_U = \sqrt{\frac{1}{N-1}\sum_{i=1}^{N}(U_i - \overline{U})^2} = \sqrt{\frac{1}{N-1}\left(\sum_{i=1}^{N} U_i^2 - N\overline{U}^2\right)} \tag{3.10}$$

$$\frac{\overline{P}}{A} = \frac{1}{2}\rho\frac{1}{N}\sum_{i=1}^{N} U_i^3 \tag{3.11}$$

$$\frac{E}{A} = \frac{1}{2}\rho\Delta t\sum_{i=1}^{N} U_i^3 = \left(\frac{\overline{P}}{A}\right)(N\Delta t) \tag{3.12}$$

$$\overline{P_w} = \frac{1}{N}\sum_{i=1}^{N} P_w(U_i) \tag{3.13}$$

$$E_w = \sum_{i=1}^{N} P_w(U_i)(\Delta t) \tag{3.14}$$

Here, ρ is the air density, A is the rotor-swept area, $P_w(U_i)$ is the power output defined by the wind turbine's power curve, and Δt represents the time interval over which observations are averaged. After this method is implemented a histogram can be used to visualise the probability of specific wind speeds - This is also one of the outputs of a WAsP wind assessment which will be discussed later in this thesis.

WAsP creates a statistical analysis of wind data to calculate wind energy production of a wind turbine [44]. Statistical analysis of wind data enables a projection of measured data from one location to another unlike other methods for wind energy production estimation. A probability distribution is the outcome of a statistical analysis and describes the probability of specific wind speeds.

The frequency of occurrence of wind speeds will be described by a probability density function $p(U)$ for wind speeds. It will describe the probability of a wind speed occurring between U_a and U_b. After that the area under the probability density curve can be calculated. If $p(U)$ is known, the mean wind speed, the standard deviation of wind speed and the mean available wind power density can be calculated:

$$p(U_a \leq U \leq U_b) = \int_{U_a}^{U_b} p(U)\,\mathrm{d}U \tag{3.15}$$

$$\int_0^{\infty} p(U)\,\mathrm{d}U = 1 \tag{3.16}$$

$$\overline{U} = \int_0^{\infty} Up(U)\,\mathrm{d}U \tag{3.17}$$

$$\sigma_U = \sqrt{\int_0^{\infty} (U-\overline{U})^2 p(U)\,\mathrm{d}U} \tag{3.18}$$

$$\frac{\overline{P}}{A} = \frac{1}{2}\rho\int_0^{\infty} U^3 p(U)\,\mathrm{d}U = \frac{1}{2}\rho\overline{U^3} \tag{3.19}$$

The total area under the probability density curve is equal to 1, ensuring that the probability density function $p(U)$ is properly normalised [44]. If $p(U)$ is known, various wind resource parameters can be calculated. The mean wind speed, $\overline{U}$, represents the average wind velocity and is determined by integrating the product of wind speed and $p(U)$ over all possible speeds. The standard deviation of wind speed, σ_U, quantifies the variability of wind speeds and is calculated as the square root of the variance, integrating the squared deviation from the mean multiplied by $p(U)$.

The mean available wind power density, $\overline{P}/A$, expresses the average wind energy per unit area and is obtained by integrating the cube of wind speed multiplied by $p(U)$, scaled by $\frac{1}{2}\rho$, where ρ is the air density. Here, $\overline{U^3}$ represents the expected value of the cube of the wind speed. Furthermore, the probability density function can be superimposed on a wind velocity histogram by appropriately scaling it to match the area of the histogram that can be obtained by the method of bins.

Probability distribution are used in wind energy resource assessments as they provide a way to model and analyse the variability of wind speeds [44]. The commonly used probability distributions in wind analysis and WAsP are the the Rayleigh and the Weibull distributions. The Rayleigh distribution has one parameter which is the mean wind speed. The Weibull distribution on the other hand is based on two parameters and can therefore represent a wider variety of wind regimens. WAsP also uses the emergent distribution, which represents the weighted sum of Weibull distributions across all directional sectors. The Rayleigh Distribution requires only knowledge of the mean wind speed $\overline{U}$ [44]. An example of a Rayleigh Distribution is illustrated in Figure 3.5. The probability density function and the cumulative distribution function are as follows:

$$p(U) = \frac{\pi}{2}\left(\frac{U}{\overline{U}^2}\right)\exp\left[-\frac{\pi}{4}\left(\frac{U}{\overline{U}}\right)^2\right] \tag{3.20}$$

$$F(U) = 1 - \exp\left[-\frac{\pi}{4}\left(\frac{U}{\overline{U}}\right)^2\right] \tag{3.21}$$

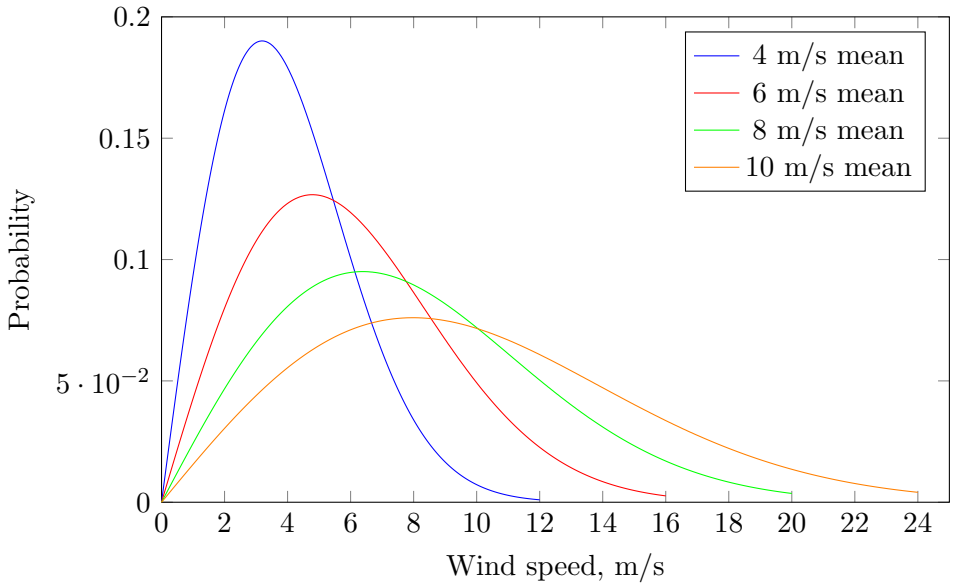

Figure 3.5: Rayleigh probability density function for different mean wind speeds.

The curves in Figure 3.5 demonstrate that as the mean wind speed increases, the peak of the distribution shifts to the right, indicating higher probabilities for larger wind speeds [44]. In Addition, the spread of the distribution increases with the mean wind speed, signifying that higher mean wind speeds are associated with greater variability in wind speeds. This means that at locations with a higher average wind speed, wind turbines will experience higher-speed winds more frequently, which contributes to greater energy production since wind power is proportional to the cube of wind speed.
As for the Weibull probability density function, two parameters are required: k, a shape factor, and c, a scale factor [44]. Both parameters depend on the mean wind speed, $\overline{U}$, and the standard deviation, σ_U. The Weibull probability density function (PDF) and cumulative distribution function (CDF) are defined as:

$$p(U) = \left(\frac{k}{c}\right)\left(\frac{U}{c}\right)^{k-1} \exp\left[-\left(\frac{U}{c}\right)^{k}\right] \tag{3.22}$$

$$F(U) = 1 - \exp\left[-\left(\frac{U}{c}\right)^{k}\right] \tag{3.23}$$

An example of a Weibull probability distribution function is shown in Figure 3.6. As the value of k increases, the curve exhibits a sharper peak, indicating reduced wind speed variation [44].

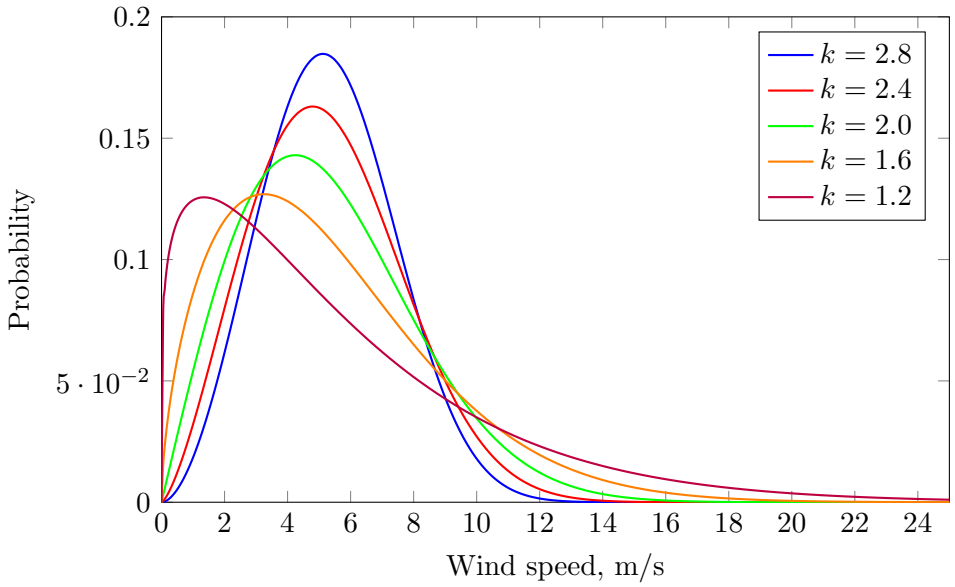

Figure 3.6: Example of Weibull probability density function for $\overline{U} = 6\,\mathrm{m/s}$.

The average wind speed for the Weibull distribution can be determined as a function of the scale parameter c, the shape parameter k, and the gamma function Γ [44]. The gamma function itself can be defined as an integral, or approximated using a series expansion. The variance of wind speed is also expressed in terms of the gamma function and the Weibull parameters. Determining c and k in terms of the mean wind speed $\overline{U}$ and the standard deviation σ_U can be done using analytical approximations. As an example k be approximated based on the ratio of σ_U to $\overline{U}$, and subsequently, c can be computed using the relationship between $\overline{U}$, c, and the gamma function [44].

$$\overline{U} = c\,\Gamma\left(1 + \frac{1}{k}\right) \tag{3.24}$$

$$\Gamma(x) = \int_0^\infty e^{-t} t^{x-1}\,\mathrm{d}t \tag{3.25}$$

$$\Gamma(x) = \left(\sqrt{2\pi x}\right)\left(x^{-1}\right) e^{-x}\left(1 + \frac{1}{12x} + \frac{1}{288x^2} - \frac{139}{51840x^3} + \dots\right) \tag{3.26}$$

$$\sigma_U^2 = \overline{U}^2\left[\frac{\Gamma(1+2/k)}{\Gamma^2(1+1/k)} - 1\right] \tag{3.27}$$

$$k = \left(\frac{\sigma_U}{\overline{U}}\right)^{-1.086} \tag{3.28}$$

$$c = \frac{\overline{U}}{\Gamma\left(1 + \frac{1}{k}\right)} \tag{3.29}$$

Statistical methods, such as Rayleigh and Weibull distributions, provide a foundation for estimating the energy production of a turbine with minimal data requirements [44].The average wind turbine power, $\overline{P_w}$, can be calculated using the probability density function

of wind speed, $p(U)$, and the turbine power curve, $P_w(U)$. This average power can also be used to compute the capacity factor (CF), which is the ratio of the actual energy output of a turbine over a period of time to the energy it would produce if it operated at its rated power (P_R) during the same period. Furthermore, the turbine power curve can be derived using the power available in the wind and the rotor power coefficient, C_p, where η is the efficiency (generator power/rotor power), ρ is the air density, and A is the rotor area. The rotor power coefficient C_p is defined as the ratio of the rotor power to the power available in the wind. Additionally, the power coefficient C_p is a function of the tip speed ratio, λ, which is the ratio of the blade tip speed to the wind speed, given by $\lambda = \frac{\Omega R}{U}$, where Ω is the angular velocity of the rotor and R is the rotor radius. Assuming a constant efficiency, the average wind turbine power can also be calculated (Equation 3.30). The annual energy production of a wind turbine can then be calculated by multiplying the average wind turbine power with the amount of hours in a year (8760 Hours) [44].

$$\overline{P_w} = \int_0^\infty P_w(U) p(U)\,\mathrm{d}U \tag{3.30}$$

$$CF = \frac{\overline{P_w}}{P_R} \tag{3.31}$$

$$P_w(U) = \frac{1}{2}\rho A C_p \eta U^3 \tag{3.32}$$

$$C_p = \frac{P_{\text{rotor}}}{\frac{1}{2}\rho A U^3} \tag{3.33}$$

$$\lambda = \frac{\Omega R}{U} \tag{3.34}$$

$$\overline{P_w} = \frac{1}{2}\rho\pi R^2 \eta \int_0^\infty C_p(\lambda) U^3 p(U)\,\mathrm{d}U \tag{3.35}$$

3.1.5 Wind Resource and Energy Yield Assessment Procedures

The theoretical explanations handled in this chapter were aimed at giving a better understanding of wind energy assessment calculations. The implementation of a wind resource assessment can be done conceptually, experimentally or statistically. The focus in this Thesis is on the wind atlas method which is used by the software WAsP.

The Wind Atlas Method relies on a mathematical model to determine the wind conditions of a site by analysing factors such as surface roughness, terrain elevations (orography), and nearby obstacles [67]. These factors are evaluated using topographical maps and on-site data about individual obstacles. When wind speed frequency distributions and characteristics of the region's atmospheric boundary layer are known the average annual wind speed at various heights can be calculated. A key requirement for this process is

converting raw data from an appropriate wind measurement station. This conversion accounts for the influence of roughness, orography, and obstacles near the measurement point. The raw data is adjusted using a long-term extrapolation procedure to the long-term climatology of the area [49]. This can be implemented using WAsP where raw data from a measurement station is processed alongside digitised information about the site's surroundings. The outcomes include the average annual wind speed, the Weibull distribution and a wind rose. The wind potential at a site is then combined with the performance characteristics of the wind energy turbine to estimate the expected annual energy yield.

After the wind resource has been analysed, an energy yield assessment can be undertaken. For the energy yield assessment, from the adjusted site wind data a reference yield is calculated at the hub height of the measuring mast from site wind data and the power curve of a chosen wind turbine [49]. Then a gross yield is calculated where terrain effects are accounted for. A potential yield is then calculated, where wake losses are accounted for and a net yield that accounts for technical or operational losses is calculated. An energy yield that accounts for the modelling uncertainty is also calculated. The energy yield calculated by WAsP is the potential annual energy production, which could potentially be produced by the wind farm when wake losses have been taken into account [49]. The net yield and an energy yield that accounts for other losses can however be calculated with other WAsP tools. The wind resource and energy yield Assessment procedures are visualised in Figure 3.7.

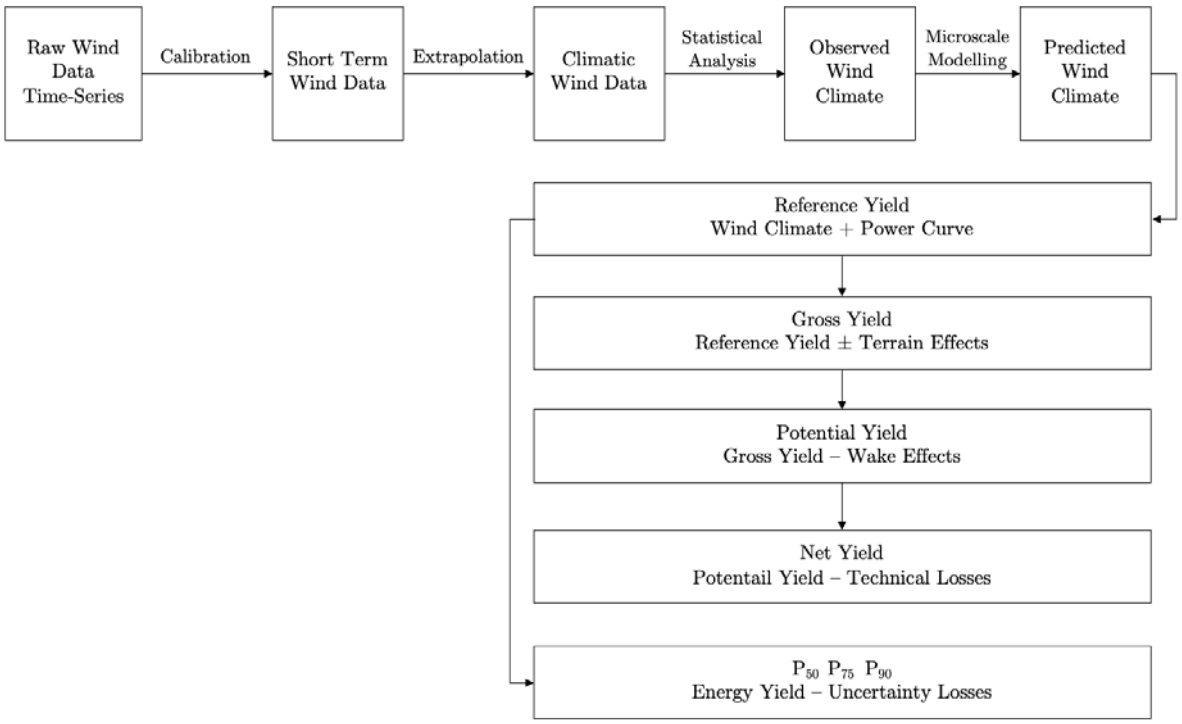

Figure 3.7: Wind Resource and Energy Yield Assessment Procedure

3.1.6 Topographical Inputs

The topographical inputs for WAsP are provided via a vector map, which may include height contour lines, roughness change lines, and attribute-free lines, such as the border of a wind farm site [49]. Sheltering obstacles can also be specified in a separate group and displayed on the map. All coordinates and elevations must be in meters, using a consistent Cartesian map coordinate system. The map's projection and datum are set in the WAsP Map Editor to embed this information in the map file. The Map Editor can transform maps between coordinate systems [49]. The inputs needed include:

- Elevation Maps: Elevation maps for WAsP can be created from digitised paper maps, databases of pre-digitised height contours, or generated using contouring software from gridded or random spot height data [49]. The map should extend at least 2-3 times the horizontal scale of significant terrain features, typically 5-10 km. High-resolution gridded elevation data can be directly used in the Map Editor or processed into vector maps using GIS Tools [49].

- Land Cover Maps: A land cover (roughness length) map classifies terrain based on land cover types, each characterised by a specific roughness length value, z_0. These maps can be created by digitising scanned maps, aerial photographs, or satellite imagery, or sourced from land cover databases [49]. The roughness map should extend at least $100 \times h$ (where h is the height of WAsP calculations). Roughness lengths are specified in meters, with water surfaces set to 0.0 m, both as a value and a flag. Maps must be systematically checked for errors like dead ends, cross points, and inconsistent roughness values using the Map Editor tools. High-resolution gridded land cover data must be converted into vector maps for WAsP [49].

- Obstacles: Terrain features such as houses, walls, shelter belts, or clusters of trees near the WAsP calculation site can be modeled either as sheltering obstacles or as roughness elements, depending on their proximity and relative height to the calculation point [49]. A general guideline is that if the calculation point (e.g., anemometer, turbine hub, or another site) is closer to the obstacle than approximately $50 \times H$ (where H is the height of the obstacle) and lower than about $3 \times H$, the feature should be treated as a sheltering obstacle and modelled using the WAsP shelter model. However, if the calculation point is farther than $50 \times H$ or higher than $3 \times H$, the feature should be considered a roughness element, contributing to the overall terrain roughness [49].

The elevation data that will be later used for the wind assessment will be extracted from the The Reference Elevation Model of Antarctica - REMA. Figure 4.13 shows different types of DEM Data illustrations available on the REMA Explorer.

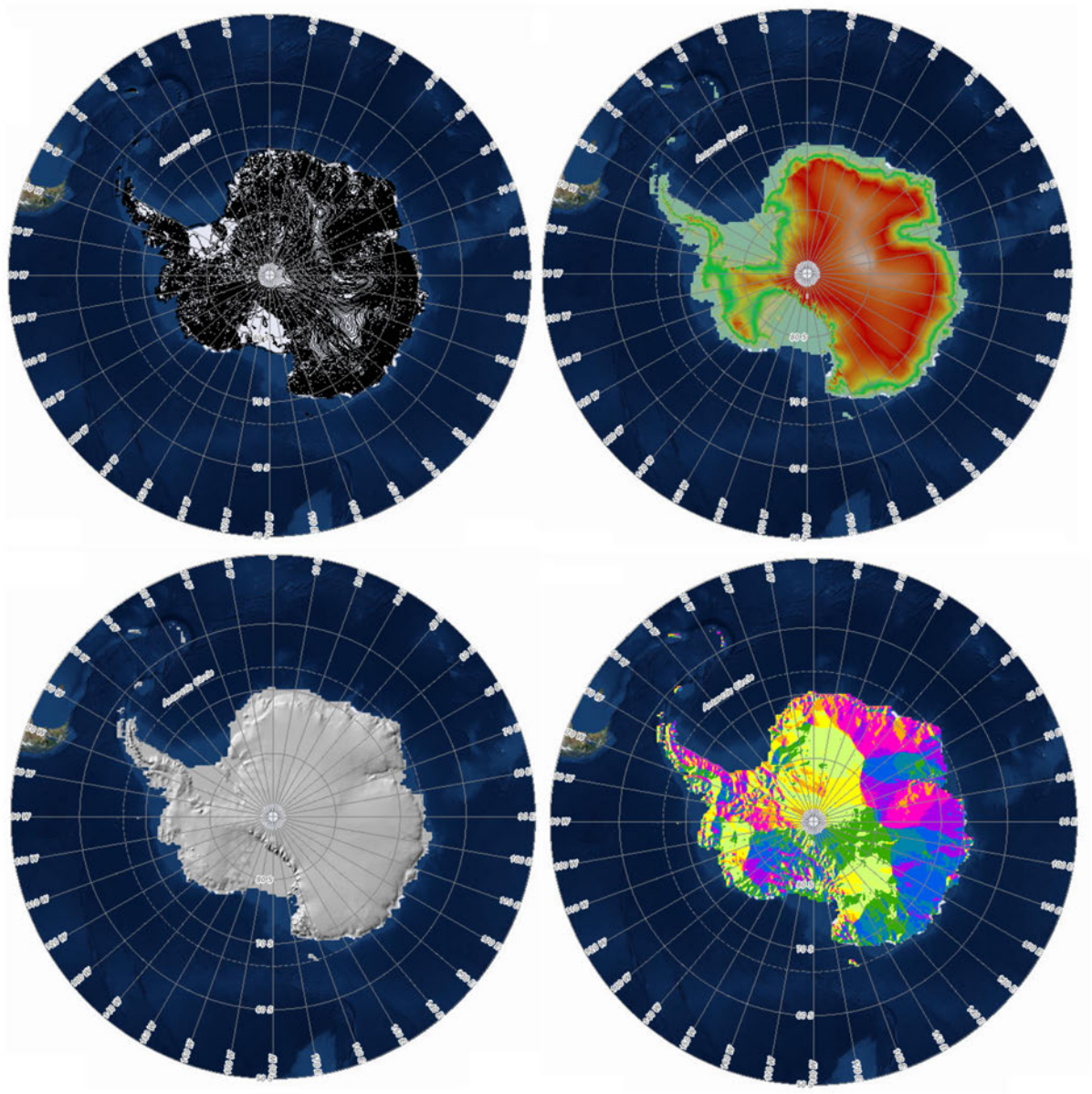

Figure 3.8: Clockwise: Contours on antarctic elevation - Elevation tinted hillshade on antarctic elevation - Hillshade on antarctic elevation - AspectMap on antarctic elevation [30]

REMA offers high-resolution (2-meter) terrain map of nearly the entire continent, with each grid point timestamped to enable elevation change measurement over time [10]. REMA was constructed from hundreds of thousands of stereoscopic Digital Elevation Models (DEMs) derived from high-resolution Maxar satellite imagery captured between 2009 and 2021. DEM files are available as time-sensitive strip files for change detection and as mosaics, compiled for larger-area consistency with timestamps and error estimates [10]. Elevation and roughness maps are crucial for the microscale flow modelling in WAsP. Acquiring the data for elevation, obstacles or roughness is usually a straightforward task.

As an example WAsP Scripts that are able to get data from multiple resources such as GWA or SRTM and to digitise maps in QGIS are available. However, the available data that the WAsP Scripts are embedded in, usually do not include Antarctica, as the data for the continent is not usually collected in DEM data campaigns. Data for Antarctica is however available in other resources where DEM data is collected only for Antarctica. Another important issues is that the data for Antarctica is usually collected in a specific projection that is only for Antarctica, which is the Projection 3031 - Antarctic Polar Stereographic. The WAsP Map editor however only accepts specific projections. A re-projection is therefore needed to be able to use the data, this will be later discussed in another chapter.

3.1.7 WAsP

In its core, WAsP is a software for horizontal and vertical extrapolation of wind data. The program contains models to calculate the effects on the wind of sheltering obstacles, surface roughness changes and terrain height variations [49]. The analysis part consists of a transformation of an observed wind climate (speed and direction distributions) to a wind atlas data set. The wind atlas data set can subsequently be applied for estimation of the wind climate and wind power potential, as well as for siting of specific wind turbines. Typical WAsP Software applications include the following [66]:

- Energy yield calculations for wind turbines and wind farms
- Wind farm wake losses and wind farm efficiency calculations
- Calculation of wind conditions for IEC site assessment like mean wind, turbulence, wind shear, extreme wind and flow inclination
- Siting of wind turbines and wind farms
- Mapping of wind resource and turbulence

Conducting a wind resource assessment with WAsP involves several steps that produce an energy yield from raw wind data. First, an analysis of time-series wind measurements through tools like the Observed Wind Climate (OWC) Wizard and the WAsP Climate Analyst can be undertaken. This will enable standardising the raw data that has been collected with measuring instruments. This analysis generates a statistical summary of the site-specific wind climate, or an observed wind climate. The analysed data can then be converted into a regional wind climate dataset or wind atlas. These wind atlas datasets are standardised and site-independent, as they are adjusted to remove the influence of specific local conditions.

Using these wind atlas datasets, WAsP can estimate the wind climate for any site by factoring in terrain descriptions and performing inverse calculations. Terrain descriptions are added through topographic maps and landcover maps using the WAsP Map editor. WAsP then estimates the total energy content of the mean wind and calculates the annual mean energy production for specific wind turbines using their power curves, the power curves can be created using the WAsP Turbine Editor. Additionally, WAsP evaluates wind farm production by analysing the layout and thrust coefficient curves of turbines, estimating wake losses, and determining the net annual energy production for individual turbines and the entire farm. An example workflow is shown in Figure 3.9

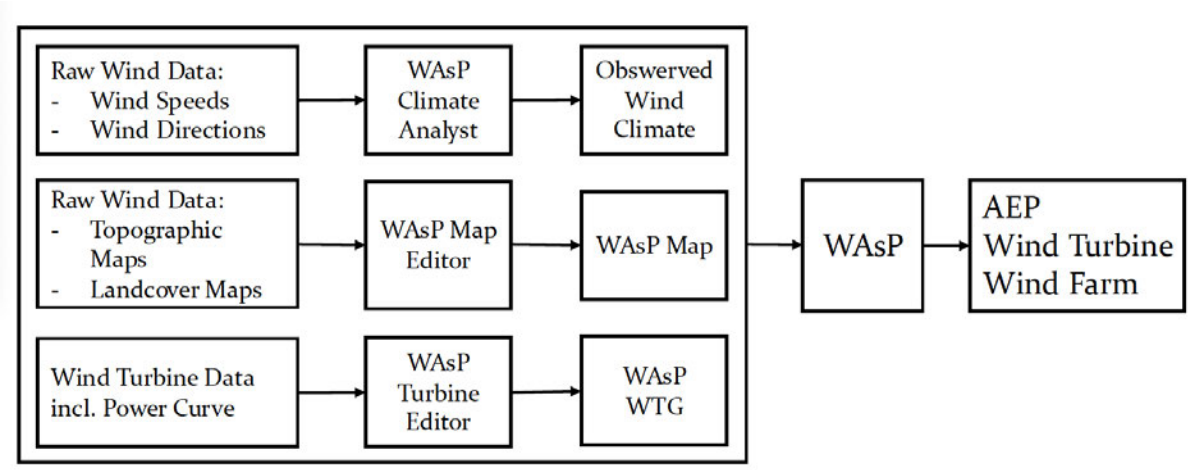

Figure 3.9: WAsP Example Workflow

3.2 Airborne Wind Energy Systems

Airborne Wind Energy Systems (AWES) will be considered for the energy supply of the Neumayer Station III. The implementation of AWES technology is in its early stages, and conducting a comprehensive wind energy resource assessment for these systems presents greater complexity compared to wind turbines as the available tools are not as adaptable and implementable like wind energy assessment tools for wind turbines. In this section, the fundamentals of AWES energy calculations will be presented. The information and the equations presented are based on the book 'Airborne Wind Energy' edited by Uwe Ahrens, Moritz Diehl and Roland Schmehl - [58].

The energy generated by an AWES results from crosswind wind power, which arises due to the aerodynamic lift force, F_L, of an airfoil, which increases with the square of the apparent airspeed, v_a, at the wing [58]. The equation for the aerodynamic lift force is shown below, where ρ represents the air density, A is the airfoil area, and C_L denotes the lift coefficient, which is dependent on the airfoil's geometry.

$$F_L = \frac{1}{2}\rho A C_L v_a^2 \tag{3.36}$$

The power P generated by a tethered airfoil operating either in drag or lift mode under idealised assumptions [58] is given by Equation 3.37 where A is the wing area, C_L is the lift coefficient, C_D is the drag coefficient, and v_w is the wind speed [58]. The lift-to-drag ratio, $\frac{C_L}{C_D}$, is a key characteristic of wings used in crosswind AWES.

$$P = \frac{2}{27}\rho A v_w^3 C_L \left(\frac{C_L}{C_D}\right)^2 \tag{3.37}$$

The power extraction formula assuming a constant wind field with speed v_w is given by Equation 3.38, where F_a is the aerodynamic force experienced by the wing and γ is the angle between the direction of the aerodynamic force and the wind direction [58]. To calculate the aerodynamic force, drag forces by the wing, tether, and an energy generation turbine must be accounted for. The drag force can be described with Equation 3.40, where C_D is the combined drag coefficient of wing and tether. An extra drag force with coefficient $C_{D,\text{Power}}$ results as an example from an energy generating turbine. The resulting equation for F_a can then be calculated in Equation 3.40. The resultant total aerodynamic force coefficient is abbreviated as C_R: Equation 3.41.

$$P_{\text{wind}} = v_w F_a \cos\gamma \tag{3.38}$$

$$F_D = \frac{1}{2}\rho A C_D v_a^2 \tag{3.39}$$

$$F_a = \frac{1}{2}\rho A v_a^2 \sqrt{C_L^2 + (C_D + C_{D,\text{power}})^2} \tag{3.40}$$

$$C_R = \sqrt{C_L^2 + (C_D + C_{D,\text{power}})^2} \tag{3.41}$$

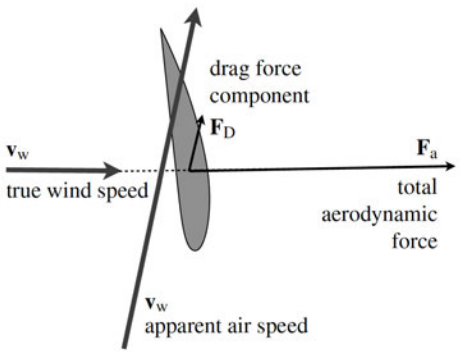

Figure 3.10: Relevant speeds and forces around a wing for wind power generation. [58]

There are multiple applications and concepts of AWESs, the focus will be on ground-based power generation AWESs as one of these systems will be considered later. Ground-based power generation uses the tether tension from fast-flying tethered wings to drive an electric generator via a rotating drum placed on the ground [58]. This method involves two phases: a reel-out phase for power production, and a reel-in phase where the tether is retracted with minimal energy by altering the wing's flight pattern to reduce lift. This cyclical process, often referred to as pumping or Yo-Yo mode, can achieve high efficiency when combined with crosswind motion. Figure 3.11 shows an example of a pumping configuration AWES. The system needed to control a single kite, is denoted as Kite Steering Unit (KSU) [47], the KSU is fixed to the ground, and electrical energy is generated through a continuous two-phase cycle. During the traction phase, the kite flies rapidly in a crosswind direction, following "figure-eight" trajectories that produce high traction forces to unreel the tethers. In this phase, the electric drives function as generators, powered by the rotation of the drums. Once the tether reaches its maximum length, the passive phase begins, during which the drives operate as motors, utilising a small portion of the previously generated energy to reel in the tethers and reposition the kite for the next traction phase [47].

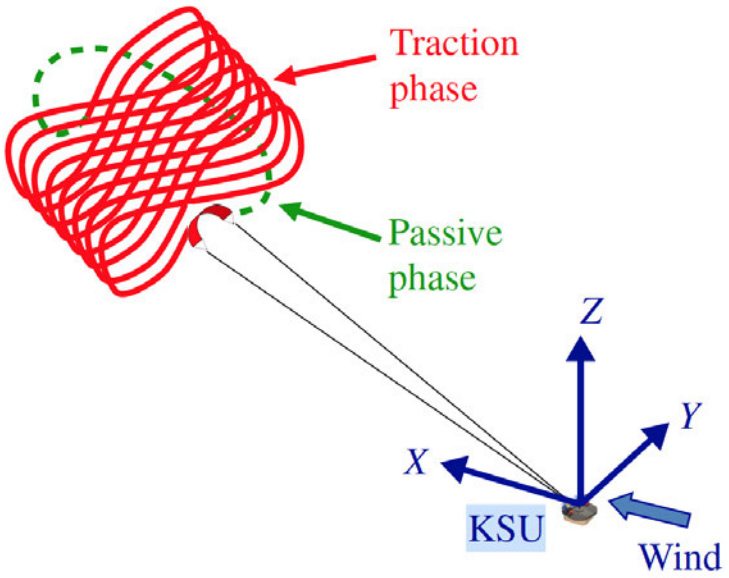

Figure 3.11: Pumping cycle AWES representation [47]

3.2.1 Energy of Pumping Cycle AWES

For a kite flying crosswind in a pumping cycle, the crosswind speed $v_{k,c}$ is proportional to the lift-to-drag ratio (C_L/C_D) of the wing, making it significantly higher than the ambient wind speed v_w [42]. The reel-out speed v_{out} of the tether during the traction phase reduces both the kite's speed and the apparent wind speed v_a, which is approximately equal to

$v_{k,c}$. For high lift-to-drag ratios, the apparent wind speed is given by:

$$v_a \simeq v_{k,c} = (v_w - v_{\text{out}})\frac{C_L}{C_D} \tag{3.42}$$

The tether force T, for large C_L/C_D ratios, is approximately equal to the lift force L, and is expressed as:

$$T \simeq L = \frac{1}{2}\rho v_a^2 A C_L \tag{3.43}$$

The mechanical power P generated during the reel-out phase is the product of the tether force T and the reel-out speed v_{out}:

$$P = T v_{\text{out}} \tag{3.44}$$

The optimal reel-out speed $v_{\text{out,opt}}$, which maximises mechanical power, is given by:

$$v_{\text{out,opt}} = \frac{1}{3}v_w \tag{3.45}$$

The maximum mechanical power produced during the traction phase is:

$$P = \frac{1}{2}\rho v_w^3 A \frac{4}{27}\frac{C_L^3}{C_D^2} \tag{3.46}$$

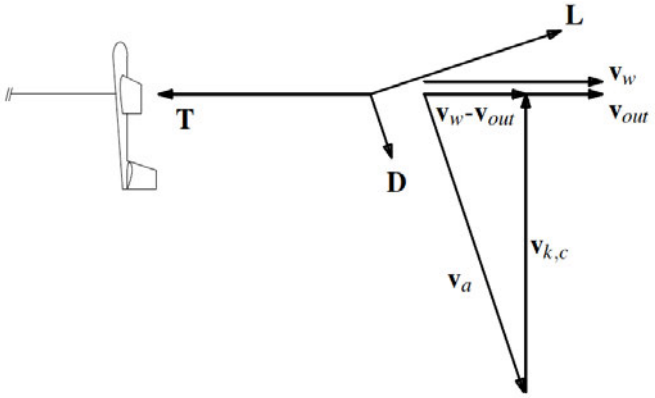

Figure 3.12: Forces and velocities of a kite flying crosswind [42]

The analysis presented does not account for the retraction phase discussed earlier. The cycle power has to be accounted for to calculate an AEP that will later be important for the wind energy assessment for a selected AWES. To account for the losses that occur do to the retraction phases, the maximum power production is considered and then the limiting forces are added.

As previously presented, a full pumping cycle includes a traction (reel-out) phase and a retraction (reel-in) phase. The reel-out speed v_{out} and the reel-in speed v_{in} that maximise

the average mechanical power P_c over one complete pumping cycle are needed [42]. Using the dimensionless factor γ_{out}, defined as $\gamma_{\text{out}} = \frac{v_{\text{out}}}{v_w}$, the tether force during the traction phase can be expressed as:

$$T_{\text{out}} = \frac{1}{2}\rho v_w^2 A(1-\gamma_{\text{out}})^2 F_{\text{out}} \tag{3.47}$$

Here, the dimensionless force factor F_{out} is given by:

$$F_{\text{out}} = \frac{C_L^3}{C_D^2} \tag{3.48}$$

Similarly, the tether force during the retraction phase can be expressed in terms of the dimensionless factor γ_{in}, where $\gamma_{\text{in}} = \frac{v_{\text{in}}}{v_w}$, as follows:

$$T_{\text{in}} = \frac{1}{2}\rho v_w^2 A(1+\gamma_{\text{in}})^2 F_{\text{in}} \tag{3.49}$$

In a pumping cycle kite power system, the reel-in phase is characterised by a dimensionless force factor F_{in}, which ideally equals the drag coefficient C_D of the kite [42]. However, in practice, F_{in} depends on the minimal tether force required to reel in the kite in a controlled way, which can exceed the drag force.

During one power cycle, where the tether length changes by l_c, the energy produced per cycle E_c is determined by the difference in tether forces between the traction and retraction phases [42], as shown in Eq. 3.50. The duration of the cycle t_c, expressed in terms of the reel-out speed γ_{out} and reel-in speed γ_{in}, is given in Eq. 3.51. The average power per cycle P_c, defined as the energy produced divided by the cycle duration, is given in Eq. 3.52 [42]. This value is normalised using the wind power density P_w (Eq. 3.53), leading to a normalised power factor f_c (Eq. 3.54). For maximal power output, reeling in should occur with minimal resistance ($F_{\text{in}} = 0$) and infinite reel-in speed ($\gamma_{\text{in}} \to \infty$), which results in the maximum normalised power factor $f_c^{\max}$, as shown in Eq. 3.55.

$$E_c = (T_{\text{out}} - T_{\text{in}})l_c = \frac{1}{2}\rho v_w^2 A\left[(1-\gamma_{\text{out}})^2 F_{\text{out}} - (1+\gamma_{\text{in}})^2 F_{\text{in}}\right] l_c \tag{3.50}$$

$$t_c = \frac{l_c}{v_{\text{out}}} + \frac{l_c}{v_{\text{in}}} = \frac{l_c}{v_w}\left(\frac{\gamma_{\text{out}}\gamma_{\text{in}}}{\gamma_{\text{out}}+\gamma_{\text{in}}}\right) \tag{3.51}$$

$$P_c = \frac{E_c}{t_c} = P_w A\left[F_{\text{out}}(1-\gamma_{\text{out}})^2 - F_{\text{in}}(1+\gamma_{\text{in}})^2\right]\left(\frac{\gamma_{\text{out}}\gamma_{\text{in}}}{\gamma_{\text{out}}+\gamma_{\text{in}}}\right) \tag{3.52}$$

$$P_w = \frac{1}{2}\rho v_w^3 \tag{3.53}$$

$$f_c = \frac{P_c}{P_w A F_{\text{out}}} = \left[(1-\gamma_{\text{out}})^2 - \frac{F_{\text{in}}}{F_{\text{out}}}(1+\gamma_{\text{in}})^2\right]\left(\frac{\gamma_{\text{out}}\gamma_{\text{in}}}{\gamma_{\text{out}}+\gamma_{\text{in}}}\right) \tag{3.54}$$

$$f_c^{\max} = \max_{\gamma_{\text{out}}} \left\{ \frac{P_c}{P_w A F_{\text{out}}} \right\} = \frac{4}{27} \tag{3.55}$$

The numerical results for the maximal cycle power of a pumping kite system are derived for general force factors F_{out} and F_{in}, where $F_{\text{out}}, F_{\text{in}} > 0$ [42]. The normalised power factor f_c is expressed as the maximum over the dimensionless reel-out and reel-in speeds (γ_{out} and γ_{in}):

$$f_c = \max_{\gamma_{\text{out}}, \gamma_{\text{in}}} \left\{ \left((1 - \gamma_{\text{out}})^2 - \frac{F_{\text{in}}}{F_{\text{out}}} (1 + \gamma_{\text{in}})^2 \right) \left(\frac{\gamma_{\text{out}} \gamma_{\text{in}}}{\gamma_{\text{out}} + \gamma_{\text{in}}} \right) \right\} \tag{3.56}$$

Now that the optimal reel in and reel out speed have been determined the power has to be limited: The optimal reel-out and reel-in speeds are typically independent of the wind speed [42]. However, at a certain wind speed v_n, referred to as the nominal wind speed, the kite power system reaches its nominal power P_{out}^n. Beyond v_n, both the tether force and reel-out power cannot increase further and must be maintained at constant values. This constraint ensures the system operates safely at higher wind speeds. Due to this limitation, the reel-out speed (Eq. 3.57) must also remain constant, while the reel-in speed can still be optimized.

For wind speeds $v_w \leq v_n$, the dimensionless reel-out and reel-in speeds (γ_{out}^n and γ_{in}^n) are independent of v_w and defined as in Eq. 3.57, Eq. 3.58, and Eq. 3.59 [42].

For wind speeds $v_w > v_n$, the power produced and cycle duration can be calculated using the procedure outlined in earlier equations. The energy produced per cycle (E_c), the cycle duration (t_c) and the average power (P_c) are given by Eq. 3.60, Eq. 3.61 and Eq. 3.62, respectively, while power factor $f_{c,\mu}$ is expressed in Eq. 3.63.

To characterize the behavior at higher wind speeds, the dimensionless velocity parameter μ is introduced (Eq. 3.64) [42]. When $\mu > 1$, the tether force and power in the traction phase are kept constant by adjusting F_{out}, typically by reducing the lift coefficient C_L, as described in Eq. 3.65.

$$v_{\text{out}}^n = \gamma_{\text{out}}^n v_n \tag{3.57}$$

$$T_{\text{out}}^n = \frac{1}{2} \rho v_n^2 A (1 - \gamma_{\text{out}}^n)^2 F_{\text{out}} \tag{3.58}$$

$$P_{\text{out}}^n = T_{\text{out}}^n v_{\text{out}}^n \tag{3.59}$$

$$E_c = (T_{\text{out}}^n - T_{\text{in}}) l_c \tag{3.60}$$

$$t_c = \frac{l_c}{v_{\text{out}}} + \frac{l_c}{v_{\text{in}}} \tag{3.61}$$

$$P_c = \frac{E_c}{t_c} = P_w \max_{\gamma_{\text{in}}} \left\{ \frac{1}{\mu^2}(1-\gamma_{\text{out}}^n)^2 - \frac{F_{\text{in}}}{F_{\text{out}}}(1+\gamma_{\text{in}})^2 \right\} \tag{3.62}$$

$$\frac{P_c}{P_w A F_{out}} = f_{c,\mu} = \max_{\gamma_{in}} \left\{ \left(\frac{1}{\mu^2}(1-\gamma_{out}^n)^2 - \frac{F_{in}}{F_{out}}(1+\gamma_{in})^2 \right) \left(\frac{\gamma_{out}^n \gamma_{in}}{\gamma_{out}^n + \mu\gamma_{in}} \right) \right\} \tag{3.63}$$

$$\mu = \frac{v_w}{v_n} \tag{3.64}$$

$$F_{\text{out},\mu} = \frac{F_{\text{out}}}{\mu^2} \frac{(1-\gamma_{\text{out}}^n)^2}{(1-\gamma_{\text{out}}^n/\mu)^2}, \quad \gamma_{\text{out}} = \frac{\gamma_{\text{out}}^n}{\mu} \tag{3.65}$$

The average mechanical power over one cycle of the pumping kite power system, at a given wind speed v_w, is defined within the range $0 \leq v_w \leq v_n$, where v_n is the nominal wind speed. This power curve depends on the dimensionless reel-out and reel-in speeds (γ_{out} and γ_{in}), as well as the tether forces during the reel-out (F_{out}) and reel-in (F_{in}) phases. The normalized average power $\frac{P_c}{AF_{\text{out}}}$ is expressed as:

$$\frac{P_c}{AF_{\text{out}}} = P_w \max_{\gamma_{\text{out}},\gamma_{\text{in}}} \left\{ \left((1-\gamma_{\text{out}})^2 - \frac{F_{\text{in}}}{F_{\text{out}}}(1+\gamma_{\text{in}})^2 \right) \left(\frac{\gamma_{\text{out}}\gamma_{\text{in}}}{\gamma_{\text{out}}+\gamma_{\text{in}}} \right) \right\} \tag{3.66}$$

This equation captures the optimisation of power generation by balancing the reel-out and reel-in speeds and accounting for the efficiency factors of the system [42].

The normalized average mechanical power for wind speeds $v_n < v_w$ is calculated using Eq. 3.67, which accounts for the effect of increasing wind speed on the reel-in phase [42].

$$\frac{P_c}{P_w A F_{\text{out}}} = P_w \max_{\gamma_{\text{in}}} \left\{ \left(\frac{1}{\mu^2}(1-\gamma_{\text{out}}^n)^2 - \frac{F_{\text{in}}}{F_{\text{out}}}(1+\gamma_{\text{in}})^2 \right) \left(\frac{\gamma_{\text{out}}^n \gamma_{\text{in}}}{\gamma_{\text{out}}^n + \mu\gamma_{\text{in}}} \right) \right\} \tag{3.67}$$

To limit the tether force to a nominal value for $v_w > v_n$ the reel-out speed is increased above its optimal value[42]. For wind speeds $v_w > v_n$, the nominal tether force T_{out}^n can be used to determine the reel-out speed. The tether force is given by Eq. 3.68 and remains constant. Using this, the reel-out speed ratio γ_{out} and the reel-out speed v_{out} can be calculated, as shown in Eq. 3.69 and Eq. 3.70. The reel-out power P_{out} is then determined by Eq. 3.71.

The energy produced per cycle (E_c), cycle duration (t_c), and average power (P_c) can be calculated using Eq. 3.72, Eq. 3.73, and Eq. 3.74, respectively.

The normalized average power $\frac{P_c}{P_w A F_{\text{out}}}$ incorporates the relationship between γ_{out}, γ_{in}, and μ (the dimensionless velocity parameter) [42]. This is shown in Eq. 3.75. For wind speeds $v_w > v_n$, P_{out} increases linearly with wind speed, while P_c increases more slowly, reaching a maximum before declining for very high wind speeds.

$$T_{\text{out}}^n = \frac{1}{2}\rho v_n^2 A(1-\gamma_{\text{out}}^n)^2 F_{\text{out}} = \frac{1}{2}\rho v_w^2 A(1-\gamma_{\text{out}})^2 F_{\text{out}} = \text{const.} \tag{3.68}$$

$$\gamma_{\text{out}} = 1 - \frac{1-\gamma_{\text{out}}^n}{\mu} \tag{3.69}$$

$$v_{\text{out}} = v_w - v_n + \gamma_{\text{out}}^n v_n \tag{3.70}$$

$$P_{\text{out}} = T_{\text{out}}^n v_{\text{out}} \tag{3.71}$$

$$E_c = (T_{\text{out}}^n - T_{\text{in}}) l_c \tag{3.72}$$

$$t_c = \frac{l_c}{v_{\text{out}}} + \frac{l_c}{v_{\text{in}}} \tag{3.73}$$

$$P_c = \frac{E_c}{t_c} \tag{3.74}$$

$$\frac{P_c}{P_w A F_{\text{out}}} = \max_{\gamma_{\text{in}}} \left\{ \left(\frac{1}{\mu^2}(1-\gamma_{\text{out}}^n)^2 - \frac{F_{\text{in}}}{F_{\text{out}}}(1+\gamma_{\text{in}})^2 \right) \frac{\gamma_{\text{in}}(\mu - 1 + \gamma_{\text{out}}^n)}{\mu\gamma_{\text{in}} + \mu - 1 + \gamma_{\text{out}}^n} \right\} \tag{3.75}$$

A three-phase strategy for pumping kite power systems divides the wind spectrum into three distinct phases based on wind speed [42]. At low wind speeds ($v_w \leq v_{n,T}$), there are no constraints on tether force or generator power. At medium wind speeds ($v_{n,T} < v_w \leq v_{n,P}$), the tether force is limited by a higher reel-out speed while the power limit is not yet reached. For high wind speeds ($v_w > v_{n,P}$), both the tether force and power limits are reached. This strategy allows for optimised performance across varying wind conditions by adjusting operational parameters accordingly.

3.2.2 Annual Energy Production of Pumping Cycle AWES

Now that the groundwork has been laid for AWES energy principles and calculations, a calculation of the annual energy production is possible. The AEP for AWES follows similar principles as the the AEP calculation for wind turbines. To account for wind speed variations a probability distribution using the Weibull probability density function is used as mentioned previously (Equation 3.76). The average wind speed $\overline{U}$ is given by Equation 3.77.

$$p(U) = \left(\frac{k}{c}\right)\left(\frac{U}{c}\right)^{k-1} \exp\left[-\left(\frac{U}{c}\right)^k\right] \tag{3.76}$$

$$\overline{U} = \int_0^\infty U p(U) dU = c\Gamma\left(1 + \frac{1}{k}\right) \tag{3.77}$$

For a pumping kite power system, the annual average power P_{av} can be calculated by integrating the product of the power curve P_c, the wind speed distribution $p(U)$, and efficiency factors over the range of wind speeds. This integration, shown in Eq. 3.78, includes contributions from two phases: (1) wind speeds below the nominal wind speed v_n, and (2) wind speeds above v_n but below the cut-out speed v_{cut}, beyond which power production ceases [42]. The efficiency factors f_c and $f_{c,\mu}$ are derived from previous equations.

$$P_{\text{av}} = \int_0^{v_n} P_w A F_{\text{out}} f_c p(U) dU + \int_{v_n}^{v_{\text{cut}}} P_w A F_{\text{out}} f_{c,\mu} p(U) dU \tag{3.78}$$

The annual mechanical energy produced by the kite power system can be determined as the product of the average cycle power P_{av} and the total number of hours in a year. This relationship is expressed in Eq. 3.79:

$$AEP = P_{\text{av}} \cdot 8760 \quad [\text{kWh}] \tag{3.79}$$

The explanations in this section regarding the energy production of AWES should function as a basis to understand the energy production of AWES. However, an easier approach can be used, if the power curve of an AWES is available, that accounts for cycle losses. In Chapter 4, the implementation of the AEP Calculation for a selected AWES will be executed using available power curves from the manufacturers where the cycle losses have already been accounted for. Assuming that the power curve is available and that therefore the three phase strategy is not relevant anymore and since $f_c = \frac{P_c}{P_w \cdot A \cdot F_{\text{out}}}$ Equation 3.78 can be simplified to:

$$P_{\text{av}} = \int_{v_{\text{in}}}^{v_{\text{cut}}} P_c \cdot p(U)\, dU \tag{3.80}$$

Where P_c is the cycle power obtained from the power curve, and $p(U)$ represents the wind speed distribution.

Chapter 4

Methodology

The set objective of evaluating the potential of new wind energy systems for the NMS-III will be implemented in this chapter. A wind resource assessment will be conducted, requiring the selection of a wind energy system to estimate the annual energy production (AEP). The aim is to replace approximately 30% of the current energy demand, presently met by diesel fuel (2645.8 MWh/a) [7], with energy generated by wind turbines. For the AWES, emphasis will be placed on power generation using a single device, as this technology has not been implemented in Antarctica or on a large scale globally. The wind assessment for the selected wind turbine will be performed using WAsP, while the AWES assessment will employ a MATLAB-based code developed from the equations presented in Chapter 3. Wind measurement data will be filtered and prepared for import into WAsP, and topographical inputs will be accounted for by creating and formatting a map for WAsP compatibility. Additionally, the technical specifications of the selected wind turbine will be prepared for import into WAsP to facilitate the analysis.

4.1 Picking a Wind Energy System

As previously discussed in Chapter 2, research stations in Antartica use a wide range of wind turbines including small-scale wind turbines and large-scale wind turbines. For the further wind assessment in this Thesis, the choice of a wind energy system plays a significant role as it affects the energy output, efficiency and economic feasibility. Picking a wind system is in addition challenging in the context of this Thesis, as the environment of Antarctica is challenging and requires additional specifications to withstand the harsh conditions. However, the currently operating wind turbines in Antarctica can be taken into account as a basis for picking a suitable wind turbine as their feasibility has already been proven. This is not the case with Airborne Wind Systems as airborne energy technology is a relatively new technology that is still in development. Nevertheless, an AWES will be picked to get an idea of how much energy an AWES could produce if

installed.

4.1.1 Selected Wind Turbine

To pick a wind turbine a requirement analysis is crucial to determine what wind turbine is best suited for the installation. Multiple manufacturers offer wind turbines specifically engineered for use in cold climate environments. For the sake of providing a feasible and validated wind turbine, the focus will be more on wind turbine models that have already been used in Antarctica.
The dutch wind turbine manufacturer EWT will be supplying 3 wind turbines from the type DW54X-1MW to the Ross Island wind farm by the end of 2024 [23]. On the other hand, the Scottish manufacturer SD Wind Energy Limited has 9 wind turbines installed in Antarctica from the model SD6 [20]. The SD6 wind turbine is a small-scale wind turbine with a rated power of 6 kW. The company also has another model that comes with a cold-climate option that could produce up to 9 kW called SD6+. The SD6+ model is similar in design of the SD6 Model, but can produce more power in higher speeds due to an additional copper winding included in the generator [21]. The American wind turbine manufacturer Bergey Windpower Company also offers wind turbines that can withstand cold climate conditions like the model BWC Excel 10 [12]. The BWC Excel 10 has a rated power of 8.9 kW and can withstand temperatures to -40°C. The BWC Excel 10 has not been however installed in Antarctica. The german wind turbine manufacturer superwind GmbH produces small-scale wind turbines that are engineered to withstand harsh weather conditions [63]. The company offers relatively low rated power wind turbines like the SW-353 model with a rated power of 350 W and the SW-1250 model with a rated power of 1250 W.
Vertical wind turbines have also been used in Antarctica as discussed in Chapter 2. The vertical wind turbine used is from the company Oy Windside Production Ltd. and has a rated power of 0.15 kW which is very low for the needed power by the NMS-III. The same manufacturer offers another model that has a rated power of 12 kW that could be considered for use at the Neumayer Station III. Table 4.1 shows an overview of the discussed candidates.

Wind Turbine	DW54X-1MW	SW-1250	SW-353	Excel-10	SD-6	SD6+	WS-12
Manufacturer	EWT	supwewind GmbH	superwind GmbH	Bergey Windpower Co.	SD Wind Energy	SD Wind Energy	Oy Windside Production Ltd.
Power Rating [kW]	1000	0.125	0.350	10	5.2	6	12
Range [m/s]	3-25	3.5-35	3.5-35	3.4-60	2.5-70	2.5-70	2-60
Rotor Diameter [m]	52	2.4	1.2	7	5.6	5.6	-
Pitch	Active	Active	Active	Fixed	Fixed	Fixed	Fixed
Generator	DD-PMG	DD-PMG	DD-PMG	DD-PMG	Brushless DD-PMG	Brushless DD-PMG	Custom
Tower	Type Conical tubular steel, internal ascent	Custom	Custom	Custom	Taperfit Monopole	Taperfit Monopole	Custom
Price [€]	1.3M - Estimate	8,000.00	3,000.00	61,334.44	40,000.00	43,000.00	-

Table 4.1: Proposed Wind Turbines [48, 11, 13, 21, 22, 63, 23, 12, 39]

To make sure the best suitable wind turbine is picked an evaluation matrix will be created. Each criteria has a score of 1-5 with 5 being the highest score. The wind turbine with the highest overall score will be picked for further investigations. The criteria will include the following:

- Power: As previously discussed, the aim in this Thesis is to replace a big portion of the current energy supply with wind energy alternatives. Wind Turbines that have a low power rating will score less as too many wind turbines will increase the possibility of maintenance works.
- Durability: The chosen wind turbine needs to have parts that can withstand the harsh weather conditions of Antarctica including high wind speeds.
- Cold Climate: This criteria is to differentiate wind turbines that have been engineered to withstand cold weather conditions.
- Off-Grid: Wind turbines that can be easily installed without the need of a network would score higher.
- Installation: This criteria is meant is to quantify the difficulty of installing a specific wind turbine. The bigger the wind turbine, the lower its score will be.
- Maintenance: This criteria is meant to quantify how often a wind turbine would need maintenance and how difficult a maintenance campaign implementation would be if needed. Larger wind turbines and turbines with break down history in Antarctica would score lower.
- Cost: The capital cost of a wind turbine would be divided by the power ratings to examine the cost in relation to the power produced. The lower the number is, the higher the score.

- Replicability: Wind turbines that have already been used in Antarctica would score higher.

The evaluation matrix is shown in Figure 4.1.

Wind Turbine \ Criteria	Power	Durability	Cold Climate	Off-Grid	Installation	Cost	Maintenance	Replicability	**Total**	**Ranking**
SD-6+	3	3	5	5	5	4	5	5	35	1
SD-6	2	3	5	5	5	4	5	5	34	2
WS-12	3	2	4	5	4	5	5	5	33	3
SW-353	1	5	5	5	5	1	5	5	32	4
SW-1250	1	5	5	5	5	1	5	5	32	4
Excel 10	3	3	2	5	4	5	5	1	28	5
DW-54X-1MW	5	5	5	1	1	5	1	5	28	5

Figure 4.1: Evaluation Matrix - Wind Turbines

The DW-54X-1MW wind turbine would present multiple challenges operationally and logistically due to its size. The Excel 10 wind turbine has not been used in Antarctica yet and doesn't qualify for the further investigations in this thesis. The wind turbines from the company superwind GmbH are the easiest to transport but have relatively low power ratings and are more expensive compared other wind turbines with similar power ratings. This narrows down the choice to the wind turbines SD6 and SD6+. The SD6 wind turbine has been used in Antarctica with no reports of break outs. It's also not difficult to transport compared to the DW-54X-1MW wind turbine and is a fair economical choice as the price is similar to other small-scale wind turbines with similar power ratings. The updated model of the SD-6 also has a cold-climate option and a higher power rating, The SD6+ is as a result the chosen wind turbine to be further investigated in this Thesis.

The SD6+ Wind Turbine

The SD6+ wind turbine (Figure 4.2) is a 6 kW turbine capable of achieving up to 9 kW under high wind conditions [21]. It can be installed on towers of varying heights—9 m, 15 m, or 20 m—using either a gin pole or hydraulic tower configuration. These towers can be anchored on fixed concrete foundations or above-ground bases, depending on site requirements [21]. The SD6+ turbine adheres to the SD6 wind turbine power curve under standard wind conditions but exhibits an increase in power output at higher wind speeds [21]. This enhanced performance is attributed to the inclusion of additional copper windings in the generator. Structurally and mechanically, the SD6+ shares the

same design as the original SD6 model [21]. The wind turbine specifications are listed in Table 4.2

Figure 4.2: SD6+ [22]

Specification	**Details**
Peak Power	6 kW @ 11 m/s
Applications	Agricultural, Domestic, Remote Islands, Utility
Solutions	Grid Tied & Battery Charge, 48 V, 300 V
Architecture	Downwind, 3-Bladed, Self-Regulating
Rotor	5.6 m Diameter
Blade Material	Glass Thermoplastic Composite
Generator	Brushless Direct Drive Permanent Magnet
Tower Options	9 m / 15 m / 20 m Taperfit Monopole - Hydraulic or Gin Pole
Tower Specification	Class 1 Rated / Galvanised Steel
Foundation Options	Pad / Root / Rock Anchor
Cut-In Speed	2.5 m/s
Cut-Out Speed	None - Continuous Operation
Survival Wind Speed	Designed to Class 1 (70 m/s)
Warranty	5 Years
Cold Climate Options	Available on Request
Colour Options	Light Grey (RAL7035), Black (RAL9005)

Table 4.2: SD6+ Wind Turbine Specification [21]

The power curve of the selected wind turbine is an important input for the wind assessment. The power curve extracted from the manufacturer's data [21] is shown in Figure 4.3

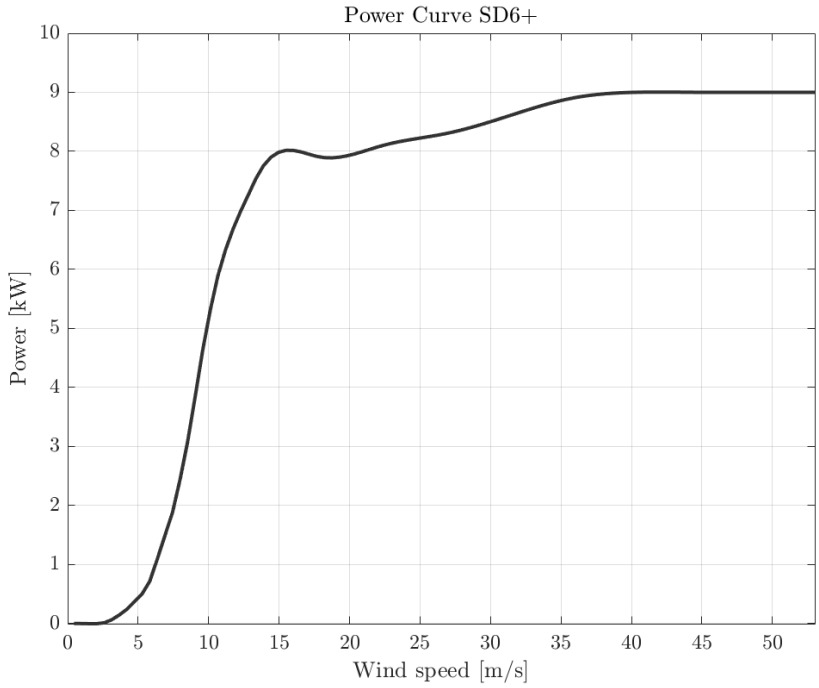

Figure 4.3: SD6+: Power Curve

4.1.2 Selected AWES

Unlike wind turbines, airborne wind energy projects are not as abundant. This leads to difficulties in finding sufficient information that describe characteristics of the systems. As an example, a power curve that accounts for cycle losses is beneficial for the AEP calculations of a selected AWES. The AWES manufacturer Kitepower has published a system with sufficient information for an analysis and their AWES is therefore selected as candidates for the energy supply of the NMS-III.

Kitepower: Falcon

The Dutch company Kitepower specialises in the production of Airborne Wind Energy Systems. The company's model Falcon is a pumping cycle AWES and has a maximum rated power of 100 kW and can produce up to 450 MWh a year [35]. The system is visualised in Figure 4.4: The system's components include a ground station(1), a tether (2), a KCU (3) and the kite (4).

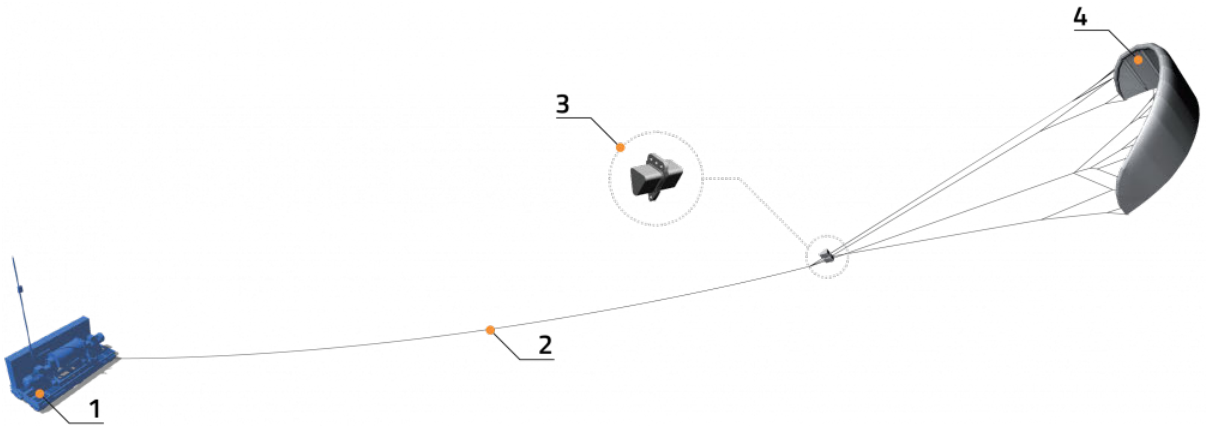

Figure 4.4: Kitepower Falcon AWES [61]

The kite consists of an inflatable and fixed fibre-glass skeleton, making it light and durable at the same time [35]. The Tether connects all the components and is made from a lightweight but strong material [35]. The KCU controls the roll, pitch and yaw of the kite and is responsible for the communication between a sensor on the kite and ground station [35]. The ground station converts the mechanical energy of the kite to electrical power and reels the kite in by using the generator as a motor [35]. The space requirements of the Falcon AWES are illustrated in Figure 4.5.

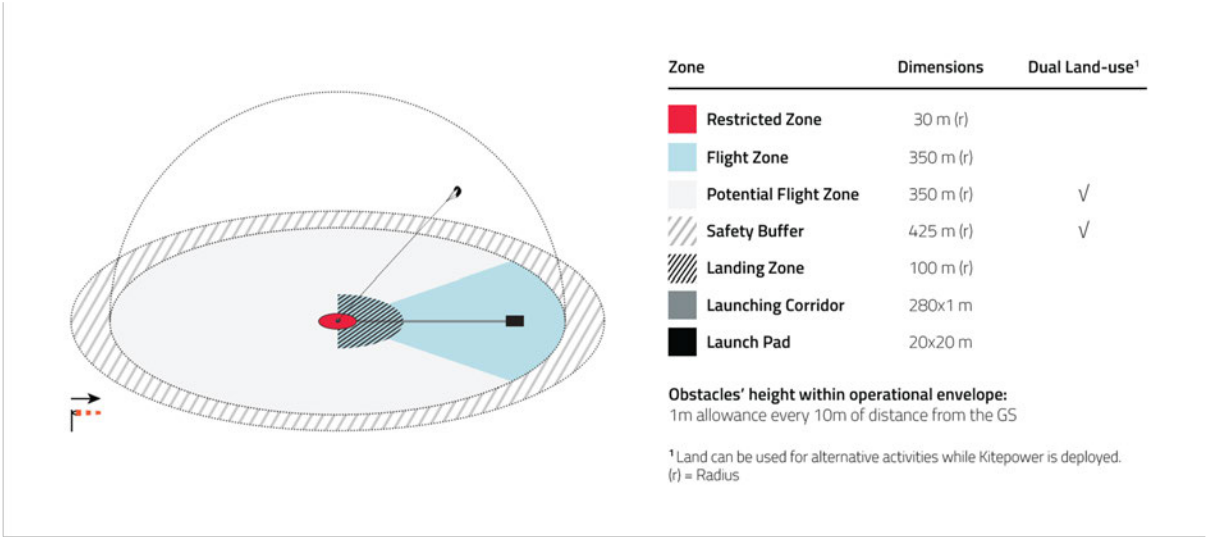

Figure 4.5: Space Requirements Kitepower Falcon [35]

The system has a cycle duration of 100s [35]. Energy production takes up about 80% of the production cycle and the rest is for the retraction phase. A system with the biggest kite variation would produce about 130 kW, of which 20kW will be used up for the retraction phase. The cycle is visualised in Figure 4.6. The AWES power curve extracted from the manufacturer's data is shown in Figure 4.7

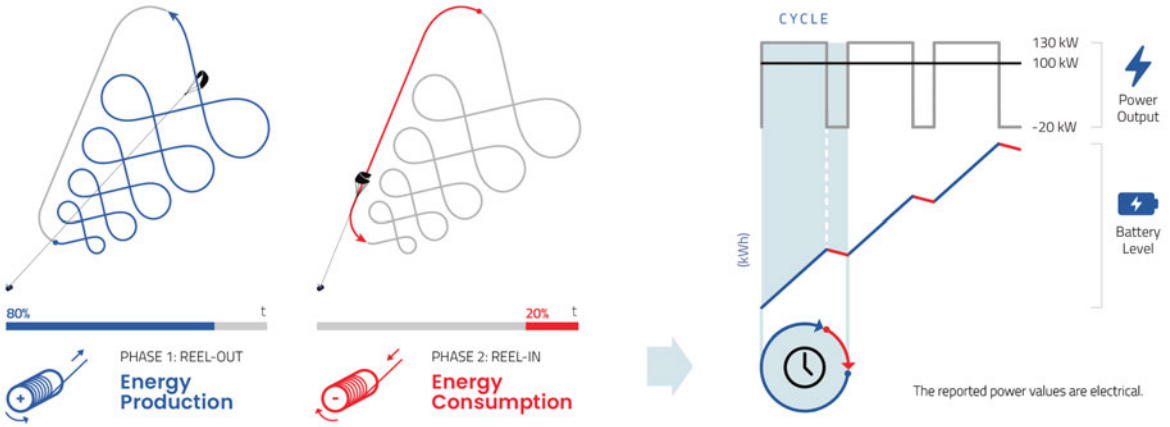

Figure 4.6: Cycle Power - Kitepower Faclon [35]

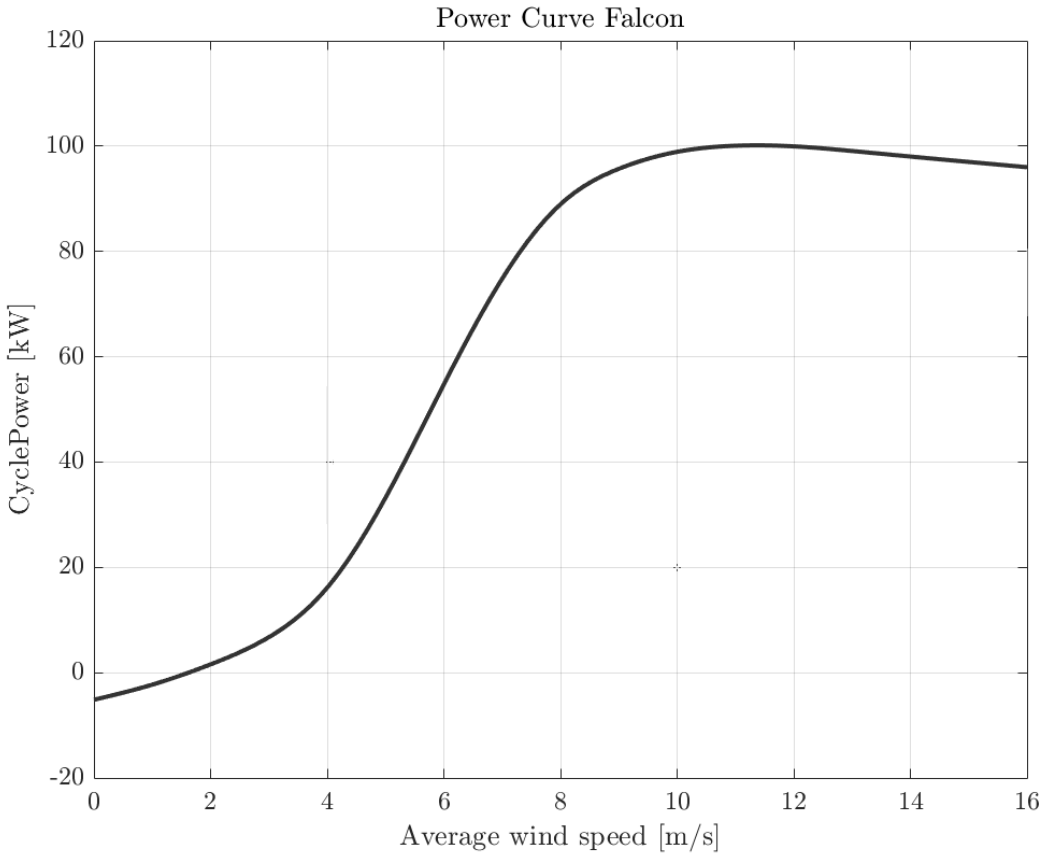

Figure 4.7: Power Curve - Kitepower Faclon [35]

4.2 Wind Resource Assessment Implementation for the selected Wind Turbine using WAsP

4.2.1 Wind Data Analysis

An analysis of wind data is required as presented in Chapter 3. The wind data that will be used for the wind energy assessment is from the Meteorological Observatory Neumayer and is available as a wind data time series. The data has to be prepared before it's imported to the WAsP Climate Analyst. A MATLAB code will be used to prepare the data for the WAsP Climate Analysis tool. The flow chart in Figure 4.8 visualises the filtering process done by the code [1].

The code presented aims to combine all files and to create files that contain the two needed parameters: Wind direction and wind speeds at 10 m height. These values are labeled as DD10 and FF10 in the files. The data covers a large period of time (1982/03 -2022/01). For the wind assessment only data in the time period from March 2016 till January 2022 will be used as this is sufficient for the wind assessment. The recording interval of the data is 60s, making the files too big to be analysed in the WAsP Climate Analysis Tool. The data from the specified time period will be therefore separated into 5 files and imported separately so that the WAsP Climate Analysis tool can analyse the data. Each file contains the time stamp, the wind direction and the wind speeds. The WAsP Climate Analysis Tools filters the data again and looks for inconsistencies in the data. The imported filtered data can then be examined and plotted. Figure 4.9 shows plots of time traces of wind direction and wind speeds and the same data in a polar representation [2].

[1] The code can be found in the Appendix.

[2] Plots for each year from the specified time period can be found in the Appendix.

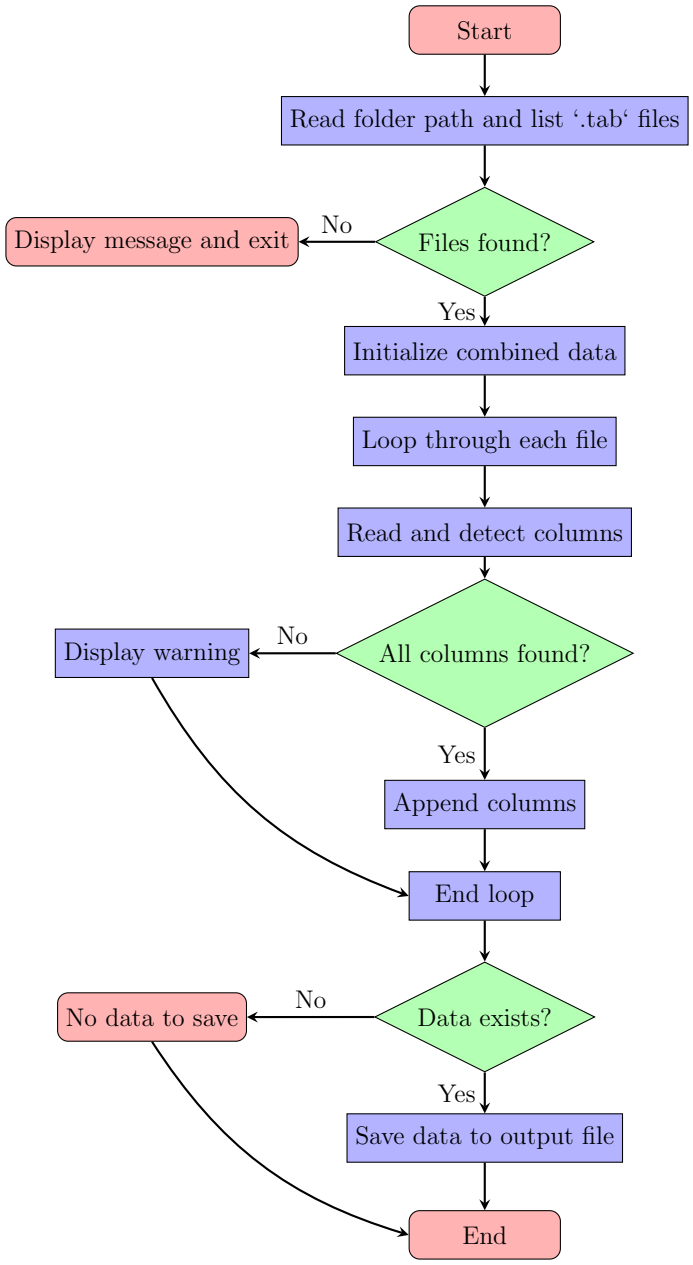

Figure 4.8: Flowchart for MATLAB Function for processing files and extracting columns

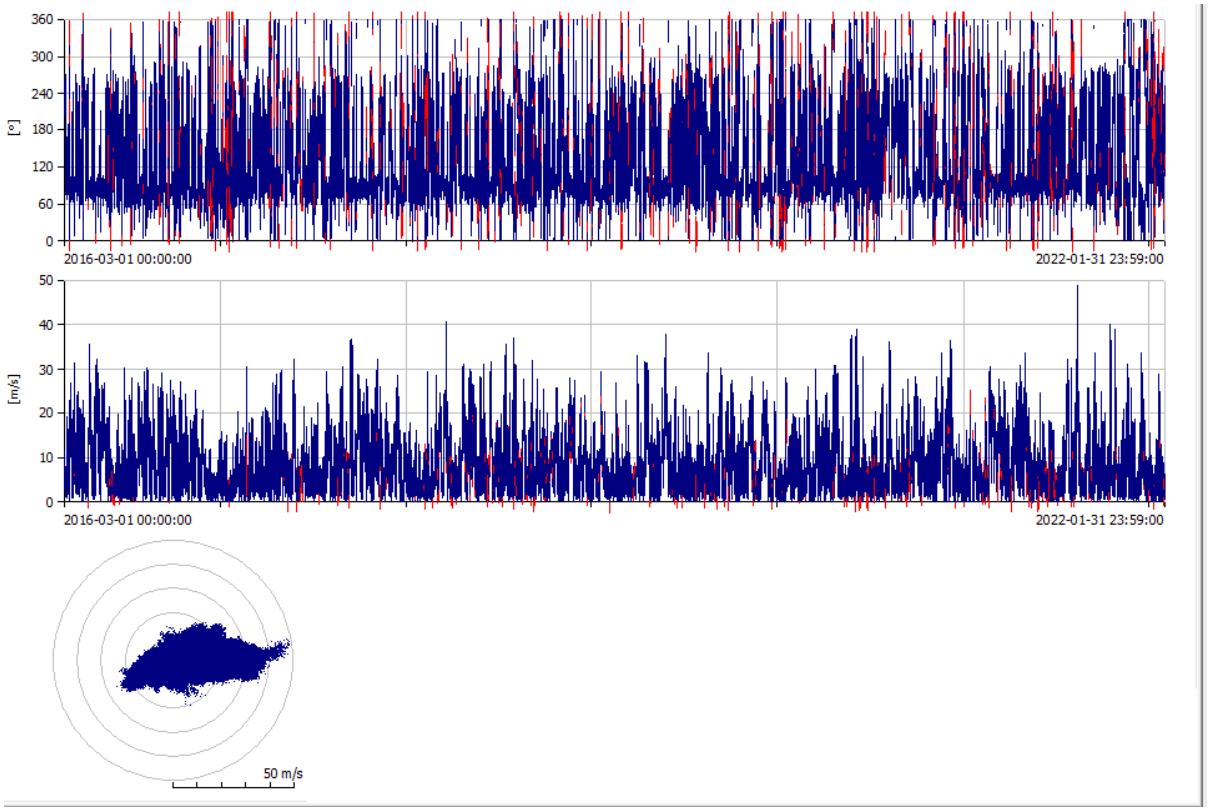

Figure 4.9: WAsP Climate Analyst - Wind Direction and Wind Speeds 2016/03-2022/01

The red points in the plot show areas where the data was not found. This is as an example to see in Figure 4.10 where a zoom to a specific data range shows that data is not available. This is because of gaps in the original data files. The corresponding data snippet of plotted range is shown in Figure 4.11.

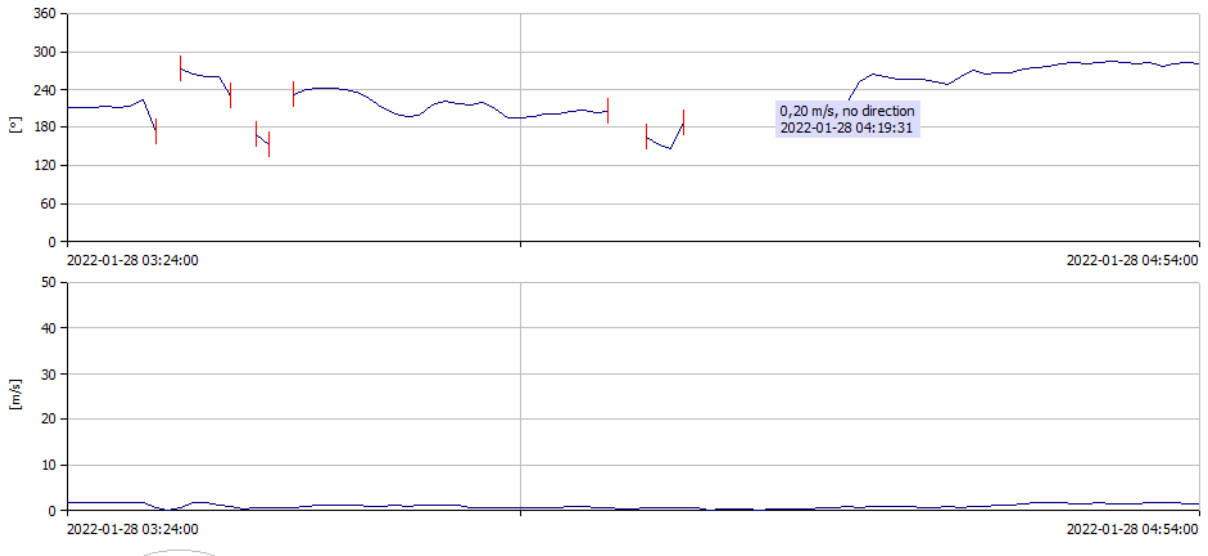

Figure 4.10: WAsP Climate Analyst Plot - Zoomed in to 28/01/2022

Date/Time	SSD	T10	DD10	FF10	T2		DD2	FF2	RH	RH	RH	RH	PoPoPo	PoPoPo+	SWD OG1	SWD RG8	UV rad
2022-01-28T04:14	1	-10.0		0.5	-11.7		0.1	89.8	90.9	82.3	81.2	982.00	982.14	41.0	28.1	3.9	196.9
2022-01-28T04:15	1	-9.9		0.1	-11.6		0.2	89.7	90.6	80.9	80.3	981.97	982.11	40.8	27.9	3.9	197.2
2022-01-28T04:16	1	-9.9		0.2	-11.7		0.5	90.0	91.2	80.3	80.2	981.94	982.08	36.2	24.3	4.0	197.3
2022-01-28T04:17	1	-9.7		0.2	-11.5		0.3	89.7	89.1	79.3	78.9	981.91	982.05	32.1	21.2	4.0	197.4
2022-01-28T04:18	1	-10.0		0.3	-11.6		0.3	89.4	91.2	80.6	80.5	981.90	982.04	27.3	17.4	4.0	197.3
2022-01-28T04:19	1	-9.8		0.1	-11.7		0.1	89.8	91.2	79.5	79.1	981.89	982.03	26.0	16.5	4.1	197.3
2022-01-28T04:20	1	-9.8		0.2	-11.9	326.9	0.5	90.1	91.6	79.2	77.8	981.89	982.03	29.5	19.3	4.1	197.3
2022-01-28T04:21	1	-9.4		0.3	-11.4		0.3	89.2	87.7	78.0	75.3	981.89	982.03	28.8	18.5	4.2	197.6
2022-01-28T04:22	1	-9.4		0.4	-11.2		0.1	87.9	88.5	78.1	77.0	981.89	982.03	32.1	21.1	4.2	197.6
2022-01-28T04:23	1	-9.4		0.4	-11.1		0.2	87.6	87.5	78.2	77.8	981.88	982.02	37.2	25.2	4.3	197.7
2022-01-28T04:24	1	-9.4	187.6	0.5	-11.0		0.3	86.2	87.5	77.9	77.5	981.88	982.02	40.8	27.9	4.3	197.6
2022-01-28T04:25	1	-9.3	208.8	0.5	-10.8		0.5	85.4	86.9	78.1	76.3	981.87	982.01	40.7	27.9	4.4	197.8

Figure 4.11: Original Data Snippet from 28/01/2022

Now that the data has been imported and filtered, a WAsP Observed Wind Climate File can be exported. The resulting OWC will be discussed in the next chapter.

4.2.2 Wind Turbine Parameters

Now that OWC has been created, the next step is to create a WTG file with the parameters presented for the SD6+ wind turbine. The WAsP Turbine Editor can be used to create the WTG file. The tool requires specific data from the wind turbine to create the WTG. All of the required data has been presented in Chapter 3 and can be extracted from the manufacturer's data. One of the inputs however, has to be calculated: The Thrust Coefficient. The thrust coefficient can be calculated with the available information and the thrust force where a is the axial induction factor, T is the thrust force, and C_P is the power coefficient [44] [3].

$$C_P = 4a(1-a)^2 \tag{4.1}$$

$$T = \frac{1}{2}\rho A U^2 \left[4a(1-a)\right] \tag{4.2}$$

$$C_T = \frac{T}{\frac{1}{2}\rho U^2 A} \tag{4.3}$$

Now that all data is available, the data is added to the WAsP turbine editor. Figure 4.12 shows a screenshot from the software tool.

[3] A table containing the power curve values and all calculated parameters can be found in the Appendix.

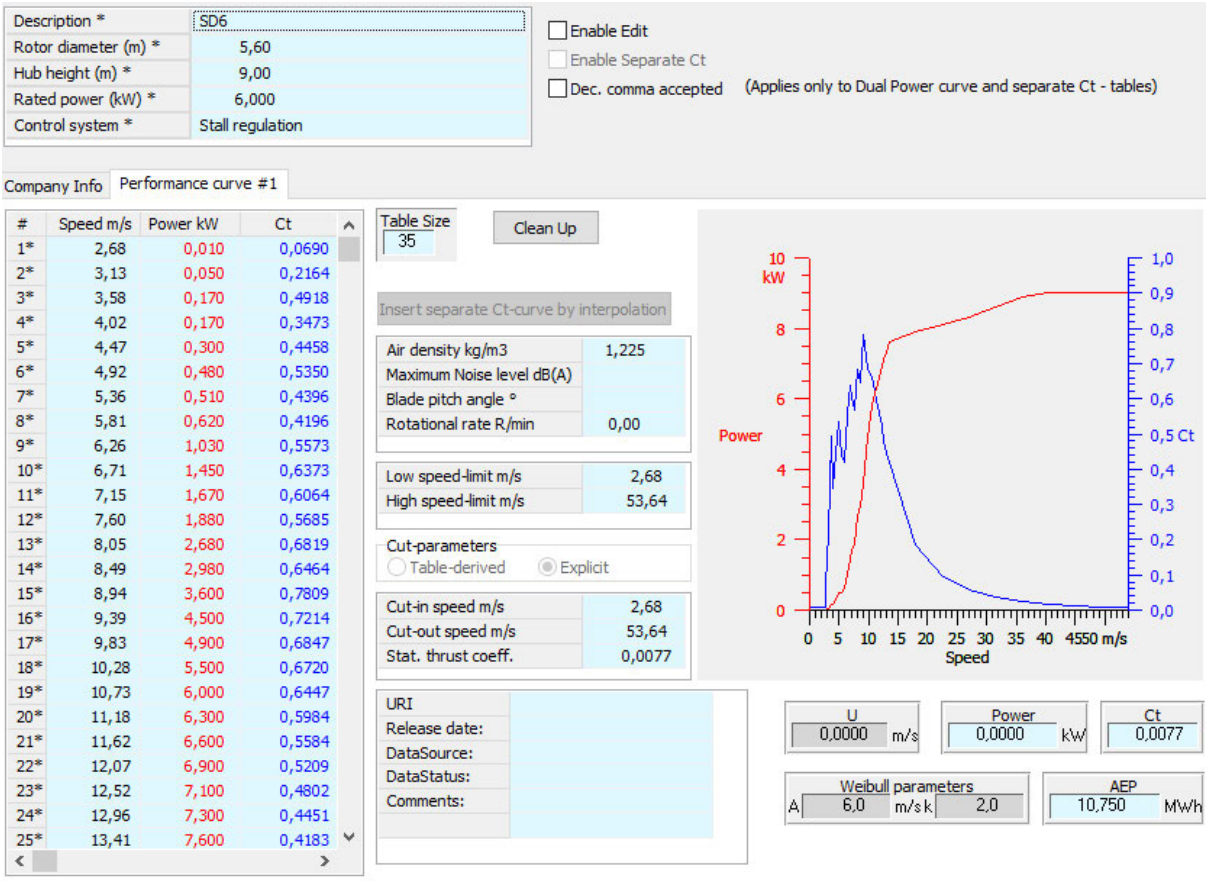

Figure 4.12: WAsP Wind Turbine Editor

4.2.3 Adding Topographical Inputs

Topographical Inputs must also be prepared for the usage in WAsP. As presented in Chapter 3, the data for the topographical map will be downloaded from the Reference Elevation Model of Antarctica (REMA) and the map for the project will be prepared using QGIS and the WAsP Map Editor. The raster data can be downloaded from the REMA Explorer[4] either from a user specified map area or as Strip DEMs. The data will be dowloaded from the REMA Explorer as this gives more room for extracting only a specific area from the map around the NMS-III Station. Figure 4.13 shows the map downloaded from the REMA Explorer with raster data.

[4]The REMA Explorer can be reached using the following URL: `https://rema.apps.pgc.umn.edu/`

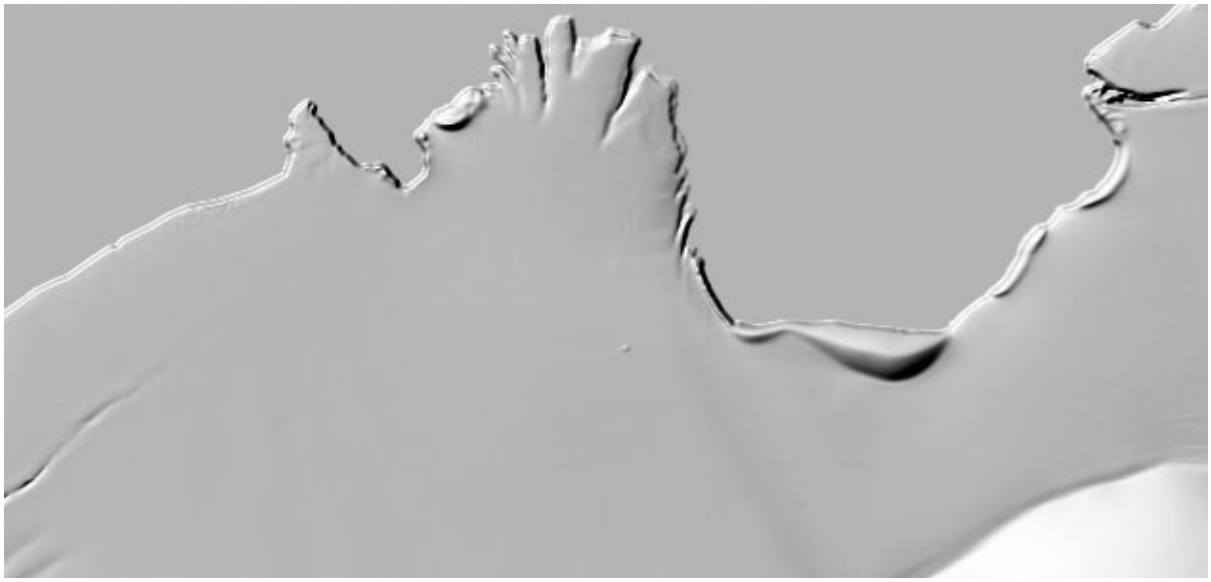

Figure 4.13: REMA Raster Map

As illustrated in Figure 4.13, the sea near the NMS-III Station is depicted with a grey colour. This is problematic, as both QGIS and the WAsP Map Editor do not interpret areas with this colour as representing an elevation of zero, which is the standard convention used for denoting sea level. The map has to be therefore edited so that the sea is depicted with a black colour: Figure 4.14.

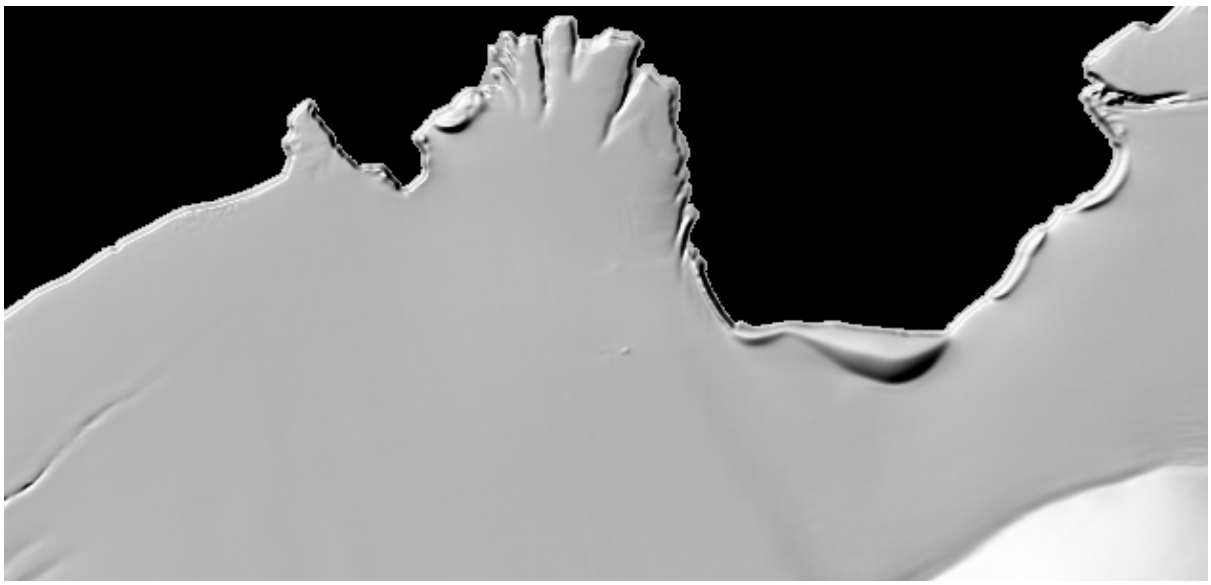

Figure 4.14: REMA Raster Map - Edited

The edited map is then imported to QGIS to convert the raster data into vector counter lines using the raster contours tool in QGIS (Figure 4.15). The coordinate reference system of the contours layer is changed from the CRS EPSG:3031 to CRS:32729 as the WAsP Map Editor can import only specific CRSs. The Projection used is WGS 84 as in the REMA Data, the UTM zone is 29S. The map is saved as a .shp file as only specific

file types can be imported to the WAsP Map Editor.

Figure 4.15: Contours Map after change of CRS

The contours map is then imported to the WAsP Map Editor as seen in Figure 4.16.

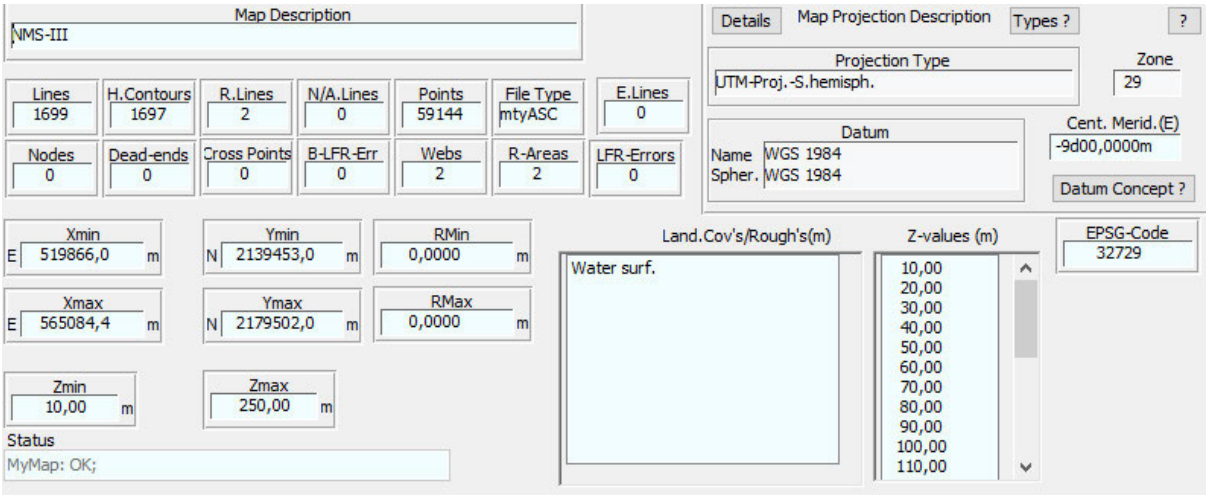

Figure 4.16: WAsP Map Editor

The WAsP Map Editor interface displays various parameters related to the spatial and topographical data of the map being used. The "Lines" parameter indicates the total number of line elements in the map, such as contour lines or boundary lines, while "H.Contours" represents the count of horizontal elevation contours derived from DEM data. "R.Lines" shows the number of roughness lines, which are used to model changes in surface roughness, such as transitions from forests to open water. The "Points" field indicates the total number of vertices defining all geometries in the map. Additionally,

diagnostic parameters such as "E.Lines," "Nodes," "Dead-ends," "Cross Points," and "B-LFR-Err" check for potential issues like crossing lines or incomplete geometries. The geographic extent of the map is described by "Xmin," "Xmax," "Ymin," and "Ymax," which define the minimum and maximum coordinates, while "Zmin" and "Zmax" provide the range of elevation values. The "Land.Cov's/Rough(s)" section describes land cover or surface roughness values and the "Z-values" list represents the elevation levels associated with the contour lines.
The Map is cropped to the area around the NMS-III as shown in Figure 4.17

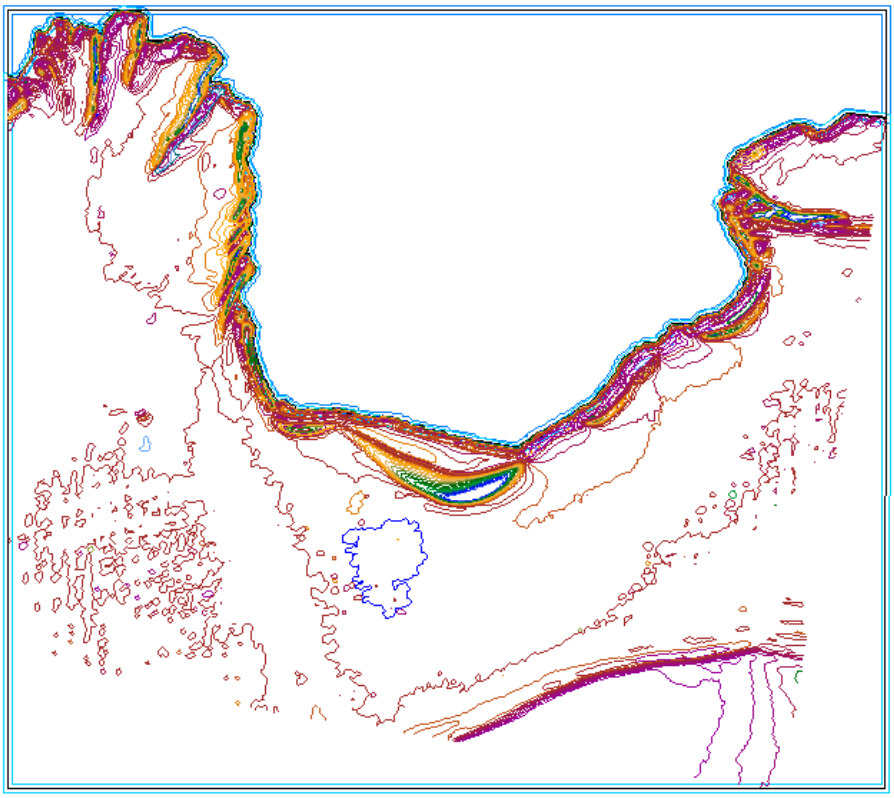

Figure 4.17: Cropped Map

The roughness information is added manually to the map to indicate the ice area and the water area as shown in Figure 4.18. The the roughness length of the Ekström Shelf near the NMS-III has been previously studied and a mean value of 0.0001m was calculated [37]. In the WAsP Map Editor, a roughness length of 0.0001 meters was applied to represent ice-covered regions. However, the WAsP Map Editor regards all roughness values less than 0.001m the same and denotes them as a water surface. Figure 4.19 shows the roughness length change lines that were added manually to the map.

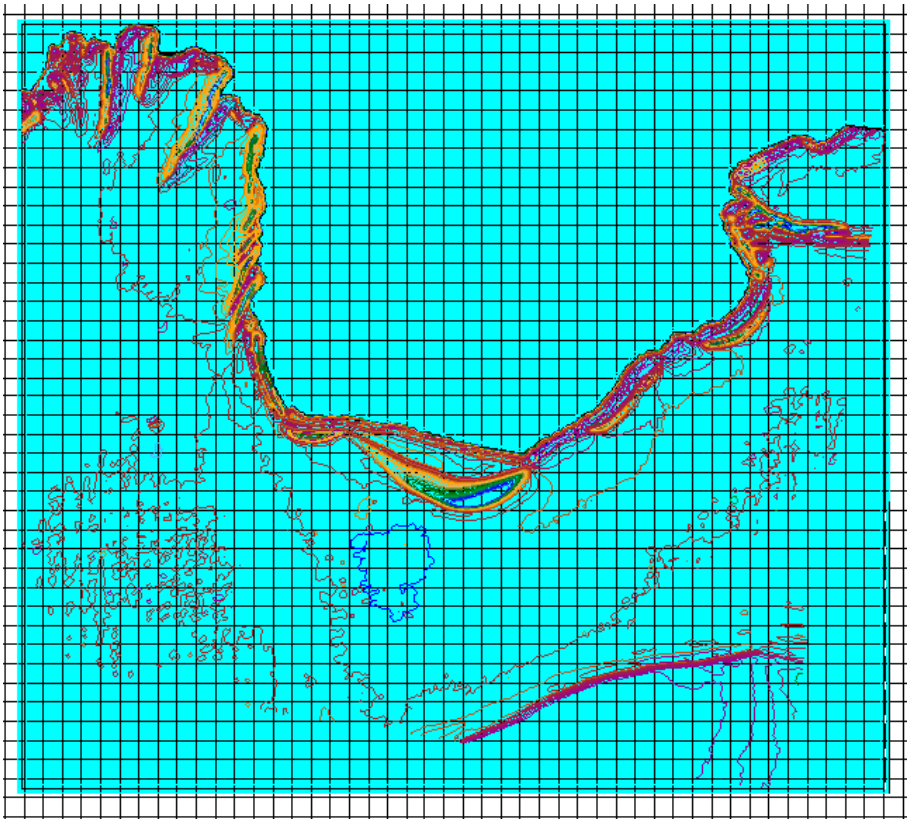

Figure 4.18: Map with Roughness Lengths

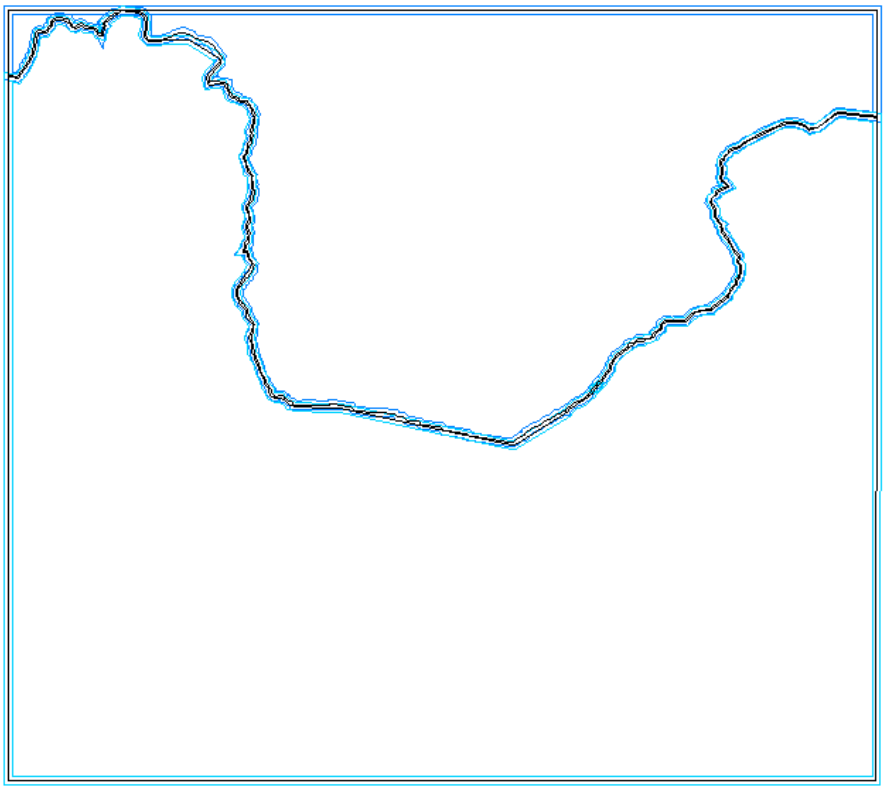

Figure 4.19: Roughness Lengths Change Lines

4.2.4 Creating the WAsP Project

After creating all the required files for an assessment with WAsP a Project can be created and the OWC, the WAsP Map and the wind turbine WTG file can all be added. As a first step a generalised wind climate (GWC) is added to the project. GWC gives a site-independent wind climate derived from the wind speed and direction measurements. In the GWC additional information about the site barometric Information can be fetched, Table 4.3 shows the fetched data in the GWC in the specified location [5].

Parameter	**Value**	**Unit**
Mean Temperature	-14.92	°
Ref. Altitude for Temperature (a.s.l.)	35.3	m
Mean Pressure	98180	Pa
Ref. Altitude for Pressure (a.s.l.)	33.3	m
Relative Humidity	75.76	%

Table 4.3: GWC - Barometric Reference Information

The meteorological station is then added to the project on the location of the Neumayer Metrological Observatory as presented in Chapter 3. Table 4.4 shows the site specification for the meteorological station [6].

Parameter	**Value**	**Unit**
Anemometer Height (a.g.l.)	10	m
Elevation (a.s.l.)	198.4	m
Net Altitude (a.s.l.)	208.4	m
Mean Air Density	1.293	kg/m^3

Table 4.4: Site Information

The calculated OWC is then added to describe the climate at the NMS-III Meteorological Observatory. A terrain analysis is needed to add the maps created, the map has two layers as previously presented, a layer for orography and a layer for roughness. The created

[5] A GWC Report created by WAsP can be found in the Appendix
[6] A Met. Station report created by WAsP can be found in the Appendix

WTG file for the SD6+ wind turbine is imported to the project. A wind farm is added with 32 turbines, each at 9 meter height. The distance between the closest wind turbine in the wind farm and the station is around 500m, the wind turbines are placed 60m from each other. The map shown in Fig 4.20 shows the imported map in WAsP after adding the NMS-III, the Meteorological Observatory, all the Wind Turbines and the borders of a wind resource grid map. The results will be discussed in the next chapter.

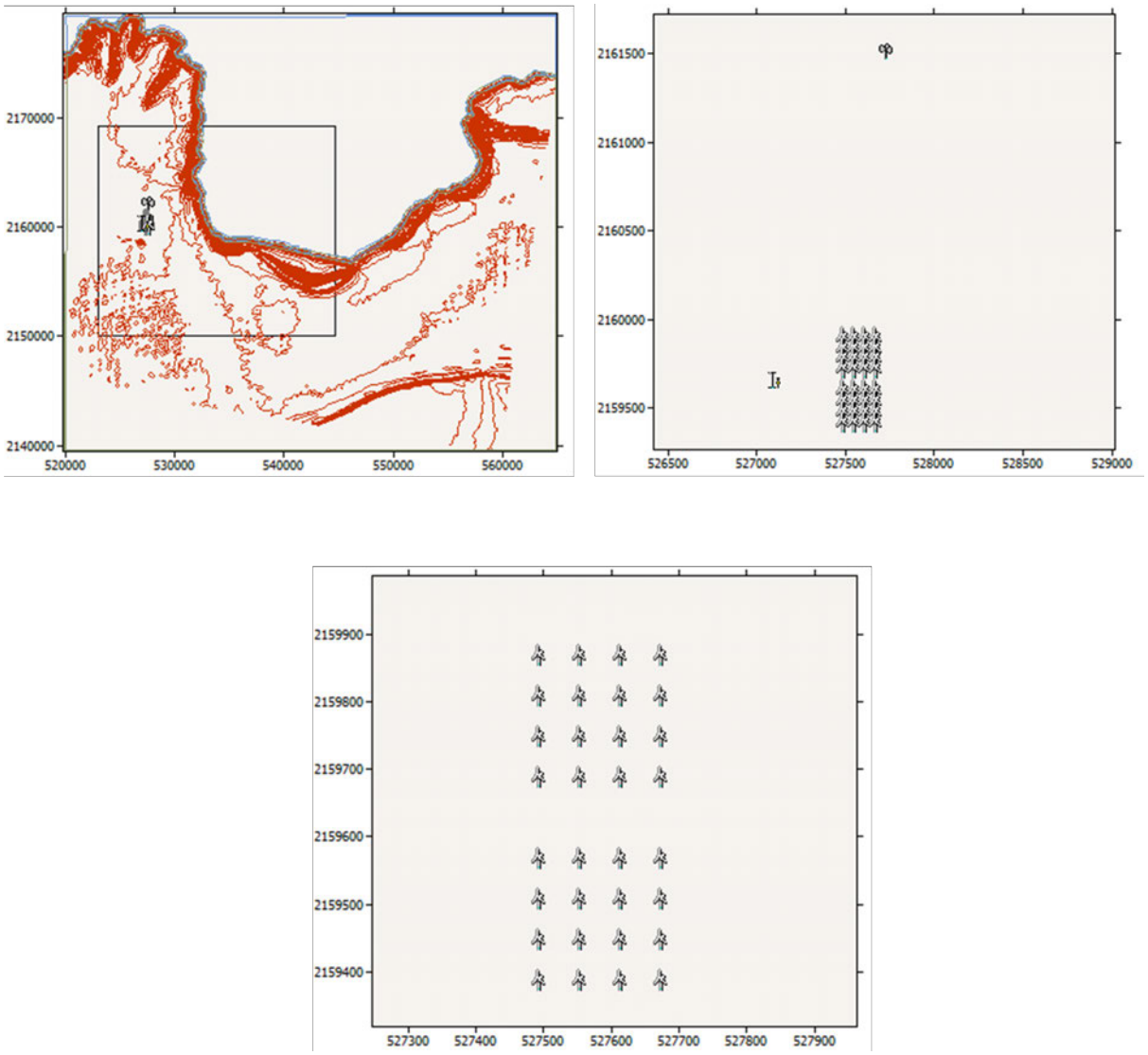

Figure 4.20: Imported Map to WAsP

Table 4.5 lists the locations from the WAsP Model in UTM Coordinates (WGS84 - 29)[7]. The final project breakdown in WAsP is shown in Figure 4.21.

[7]The location of the wind farm corresponds to a wind turbine in the middle of the presented wind farm

Description	Location
NMS-III	(527095.6 - 2159616.0)
Measuring Site	(527734.4 - 2161467.0)
Wind Farm	(527555.6 - 2159676.0)

Table 4.5: Locations of NMS-III, Measuring Site and Wind Farm

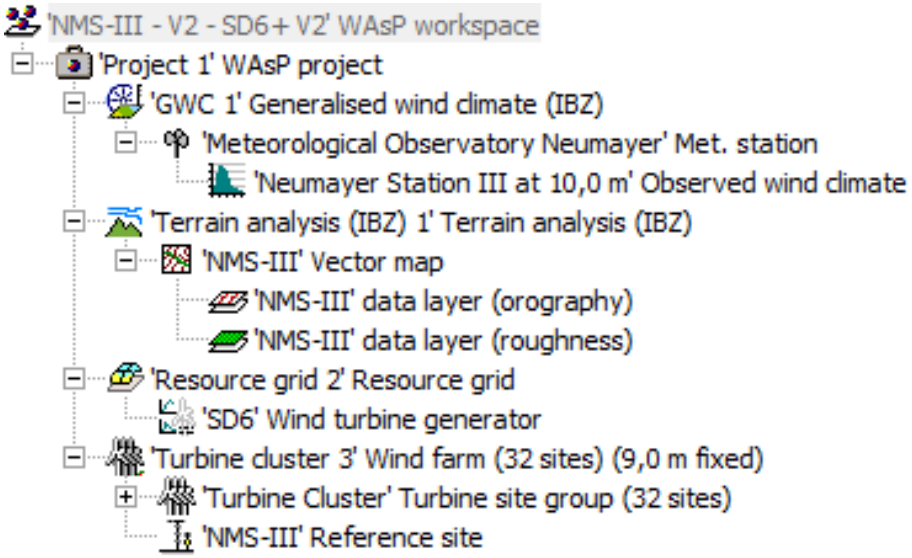

Figure 4.21: Final WAsP Project Overview

4.3 Wind Energy Assessment Implementation: AWES

Calculating an Annual Energy Production of an AWES is rather difficult to implement with a software or a simulation tool as the technology is not as widespread as is the case for wind turbines. Calculating the AEP in accordance with examples from literature as presented in Chapter 3 will therefore be implemented. As previously discussed, There are several methodologies available for obtaining data to calculate the AEP for AWES. the radiosonde data from the NMS-III will be utilised as the primary source for the AEP calculation. This choice is based on the fact that radiosonde data provides direct, empirical measurements of atmospheric conditions, thereby avoiding the assumptions inherent in alternative methods such as the power law or reanalysis datasets like ERA5. MATLAB scripts will be used to analyse wind speed data to determine the AEP. The process involves detailed data filtering, statistical analysis, and mathematical modelling using the Weibull distribution and the AWES power curve. The methodology implemented in the MATLAB scripts uses a simplified approach that nevertheless accounts for the various methods presented for the calculation of AEP for AWESs.

Radiosonde data from January 2015 till December 2020 are filtered so that only the date-time series, altitude, wind speeds and wind directions are left. A MATLAB script is then used to perform a statistical analysis of wind speed variations across different altitude ranges to visualise the vertical wind profile [8]. After importing the data, the altitude range is divided into bins of 100 meters to facilitate the analysis of wind speed distributions within discrete vertical segments. For each altitude bin, the script calculates the median wind speed, which represents the central value of the sorted wind speed data, and determines percentiles ranging from the 10th to the 90th, capturing the spread and variability of wind speeds similar to an approach implemented by another study [65]. The median wind speed values are then smoothed using a moving average technique to enhance visualisation. Two key plots are generated shown in Figure 4.22: one illustrating the wind speed profile across the full altitude range and another zoomed in to focus on altitudes below 500 meters.

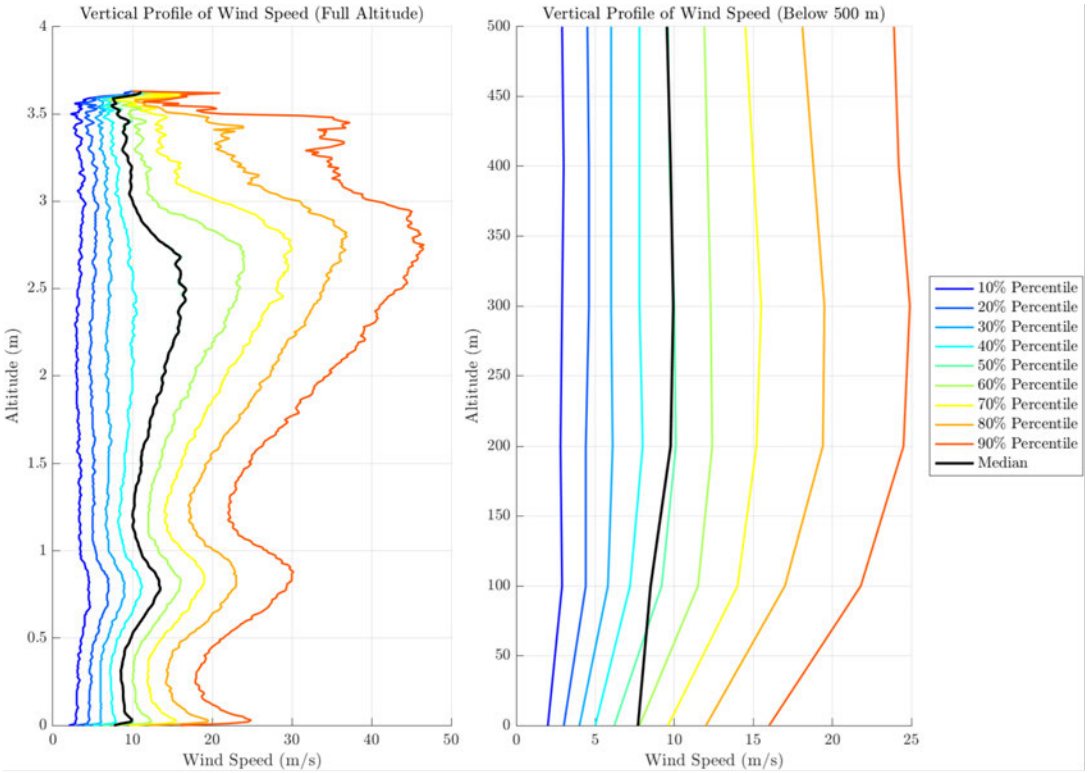

Figure 4.22: Extracted Vertical Wind Profile from Wind Data - All Altitudes and 500 Meters

The methodology for the AEP calculation [9] begins by filtering wind speed data to isolate measurements within a specified altitude range, defined as 70 to 350 meters as this is the range set by the manufacturer. Invalid or negative wind speeds are excluded to ensure the integrity of the analysis. The wind speed distribution is then modelled using the Weibull

[8]The MATLAB Script for the vertical wind profile can be found in the Appendix
[9]The MATLAB Script for the AEP Calculation can be found in the Appendix

probability density function. The code fits the Weibull distribution to the filtered data to determine the Weibull parameters. Once the Weibull distribution is established, the script uses the previously presented power curve for the Falcon AWES to estimate energy production. Interpolation is applied to ensure smooth transitions between discrete power curve values. To calculate the average power output, the script integrates the product of the power curve and the Weibull PDF over the AWES operational wind speed range, defined by the cut-in and cut-out speeds (5 m/s and 15 m/s). Finally, the total AEP is determined by multiplying the average power output by the number of hours in a year as presented previously. The equations presented in chapter 3 for the average power and the AEP are used with a slight change to the AEP formula: As 20% of a cycle is used for the retraction, the amount of hours in a year is multiplied with the factor 0.8.

$$P_{\text{av}} = \int_{v_{\text{in}}}^{v_{\text{cut}}} P_c \cdot p(U)\, dU \tag{3.80}$$

$$\text{AEP} = 0.8 \cdot P_{\text{av}} \cdot 8760 \quad [\text{kWh}] \tag{4.4}$$

The results of the AEP analysis include the Weibull distribution parameters, average power output, and total AEP. The results of the AEP calculation will be presented in the next chapter.

Chapter 5

Results

5.1 Wind Energy Resource Assessment: Wind Farm

The first important outcome is the OWC which represents the long-term wind climate at anemometer height at the position of the meteorological mast [49]. The OWC includes a Weibull distributions to represent the sector-wise wind speed distributions and an emergent distribution for the total (omni-directional) distribution. The difference between the fitted and the observed wind speed distributions should be small: less than about 1% for mean power density and less than a few per cent for mean wind speed [49]. This is the case according to the results from the OWC as shown in Table 5.1 and Figure 5.1 which includes the Weibull-A, Weibull-k, mean speeds and power densities of the respective distributions [1].

[1] A statistics report and a generation report created by WAsP can be found in the Appendix.

Data	Weibull-A [m/s]	Weibull-k	Mean speed [m/s]	Power density [W/m^2]
Source Data	-	-	8.72	1239
Fitted	9.1	1.3	8.38	1240
Emergent	-	-	8.27	1239
Combined	9.6	1.39	8.27	1239

Table 5.1: OWC Results

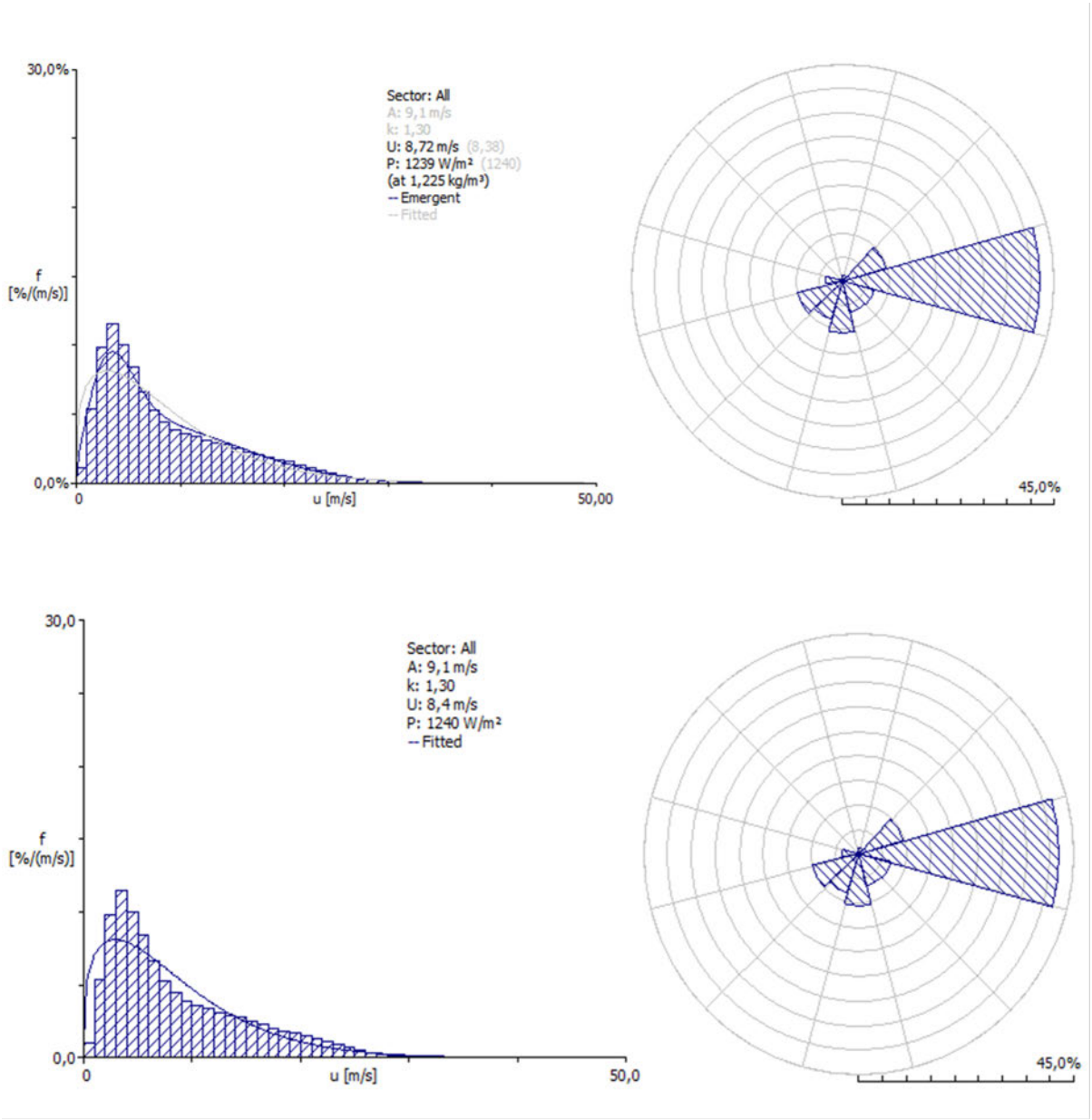

Figure 5.1: Observed Wind Climate - Emergent and Fitted

The OWC results show that most of the wind is coming from the east or section 4.

Figure 5.2 shows the hourly mean wind speeds by month.

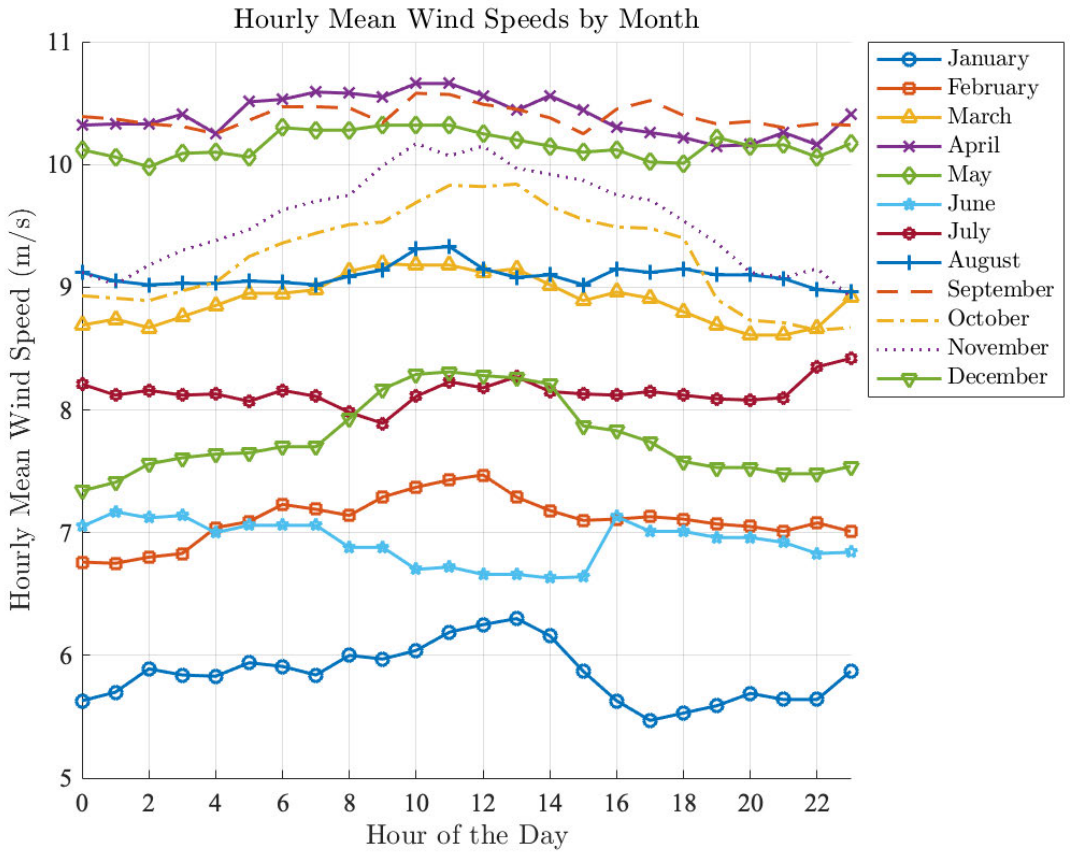

Figure 5.2: Hourly Mean Wind Speeds by Month

In Addition to the OWC, the WAsP Climate analysis tool creates an Observed Extreme Wind Climate (OEWC). An OEWC is a statistical representation of the extreme wind conditions at the site [29] and describes the magnitude of the strongest winds at a site and the way in which the maximum wind observed varies with the length of the observation time [29]. There are two methods for OEWC analysis: Annual Maxima and Peak Over Threshold (POT). While both approaches use the same dataset, they differ in data requirements and their handling of extreme wind events [29]. The Annual Maxima method identifies the highest wind speeds recorded annually and requires at least two years of data [29]. This approach provides a comprehensive distribution of extreme wind speeds, including the derived 50-year return wind speed (U50) and the Gumbel distribution parameter. Additionally, the method associates annual maxima with their corresponding wind directions, offering insights into directional trends in extreme winds [29]. The OEWC is shown in Figure 5.3

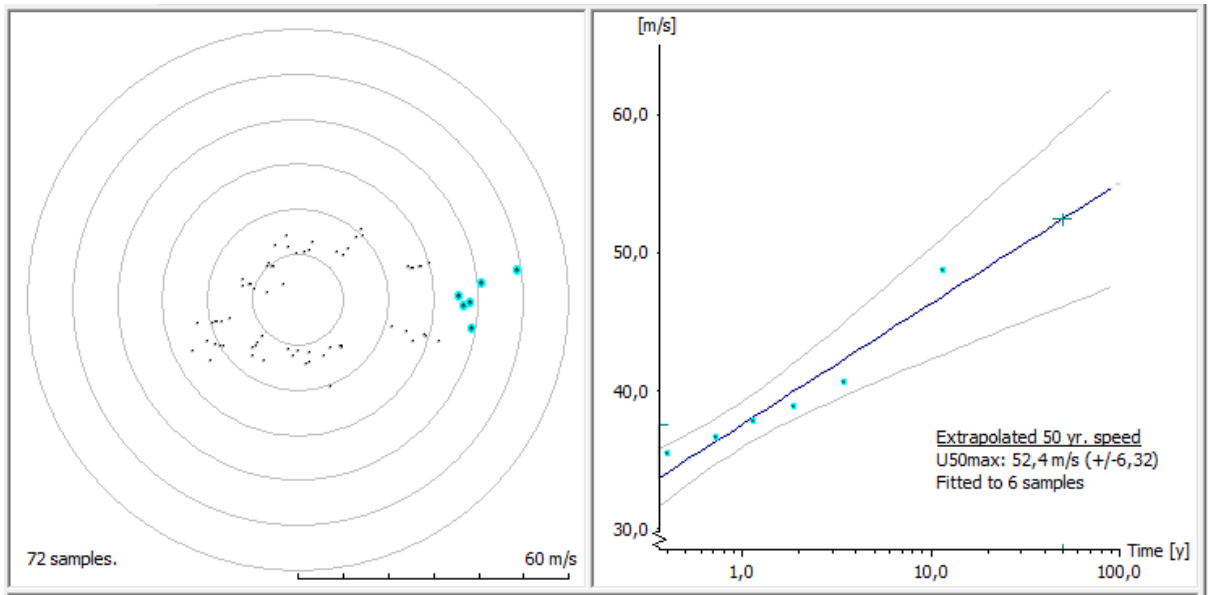

#	1	2	3	4	5	6
Dir [°]	88	92	85	91	99	82
U [m/s]	35,60	36,70	40,70	37,90	38,90	48,80
Rank	1	2	5	3	4	6

Figure 5.3: Annual Maxima OWEC

In contrast, the POT method focuses on wind events exceeding a defined threshold and requires less data, making it suitable for shorter datasets [49]. However, the accuracy of this method improves significantly with more extensive records. The POT approach primarily estimates U50 along with associated uncertainties. The OEWC-POT Plot is shown in Figure 5.4.

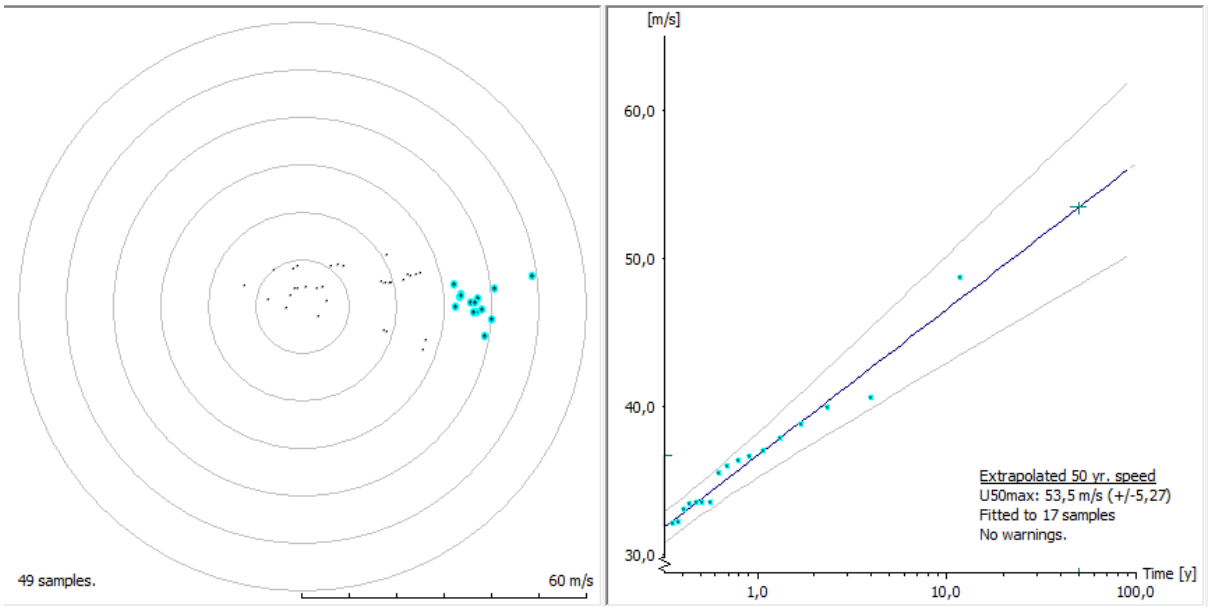

Figure 5.4: Peak Over Threshold OWEC

With the OWC results now presented, the analysis can proceed to the GWC results. Table 5.2 provides the wind speed distribution parameters across various heights (10 m

to 200 m) and directional sectors (0° to 330°). For each height and sector, it lists the Weibull scale factor (A), the Weibull shape factor (k), and the mean wind speed (U). Additionally, the bottom row shows the frequency distribution (%) of wind occurrences for each sector, highlighting the prevailing wind directions and their contributions to the overall wind profile.

Height (m)	Parameter (Unit)	Sec. 1 (0°)	Sec. 2 (30°)	Sec. 3 (60°)	Sec. 4 (90°)	Sec. 5 (120°)	Sec. 6 (150°)	Sec. 7 (180°)	Sec. 8 (210°)	Sec. 9 (240°)	Sec. 10 (270°)	Sec. 11 (300°)	Sec. 12 (330°)
10.0	A (m/s)	3.2	6.3	9.6	14.5	6.2	3.9	4.4	4.4	6.8	6.4	4.1	3.6
	k (–)	1.18	1.48	1.79	2.20	1.11	1.86	2.15	2.08	1.72	1.79	1.52	1.62
	U (m/s)	3.06	5.70	8.50	12.85	5.96	3.50	3.88	3.91	6.09	5.68	3.66	3.24
25.0	A (m/s)	3.7	7.0	10.5	15.8	6.9	4.7	5.1	5.0	7.6	7.1	4.6	4.1
	k (–)	1.27	1.54	1.82	2.22	1.15	2.13	2.42	2.31	1.78	1.88	1.65	1.76
	U (m/s)	3.44	6.30	9.29	14.02	6.58	4.13	4.48	4.47	6.73	6.28	4.12	3.63
50.0	A (m/s)	4.1	7.6	11.2	16.9	7.6	5.5	5.8	5.7	8.2	7.7	5.1	4.5
	k (–)	1.29	1.61	1.87	2.26	1.20	2.34	2.53	2.37	1.85	1.92	1.63	1.74
	U (m/s)	3.83	6.85	9.96	14.97	7.17	4.88	5.11	5.03	7.32	6.85	4.59	4.04
100.0	A (m/s)	4.7	8.5	12.1	18.1	8.6	6.7	6.5	6.4	9.1	8.5	5.8	5.2
	k (–)	1.28	1.61	1.88	2.31	1.26	2.51	2.58	2.38	1.85	1.91	1.61	1.71
	U (m/s)	4.39	7.58	10.76	16.04	7.96	5.93	5.80	5.64	8.05	7.58	5.24	4.60
200.0	A (m/s)	5.6	9.6	13.2	19.6	9.9	7.7	6.7	6.5	10.0	9.6	6.7	5.9
	k (–)	1.27	1.62	1.89	2.32	1.30	2.62	2.59	2.41	1.86	1.90	1.59	1.68
	U (m/s)	5.17	8.60	11.76	17.35	9.10	6.85	5.97	5.79	8.86	8.50	6.02	5.30
Freq. (%)		0.4	1.3	9.3	40.7	8.1	7.0	10.7	8.2	9.6	7.0	3.5	0.7

Table 5.2: GWC Results for different heights

In addition, wind resource grid maps are generated to analyse the results. For each point in the grid, data like elevation, RIX, mean wind speed, and other parameters are calculated. Figure 5.5 shows a collection of the generated grid maps. The wind resource grid maps provide a comprehensive analysis of key parameters influencing wind energy potential. The elevation map highlights terrain variations that affect wind flow, while the AEP map estimates the site's energy output potential in kWh. The mean speed map shows average wind speeds in meters per second. The RIX (Ruggedness Index) map depicts terrain ruggedness, which can impact wind flow and turbine performance. Additionally, the power density map indicates the available wind energy in W/m^2, and the capacity factor map represents the efficiency of energy production, reflecting the ratio of actual to maximum possible output.

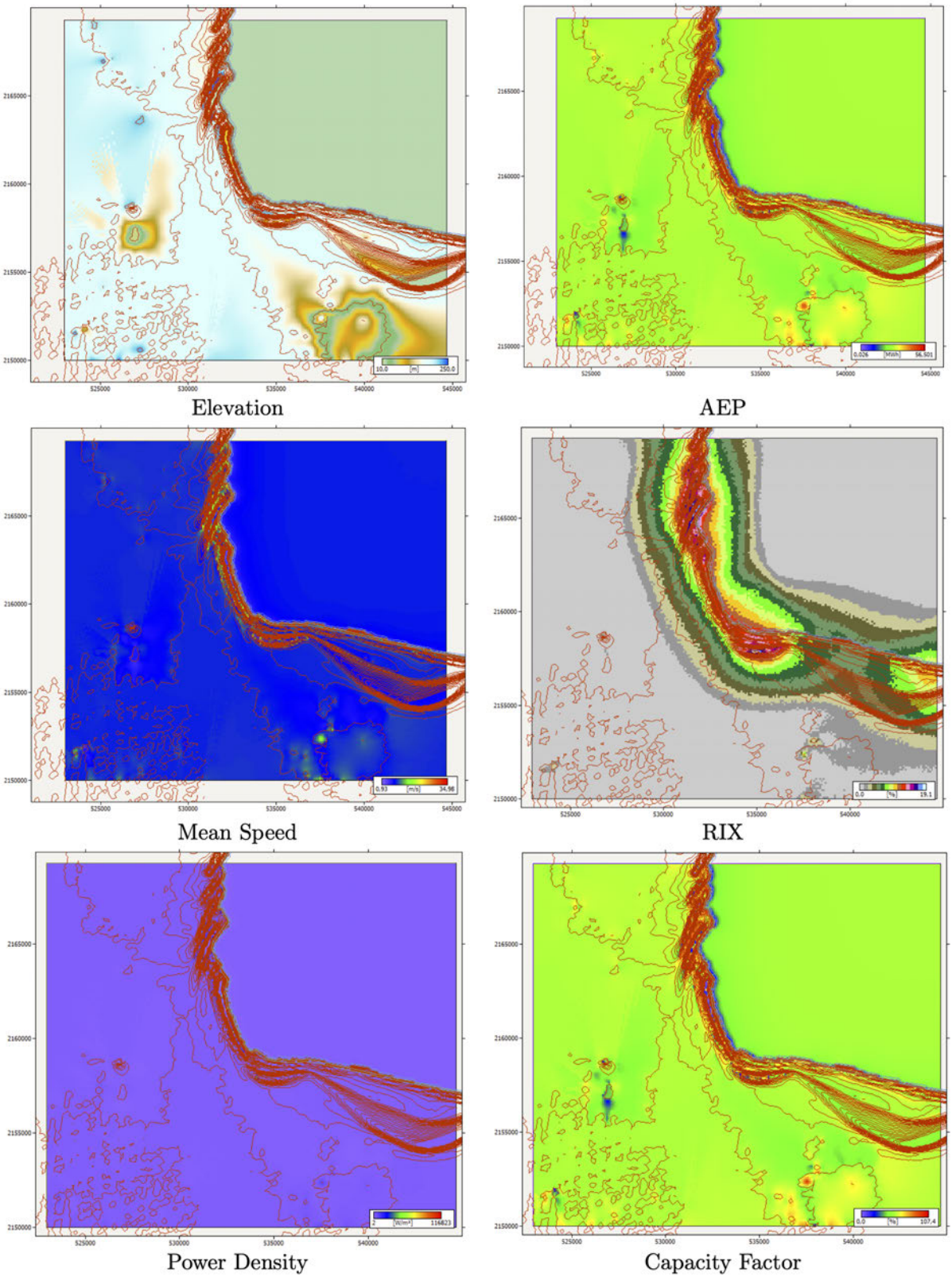

Figure 5.5: Generated Grid Maps in WAsP

The AEP results from the wind farm are listed in Table 5.3. The system demonstrates a total AEP of 828.33 MWh, with a net AEP of 809.95 MWh after accounting for proportional wake losses of 2.22%. The capacity factor is reported at 48.1%, reflecting the ratio

of actual energy output to the maximum possible output over the operational period. The mean wind speed is observed to be 8.18 m/s, while the wake-reduced mean speed slightly decreases to 8.08 m/s. The air density averages at 1.298 kg/m^3, with power density values ranging from 950 W/m^2 to 1,257 W/m^2. The RIX, a measure of terrain complexity, remains negligible, ranging from 0.0% to 0.1%. These parameters provide insights into the system's energy yield and environmental operating conditions. The wake losses can be avoided if the wind turbines are arranged differently. An optimal arrangement to avoid wake losses would be to position the wind turbines in a straight line, this will however make the distance to the farthest wind turbine from the station higher.

Variable	**Total**	**Mean**	**Min**	**Max**
Total gross AEP [MWh]	828,325	25,885	24,615	27,436
Total net AEP [MWh]	809,953	25,311	24,417	27,216
Proportional wake loss [%]	2.22	-	0.19	3.21
Capacity factor [%]	48.1	-	46.4	51.7
Mean speed [m/s]	-	8.18	7.84	8.59
Mean speed (wake-reduced) [m/s]	-	8.08	7.83	8.55
Air density [kg/m^3]	-	1.298	1.293	1.302
Power density [W/m^2]	-	1095	950	1257
RIX [%]	-	-	0.0	0.1

Table 5.3: AEP Results

Figure 5.6 shows the power curve of the wind farm. The power curve was created by taking the given wind speed and average power outputs from all sections and fitting a smoothing spline to the dataset. The wind speeds, ranging from 2 m/s to 55 m/s, were used as input along with their corresponding average power outputs in kW.

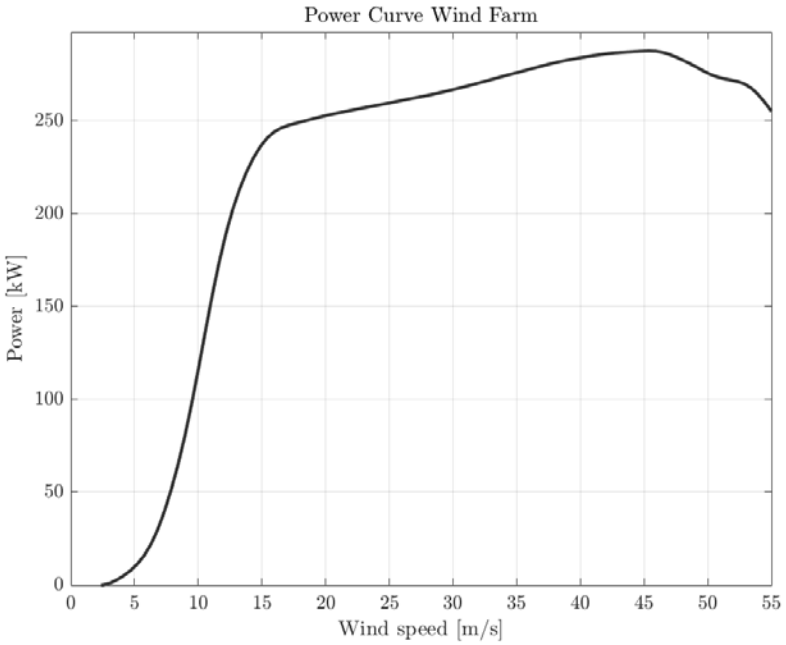

Figure 5.6: Power Curve: Wind Farm

5.2 Wind Energy Resource Assessment: AWES

The results of the AEP calculation, performed using the methodology described in the previous chapter, provide an estimation of the Kitepower Falcon AWES energy output under realistic operating conditions. By integrating the power curve with the Weibull probability density function over the specified operational wind speed range, the analysis accounts for the variability of wind speeds at the specified altitude range (70–350 meters). The filtering of wind speed data ensured high-quality inputs, while the Weibull distribution fitting enabled modelling of wind speed variability. The incorporation of interpolation into the power curve calculation allowed for smooth and accurate power estimates across varying wind speeds, mitigating any potential inaccuracies from discrete power curve data. The calculated AEP demonstrates the Falcon AWES's potential to harness wind energy efficiently within the manufacturer's specified altitude and operational wind speed ranges.

Figure 5.7 illustrates the Weibull wind speed distribution and the output parameters of the distribution and the AEP Results are presented in Table 5.4. The average power is at 42.96 kW and the calculated AEP is at around 300 MWh per year.

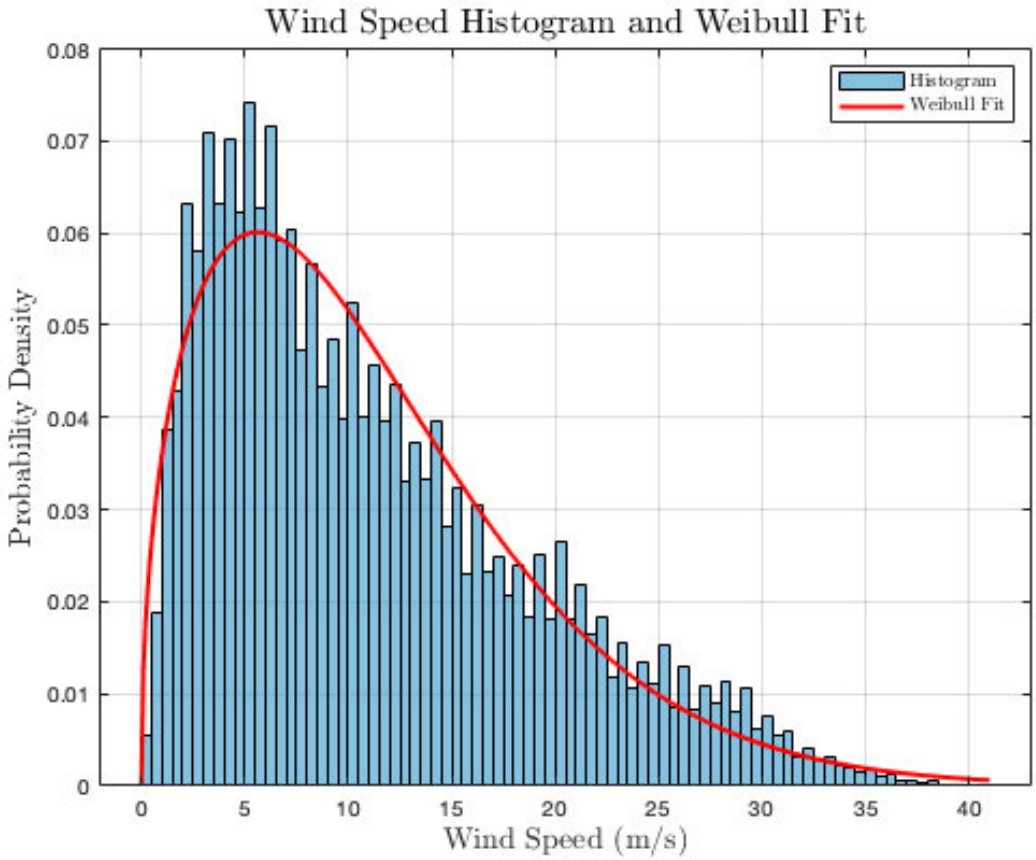

Figure 5.7: Weibull Wind Speed Distribution - 350m

Parameter	**Value**	**Unit**
Weibull-A	12.33	m/s
Weibull-k	1.46	–
Average Power (P_{av})	42.96	kW
AEP	301.06	MWh/year

Table 5.4: Results Weibull Distribution and AEP

Chapter 6

Financial Analysis

This chapter presents a comprehensive financial analysis of the proposed wind farm and AWES. The primary objective of this analysis is to determine the Cost of Energy (COE) for the systems under consideration. The analysis aims to assess the anticipated economic outcomes, including potential gains or losses, that would result from implementing these systems. By substituting a portion of diesel-based energy generation with these renewable systems, the analysis seeks to quantify the expected cost savings and overall financial feasibility. The financial estimation for the AWES poses a greater challenge due to the limited availability of literature compared to conventional wind turbines. Therefore, an alternative methodology will be used to conduct the financial analysis for the AWES.

6.1 Wind Farm

The formula for the COE is defined in Equation 6.1 where C_c represents the system's capital cost, FCR is the fixed charge rate that accounts for the present value of factors such as utility debt and equity costs, taxes, and insurance. $C_{O\&M}$ denotes the annual operation and maintenance expenses [44].

$$COE = \frac{C_c \times FCR + C_{O\&M}}{\text{AEP}} \tag{6.1}$$

The cost of a single wind turbine is approximately 43,000 € according to the manufacturer, resulting in a total cost of 1,376,000 € for a wind farm consisting of 32 turbines. To estimate the capital costs more comprehensively, additional factors such as transportation must be considered.

It is assumed that the wind turbines will be transported to Neumayer Station III (NMS-III) using the station's regular logistical supply chain, which includes the research vessel RV Polarstern. The RV Polarstern has a cargo capacity sufficient for 80 20-ft containers [25], providing adequate space to accommodate the 32 wind turbines. The RV Polarstern typically requires approximately 900 metric tons of fuel per month for its operations [2],

and an expedition to Antarctica generally lasts one month. Assuming that 25% of the vessel's cargo capacity is utilized for the wind turbine shipment, and at a marine gas oil (MGO) fuel price of 455 €/metric ton [50], the transportation cost contribution can be calculated as follows:

$$C_c = C_{\text{turbines}} + (f_{\text{Space}} \times P_{\text{fuel}} \times M_{\text{fuel}}) \quad (\text{in } €) \tag{6.2}$$

The Net Present Value (NPV) is calculated by summing the discounted value of annual savings (S) over the project lifetime:

$$NPV = \sum_{j=1}^{N} \frac{\text{Annual Savings (S)}}{(1+r)^j} \tag{6.3}$$

If the discount rate is zero ($r = 0$), the equation simplifies to:

$$NPV = S \times N \quad (\text{in } €) \tag{6.4}$$

The annual cost savings from replacing the fuel (E_{Fuel}) with wind energy is:

$$S = E_{\text{Fuel}} \times P_{\text{Diesel}} \quad (\text{in } €) \tag{6.5}$$

To calculate the amount of diesel required to generate the energy replaced by the wind turbine, the following equation is used:

$$E_{\text{Fuel}} = \frac{\text{AEP}_{\text{Wind Turbine}} \times 1000}{C \times \eta_{\text{Generator}}} \quad (\text{in liters/year}) \tag{6.6}$$

The Capital Recovery Factor is calculated as [44]:

$$CRF = \frac{1}{N} \quad (\text{dimensionless}) \tag{6.7}$$

The Fixed Charge Rate considers the CRF and the NPV [56]:

$$FCR = CRF \times \frac{NPV}{C_{\text{turbines}}} \quad (\text{dimensionless}) \tag{6.8}$$

Another important value for the calculation of the COE is the annual operation and maintenance expenses factor $C_{O\&M}$. The cumulative costs for O&M represent as much as 65-90% of a turbine's investment cost [18]. The higher end of the estimate will be taken into account as the project is being executed in a cold environment. $C_{O\&M}$ can then be calculated as follows:

$$C_{O\&M} = \frac{C_c \cdot 0.9}{N} \tag{6.9}$$

$$COE = \frac{(C_{\text{turbines}} + (f_{\text{Space}} \times P_{\text{fuel}} \times M_{\text{fuel}})) \times \frac{S}{C_{\text{turbines}}} + \frac{(C_c \cdot 0.9)}{N}}{\text{AEP}_{\text{Wind Turbine}}} \quad (\text{in } €/\text{kWh}) \tag{6.10}$$

$$\begin{aligned} COE &= \frac{\left(1,376,000.00 € + \left(0.25 \times 455 \, \frac{€}{\text{MT}} \times 900 \, \text{MT}\right)\right) \times \frac{303{,}732{,}3.75 €}{1{,}376{,}000.00 €} + \frac{(1{,}478{,}375.00 € \cdot 0.9)}{25 \, \text{years}}}{809.96 \, \text{kWh/year}} \\ &= 3.82 \, \frac{€}{\text{kWh}} \end{aligned} \tag{6.11}$$

Parameter	Value	Description
C_{turbines}	1,376,000.00 €*	Wind turbines capital cost
f_{Space}	0.25**	Space factor or area-related multiplier
P_{fuel}	455 €/MT [50]	Price of fuel
M_{fuel}	900 MT [2]	Quantity of fuel used in a month
S	303,732,3.75 €	Annual cost savings from replacing fuel with wind energy
C_c	1,478,375.00 €	Cumulative capital cost
N	25 years [21]	Project lifetime
E_{Fuel}	222,250.00 kWh/year****	Energy replaced by the wind farm
P_{Diesel}	15 €/liter*** [14]	Price of diesel
$\text{AEP}_{\text{Wind Turbine}}$	809.96 kWh/year	Annual Energy Production from the wind farm
COE	**3.82 €/kWh**	**Cost of Energy**

Table 6.1: Parameters, values, and descriptions for the financial analysis

* Based on prices from the manufacturer at 43.000 € per wind turbine
** Based on an assumption on the wind turbines size and weight
*** Assumed Diesel Cost in Antarctica
**** Assumed Generator Efficiency at 40%

6.2 AWES

The financial analysis for the selected AWES will be implemented using a reference economic model from the IEA Wind TCP Task 48 [31]. The model is a helpful tool to estimate the cost of energy for an AWES as data on such systems is usually not available and the small number of implemented projects worldwide is small compared to wind turbines which leads to less accuracy in the estimation. The model is available as a MATLAB code to implement with user-specified inputs. The reference model combines site specific inputs and system specific inputs to generate important economic outputs. Figure 6.1 illustrates the workflow of the MATLAB code.

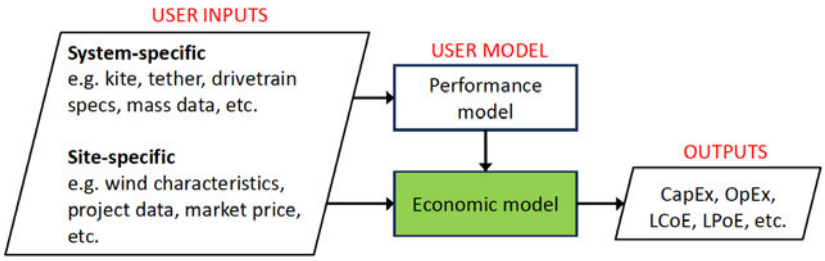

Figure 6.1: Representation of Inputs and Outputs of the Reference Economic Model for AWES [31]

The LCOE is calculated in the tool as follows [31]:

$$\text{LCOE} = \frac{\sum_{y=0}^{N_y} \frac{\text{CapEx}_y + \text{OpEx}_y}{(1+r)^y}}{\sum_{y=0}^{N_y} \frac{\text{AEP}_y}{(1+r)^y}} \tag{6.12}$$

In the equation, CapEx is the capital expenditure, OpEx is the operational expenditure, r is the discount rate, AEP is the annual energy produced, y is the instantaneous year, and Ny is the project lifetime [31]. The cost modeling framework accounts for all key components and subcomponents of the AWES. CapEx and OpEx account for costs for critical elements such as the kite, tether and the ground station. Balance of system and balance of plant parameters are also accounted for in the model. Figure 6.2 shows the components that the model accounts for.

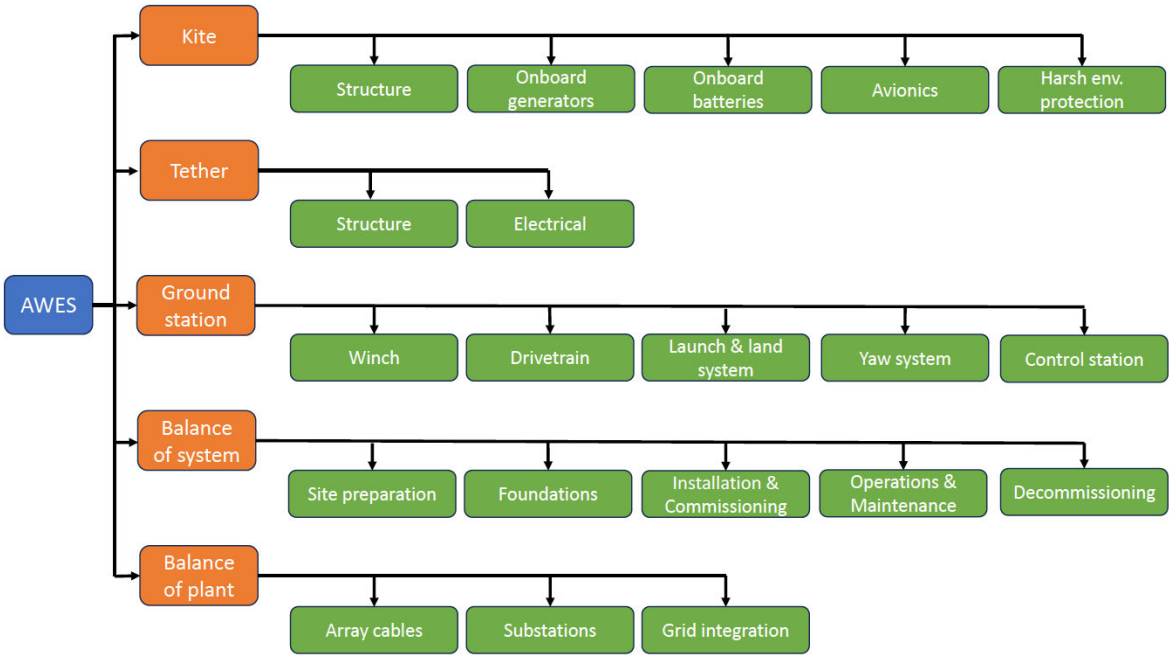

Figure 6.2: Components considered in the Reference Economic Model for AWES [31]

The model's parameters are derived from a system developed by the same company as the selected AWES [31], increasing accuracy in the calculations. However, several input values

will either be assumed or set to default due to the unavailability of certain parameters for the selected AWES. As an input the type of AWES must be added. For this model, the selected configuration is Ground Generation (GG) with a soft kite. The project lifetime is set to 25 years, which is used as a default value. The Weibull shape factor ($k = 1.46$) and scale factor ($A = 12.33$) are derived from the Annual Energy Production (AEP) calculations presented in Chapter 5. The wind speed range is specified as [5, 15] m/s, based on the AWES specifications. The kite replacement frequency is set at 1 per year because the specifications indicate a lifetime of 4000 operational hours for the kite. The onboard generator power is set to 1000 W, and the onboard battery energy is set to 0 kWh, both are default values due to insufficient available data. The tether diameter is 0.04 m, determined from a study on the selected AWES. The tether length (350 m) and material density (970 kg/m^3) are taken from the system's specifications. The tether replacement frequency is set to -1 as a default, meaning no replacement is considered. The tether force values, ranging from 4083 N to 87500 N, are calculated using a linear approach based on the original power curve. The peak mechanical power is specified as 130 kW, derived from the system's specifications, and the average electrical power values, ranging from 10 kW to 100 kW, are based on the provided power curve. All ground station parameters are set to default values due to a lack of specific data. However, these values are based on a similar system developed by the same company, making it highly likely that they are applicable to the current system. Table 6.2 provides a comprehensive overview of the input parameters used in the model. The outputs of the MATLAB Code[1] are shown in Table 6.3.

Although the reference model used accounts for multiple factors and it was created through a project combining multiple researchers from the AWES sector, it is important to note out that no financial numbers from the manufacturer were used for the calculation. As an example, the financial analysis for the wind turbines included realistic capital costs and logistical costs. An AWES is nevertheless cheaper compared to a wind turbine as the costs for foundations, installation and components are lower in general, not to to mention the logistical advantages that reduce the total cost in this case for AWES.

[1]The code used to generate the outputs can be found in the Appendix.

Parameter	Value	Unit	Source
General System Information			
System Type	GG (Ground-Gen)		Manufacturer
Kite Type	Soft		Manufacturer
Project Lifetime	25	years	Manufacturer
Wind Conditions			
Weibull Shape Factor (k)	1.46		AEP Calculation
Weibull Scale Factor (A)	12.33		AEP Calculation
Wind Speed Range	[5, 15]	m/s	Manufacturer
Kite Parameters			
Kite Area	80	m^2	Manufacturer
Kite Replacement Frequency	1	replacements/year	Manufacturer
Onboard Generator Power	1000	W	Default
Onboard Battery Energy	0	kWh	Default
Tether Parameters			
Tether Diameter	0.04	m	Literature [71]
Tether Length	350	m	Manufacturer
Tether Material Density	970	kg/m^3	Manufacturer
Tether Replacement Frequency	-1	replacements/year	Default
Tether Force	[4083, ..., 87500]	N	Derived
System Performance			
Peak Mechanical Power	130	kW	Manufacturer
Average Electrical Power	[10, 20, ..., 100]	kW	Manufacturer
Cycle Duration	100	s	Manufacturer
Ground Station Parameters			
Ultracapacitor Energy Capacity	2.5	kWh	Default
Ultracapacitor Usable Energy	1.25	kWh	Default
Ultracapacitor Replacement	-1	replacements/year	Default
Battery Energy Capacity	0.098	kWh	Default
Battery Usable Energy	1.25	kWh	Default
Battery Replacement	-1	replacements/year	Default
Hydraulic Accumulator Energy	2.5	kWh	Default
Hydraulic Usable Energy	1.25	kWh	Default
Hydraulic Accumulator Replacement	0.1	replacements/year	Default
Hydraulic Motor Replacement	0.083	replacements/year	Default
Pump Motor Replacement	0.125	replacements/year	Default

Table 6.2: Reference Economic Model for AWES - Input Parameters

Parameter	Value	Explanation
Capacity Factor (CF)	0.27	Ratio of energy output to maximum output
Levelized Cost of Energy (LCoE)	175 EUR/MWh	Energy cost over system's lifetime
Cost of Variable Expenses (CoVE)	92 EUR/MWh	Variable operating costs
Levelized Revenue of Energy (LRoE)	182 EUR/MWh	Revenue per unit of energy
Levelized Profit of Energy (LPoE)	7 EUR/MWh	Profit per unit of energy
Net Present Value (NPV)	16 k EUR	Net cash flows over project lifetime
Internal Rate of Return (IRR)	0.097	Project rate of return

Table 6.3: Reference Economic Model for AWES - Output Parameters

Figure 6.3 illustrates the cost distribution for an Airborne Wind Energy System (AWES) across three economic metrics: CapEx, OpEx, and LCoE. CapEx is dominated by the ground station winch (35%), ultracapacitors (19%), and tether costs (13%). OpEx is primarily influenced by Balance of System (BoS) operations and maintenance (39%) and kite structure replacement (28%). LCoE reflects contributions from both CapEx and OpEx, with the winch (22%) and BoS (15%) being major contributors.

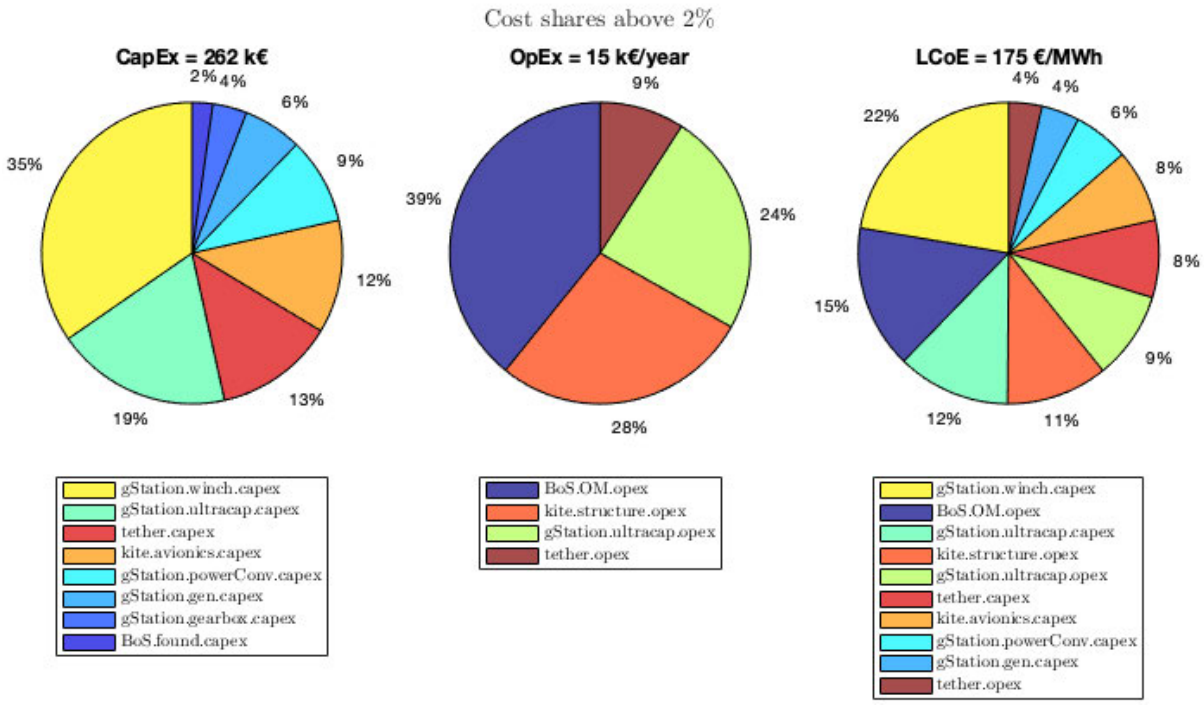

Figure 6.3: Reference Economic Model for AWES: Output Results Breakdown

Chapter 7

Discussion

The wind data analysis results align closely with data from other sources regarding wind direction and speed [36]. The difference between the emergent and fitted results is within the accepted range. The analysis revealed that hourly mean wind speeds are slowest during the latter half of the summer months (December, January, and February) similar to expected results as presented in the literature review, suggesting the necessity of energy storage solutions to optimise the utilisation of wind energy. The calculated Annual Energy Production (AEP) aligns with expectations for the chosen wind turbines. Annual Maxima and Peak Over Threshold methods were employed as validation mechanisms, both yielding satisfactory results.

Grid maps provided an overview of the mean wind speeds expected in the area based on the terrain. However, adjustments made during vectorisation may have introduced inaccuracies, especially near the map borders. Despite this, pre-edit evaluations yielded similar results, confirming the reliability of the data. It is also noteworthy that the coast is not in the required range by WAsP and the map is bigger than the minimum area required by WAsP.

The chosen wind turbine model has a track record in Antarctica, enhancing confidence in its feasibility for this project. However, significant challenges remain, particularly in installation and commissioning. Transportation of the wind turbines from the coast to the station is a notable challenge. The integration of the wind farm into the station's existing electrical grid is another area of concern. Additional costs may arise from necessary upgrades or modifications to the grid.

The proposed wind farm consists of 32 turbines. This configuration requires more maintenance compared to a single large turbine and demands additional equipment. However, larger turbines present their own unique logistical and operational challenges, including higher transportation costs and the need for specialised infrastructure. While a single larger turbine could potentially have its perks, logistical challenges such as transportation and installation in Antarctica's extreme conditions increase complexity and risk. More-

over, data on larger wind turbines in similar environments is often inaccessible, making feasibility assessments challenging.

Financial calculations employed higher thresholds to ensure realistic estimations. While the Cost of Energy (COE) remains high compared to other studies in literature, it is still advantageous compared to the cost of diesel-generated electricity. Moreover, the environmental benefits are significant. Assuming diesel emits 370g CO_2/kWh [1] and the energy that would be replaced by the wind farm is at 222,250.00 kWh, around 80 MT of CO_2 and 2000 MT of CO_2 over the project's lifetime would be saved.

AWES presented several advantages over the wind farm. One notable benefit is their ease of transportation as an AWES unit is significantly more compact and lightweight compared to wind turbines, making logistical operations more feasible. Additionally, a single AWES unit has the potential to generate approximately one third of the energy output of a the wind farm, offering a promising alternative.

However, a major limitation of AWES technology is the lack of comprehensive data and studies, especially concerning its operational feasibility in Antarctica or cold regions. Currently, no detailed research exists on how AWES performs under extreme conditions such as low temperatures, high winds, and icing. This poses a challenge to assessing the practicality and reliability of the proposed AWES.

The estimation of the AEP for the AWES was conducted analytically without utilising tools or WAsP. AWES operate at higher altitudes compared to wind turbines, where wind conditions are less influenced by ground-level topographical features. Nevertheless, it is important to note that the calculations did not incorporate the effects of local terrain. Despite this limitation, the resulting AEP aligns well with the performance data provided by the AWES manufacturer.

From a financial perspective, AWES offers additional advantages. The costs associated with AWES are considerably lower than those for the current diesel generators or the wind farm. The system's reduced transportation and installation requirements further enhance its cost-effectiveness. However, it is critical to not that certain cost factors, such as logistical expenses and potential maintenance challenges specific to Antarctic conditions, were not included in the financial analysis. These costs could impact the overall feasibility.

The primary issue with the AWES assessment is that the technology lacks feasibility, both globally or in Antarctica. While AWES systems show theoretical promise, there isn't enough data validating their performance in real-world applications on a large scale. This issue is magnified in extreme climates, where factors such as icing, turbulent wind conditions, and operational durability remain largely untested. Addressing these uncertainties would require dedicated studies and experiments to evaluate AWES under Antarctic conditions.

Chapter 8

Conclusion

The research undertaken in this thesis laid a basis for the wind resource assessment and the results expected. Antarctica's wind energy resource was explored and the continent's atmospheric characteristics were taken into account. Operational aspects for the utilisation of wind energy in cold climates were explored to get a better understanding of the challenges that wind turbines face in similar environments. The NMS-III was further investigated to get an idea of the current status of energy supply at the station and to set an objective for the wind energy generation. An overview of the research stations currently utilising wind energy for their energy supply gave important information and offered a good starting point to pick a wind turbine for the wind resource assessment. Multiple wind turbine models were investigated and a choice was met with important factors taken into account. The fundamentals of wind resources energy assessment were explored to provide the knowledge needed for the subsequent WAsP modelling. Topographical inputs were extracted from REMA, wind measurements were extracted from the Meteorological Observatory Neumayer data and the wind turbine data was extracted from the manufacturer's data. A WAsP project was created and a wind farm with 32 wind turbines was added to reach the set objective. The AEP of the wind farm was calculated and a financial analysis that took into account important factors was implemented. The resulting COE showed that using wind energy would offer a financial advantage as is the case with other wind energy projects in Antarctica.

As for AWES, the fundamentals of ground-based AWES technology were examined, with a focus on methods for calculating the AEP of a selected system. While a straightforward approach was employed for the AEP calculation, additional tools and studies were also discussed. To enhance accuracy, radiosonde data was extracted from the Meteorological Observatory Neumayer data and used for the AEP estimation. Furthermore, a MATLAB model was utilised to perform a financial analysis of AWES, providing assumptions about the costs associated with implementing the technology. The AWES assessment offered optimistic results in regard to AEP and financial costs.

8.1 Outlook

The proposed wind energy systems offer a sustainable and environmentally friendly alternative to diesel-powered energy generation. Despite challenges in logistics, installation, and grid integration, the feasibility of the project is supported by data, past experiences with similar wind turbines, and the environmental benefits of reduced CO_2 emissions. Further detailed assessments of logistical requirements, grid integration, and storage options are recommended to optimise the project's implementation and performance. Although the wind resources assessment was implemented with a selected wind turbine, the assessment can be easily adjusted and be used for other wind turbines.

Airborne Wind Energy Systems represented a good alternative for the energy generation. Their advantages, including ease of transportation, high energy yield per unit, and lower operational costs, make them an attractive alternative to the wind farm. However, the current lack of data and field studies on AWES, particularly in Antarctic conditions, underscores the need for further research. Rigorous testing and feasibility analyses will be essential to determine whether AWES can become a reliable component of Antarctica's renewable energy infrastructure.

Bibliography

[1] U.S. Energy Information Administration. How much carbon dioxide is produced per kilowatthour of u.s. electricity generation? https://www.eia.gov/tools/faqs/faq.php?id=74&t=11. Accessed: 26/01/2025.

[2] Alfred-Wegener-Institut. An icon of german polar research https://www.awi.de/en/fleet-stations/research-vessel-and-cutter/research-vessel-and-icebreaker-polarstern/the-symbol-of-german-polar-research.html#:~:text=In%20a%20month%20of%20operations,consumed%20in%20the%20mess%20hall., . Accessed: 26/12/2024.

[3] Alfred-Wegener-Institut. Standard meteorological measurements https://www.awi.de/en/science/long-term-observations/atmosphere/antarctic-neumayer/meteorology/meteorological-measurements/standard-meteorological-measurements.html, . Accessed: 18/11/2024.

[4] Alfred-Wegener-Institut. Construction of the neumayer station iii https://www.awi.de/en/fleet-stations/stations/neumayer-station-iii/construction-of-neumayer-station-iii.html, . Accessed: 18/11/2024.

[5] Ian Baring-Gould, René Cattin, Michael Durstewitz, Mira Hulkkonen, Andreas Krenn, Timo Laakso, Antoine Lacroix, Esa Peltola, Göran Ronsten, Lars Tallhaug, and Tomas Wallenius. Wind energy in cold climates. In *IEA Wind Recommended Practice 13*. International Energy Agency, 2012.

[6] Lorenzo Battisti. *Wind Turbines in Cold Climates: Icing Impacts and Mitigation Systems*. Number ISBN 978-3-319-05190-1. Springer International Publishing Switzerland, 2015.

[7] Franziska Bockelmann, Ann-Kathrin Dreier, Joris Zimmermann, and Markus Peter. Renewable energy in antartica - photovoltaic for neumayer station iii. *Solar Energy Advances*, 2(100026), 2022.

[8] G.J. Bowden, Joan Adler, T. Dabbs, and J. Walter. The potential of wind energy in antarctica. 4(3):163–176, 1980.

[9] Thomas Bunge and Ellen Roß-Reginek. *Final Comprehensive Environmental Evaluation of the proposed activities: Construction if the Neumayer III Station, Operation of the Neumayer II Station and Dismantling of the existing Neumayer II Station and Removal of Materials from Antarctica*. German Federal Environmental Agency, 2005.

[10] The Polar Geospatial Center. Rema `https://www.pgc.umn.edu/data/rema/`. Accessed: 9/12/2024.

[11] Climatebiz. Commercial wind turbine cost `https://climatebiz.com/commercial-wind-turbine-cost/`. Accessed: 08/01/2025.

[12] Bergey Windpower Co. Designed for high reliability `https://www.bergey.com/products/off-grid-turbines/excel-10-off-grid/`. Accessed: 08/01/2025.

[13] BERGEY WINDPOWER CO. Retail price list `https://www.bergey.com/wp-content/uploads/2012/05/685d0a6f733ef2bbd913a05d15e442cd.pdf`. Accessed: 08/01/2025.

[14] COSMOS. Permanent antarctic home – hard, expensive and potentially bad for your health `https://cosmosmagazine.com/news/permanent-antarctic-home-bad-for-health/`. Accessed: 26/12/2024.

[15] Magnus de Witt, Changhyun Chung, and Joohan Lee. Mapping renewable energy among antarctic research stations. *Sustainability*, 16(426), 2024.

[16] Australian Antarctic Division. Up and running - antarctic's first major wind turbine. `https://www.antarctica.gov.au/news/2003/up-and-running-antarctics-first-major-wind-turbine/`, . Accessed: 11/11/2024.

[17] Australian Antartic Division. Wind power `https://www.antarctica.gov.au/antarctic-operations/stations/amenities-and-operations/renewable-energy/wind-power/`, . Accessed: 15/11/2024.

[18] Idriss El-Thalji, Imad Alsyouf, and Göran Ronsten. A model for assessing operation and maintenance cost adapted to wind farms in cold climate environment: based on onshore and offshore case studies. In *European Offshore Wind Conference proceedings*, Stockholm, Sweden, September 2009.

[19] SD Wind Energy. Research stations in antarctica: Top 8 antarctic bases `https://www.antarcticacruises.com/guide/research-stations-in-antarctica`, . Accessed: 28/01/2025.

[20] SD Wind Energy. Case studies https://sd-windenergy.com/wind-turbine-installation-case-studies/, . Accessed: 15/11/2024.

[21] SD Wind Energy. Sd6+ product specification https://sd-windenergy.com/files/4017/1155/4933/SD6__Product_Leaflet.pdf, . Accessed: 17/12/2024.

[22] SD Wind Energy. The small wind turbine of choice https://sd-windenergy.com/small-wind-turbines/sd6-6kw-wind-turbine/, . Accessed: 17/12/2024.

[23] EWT. Ewt to supply and install 3 dw54x-1mw turbines at ross island, antarctica https://ewtdirectwind.com/news/ewt-to-supply-and-install-3-dw54x-1mw-turbines-at-ross-island-antarctica/. Accessed: 15/11/2024.

[24] Uwe Fechner and Roland Schmehl. Airborne wind energy simulation software - a review. Delft University of Technology, 2024.

[25] Alfred-Wegener-Institut Helmholtz-Zentrum für Polar-und Meeresforschung. Polar research and supply vessel polarstern operated by the alfred-wegener-institute. *Journal of Large-Scale Research Facilities*, 3:A119, 2017. doi: 10.17815/jlsrf-3-163. URL http://dx.doi.org/10.17815/jlsrf-3-163.

[26] Patrice Godon. Dumont d'urville wind turbine. https://www.patricegodonpolarengineering.eu/wind-turbine/. Accessed: 15/11/2024.

[27] Antoine Guichard, Peter Magill, Patrice Godon, David Lyons, and Chris Brown. Potential for significant wind power generation at antarctic stations. *Seventh Symposium on Antarctic and Logistics Operations*, August 1996.

[28] Julia Hager. "princess elisabeth antarctica": zero emmission polar research https://polarjournal.ch/en/2022/05/30/princess-elisabeth-antarctica-zero-emission-polar-research/. Accessed: 15/11/2024.

[29] Duncan N. Heathfield, Cristopher A. Tenwolde, Niels G. Mortenson, and Hans E. Jorgensen. *WAsP Climate Analyst 3 Help Ficility*. Number ISBN 978-87-550-3609-3. Risø National Laboratory, Technical University of Denmark, Roskilde, Denmark.

[30] Ian Howat, Claire Porter, Myoung-Jon Noh, Erik Husby, Samuel Khuvis, Evan Danish, Karen Tomko, Judith Gardiner, Adelaide Negrete, Bidhyananda Yadav, James Klassen, Cole Kelleher, Michael Cloutier, Jesse Bakker, Jeremy Enos, Galen Arnold, Greg Bauer, and Paul Morin. The Reference Elevation Model of Antarctica - Mosaics, Version 2, 2022. URL https://doi.org/10.7910/DVN/EBW8UC.

[31] Rishikesh Joshi and Filippo Trevisi. Reference economic model for airborne wind energy systems (version 1). iea wind tcp task 48. https://doi.org/10.5281/zenodo.10959930. Technical report, June 2024.

[32] Rishikesh Joshi, Roland Schmehl, and Michiel Kruijff. Power curve modelling and scaling of fixed-wing ground-generation airborne wind energy systems. *Wind Energy Science*, 9:2195–2215, November 2024.

[33] WANG Kai-shana, WU Di, ZHENG Chong-wei, TAO Gui-sheng, LI Weia, GAO Yuan-bo, YU Yue, and WU Kai. A detail investigation on the antarctic wind energy. *China Ocean Eng.*, 37(4):698–708, 2023.

[34] Klaus Kerwel. Die neumayer-station iii `https://www.menschundtechnik.com/die-neumayer-station-iii/`. Accessed: 2/1/2025.

[35] Kitepower. Product summary - the kitepower falcon.

[36] Milan Klöwer, Thomas Jung, Gert König-Langlo, and Tido Semmler. Aspects of weather parameters at neumayer station, antarctica, and their representation in reanalysis and climate model data. *Meteorologische Zeitschrift*, (DOI: 10.1127/0941-2948/2013/0505), 2013.

[37] Gert König. Roughness length of an antaretie lee shelf. *Polarforschung*, 55(1):27–32, 1985.

[38] Lei Li. *Understanding seismic body waves retrieved from noise correlations :Toward a passive deep Earth imaging.* PhD thesis, Université Grenoble Alpes, November 2018.

[39] Oy Windside Production Ltd. Ws-12 `https://windside.com/products/ws-12/`, . Accessed: 08/01/2025.

[40] Oy Windside Production Ltd. Ws-0,15, . Accessed: 22/01/2025.

[41] Juan José Lucci, Maria Alegre, and Leonard Vigna. Renewables in antarctica: an assessment of progress to decarbonize the energy matrix of research facilities. *Antartic Science*, 34(5), 2022.

[42] Rolf H. Luchsinger. *Airborne Wind Energy.* Springer-Verlag, 2013.

[43] E.C. Malz, V. Verendel, and S. Gros. Computing the power profiles for an airborne wind energy system based on large-scale wind data. *Renewable Energy*, 162:766–778, August 2020.

[44] James Manwell, Jon McGowan, and Anthony Rogers. *Wind Energy Explained.* John Wiley and Sons Ltd., second edition, 2009.

[45] Jennifer Matthews. Arctic weather and climate. `https://nsidc.org/learn/parts-cryosphere/arctic-weather-and-climate/why-arctic-weather-and-climate-matter`. Accessed: 12/11/2024.

[46] XXXIII Antartic Treaty Consuliative Meeting. Ross island wind energy project: Sustainability through collaboration. 2010.

[47] Mario Milanese, Franco Taddei, and Stefano Milanese. *Airborne Wind Energy*. Springer-Verlag, 2013.

[48] Inc. Mission Critical Energy. Superwind micro wind turbines `https://missioncriticalenergy.com/superwind-micro-wind-turbines/`. Accessed: 08/01/2025.

[49] Niels Mortensen. *Wind resource assessment using the WAsP software*. Number 174. DTU Wind Energy, 2018.

[50] PBT International NV. Oil price information `https://pbt-international.com/price-information/`. Accessed: 26/12/2024.

[51] American Museum of Natural History. Katabatic winds. `https://www.amnh.org/learn-teach/curriculum-collections/antarctica/extreme-winds/katabatic-winds`. Accessed: 11/11/2024.

[52] Thomas R. Parish and David H. Bromwich. Reexamination of the near-surface airflow over the antarctic continent and implications on atmospheric circulations at high southern latitudes. 135:1964, 8 2006.

[53] Francesco Pellegrino. Energy: Antarctica, the mario zucchelli station becomes increasingly "renewable" `https://www.media.enea.it/en/press-releases-and-news/years-archive/year-2024/energy-antarctica-the-mario-zucchelli-station-becomes-increasingly-renewable.html`. Accessed: 15/11/2024.

[54] The Wind Power. Ross island wind power `https://www.thewindpower.net/windfarm_en_7204_ross-island.php`. Accessed: 15/11/2024.

[55] Pavel Prošek, Miloš Barták, Kamil Láska, Alois Suchánek, Josef Hájek, and Pavel Kapler. Facilities of j. g. mendel antarctic station: Technical and technological solutions with a special respect to energy sources. *Czech Polar Reports*, 3(1):38–57, March 2013.

[56] LLC RE Vision Consulting. Economic methodology for the evaluation of emerging renewable technologies, 10 2011.

[57] Mark Schelbergen, Peter C. Kalverla, Roland Schmehl, and Simon J. Watson. Clustering wind profile shapes to estimate airborne wind energy production. 5:1097–1120, August 2020.

[58] Roland Schmehl, Michael Noom, and Rolf van der Vlugt. *Airborne Wind Energy*. Springer-Verlag, 2013.

[59] Holger Schmithüsen. Continuous meteorological observations at Neumayer station (1982-03 et seq), 2023. URL https://doi.org/10.1594/PANGAEA.962313.

[60] Holger Schmithüsen and Hanno Müller. Radiosonde measurements from Neumayer Station (2018-10). PANGAEA, 2019. doi: 10.1594/PANGAEA.900640. URL https://doi.org/10.1594/PANGAEA.900640.

[61] Paul Smits. Kitepower's kite generates energy by spinning in figures of 8 at high altitude https://innovationorigins.com/en/kitepowers-kite-generates-energy-by-spinning-in-figures-of-8-at-high-altitude/, 2025. Accessed: 08/01/2025.

[62] Thomas Steuer. Windkraftanlage wind generator https://commons.wikimedia.org/wiki/File:2011_Versorgung_TSteuer-003.jpg. Accessed: 15/11/2024.

[63] superwind GmbH. Homepage https://www.superwind.com/. Accessed: 08/01/2025.

[64] Umweltbundesamt. Antarctica https://www.umweltbundesamt.de/en/topics/sustainability-strategies-international/antarctic/antarctica. Accessed: 22/01/2025.

[65] Étienne Vignon, Olivier Traullé, and Alexis Berne. On the fine vertical structure of the low troposphere over the coastal margins of east antarctica. *Atmospheric Chemistry and Physics*, 19:4659–4683, 2019.

[66] DTU Wind. Wind atlas analysis and application program. https://www.wasp.dk/. Accessed: 4/12/2024.

[67] windtest grevenbroich gmbh. Yield report https://www.windtest-nrw.de/worldwide/english/energy-assessment/standortbeurteilung-eng/yield-report.html. Accessed: 5/12/2024.

[68] Kate Winter. Antarctica's first zero emission research station shows that sustainable living is possible anywhere https://theconversation.com/antarcticas-first-zero-emission-research-station-shows-that-sustainable-living-is-possible-anywhere-113977. Accessed: 15/11/2024.

[69] ZARGES. The german antarctic research centre – neumayer-station iii https://www.zarges.com/en/the-german-antarctic-research-centre-neumayer-station-iii/. Accessed: 2/1/2025.

[70] Antarctica New Zealand. Wind farm upgrade https://www.scottbaseredevelopment.govt.nz/wind-farm-upgrade. Accessed: 15/11/2024.

[71] Mehrad Zolfaghari, Farhood Azarsina, and Alireza Kani. Feasibility analysis of airborne wind energy system (awes) pumping kite (pk). *Journal of Advanced Research in Fluid Mechanics and Thermal Sciences*, (74):133–143, 2020.

A Meteorological Observatory Neumayer Met. Station report

'Meteorological Observatory Neumayer' Met. Station report

Produced on 30/12/2024 at 15:43:08 by licenced user: Thomas Stegmann using WAsP Version: 12.09.0034

Site information

Anemometer height a.g.l	10m
Elevation a.s.l	198,4 m
Net altitude a.s.l	208,4 m
Mean air density	1,293 kg/m³

The observed wind climate anemometer data were collected at -70,65°N -8,25°E

The Met. station is located at co-ordinates (527734,2161467) in a map called 'NMS-III'.

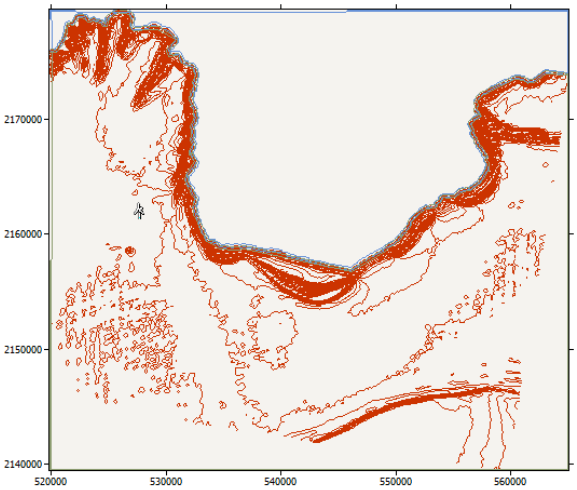

Site effects

Sector	Angle [°]	Or.Spd [%]	Or.Tur [°]	Or.Ti [%]	Or.Inc [°]	Obs.Spd [%]	Rgh.Spd [%]	Rix [%]
1	0	1,6	0,9	-1,0	-9.999,0	0,0	0,0	0,0
2	30	3,5	1,0	-1,0	-9.999,0	0,0	0,0	0,0
3	60	4,6	0,1	-1,0	-9.999,0	0,0	0,0	0,0
4	90	3,9	-0,9	-1,0	-9.999,0	0,0	0,0	0,0
5	120	1,9	-1,0	-1,0	-9.999,0	0,0	0,0	0,0
6	150	0,8	-0,1	-1,0	-9.999,0	0,0	0,0	0,0
7	180	1,6	0,9	-1,0	-9.999,0	0,0	0,0	0,0
8	210	3,5	1,0	-1,0	-9.999,0	0,0	0,0	0,7
9	240	4,6	0,1	-1,0	-9.999,0	0,0	0,0	0,0
10	270	3,9	-0,9	-1,0	-9.999,0	0,0	0,0	0,0
11	300	1,9	-1,0	-1,0	-9.999,0	0,0	0,0	0,0
12	330	0,8	-0,1	-1,0	-9.999,0	0,0	0,0	0,0

The all-sector RIX (ruggedness index) for the site is 0,1%

The observed wind climate for the site

> **Note:** The observed wind climate power density values are calculated for standard air density 1,225 kg/m³.

-	Weibull fit	Combined	Discrepancy
Mean wind speed	8,38 m/s	8,72 m/s	4,10%

Mean power density	1240 W/m²	1239 W/m²	-0,02%

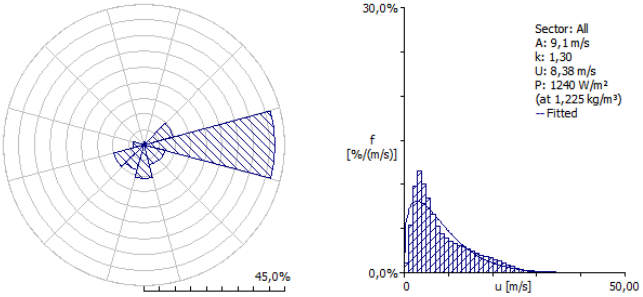

The self-prediction for the met. station

Note: The predicted power density values are calculated for site air density 1,293 kg/m³.

-	Observed	Predicted	Discrepancy
Mean wind speed	8,38 m/s	8,71 m/s	3,95%
Mean power density	1240 W/m²	1309 W/m²	5,59%

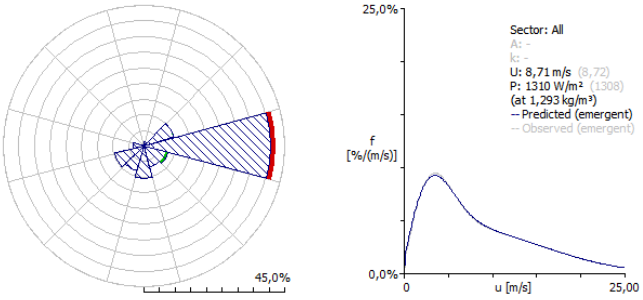

Data origins information

The Observed wind climate 'Neumayer Station III at 10,0 m' associated with this Met. station was imported by 'yazen' from a file called 'C:\Users\yazen\Desktop\OWC\Final\Neumayer Station III at 10,0 m.owc' , on a computer called 'DESKTOP-0EC4SNG'. The Observed wind climate file data were last modified on the 19/12/2024 at 17:07:14

There is no information about the origin of the 'GWC 1' Generalised wind climate associated with this Met. station.

WAsP project parameters

All of the WAsP project parameters have default values.

The Met. station is in a project called 'Project 1'.

GWC Profile model

Using the T-star profile model, with:

Sector	1	2	3	4	5	6	7	8	9	10	11	12
T-star (land) [K]	-0,073	-0,056	-0,042	-0,083	-0,168	-0,121	-0,101	-0,106	-0,108	-0,068	-0,066	-0,077
T-star std.dev (land) [K]	0,084	0,069	0,046	0,048	0,045	0,039	0,037	0,040	0,047	0,057	0,081	0,078
H-star (land) [/s]	1.368	1.117	1.650	1.982	1.011	486	380	461	779	1.049	1.286	1.045
T-star (water) [K]	-0,028	-0,031	-0,020	-0,021	-0,064	-0,076	-0,052	-0,040	-0,030	-0,026	-0,027	-0,024
T-star std.dev (water) [K]	0,035	0,035	0,026	0,025	0,043	0,039	0,041	0,040	0,035	0,034	0,036	0,034
H-star (water) [/s]	1.983	1.877	1.737	1.593	1.810	1.003	659	650	871	1.328	1.474	1.639

Geostrophic wind shear vectors:

Sector	1	2	3	4	5	6	7	8	9	10	11	12
Direction [°]	45	-5	-150	171	178	174	-180	-160	-118	-131	-154	-141
Magnitude [m/s]	0,00183	0,00167	0,00344	0,00367	0,00546	0,00508	0,00357	0,00269	0,00408	0,00419	0,00449	0,00254

B Generalised wind climate report

'GWC 1' Generalised wind climate report

Produced on 30/12/2024 at 11:08:27 by licenced user: Thomas Stegmann using WAsP Version: 12.09.0034

Reference conditions

Number of roughness lengths	5
Number of heights	5
Number of sectors	12
Roughness lengths	0,000 m; 0,030 m; 0,100 m; 0,400 m; 1,500 m
Heights a.g.l	10 m; 25 m; 50 m; 100 m; 200 m

Climate context

The generalised wind climate is located at -70,65°N -8,25°E

The Met. station is located at co-ordinates (527734,2161467) in a map called 'NMS-III'.

Barometric reference information

Mean temperature	-14,92 °
Ref. altitude for temperature a.s.l	35,3 m
Mean pressure	98.180 Pa
Ref. altitude for pressure a.s.l	33,3 m
Relative humidity	75,75772 %

Data source for barometric reference information

Barometric reference source: Rogier Floors from DTU 2020-11-25. Period: 2010-01-01-2020-01-01. Averaging method: mean of monthly means. Source data time interval: 1hr. Source data: ERA5 surface variables (https://cds.climate.copernicus.eu/cdsapp#!/dataset/reanalysis-era5-single-levels-monthly-means?tab=overview) and pressure levels (https://cds.climate.copernicus.eu/cdsapp#!/dataset/reanalysis-era5-pressure-levels-monthly-means)

Profile model

Using the T-star profile model, with:

Sector	1	2	3	4	5	6	7	8	9	10	11	12
T-star (land) [K]	-0,073	-0,056	-0,042	-0,083	-0,168	-0,121	-0,101	-0,106	-0,108	-0,068	-0,066	-0,077
T-star std.dev (land) [K]	0,084	0,069	0,046	0,048	0,045	0,039	0,037	0,040	0,047	0,057	0,081	0,078
H-star (land) [/s]	1.368	1.117	1.650	1.982	1.011	486	380	461	779	1.049	1.286	1.045
T-star (water) [K]	-0,028	-0,031	-0,020	-0,021	-0,064	-0,076	-0,052	-0,040	-0,030	-0,026	-0,027	-0,024
T-star std.dev (water) [K]	0,035	0,035	0,026	0,025	0,043	0,039	0,041	0,040	0,035	0,034	0,036	0,034
H-star (water) [/s]	1.983	1.877	1.737	1.593	1.810	1.003	659	650	871	1.328	1.474	1.639

The stability model inputs have the following origin information

Stability model inputs source: Stability input data imported by WAsP GUI, version 12.09.0034 at 2024-10-01T21:31:30Rogier Floors from DTU Wind Energy. 2022-05-18 (baro) and 2023-01-25 (meso). Period: 2011-01-01 to 2020-12-31. Averaging method: mean of monthly means. Source data time interval: 1hr. Source data: ERA5 surface variables (https://cds.climate.copernicus.eu/cdsapp#!/dataset/reanalysis-era5-single-levels-monthly-means?tab=overview) and pressure levels (https://cds.climate.copernicus.eu/cdsapp#!/dataset/reanalysis-era5-pressure-levels-monthly-means)Assembly: Rvea0359-32, Version=1.0.0.28, Culture=neutral, PublicKeyToken=null, built at UTC time: 2023-12-29T12:46:42Z

Geostrophic wind shear vectors:

Sector	1	2	3	4	5	6	7	8	9	10	11	12
Direction [°]	45	-5	-150	171	178	174	-180	-160	-118	-131	-154	-141
Magnitude [m/s]	0,00183	0,00167	0,00344	0,00367	0,00546	0,00508	0,00357	0,00269	0,00408	0,00419	0,00449	0,00254

The geostrophic shear vectors have the following origin information

Geostrophic shear vectors source: Geostrophic shear data imported by WAsP GUI, version 12.09.0034 at 2024-10-01T21:31:30Rogier Floors from DTU Wind Energy. 2022-05-18 (baro) and 2023-01-25 (meso). Period: 2011-01-01 to 2020-12-31. Averaging method: mean of monthly means. Source data time interval: 1hr. Source data: ERA5 surface variables (https://cds.climate.copernicus.eu/cdsapp#!/dataset/reanalysis-era5-single-levels-monthly-means?tab=overview) and pressure levels (https://cds.climate.copernicus.eu/cdsapp#!/dataset/reanalysis-era5-pressure-levels-monthly-means)Assembly: Rvea0359-32, Version=1.0.0.28, Culture=neutral, PublicKeyToken=null, built at UTC time: 2023-12-29T12:46:42Z

Generalised wind climate summary

		Roughness length 0,000 m	Roughness length 0,030 m	Roughness length 0,100 m	Roughness length 0,400 m	Roughness length 1,500 m
Height 10,0 m	Weibull A [m/s]	9,21	6,58	5,77	4,60	3,11
	Weibull k	1,39	1,31	1,31	1,31	1,31
	Mean speed U [m/s]	8,40	6,06	5,32	4,24	2,87
Height 25,0 m	Weibull A [m/s]	10,17	7,92	7,21	6,16	4,83
	Weibull k	1,42	1,37	1,37	1,37	1,37
	Mean speed U [m/s]	9,25	7,25	6,60	5,63	4,42

Height 50,0 m	Weibull A [m/s]	11,05	9,20	8,55	7,58	6,36
	Weibull k	1,47	1,44	1,44	1,44	1,44
	Mean speed U [m/s]	10,00	8,35	7,76	6,88	5,77
Height 100,0 m	Weibull A [m/s]	12,08	10,79	10,20	9,34	8,25
	Weibull k	1,52	1,54	1,54	1,54	1,54
	Mean speed U [m/s]	10,89	9,71	9,18	8,41	7,42
Height 200,0 m	Weibull A [m/s]	13,15	12,58	12,12	11,43	10,53
	Weibull k	1,53	1,56	1,58	1,59	1,62
	Mean speed U [m/s]	11,84	11,30	10,89	10,26	9,43

Detailed descriptions

Roughness length 0,000 m

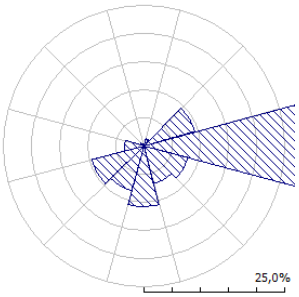

		Sec. 1 0°	Sec. 2 30°	Sec. 3 60°	Sec. 4 90°	Sec. 5 120°	Sec. 6 150°	Sec. 7 180°	Sec. 8 210°	Sec. 9 240°	Sec. 10 270°	Sec. 11 300°	Sec. 12 330°
Height 10,0 m	A [m/s]	3,2	6,3	9,6	14,5	6,2	3,9	4,4	4,4	6,8	6,4	4,1	3,6
	k	1,18	1,48	1,79	2,20	1,11	1,86	2,15	2,08	1,72	1,79	1,52	1,62
	U [m/s]	3,06	5,70	8,50	12,85	5,96	3,50	3,88	3,91	6,09	5,68	3,66	3,24
Height 25,0 m	A [m/s]	3,7	7,0	10,5	15,8	6,9	4,7	5,1	5,0	7,6	7,1	4,6	4,1
	k	1,27	1,54	1,82	2,22	1,15	2,13	2,42	2,31	1,78	1,88	1,65	1,76
	U [m/s]	3,44	6,30	9,29	14,02	6,58	4,13	4,48	4,47	6,73	6,28	4,12	3,63
Height 50,0 m	A [m/s]	4,1	7,6	11,2	16,9	7,6	5,5	5,8	5,7	8,2	7,7	5,1	4,5
	k	1,29	1,61	1,87	2,26	1,20	2,34	2,53	2,37	1,85	1,92	1,63	1,74
	U [m/s]	3,83	6,85	9,96	14,97	7,17	4,88	5,11	5,03	7,32	6,85	4,59	4,04
Height 100,0 m	A [m/s]	4,7	8,5	12,1	18,1	8,6	6,7	6,5	6,4	9,1	8,5	5,8	5,2
	k	1,28	1,61	1,88	2,31	1,26	2,51	2,58	2,38	1,85	1,91	1,61	1,71
	U [m/s]	4,39	7,58	10,76	16,04	7,96	5,93	5,80	5,64	8,05	7,58	5,24	4,60
Height 200,0 m	A [m/s]	5,6	9,6	13,2	19,6	9,9	7,7	6,7	6,5	10,0	9,6	6,7	5,9
	k	1,27	1,62	1,89	2,32	1,30	2,62	2,59	2,41	1,86	1,90	1,59	1,68
	U [m/s]	5,17	8,60	11,76	17,35	9,10	6,85	5,97	5,79	8,86	8,50	6,02	5,30
Freq. [%]		0,4	1,3	9,3	40,7	8,1	7,0	10,7	8,2	9,6	3,5	0,7	0,4

Roughness length 0,030 m

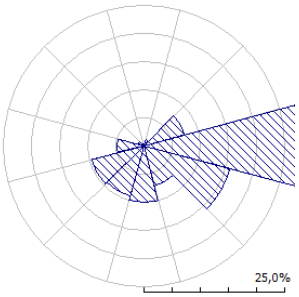

		Sec. 1 0°	Sec. 2 30°	Sec. 3 60°	Sec. 4 90°	Sec. 5 120°	Sec. 6 150°	Sec. 7 180°	Sec. 8 210°	Sec. 9 240°	Sec. 10 270°	Sec. 11 300°	Sec. 12 330°
Height 10,0 m	A [m/s]	2,3	4,4	7,2	10,4	8,3	2,9	2,9	2,9	4,1	4,5	3,6	2,7
	k	1,12	1,37	1,75	2,06	1,49	1,06	1,88	1,85	1,43	1,65	1,43	1,40
	U [m/s]	2,22	4,01	6,43	9,26	7,54	2,82	2,58	2,58	3,76	4,07	3,30	2,46
Height 25,0 m	A [m/s]	3,1	5,3	8,5	12,3	10,0	3,7	3,8	3,8	5,2	5,5	4,5	3,5
	k	1,36	1,47	1,80	2,11	1,54	1,16	2,19	2,20	1,57	1,79	1,63	1,71
	U [m/s]	2,85	4,81	7,56	10,88	8,97	3,49	3,32	3,36	4,63	4,93	4,07	3,16
Height 50,0 m	A [m/s]	4,0	6,2	9,6	13,9	11,5	4,5	4,6	4,7	6,2	6,5	5,5	4,5
	k	1,49	1,62	1,88	2,19	1,63	1,31	2,49	2,51	1,76	1,95	1,76	1,85
	U [m/s]	3,59	5,58	8,53	12,29	10,29	4,20	4,08	4,21	5,54	5,80	4,89	3,98

Height 100,0 m	A [m/s]	5,3	7,4	11,0	15,8	13,5	5,6	5,4	5,8	7,7	7,9	6,9	5,9
	k	1,50	1,65	1,97	2,34	1,78	1,43	2,62	2,69	1,89	2,01	1,76	1,89
	U [m/s]	4,75	6,62	9,71	14,00	12,04	5,11	4,78	5,12	6,83	7,00	6,10	5,19
Height 200,0 m	A [m/s]	7,1	9,0	12,7	18,4	16,4	6,5	5,2	5,8	9,5	9,7	8,8	7,5
	k	1,53	1,67	2,01	2,44	1,97	1,50	2,38	2,59	2,04	2,08	1,77	1,94
	U [m/s]	6,36	8,03	11,27	16,30	14,52	5,89	4,64	5,18	8,42	8,61	7,80	6,65
Freq. [%]		0,4	1,1	7,4	32,9	15,7	7,3	10,0	9,1	9,6	4,8	1,2	0,4

Roughness length 0,100 m

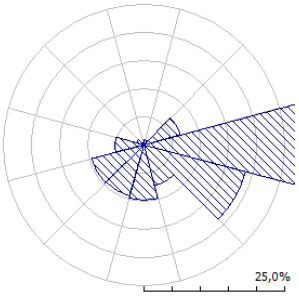

		Sec. 1 0°	Sec. 2 30°	Sec. 3 60°	Sec. 4 90°	Sec. 5 120°	Sec. 6 150°	Sec. 7 180°	Sec. 8 210°	Sec. 9 240°	Sec. 10 270°	Sec. 11 300°	Sec. 12 330°
Height 10,0 m	A [m/s]	2,1	3,8	6,4	9,1	7,9	2,6	2,5	2,5	3,5	4,0	3,3	2,4
	k	1,16	1,36	1,76	2,06	1,62	1,03	1,87	1,87	1,40	1,65	1,47	1,41
	U [m/s]	1,95	3,44	5,68	8,09	7,09	2,58	2,24	2,25	3,16	3,55	2,98	2,20
Height 25,0 m	A [m/s]	2,9	4,7	7,8	11,1	9,8	3,4	3,4	3,4	4,5	5,0	4,2	3,3
	k	1,42	1,46	1,81	2,11	1,68	1,10	2,18	2,22	1,54	1,80	1,67	1,71
	U [m/s]	2,60	4,27	6,91	9,85	8,74	3,27	2,98	3,03	4,04	4,45	3,79	2,92
Height 50,0 m	A [m/s]	3,7	5,6	9,0	12,8	11,5	4,2	4,2	4,4	5,5	6,0	5,2	4,2
	k	1,53	1,61	1,89	2,19	1,76	1,22	2,48	2,53	1,73	1,96	1,79	1,85
	U [m/s]	3,35	5,06	7,96	11,35	10,22	3,96	3,74	3,88	4,95	5,33	4,63	3,73
Height 100,0 m	A [m/s]	5,0	6,8	10,4	14,8	13,7	5,3	5,1	5,5	7,0	7,4	6,6	5,6
	k	1,55	1,63	1,99	2,34	1,93	1,34	2,63	2,74	1,87	2,01	1,80	1,89
	U [m/s]	4,51	6,09	9,20	13,14	12,12	4,86	4,52	4,85	6,21	6,53	5,83	4,94
Height 200,0 m	A [m/s]	6,9	8,4	12,2	17,5	16,7	6,4	5,1	5,8	8,8	9,2	8,5	7,3
	k	1,57	1,65	2,03	2,45	2,13	1,43	2,51	2,70	2,03	2,08	1,81	1,94
	U [m/s]	6,15	7,51	10,81	15,50	14,78	5,81	4,56	5,13	7,82	8,16	7,55	6,48
Freq. [%]		0,4	1,0	6,7	29,9	18,5	7,4	9,8	9,5	9,6	5,3	1,4	0,5

Roughness length 0,400 m

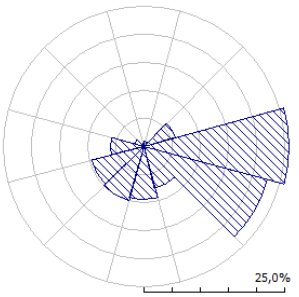

		Sec. 1 0°	Sec. 2 30°	Sec. 3 60°	Sec. 4 90°	Sec. 5 120°	Sec. 6 150°	Sec. 7 180°	Sec. 8 210°	Sec. 9 240°	Sec. 10 270°	Sec. 11 300°	Sec. 12 330°
Height 10,0 m	A [m/s]	1,7	2,9	5,1	7,2	6,7	2,2	2,0	2,0	2,6	3,1	2,7	2,0
	k	1,24	1,34	1,80	2,05	1,76	1,02	1,87	1,92	1,39	1,67	1,54	1,43
	U [m/s]	1,57	2,64	4,57	6,38	6,00	2,17	1,75	1,78	2,38	2,79	2,44	1,79
Height 25,0 m	A [m/s]	2,5	3,9	6,7	9,4	8,9	3,0	2,8	2,9	3,6	4,2	3,7	2,9
	k	1,53	1,44	1,85	2,11	1,83	1,08	2,18	2,28	1,54	1,81	1,74	1,73
	U [m/s]	2,25	3,51	5,96	8,34	7,92	2,93	2,49	2,57	3,28	3,76	3,32	2,54
Height 50,0 m	A [m/s]	3,4	4,8	8,0	11,3	10,8	3,9	3,7	3,9	4,7	5,3	4,7	3,8
	k	1,61	1,60	1,93	2,19	1,92	1,18	2,47	2,58	1,72	1,96	1,86	1,85
	U [m/s]	3,00	4,32	7,12	9,97	9,61	3,65	3,26	3,43	4,18	4,67	4,19	3,36
Height 100,0 m	A [m/s]	4,6	6,0	9,6	13,4	13,2	5,0	4,6	5,0	6,1	6,6	6,1	5,1
	k	1,63	1,61	2,04	2,33	2,10	1,29	2,64	2,82	1,86	2,01	1,86	1,89
	U [m/s]	4,16	5,35	8,47	11,88	11,71	4,58	4,11	4,45	5,43	5,88	5,40	4,56

Height 200,0 m	A [m/s]	6,5	7,6	11,5	16,2	16,4	6,2	4,9	5,6	8,0	8,5	8,0	6,9
	k	1,65	1,63	2,08	2,45	2,33	1,39	2,58	2,83	2,03	2,09	1,87	1,94
	U [m/s]	5,83	6,76	10,18	14,33	14,57	5,67	4,39	4,99	7,05	7,52	7,13	6,16
Freq. [%]		0,4	0,9	5,7	25,7	22,7	7,6	9,4	10,0	9,6	5,9	1,7	0,5

Roughness length 1,500 m

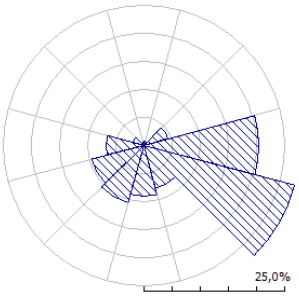

		Sec. 1 0°	Sec. 2 30°	Sec. 3 60°	Sec. 4 90°	Sec. 5 120°	Sec. 6 150°	Sec. 7 180°	Sec. 8 210°	Sec. 9 240°	Sec. 10 270°	Sec. 11 300°	Sec. 12 330°
Height 10,0 m	A [m/s]	1,2	1,8	3,5	4,8	4,8	1,6	1,3	1,4	1,7	2,1	1,9	1,4
	k	1,36	1,32	1,85	2,05	1,89	1,04	1,90	1,99	1,40	1,69	1,63	1,48
	U [m/s]	1,08	1,69	3,14	4,26	4,24	1,58	1,16	1,21	1,52	1,87	1,69	1,25
Height 25,0 m	A [m/s]	2,0	2,9	5,3	7,3	7,3	2,6	2,2	2,3	2,7	3,3	3,0	2,3
	k	1,69	1,42	1,91	2,10	1,96	1,11	2,23	2,39	1,57	1,85	1,84	1,79
	U [m/s]	1,78	2,60	4,74	6,44	6,47	2,46	1,92	2,02	2,43	2,91	2,65	2,04
Height 50,0 m	A [m/s]	2,8	3,8	6,8	9,3	9,5	3,5	3,0	3,2	3,7	4,4	4,0	3,2
	k	1,70	1,55	1,99	2,19	2,07	1,20	2,49	2,66	1,73	1,97	1,92	1,86
	U [m/s]	2,54	3,42	6,05	8,23	8,38	3,25	2,69	2,88	3,33	3,86	3,57	2,87
Height 100,0 m	A [m/s]	4,1	5,0	8,5	11,6	12,1	4,6	4,0	4,4	5,1	5,7	5,4	4,6
	k	1,72	1,57	2,10	2,34	2,25	1,31	2,69	2,91	1,88	2,03	1,92	1,90
	U [m/s]	3,66	4,45	7,54	10,29	10,69	4,25	3,59	3,95	4,57	5,09	4,80	4,07
Height 200,0 m	A [m/s]	6,0	6,5	10,6	14,5	15,5	6,0	4,6	5,3	7,0	7,6	7,4	6,4
	k	1,74	1,59	2,15	2,46	2,51	1,42	2,68	2,99	2,06	2,10	1,93	1,94
	U [m/s]	5,32	5,83	9,39	12,86	13,77	5,49	4,09	4,73	6,21	6,75	6,54	5,70
Freq. [%]		0,4	0,8	4,4	20,4	27,7	7,8	9,0	10,6	9,7	6,7	2,0	0,5

C Resource grid report

'Resource grid 2' Resource grid report

Produced on 30/12/2024 at 14:38:38 by licenced user: Thomas Stegmann using WAsP Version: 12.09.0034

Grid Setup

Column count	217
Row count	193
Calculation sites	41881
Resolution	100 m
Boundary extent	(522950, 2150015) to (544650, 2169315)
Nodes extent	(523000, 2150065) to (544600, 2169265)
Height a.g.l.	9m

Results

Mean Speed [m/s]

Maximum Value	34,98 m/s at (531400, 2167765)
Minimum Value	0,93 m/s at (533200, 2160165)
Mean Value	8,38 m/s

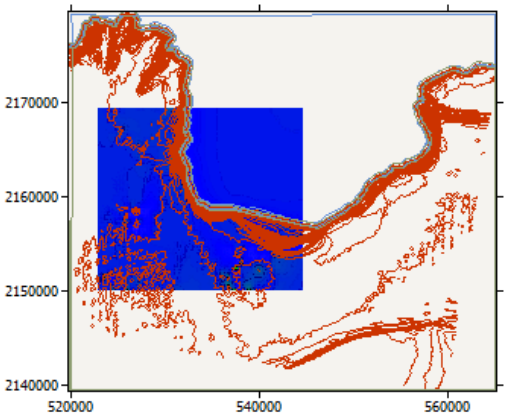

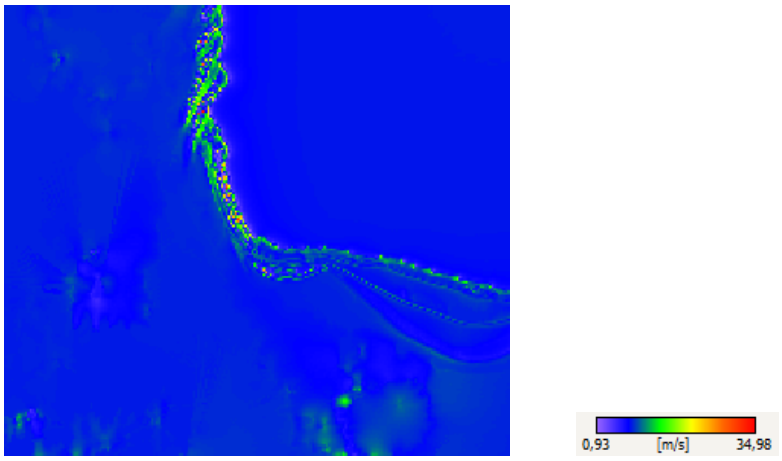

Power Density [W/m²]

Maximum Value	116823 W/m² at (531400, 2167765)
Minimum Value	2 W/m² at (533200, 2160165)
Mean Value	1290 W/m²

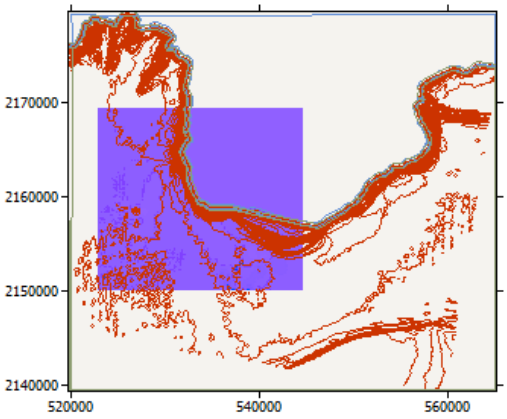

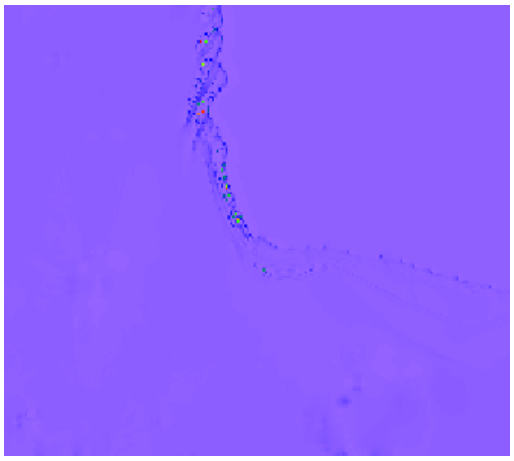

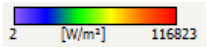

AEP [MWh]

Maximum Value	56,501 MWh at (531900, 2168365)
Minimum Value	0,026 MWh at (533200, 2160165)
Mean Value	28,245 MWh

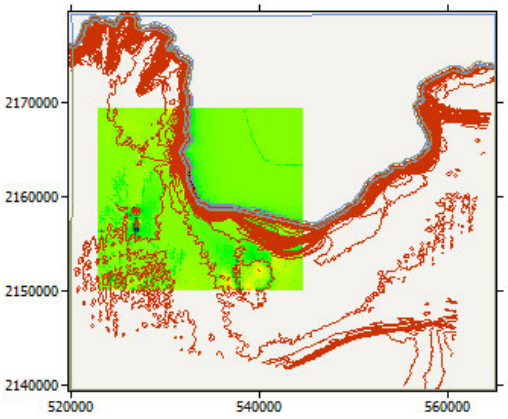

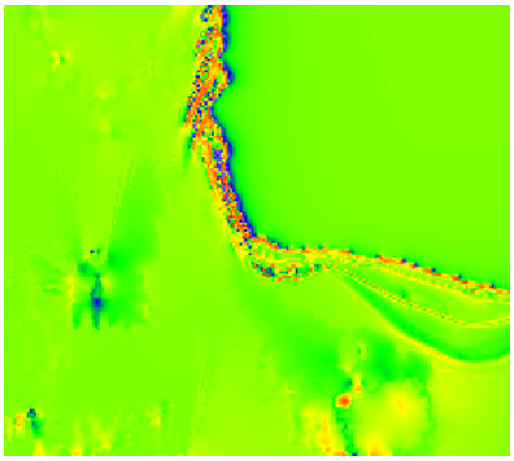

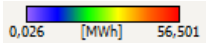

Capacity factor [%]

Maximum Value	107,4% at (531900, 2168365)
Minimum Value	0,0% at (533200, 2160165)
Mean Value	53,7%

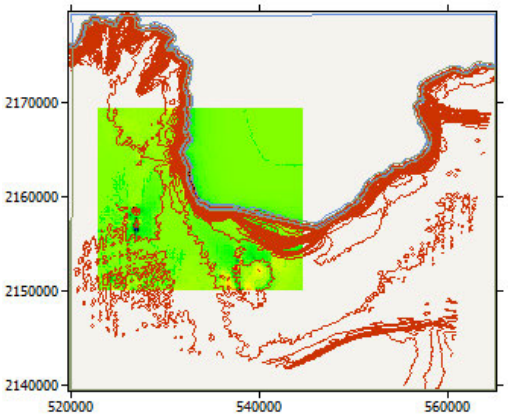

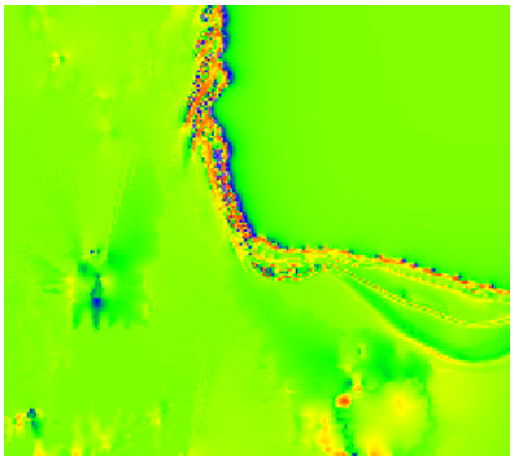

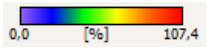

RIX [%]

Maximum Value	19,1% at (534800, 2157865)
Minimum Value	0,0% at (544600, 2169265)
Mean Value	2,4%

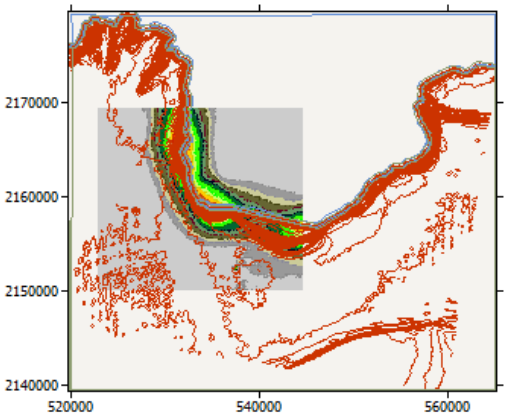

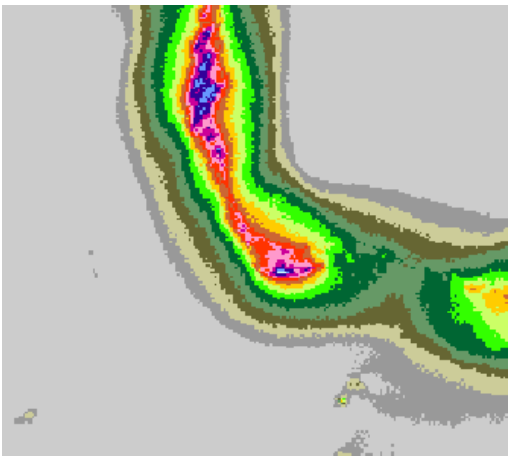

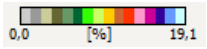

Wind turbine generator and adaptation policy

A wind turbine generator called 'SD6' was used to calculate the AEP.

The turbine is stall controlled.

The turbine has a rated power of 6 kW.

The WTG's only performance table was used for calculations with adaptation (extrapolation). The table used has an air density of 1,225 kg/m³.

The IEC method was used.

Data origins information

The Vector map ''NMS-III'' associated with this Resource grid contains the following vector data layers:

- Elevation layer named 'NMS-III' was imported by 'yazen' from a file called 'C:\Users\yazen\Desktop\SRB-SEND\WAsP-Final-V2.map' , on a computer called 'DESKTOP-0EC4SNG'. The NMS-III file data were last modified on the 12/12/2024 at 16:05:38
- Roughness layer named 'NMS-III' was imported by 'yazen' from a file called 'C:\Users\yazen\Desktop\SRB-SEND\WAsP-Final-V2.map' , on a computer called 'DESKTOP-0EC4SNG'. The NMS-III file data were last modified on the 12/12/2024 at 16:05:38

There is no information about the origin of the 'GWC 1' Generalised wind climate associated with this Resource grid.

The Wind turbine generator 'SD6' associated with this Resource grid was imported by 'yazen' from a file called 'C:\Users\yazen\Desktop\Master Arbeit\Execution\WaSP\SD6+.wtg' , on a computer called 'DESKTOP-0EC4SNG'. The Wind turbine generator file data were last modified on the 23/11/2024 at 00:23:37

WAsP project parameters

All of the WAsP project parameters have default values.

The Resource grid is in a project called 'Project 1'.

Terrain analysis (IBZ) parameters

All of the Terrain analysis (IBZ) parameters have default values.

D Wind farm report

'Turbine cluster 3' Wind farm report

Produced on 30/12/2024 at 14:46:08 by licenced user: Thomas Stegmann using WAsP Version: 12.09.0034

Site information

Site count	32
Uniform hub height a.g.l	9 m

The Wind farm lies in a map called 'NMS-III'.

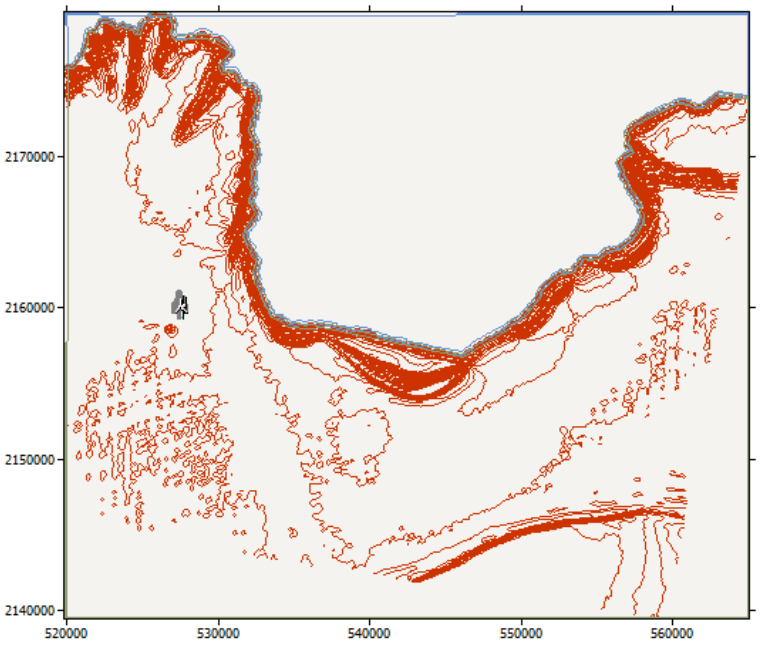

Summary results

	Total	Average	Minimum	Maximum
Net AEP [MWh]	809,953	25,311	24,417	27,216
Gross AEP [MWh]	828,325	25,885	24,615	27,436
Wake loss [%]	2,22	-	-	-
Capacity factor [%]	48,1	-	46,4	51,7

Site results

Site	Location [m]	Turbine	Elevation [m] a.s.l.	Height [m] a.g.l.	Air density [kg/m³]	Net AEP [MWh]	Wake loss [%]	Capacity factor [%]
Turbine site-1	(527495,6, 2159856,0)	SD6	200,4	9,0	1,293	26,695	2,52	50,8

Turbine site-2	(527495,6, 2159796,0)	SD6	200,3	9,0	1,293	26,606	2,78	50,6
Turbine site-3	(527495,6, 2159736,0)	SD6	200,3	9,0	1,293	26,608	2,81	50,6
Turbine site-4	(527495,6, 2159676,0)	SD6	200,2	9,0	1,293	26,612	2,65	50,6
Turbine site-5	(527495,6, 2159556,0)	SD6	200,0	9,0	1,293	26,658	2,59	50,7
Turbine site-6	(527495,6, 2159496,0)	SD6	199,9	9,0	1,293	26,536	2,75	50,5
Turbine site-7	(527495,6, 2159436,0)	SD6	164,5	9,0	1,299	24,674	3,14	46,9
Turbine site-8	(527495,6, 2159376,0)	SD6	165,6	9,0	1,299	24,777	2,76	47,1
Turbine site-9	(527555,6, 2159856,0)	SD6	200,3	9,0	1,293	26,679	2,56	50,7
Turbine site-10	(527555,6, 2159796,0)	SD6	157,1	9,0	1,301	24,744	3,21	47,0
Turbine site-11	(527555,6, 2159736,0)	SD6	158,2	9,0	1,300	24,695	3,17	47,0
Turbine site-12	(527555,6, 2159676,0)	SD6	159,3	9,0	1,300	24,851	2,83	47,2
Turbine site-13	(527555,6, 2159556,0)	SD6	161,4	9,0	1,300	24,741	2,95	47,0
Turbine site-14	(527555,6, 2159496,0)	SD6	162,4	9,0	1,300	24,652	3,16	46,9
Turbine site-15	(527555,6, 2159436,0)	SD6	163,5	9,0	1,299	24,675	3,08	46,9
Turbine site-16	(527555,6, 2159376,0)	SD6	164,8	9,0	1,299	24,679	2,58	46,9
Turbine site-17	(527615,6, 2159856,0)	SD6	155,8	9,0	1,301	24,922	2,63	47,4
Turbine site-18	(527615,6, 2159796,0)	SD6	156,7	9,0	1,301	24,769	2,73	47,1
Turbine site-19	(527615,6, 2159736,0)	SD6	158,1	9,0	1,300	24,769	2,68	47,1
Turbine site-20	(527615,6, 2159676,0)	SD6	200,0	9,0	1,293	26,785	2,04	50,9
Turbine site-21	(527615,6, 2159556,0)	SD6	155,3	9,0	1,301	24,590	2,57	46,8
Turbine site-22	(527615,6, 2159496,0)	SD6	156,3	9,0	1,301	24,523	2,70	46,6
Turbine site-23	(527615,6, 2159436,0)	SD6	158,2	9,0	1,300	24,417	2,63	46,4
Turbine site-24	(527615,6, 2159376,0)	SD6	160,1	9,0	1,300	24,634	2,10	46,8
Turbine site-25	(527675,6, 2159856,0)	SD6	200,1	9,0	1,293	27,216	0,80	51,7
Turbine site-26	(527675,6, 2159796,0)	SD6	151,1	9,0	1,302	25,040	0,80	47,6
Turbine site-27	(527675,6, 2159736,0)	SD6	152,0	9,0	1,301	25,157	0,72	47,8

Turbine site-28	(527675,6, 2159676,0)	SD6	153,9	9,0	1,301	25,139	0,46	47,8
Turbine site-29	(527675,6, 2159556,0)	SD6	156,6	9,0	1,301	25,062	0,77	47,7
Turbine site-30	(527675,6, 2159496,0)	SD6	152,6	9,0	1,301	24,839	0,73	47,2
Turbine site-31	(527675,6, 2159436,0)	SD6	153,4	9,0	1,301	24,641	0,61	46,8
Turbine site-32	(527675,6, 2159376,0)	SD6	154,0	9,0	1,301	24,569	0,19	46,7

Site wind climates

Site	Location [m]	H [m]	A [m/s]	k	U [m/s]	E [W/m²]	RIX [%]	dRIX [%]
Turbine site-1	(527495,6, 2159856,0)	9,0	9,4	1,39	8,58	1252	0,1	0,1
Turbine site-2	(527495,6, 2159796,0)	9,0	9,4	1,39	8,58	1250	0,0	0,0
Turbine site-3	(527495,6, 2159736,0)	9,0	9,4	1,39	8,58	1251	0,1	0,1
Turbine site-4	(527495,6, 2159676,0)	9,0	9,4	1,39	8,56	1238	0,0	0,0
Turbine site-5	(527495,6, 2159556,0)	9,0	9,4	1,39	8,57	1240	0,1	0,0
Turbine site-6	(527495,6, 2159496,0)	9,0	9,4	1,40	8,53	1221	0,1	0,0
Turbine site-7	(527495,6, 2159436,0)	9,0	8,9	1,38	8,08	1056	0,0	0,0
Turbine site-8	(527495,6, 2159376,0)	9,0	8,8	1,39	8,07	1048	0,0	0,0
Turbine site-9	(527555,6, 2159856,0)	9,0	9,4	1,39	8,58	1252	0,1	0,0
Turbine site-10	(527555,6, 2159796,0)	9,0	8,9	1,38	8,10	1069	0,1	0,0
Turbine site-11	(527555,6, 2159736,0)	9,0	8,9	1,38	8,09	1064	0,0	0,0
Turbine site-12	(527555,6, 2159676,0)	9,0	8,9	1,38	8,10	1071	0,0	0,0
Turbine site-13	(527555,6, 2159556,0)	9,0	8,9	1,38	8,08	1057	0,1	0,0
Turbine site-14	(527555,6, 2159496,0)	9,0	8,8	1,38	8,07	1052	0,0	0,0
Turbine site-15	(527555,6, 2159436,0)	9,0	8,8	1,39	8,07	1047	0,0	0,0
Turbine site-16	(527555,6, 2159376,0)	9,0	8,8	1,39	8,03	1032	0,0	0,0
Turbine site-17	(527615,6, 2159856,0)	9,0	8,9	1,38	8,10	1071	0,1	0,0
Turbine site-18	(527615,6, 2159796,0)	9,0	8,8	1,38	8,07	1059	0,1	0,0

Turbine site-19	(527615,6, 2159736,0)	9,0	8,8	1,38	8,07	1053	0,1	0,0
Turbine site-20	(527615,6, 2159676,0)	9,0	9,4	1,39	8,56	1246	0,1	0,0
Turbine site-21	(527615,6, 2159556,0)	9,0	8,8	1,38	8,01	1031	0,0	0,0
Turbine site-22	(527615,6, 2159496,0)	9,0	8,8	1,38	8,00	1028	0,0	0,0
Turbine site-23	(527615,6, 2159436,0)	9,0	8,7	1,39	7,97	1010	0,1	0,0
Turbine site-24	(527615,6, 2159376,0)	9,0	8,8	1,39	7,99	1016	0,1	0,0
Turbine site-25	(527675,6, 2159856,0)	9,0	9,4	1,39	8,59	1258	0,1	0,0
Turbine site-26	(527675,6, 2159796,0)	9,0	8,8	1,38	8,01	1036	0,1	0,0
Turbine site-27	(527675,6, 2159736,0)	9,0	8,8	1,38	8,04	1045	0,0	0,0
Turbine site-28	(527675,6, 2159676,0)	9,0	8,8	1,38	8,02	1038	0,0	0,0
Turbine site-29	(527675,6, 2159556,0)	9,0	8,8	1,38	8,02	1032	0,0	0,0
Turbine site-30	(527675,6, 2159496,0)	9,0	8,7	1,39	7,95	1002	0,1	0,0
Turbine site-31	(527675,6, 2159436,0)	9,0	8,6	1,40	7,89	969	0,0	0,0
Turbine site-32	(527675,6, 2159376,0)	9,0	8,6	1,40	7,84	952	0,0	0,0

Calculation of annual output for 'Turbine cluster 3'

Sector 1 (0°)

Site	A [m/s]	k	Freq. [%]	U [m/s]	MWh (free)	MWh (Park 2)	Eff. [%]
Turbine site-1	3,3	1,17	0,44	3,11	0,018	0,018	100,00
Turbine site-2	3,3	1,17	0,44	3,11	0,018	0,017	92,62
Turbine site-3	3,3	1,17	0,44	3,11	0,018	0,017	91,82
Turbine site-4	3,3	1,17	0,44	3,12	0,019	0,017	91,32
Turbine site-5	3,3	1,18	0,45	3,13	0,019	0,018	96,36
Turbine site-6	3,3	1,18	0,45	3,14	0,019	0,017	90,08
Turbine site-7	3,5	1,16	0,49	3,31	0,025	0,022	90,47
Turbine site-8	3,5	1,16	0,50	3,33	0,025	0,023	89,98
Turbine site-9	3,3	1,17	0,44	3,11	0,018	0,018	100,00
Turbine site-10	3,3	1,15	0,47	3,14	0,020	0,019	92,83
Turbine site-11	3,4	1,16	0,47	3,18	0,021	0,020	92,16
Turbine site-12	3,3	1,15	0,47	3,18	0,021	0,020	91,35
Turbine site-13	3,4	1,16	0,48	3,24	0,023	0,022	95,79
Turbine site-14	3,5	1,16	0,49	3,29	0,024	0,022	89,45

Turbine site-15	3,5	1,16	0,49	3,30	0,024	0,022	88,47
Turbine site-16	3,5	1,16	0,50	3,36	0,026	0,023	89,05
Turbine site-17	3,2	1,15	0,46	3,08	0,019	0,019	100,00
Turbine site-18	3,3	1,15	0,47	3,17	0,021	0,020	92,99
Turbine site-19	3,4	1,16	0,48	3,20	0,022	0,020	92,08
Turbine site-20	3,3	1,17	0,44	3,12	0,019	0,017	90,90
Turbine site-21	3,4	1,16	0,48	3,23	0,023	0,022	95,81
Turbine site-22	3,4	1,16	0,49	3,26	0,024	0,021	89,36
Turbine site-23	3,5	1,16	0,50	3,33	0,025	0,023	88,73
Turbine site-24	3,5	1,16	0,50	3,33	0,025	0,022	88,78
Turbine site-25	3,3	1,17	0,44	3,11	0,018	0,018	100,00
Turbine site-26	3,3	1,15	0,47	3,14	0,021	0,019	92,86
Turbine site-27	3,3	1,15	0,47	3,12	0,020	0,019	91,87
Turbine site-28	3,4	1,16	0,48	3,18	0,022	0,020	91,67
Turbine site-29	3,4	1,16	0,48	3,22	0,022	0,022	96,52
Turbine site-30	3,4	1,16	0,49	3,27	0,024	0,022	90,61
Turbine site-31	3,5	1,16	0,51	3,36	0,027	0,024	90,31
Turbine site-32	3,6	1,17	0,53	3,43	0,029	0,026	90,38
Sector 1 total	-	-	-	-	0,701	0,648	92,37

Sector 2 (30°)

Site	A [m/s]	k	Freq. [%]	U [m/s]	MWh (free)	MWh (Park 2)	Eff. [%]
Turbine site-1	6,5	1,47	1,30	5,85	0,201	0,201	100,00
Turbine site-2	6,5	1,47	1,30	5,85	0,200	0,197	98,18
Turbine site-3	6,5	1,47	1,30	5,85	0,200	0,192	95,87
Turbine site-4	6,6	1,47	1,34	5,94	0,212	0,201	94,61
Turbine site-5	6,6	1,47	1,36	6,00	0,220	0,209	94,81
Turbine site-6	6,8	1,47	1,43	6,15	0,242	0,231	95,24
Turbine site-7	6,1	1,47	1,28	5,48	0,174	0,161	92,86
Turbine site-8	6,2	1,47	1,36	5,65	0,195	0,180	92,25
Turbine site-9	6,5	1,47	1,30	5,85	0,200	0,200	100,00
Turbine site-10	5,9	1,47	1,24	5,35	0,160	0,157	97,98
Turbine site-11	5,9	1,47	1,23	5,33	0,158	0,150	95,11
Turbine site-12	5,9	1,47	1,24	5,35	0,159	0,149	93,57
Turbine site-13	6,0	1,47	1,27	5,45	0,170	0,161	94,27
Turbine site-14	6,1	1,47	1,32	5,56	0,184	0,175	95,17
Turbine site-15	6,2	1,47	1,34	5,61	0,190	0,179	94,11
Turbine site-16	6,4	1,48	1,42	5,76	0,212	0,199	93,65
Turbine site-17	5,9	1,47	1,24	5,35	0,160	0,160	100,00
Turbine site-18	5,9	1,47	1,23	5,32	0,157	0,154	97,86

Turbine site-19	5,9	1,47	1,24	5,35	0,160	0,153	95,74
Turbine site-20	6,5	1,47	1,32	5,90	0,207	0,199	96,14
Turbine site-21	6,0	1,47	1,27	5,40	0,167	0,162	97,10
Turbine site-22	6,0	1,47	1,29	5,45	0,173	0,168	97,17
Turbine site-23	6,2	1,47	1,36	5,59	0,193	0,184	95,78
Turbine site-24	6,3	1,48	1,39	5,67	0,202	0,193	95,43
Turbine site-25	6,5	1,47	1,30	5,86	0,201	0,201	100,00
Turbine site-26	5,9	1,47	1,24	5,29	0,156	0,156	100,00
Turbine site-27	5,9	1,47	1,24	5,31	0,157	0,157	100,00
Turbine site-28	5,9	1,47	1,24	5,30	0,156	0,156	100,00
Turbine site-29	6,0	1,47	1,28	5,43	0,171	0,171	100,00
Turbine site-30	6,3	1,48	1,40	5,66	0,203	0,203	100,00
Turbine site-31	6,5	1,49	1,52	5,85	0,234	0,234	100,00
Turbine site-32	6,6	1,50	1,61	5,97	0,257	0,257	100,00
Sector 2 total	-	-	-	-	6,031	5,847	96,95

Sector 3 (60°)

Site	A [m/s]	k	Freq. [%]	U [m/s]	MWh (free)	MWh (Park 2)	Eff. [%]
Turbine site-1	10,2	1,77	10,06	9,08	3,163	3,163	100,00
Turbine site-2	10,2	1,77	10,00	9,04	3,129	3,040	97,16
Turbine site-3	10,2	1,77	10,02	9,06	3,142	3,029	96,40
Turbine site-4	10,2	1,77	10,16	9,12	3,212	3,095	96,36
Turbine site-5	10,3	1,77	10,30	9,20	3,295	3,258	98,90
Turbine site-6	10,4	1,77	10,38	9,23	3,334	3,246	97,37
Turbine site-7	8,9	1,78	8,85	7,96	2,312	2,202	95,25
Turbine site-8	9,0	1,78	8,85	7,98	2,322	2,207	95,06
Turbine site-9	10,2	1,77	10,00	9,05	3,132	3,132	100,00
Turbine site-10	9,0	1,78	8,99	8,03	2,381	2,305	96,83
Turbine site-11	9,0	1,78	8,93	7,99	2,347	2,263	96,40
Turbine site-12	9,0	1,78	8,95	8,02	2,366	2,282	96,44
Turbine site-13	9,0	1,78	8,94	8,00	2,355	2,342	99,46
Turbine site-14	9,0	1,78	8,89	7,98	2,332	2,262	96,96
Turbine site-15	9,0	1,78	8,88	7,98	2,332	2,249	96,45
Turbine site-16	8,9	1,78	8,80	7,93	2,288	2,207	96,43
Turbine site-17	9,0	1,78	9,00	8,04	2,391	2,391	100,00
Turbine site-18	9,0	1,78	8,94	7,98	2,345	2,308	98,43
Turbine site-19	9,0	1,78	8,97	7,99	2,357	2,323	98,52
Turbine site-20	10,2	1,77	10,13	9,10	3,198	3,163	98,91
Turbine site-21	8,9	1,78	8,92	7,92	2,315	2,315	100,00
Turbine site-22	8,9	1,78	8,88	7,90	2,292	2,257	98,48

Turbine site-23	8,8	1,78	8,78	7,84	2,242	2,208	98,47
Turbine site-24	8,9	1,78	8,81	7,88	2,269	2,235	98,50
Turbine site-25	10,3	1,77	10,14	9,13	3,213	3,213	100,00
Turbine site-26	8,9	1,78	8,95	7,93	2,326	2,326	100,00
Turbine site-27	9,0	1,78	8,98	7,96	2,348	2,348	100,00
Turbine site-28	8,9	1,78	8,94	7,92	2,321	2,321	100,00
Turbine site-29	8,9	1,78	8,94	7,94	2,327	2,327	100,00
Turbine site-30	8,9	1,78	8,89	7,88	2,289	2,289	100,00
Turbine site-31	8,8	1,78	8,75	7,80	2,216	2,216	100,00
Turbine site-32	8,7	1,78	8,66	7,74	2,165	2,165	100,00
Sector 3 total	-	-	-	-	82,055	80,686	98,33

Sector 4 (90°)

Site	A [m/s]	k	Freq. [%]	U [m/s]	MWh (free)	MWh (Park 2)	Eff. [%]
Turbine site-1	14,8	2,19	40,17	13,10	19,518	18,967	97,18
Turbine site-2	14,8	2,19	40,22	13,10	19,536	19,004	97,28
Turbine site-3	14,8	2,19	40,20	13,10	19,531	19,000	97,28
Turbine site-4	14,7	2,19	40,02	13,06	19,396	18,861	97,24
Turbine site-5	14,7	2,19	39,87	13,06	19,319	18,789	97,26
Turbine site-6	14,7	2,19	39,69	12,99	19,168	18,634	97,22
Turbine site-7	14,0	2,19	38,92	12,36	18,019	17,450	96,84
Turbine site-8	13,9	2,19	38,88	12,33	17,980	17,409	96,82
Turbine site-9	14,8	2,19	40,22	13,10	19,546	19,057	97,50
Turbine site-10	14,0	2,19	39,78	12,42	18,500	17,972	97,14
Turbine site-11	14,0	2,19	39,52	12,40	18,343	17,818	97,14
Turbine site-12	14,0	2,19	39,58	12,42	18,414	17,881	97,11
Turbine site-13	14,0	2,19	39,28	12,37	18,203	17,680	97,13
Turbine site-14	13,9	2,19	39,05	12,34	18,061	17,539	97,11
Turbine site-15	13,9	2,19	39,01	12,33	18,032	17,512	97,12
Turbine site-16	13,8	2,19	38,64	12,25	17,766	17,245	97,07
Turbine site-17	14,0	2,19	40,03	12,44	18,640	18,187	97,57
Turbine site-18	14,0	2,19	39,54	12,38	18,338	17,903	97,63
Turbine site-19	14,0	2,19	39,45	12,36	18,274	17,840	97,63
Turbine site-20	14,8	2,19	40,06	13,07	19,428	19,023	97,92
Turbine site-21	13,8	2,19	39,21	12,26	18,038	17,601	97,58
Turbine site-22	13,8	2,19	39,02	12,24	17,923	17,485	97,55
Turbine site-23	13,7	2,19	38,60	12,17	17,635	17,196	97,51
Turbine site-24	13,8	2,19	38,70	12,19	17,714	17,273	97,51
Turbine site-25	14,8	2,19	40,13	13,12	19,516	19,516	100,00
Turbine site-26	13,9	2,19	39,58	12,28	18,235	18,235	100,00

Turbine site-27	13,9	2,19	39,73	12,32	18,357	18,357	100,00
Turbine site-28	13,9	2,19	39,40	12,28	18,155	18,155	100,00
Turbine site-29	13,8	2,19	39,27	12,27	18,069	18,069	100,00
Turbine site-30	13,7	2,19	38,98	12,13	17,766	17,766	100,00
Turbine site-31	13,6	2,19	38,38	12,01	17,330	17,330	100,00
Turbine site-32	13,4	2,19	37,96	11,91	17,015	17,015	100,00
Sector 4 total	-	-	-	-	589,766	577,767	97,97

Sector 5 (120°)

Site	A [m/s]	k	Freq. [%]	U [m/s]	MWh (free)	MWh (Park 2)	Eff. [%]
Turbine site-1	6,2	1,11	7,94	5,99	1,322	1,256	95,02
Turbine site-2	6,2	1,11	7,96	6,00	1,325	1,263	95,28
Turbine site-3	6,2	1,11	7,95	6,00	1,324	1,275	96,30
Turbine site-4	6,2	1,11	7,92	5,99	1,316	1,296	98,47
Turbine site-5	6,2	1,11	7,89	5,98	1,308	1,243	95,04
Turbine site-6	6,2	1,11	7,86	5,96	1,297	1,236	95,24
Turbine site-7	7,9	1,23	10,27	7,35	2,293	2,225	97,01
Turbine site-8	7,8	1,23	10,16	7,31	2,256	2,256	100,00
Turbine site-9	6,2	1,11	7,95	6,00	1,325	1,277	96,43
Turbine site-10	7,2	1,18	9,46	6,77	1,881	1,821	96,80
Turbine site-11	7,4	1,20	9,77	6,98	2,027	1,977	97,53
Turbine site-12	7,4	1,19	9,68	6,93	1,989	1,980	99,52
Turbine site-13	7,6	1,21	9,86	7,09	2,094	2,029	96,92
Turbine site-14	7,7	1,22	10,04	7,21	2,184	2,116	96,91
Turbine site-15	7,7	1,22	10,05	7,23	2,195	2,136	97,32
Turbine site-16	7,9	1,24	10,32	7,40	2,331	2,331	100,00
Turbine site-17	6,9	1,16	9,25	6,59	1,767	1,743	98,62
Turbine site-18	7,4	1,19	9,74	6,94	2,007	1,981	98,70
Turbine site-19	7,4	1,20	9,75	6,99	2,027	2,001	98,72
Turbine site-20	6,2	1,11	7,93	5,99	1,318	1,318	100,00
Turbine site-21	7,6	1,21	9,95	7,09	2,111	2,085	98,74
Turbine site-22	7,7	1,22	10,14	7,20	2,203	2,174	98,70
Turbine site-23	8,0	1,25	10,48	7,41	2,371	2,341	98,71
Turbine site-24	7,9	1,24	10,31	7,34	2,304	2,304	100,00
Turbine site-25	6,2	1,11	7,93	5,99	1,316	1,316	100,00
Turbine site-26	7,3	1,19	9,67	6,85	1,957	1,957	100,00
Turbine site-27	7,2	1,18	9,52	6,76	1,889	1,889	100,00
Turbine site-28	7,4	1,20	9,84	6,98	2,045	2,045	100,00
Turbine site-29	7,5	1,21	9,85	7,03	2,070	2,070	100,00
Turbine site-30	7,6	1,22	9,95	7,10	2,120	2,120	100,00

Turbine site-31	7,9	1,26	10,42	7,37	2,343	2,343	100,00
Turbine site-32	8,1	1,28	10,73	7,53	2,490	2,490	100,00
Sector 5 total	-	-	-	-	60,807	59,894	98,50

Sector 6 (150°)

Site	A [m/s]	k	Freq. [%]	U [m/s]	MWh (free)	MWh (Park 2)	Eff. [%]
Turbine site-1	3,9	1,83	6,83	3,49	0,209	0,185	88,54
Turbine site-2	3,9	1,83	6,85	3,49	0,211	0,189	89,71
Turbine site-3	3,9	1,83	6,84	3,49	0,210	0,192	91,10
Turbine site-4	3,9	1,78	6,86	3,51	0,223	0,202	90,67
Turbine site-5	3,9	1,74	6,85	3,51	0,230	0,208	90,46
Turbine site-6	4,0	1,67	6,88	3,54	0,254	0,237	93,26
Turbine site-7	3,9	1,76	7,55	3,51	0,250	0,242	97,00
Turbine site-8	4,0	1,67	7,53	3,53	0,275	0,275	100,00
Turbine site-9	3,9	1,83	6,84	3,49	0,210	0,189	90,12
Turbine site-10	3,9	1,84	7,34	3,42	0,207	0,188	90,69
Turbine site-11	3,9	1,84	7,42	3,44	0,213	0,197	92,37
Turbine site-12	3,9	1,84	7,40	3,44	0,213	0,195	91,53
Turbine site-13	3,9	1,78	7,44	3,47	0,232	0,210	90,62
Turbine site-14	3,9	1,72	7,49	3,50	0,255	0,237	93,11
Turbine site-15	3,9	1,69	7,49	3,51	0,264	0,256	97,09
Turbine site-16	4,0	1,61	7,57	3,56	0,299	0,299	100,00
Turbine site-17	3,8	1,84	7,29	3,40	0,202	0,188	93,16
Turbine site-18	3,9	1,84	7,41	3,43	0,211	0,198	93,77
Turbine site-19	3,9	1,84	7,41	3,44	0,213	0,204	95,89
Turbine site-20	3,9	1,79	6,85	3,50	0,218	0,209	95,74
Turbine site-21	3,9	1,78	7,46	3,45	0,227	0,211	92,74
Turbine site-22	3,9	1,75	7,52	3,47	0,241	0,225	93,61
Turbine site-23	3,9	1,65	7,61	3,51	0,278	0,269	97,00
Turbine site-24	3,9	1,63	7,57	3,52	0,284	0,284	100,00
Turbine site-25	3,9	1,83	6,80	3,48	0,207	0,207	100,00
Turbine site-26	3,8	1,84	7,40	3,40	0,204	0,204	100,00
Turbine site-27	3,8	1,84	7,36	3,40	0,203	0,203	100,00
Turbine site-28	3,8	1,84	7,43	3,42	0,209	0,209	100,00
Turbine site-29	3,9	1,77	7,44	3,45	0,229	0,229	100,00
Turbine site-30	3,9	1,63	7,47	3,48	0,269	0,269	100,00
Turbine site-31	3,9	1,53	7,60	3,55	0,320	0,320	100,00
Turbine site-32	4,0	1,47	7,69	3,60	0,355	0,355	100,00
Sector 6 total	-	-	-	-	7,626	7,287	95,56

Sector 7 (180°)

Site	A [m/s]	k	Freq. [%]	U [m/s]	MWh (free)	MWh (Park 2)	Eff. [%]
Turbine site-1	4,4	2,11	10,65	3,92	0,407	0,357	87,85
Turbine site-2	4,4	2,11	10,66	3,92	0,407	0,358	87,90
Turbine site-3	4,4	2,11	10,66	3,92	0,408	0,360	88,36
Turbine site-4	4,4	2,11	10,70	3,94	0,415	0,397	95,81
Turbine site-5	4,5	2,11	10,71	3,95	0,418	0,376	89,90
Turbine site-6	4,5	2,11	10,78	3,96	0,426	0,389	91,29
Turbine site-7	4,2	2,11	10,66	3,75	0,346	0,316	91,34
Turbine site-8	4,3	2,11	10,75	3,78	0,358	0,358	100,00
Turbine site-9	4,4	2,11	10,65	3,92	0,406	0,355	87,37
Turbine site-10	4,2	2,12	10,57	3,70	0,325	0,278	85,62
Turbine site-11	4,2	2,12	10,56	3,70	0,326	0,282	86,63
Turbine site-12	4,2	2,12	10,57	3,71	0,329	0,311	94,67
Turbine site-13	4,2	2,12	10,66	3,74	0,342	0,307	89,90
Turbine site-14	4,2	2,12	10,71	3,76	0,349	0,316	90,46
Turbine site-15	4,3	2,12	10,73	3,76	0,353	0,322	91,32
Turbine site-16	4,3	2,11	10,81	3,79	0,364	0,364	100,00
Turbine site-17	4,2	2,12	10,53	3,68	0,317	0,273	86,11
Turbine site-18	4,2	2,12	10,56	3,69	0,324	0,277	85,64
Turbine site-19	4,2	2,12	10,62	3,71	0,332	0,285	85,89
Turbine site-20	4,4	2,11	10,69	3,93	0,412	0,392	95,19
Turbine site-21	4,2	2,12	10,66	3,71	0,331	0,298	89,94
Turbine site-22	4,2	2,12	10,68	3,72	0,334	0,302	90,43
Turbine site-23	4,2	2,11	10,74	3,74	0,344	0,314	91,42
Turbine site-24	4,2	2,11	10,78	3,75	0,351	0,351	100,00
Turbine site-25	4,4	2,11	10,62	3,92	0,404	0,359	88,95
Turbine site-26	4,1	2,12	10,57	3,67	0,316	0,277	87,67
Turbine site-27	4,1	2,12	10,57	3,67	0,316	0,279	88,31
Turbine site-28	4,2	2,12	10,60	3,68	0,322	0,308	95,69
Turbine site-29	4,2	2,12	10,68	3,71	0,333	0,300	89,88
Turbine site-30	4,2	2,12	10,81	3,73	0,344	0,311	90,38
Turbine site-31	4,2	2,11	10,93	3,76	0,359	0,327	91,32
Turbine site-32	4,3	2,11	11,03	3,78	0,370	0,370	100,00
Sector 7 total	-	-	-	-	11,487	10,472	91,17

Sector 8 (210°)

Site	A [m/s]	k	Freq. [%]	U [m/s]	MWh (free)	MWh (Park 2)	Eff. [%]
Turbine site-1	4,5	2,05	8,39	4,01	0,358	0,358	100,00

Turbine site-2	4,5	2,05	8,37	4,00	0,356	0,356	100,00
Turbine site-3	4,5	2,05	8,38	4,01	0,357	0,357	100,00
Turbine site-4	4,5	2,03	8,41	4,03	0,370	0,370	100,00
Turbine site-5	4,6	2,03	8,46	4,05	0,380	0,380	100,00
Turbine site-6	4,6	1,99	8,49	4,07	0,398	0,398	100,00
Turbine site-7	4,1	2,02	7,82	3,68	0,251	0,251	100,00
Turbine site-8	4,2	1,99	7,89	3,72	0,270	0,270	100,00
Turbine site-9	4,5	2,05	8,37	4,00	0,357	0,331	92,87
Turbine site-10	4,1	2,05	7,87	3,66	0,243	0,224	92,38
Turbine site-11	4,1	2,05	7,82	3,64	0,238	0,226	94,98
Turbine site-12	4,1	2,05	7,84	3,66	0,242	0,229	94,70
Turbine site-13	4,2	2,03	7,88	3,68	0,252	0,233	92,37
Turbine site-14	4,2	2,01	7,89	3,70	0,261	0,245	93,83
Turbine site-15	4,2	1,99	7,90	3,71	0,267	0,259	97,04
Turbine site-16	4,2	1,96	7,92	3,74	0,281	0,281	100,00
Turbine site-17	4,1	2,05	7,87	3,65	0,242	0,215	89,15
Turbine site-18	4,1	2,05	7,83	3,64	0,237	0,214	90,39
Turbine site-19	4,1	2,05	7,86	3,66	0,242	0,222	91,81
Turbine site-20	4,5	2,04	8,41	4,02	0,365	0,337	92,25
Turbine site-21	4,1	2,03	7,86	3,65	0,243	0,220	90,56
Turbine site-22	4,1	2,02	7,85	3,65	0,245	0,228	92,92
Turbine site-23	4,1	1,98	7,85	3,67	0,257	0,249	96,97
Turbine site-24	4,2	1,97	7,90	3,70	0,268	0,268	100,00
Turbine site-25	4,5	2,05	8,41	4,01	0,361	0,324	89,58
Turbine site-26	4,1	2,05	7,84	3,62	0,232	0,206	88,70
Turbine site-27	4,1	2,05	7,86	3,63	0,235	0,212	90,01
Turbine site-28	4,1	2,05	7,83	3,62	0,233	0,210	90,18
Turbine site-29	4,1	2,03	7,89	3,66	0,247	0,223	90,33
Turbine site-30	4,2	1,97	7,97	3,70	0,270	0,251	93,17
Turbine site-31	4,2	1,92	7,98	3,73	0,287	0,279	97,07
Turbine site-32	4,2	1,90	8,01	3,75	0,301	0,301	100,00
Sector 8 total	-	-	-	-	9,148	8,730	95,43

Sector 9 (240°)

Site	A [m/s]	k	Freq. [%]	U [m/s]	MWh (free)	MWh (Park 2)	Eff. [%]
Turbine site-1	7,0	1,71	9,65	6,27	1,648	1,648	100,00
Turbine site-2	7,0	1,71	9,64	6,26	1,643	1,643	100,00
Turbine site-3	7,0	1,71	9,64	6,26	1,645	1,645	100,00
Turbine site-4	7,0	1,71	9,60	6,26	1,638	1,638	100,00
Turbine site-5	7,0	1,71	9,60	6,28	1,645	1,645	100,00

Turbine site-6	7,0	1,71	9,54	6,26	1,625	1,625	100,00
Turbine site-7	6,4	1,71	9,05	5,69	1,257	1,257	100,00
Turbine site-8	6,4	1,71	9,06	5,71	1,265	1,265	100,00
Turbine site-9	7,0	1,71	9,65	6,26	1,645	1,612	97,98
Turbine site-10	6,4	1,71	9,25	5,73	1,306	1,275	97,64
Turbine site-11	6,4	1,71	9,18	5,70	1,282	1,252	97,63
Turbine site-12	6,4	1,71	9,20	5,72	1,296	1,296	100,00
Turbine site-13	6,4	1,71	9,15	5,72	1,285	1,255	97,63
Turbine site-14	6,4	1,71	9,10	5,71	1,271	1,243	97,79
Turbine site-15	6,4	1,71	9,09	5,71	1,271	1,242	97,79
Turbine site-16	6,4	1,71	9,01	5,67	1,242	1,242	100,00
Turbine site-17	6,4	1,71	9,30	5,73	1,314	1,243	94,64
Turbine site-18	6,4	1,71	9,19	5,70	1,280	1,211	94,59
Turbine site-19	6,4	1,71	9,18	5,71	1,286	1,225	95,24
Turbine site-20	7,0	1,71	9,62	6,26	1,641	1,629	99,25
Turbine site-21	6,4	1,71	9,13	5,67	1,255	1,187	94,56
Turbine site-22	6,3	1,71	9,08	5,65	1,239	1,174	94,72
Turbine site-23	6,3	1,71	8,98	5,61	1,207	1,150	95,28
Turbine site-24	6,3	1,71	9,01	5,64	1,226	1,226	100,00
Turbine site-25	7,0	1,71	9,67	6,28	1,659	1,559	93,97
Turbine site-26	6,3	1,71	9,20	5,66	1,264	1,173	92,84
Turbine site-27	6,4	1,71	9,24	5,68	1,280	1,205	94,12
Turbine site-28	6,4	1,71	9,17	5,66	1,259	1,229	97,63
Turbine site-29	6,4	1,71	9,15	5,68	1,263	1,170	92,63
Turbine site-30	6,3	1,71	9,10	5,64	1,237	1,150	92,96
Turbine site-31	6,3	1,71	8,96	5,58	1,187	1,122	94,50
Turbine site-32	6,2	1,71	8,86	5,54	1,154	1,154	100,00
Sector 9 total	-	-	-	-	43,713	42,587	97,42

Sector 10 (270°)

Site	A [m/s]	k	Freq. [%]	U [m/s]	MWh (free)	MWh (Park 2)	Eff. [%]
Turbine site-1	6,5	1,78	3,49	5,79	0,495	0,495	100,00
Turbine site-2	6,5	1,78	3,50	5,78	0,495	0,495	100,00
Turbine site-3	6,5	1,78	3,50	5,79	0,495	0,495	100,00
Turbine site-4	6,5	1,78	3,48	5,77	0,490	0,490	100,00
Turbine site-5	6,5	1,78	3,47	5,77	0,487	0,487	100,00
Turbine site-6	6,4	1,78	3,45	5,74	0,480	0,480	100,00
Turbine site-7	6,2	1,78	3,80	5,50	0,478	0,478	100,00
Turbine site-8	6,2	1,78	3,72	5,49	0,465	0,465	100,00
Turbine site-9	6,5	1,78	3,50	5,79	0,496	0,462	93,22

Turbine site-10	6,2	1,78	3,81	5,52	0,484	0,449	92,64
Turbine site-11	6,2	1,78	3,84	5,52	0,487	0,451	92,62
Turbine site-12	6,2	1,78	3,82	5,53	0,487	0,451	92,65
Turbine site-13	6,2	1,78	3,76	5,50	0,473	0,438	92,59
Turbine site-14	6,2	1,78	3,74	5,49	0,468	0,433	92,61
Turbine site-15	6,2	1,78	3,72	5,48	0,465	0,433	93,14
Turbine site-16	6,1	1,78	3,68	5,45	0,453	0,422	93,09
Turbine site-17	6,2	1,78	3,83	5,53	0,488	0,448	91,76
Turbine site-18	6,2	1,78	3,83	5,51	0,484	0,446	92,03
Turbine site-19	6,2	1,78	3,79	5,50	0,477	0,439	92,01
Turbine site-20	6,5	1,78	3,48	5,77	0,491	0,455	92,75
Turbine site-21	6,1	1,78	3,77	5,46	0,465	0,428	91,91
Turbine site-22	6,1	1,78	3,77	5,45	0,464	0,427	91,91
Turbine site-23	6,1	1,78	3,75	5,42	0,455	0,418	91,87
Turbine site-24	6,1	1,78	3,70	5,42	0,451	0,414	91,93
Turbine site-25	6,5	1,78	3,49	5,79	0,496	0,458	92,33
Turbine site-26	6,1	1,78	3,82	5,46	0,473	0,432	91,40
Turbine site-27	6,2	1,78	3,81	5,48	0,476	0,436	91,46
Turbine site-28	6,1	1,78	3,81	5,47	0,473	0,430	90,99
Turbine site-29	6,1	1,78	3,75	5,45	0,463	0,423	91,41
Turbine site-30	6,1	1,78	3,66	5,39	0,438	0,399	91,21
Turbine site-31	6,0	1,78	3,60	5,33	0,420	0,383	91,08
Turbine site-32	5,9	1,78	3,55	5,29	0,406	0,369	90,95
Sector 10 total	-	-	-	-	15,119	14,230	94,12

Sector 11 (300°)

Site	A [m/s]	k	Freq. [%]	U [m/s]	MWh (free)	MWh (Park 2)	Eff. [%]
Turbine site-1	4,1	1,50	0,70	3,68	0,034	0,034	100,00
Turbine site-2	4,1	1,50	0,71	3,68	0,034	0,034	100,00
Turbine site-3	4,1	1,50	0,71	3,68	0,034	0,034	100,00
Turbine site-4	4,1	1,50	0,70	3,67	0,034	0,034	100,00
Turbine site-5	4,1	1,50	0,70	3,67	0,034	0,034	100,00
Turbine site-6	4,1	1,50	0,70	3,66	0,033	0,033	100,00
Turbine site-7	4,5	1,50	0,91	4,03	0,058	0,058	100,00
Turbine site-8	4,5	1,50	0,90	4,02	0,056	0,056	100,00
Turbine site-9	4,1	1,50	0,71	3,68	0,034	0,034	100,00
Turbine site-10	4,3	1,49	0,84	3,86	0,047	0,046	97,51
Turbine site-11	4,3	1,49	0,86	3,92	0,051	0,050	97,59
Turbine site-12	4,3	1,49	0,85	3,91	0,050	0,049	97,57
Turbine site-13	4,4	1,49	0,87	3,95	0,052	0,052	100,00

Turbine site-14	4,4	1,49	0,89	3,99	0,055	0,053	97,67
Turbine site-15	4,4	1,49	0,89	3,99	0,055	0,054	97,68
Turbine site-16	4,5	1,50	0,91	4,04	0,058	0,056	97,38
Turbine site-17	4,2	1,49	0,82	3,81	0,044	0,044	100,00
Turbine site-18	4,3	1,49	0,86	3,91	0,050	0,048	94,99
Turbine site-19	4,3	1,49	0,86	3,92	0,051	0,048	94,11
Turbine site-20	4,1	1,50	0,70	3,68	0,034	0,032	93,32
Turbine site-21	4,4	1,49	0,88	3,94	0,052	0,052	99,11
Turbine site-22	4,4	1,49	0,90	3,97	0,055	0,052	94,92
Turbine site-23	4,5	1,50	0,93	4,03	0,058	0,055	94,40
Turbine site-24	4,4	1,50	0,91	4,01	0,057	0,053	93,95
Turbine site-25	4,1	1,50	0,70	3,68	0,034	0,034	100,00
Turbine site-26	4,3	1,49	0,85	3,87	0,048	0,045	94,06
Turbine site-27	4,3	1,49	0,84	3,84	0,047	0,043	91,80
Turbine site-28	4,3	1,49	0,87	3,91	0,051	0,046	91,54
Turbine site-29	4,3	1,49	0,87	3,92	0,051	0,050	97,49
Turbine site-30	4,3	1,49	0,88	3,92	0,052	0,048	93,43
Turbine site-31	4,4	1,51	0,92	3,99	0,056	0,052	92,06
Turbine site-32	4,5	1,51	0,95	4,03	0,059	0,054	91,69
Sector 11 total	-	-	-	-	1,517	1,467	96,68

Sector 12 (330°)

Site	A [m/s]	k	Freq. [%]	U [m/s]	MWh (free)	MWh (Park 2)	Eff. [%]
Turbine site-1	3,6	1,61	0,36	3,25	0,011	0,011	100,00
Turbine site-2	3,6	1,61	0,37	3,25	0,011	0,011	100,00
Turbine site-3	3,6	1,61	0,37	3,25	0,011	0,011	100,00
Turbine site-4	3,6	1,60	0,37	3,26	0,011	0,011	100,00
Turbine site-5	3,6	1,60	0,37	3,26	0,011	0,011	100,00
Turbine site-6	3,6	1,60	0,37	3,27	0,011	0,011	100,00
Turbine site-7	3,6	1,57	0,40	3,22	0,012	0,012	100,00
Turbine site-8	3,6	1,57	0,40	3,23	0,012	0,012	100,00
Turbine site-9	3,6	1,61	0,37	3,25	0,011	0,011	100,00
Turbine site-10	3,5	1,58	0,39	3,16	0,011	0,010	96,97
Turbine site-11	3,5	1,57	0,39	3,17	0,011	0,010	93,75
Turbine site-12	3,5	1,57	0,39	3,17	0,011	0,010	92,80
Turbine site-13	3,6	1,58	0,39	3,20	0,011	0,011	95,50
Turbine site-14	3,6	1,57	0,40	3,21	0,012	0,011	95,77
Turbine site-15	3,6	1,57	0,40	3,22	0,012	0,011	93,54
Turbine site-16	3,6	1,57	0,41	3,25	0,012	0,011	93,14
Turbine site-17	3,5	1,58	0,38	3,14	0,010	0,010	100,00

Turbine site-18	3,5	1,57	0,39	3,16	0,011	0,010	96,97
Turbine site-19	3,5	1,58	0,39	3,17	0,011	0,010	93,07
Turbine site-20	3,6	1,61	0,37	3,25	0,011	0,010	91,32
Turbine site-21	3,5	1,57	0,39	3,17	0,011	0,010	91,66
Turbine site-22	3,5	1,57	0,40	3,19	0,011	0,010	92,52
Turbine site-23	3,6	1,57	0,41	3,21	0,012	0,011	91,05
Turbine site-24	3,6	1,57	0,40	3,22	0,012	0,011	89,92
Turbine site-25	3,6	1,61	0,36	3,24	0,011	0,011	100,00
Turbine site-26	3,5	1,57	0,39	3,14	0,010	0,010	97,15
Turbine site-27	3,5	1,58	0,39	3,14	0,010	0,010	93,18
Turbine site-28	3,5	1,57	0,39	3,15	0,011	0,010	90,48
Turbine site-29	3,5	1,58	0,39	3,17	0,011	0,010	90,51
Turbine site-30	3,5	1,58	0,40	3,19	0,011	0,010	91,10
Turbine site-31	3,6	1,57	0,41	3,22	0,012	0,011	89,93
Turbine site-32	3,6	1,57	0,42	3,24	0,013	0,011	88,82
Sector 12 total	-	-	-	-	0,356	0,339	95,20

All Sectors

Turbine	Location [m]	MWh (free)	MWh (Park 2)	Eff. [%]
Turbine site-1	(527495,6, 2159856,0)	27,384	26,695	97,48
Turbine site-2	(527495,6, 2159796,0)	27,366	26,606	97,22
Turbine site-3	(527495,6, 2159736,0)	27,378	26,608	97,19
Turbine site-4	(527495,6, 2159676,0)	27,335	26,612	97,35
Turbine site-5	(527495,6, 2159556,0)	27,366	26,658	97,41
Turbine site-6	(527495,6, 2159496,0)	27,287	26,536	97,25
Turbine site-7	(527495,6, 2159436,0)	25,474	24,674	96,86
Turbine site-8	(527495,6, 2159376,0)	25,480	24,777	97,24
Turbine site-9	(527555,6, 2159856,0)	27,379	26,679	97,44
Turbine site-10	(527555,6, 2159796,0)	25,565	24,744	96,79
Turbine site-11	(527555,6, 2159736,0)	25,504	24,695	96,83
Turbine site-12	(527555,6, 2159676,0)	25,576	24,851	97,17
Turbine site-13	(527555,6, 2159556,0)	25,493	24,741	97,05
Turbine site-14	(527555,6, 2159496,0)	25,455	24,652	96,84
Turbine site-15	(527555,6, 2159436,0)	25,459	24,675	96,92
Turbine site-16	(527555,6, 2159376,0)	25,331	24,679	97,42
Turbine site-17	(527615,6, 2159856,0)	25,594	24,922	97,37
Turbine site-18	(527615,6, 2159796,0)	25,465	24,769	97,27
Turbine site-19	(527615,6, 2159736,0)	25,451	24,769	97,32
Turbine site-20	(527615,6, 2159676,0)	27,342	26,785	97,96
Turbine site-21	(527615,6, 2159556,0)	25,240	24,590	97,43

Turbine site-22	(527615,6, 2159496,0)	25,204	24,523	97,30
Turbine site-23	(527615,6, 2159436,0)	25,076	24,417	97,37
Turbine site-24	(527615,6, 2159376,0)	25,163	24,634	97,90
Turbine site-25	(527675,6, 2159856,0)	27,436	27,216	99,20
Turbine site-26	(527675,6, 2159796,0)	25,241	25,040	99,20
Turbine site-27	(527675,6, 2159736,0)	25,339	25,157	99,28
Turbine site-28	(527675,6, 2159676,0)	25,255	25,139	99,54
Turbine site-29	(527675,6, 2159556,0)	25,256	25,062	99,23
Turbine site-30	(527675,6, 2159496,0)	25,022	24,839	99,27
Turbine site-31	(527675,6, 2159436,0)	24,792	24,641	99,39
Turbine site-32	(527675,6, 2159376,0)	24,615	24,569	99,81
Wind farm	-	828,325	809,953	97,78

Wake effects modelling

Wake losses are modelled using PARK2, using default coefficient (0,06) for offshore.

Generalised wind climate

A generalised wind climate called 'GWC 1' was used to calculate the predicted wind climates

Data origins information

The Vector map ''NMS-III'' associated with this Wind farm contains the following vector data layers:

- Elevation layer named 'NMS-III' was imported by 'yazen' from a file called 'C:\Users\yazen\Desktop\SRB-SEND\WAsP-Final-V2.map' , on a computer called 'DESKTOP-0EC4SNG'. The NMS-III file data were last modified on the 12/12/2024 at 16:05:38
- Roughness layer named 'NMS-III' was imported by 'yazen' from a file called 'C:\Users\yazen\Desktop\SRB-SEND\WAsP-Final-V2.map' , on a computer called 'DESKTOP-0EC4SNG'. The NMS-III file data were last modified on the 12/12/2024 at 16:05:38

There is no information about the origin of the wind atlas associated with this Wind farm.

There is no information about the origin of the wind turbine generator associated with this Wind farm.

WAsP project parameters

All of the WAsP project parameters have default values.

The Wind farm is in a project called 'Project 1'.

Terrain analysis (IBZ) parameters

All of the Terrain analysis (IBZ) parameters have default values.

E WAsP Climate Analysis: Data Plots for each year

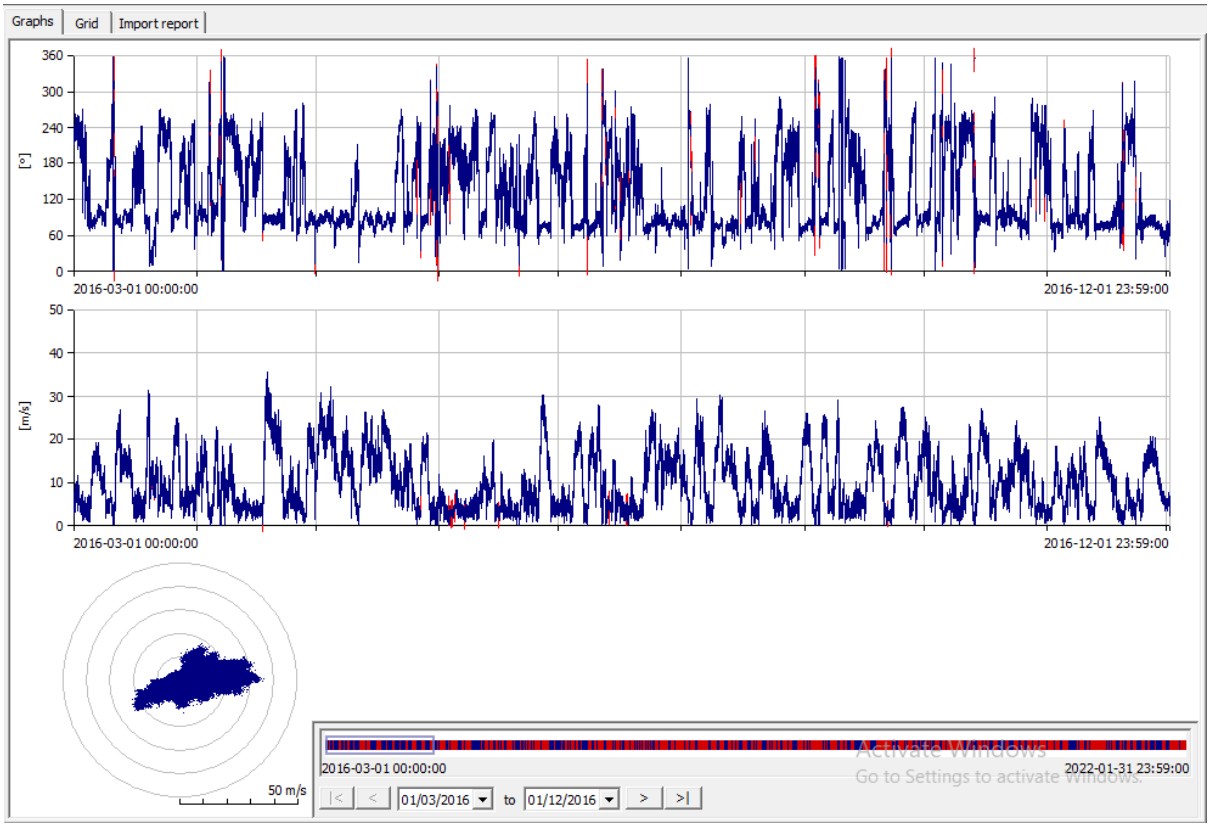

Figure A.1: WAsP Climate Analyst Data Plot - 2016

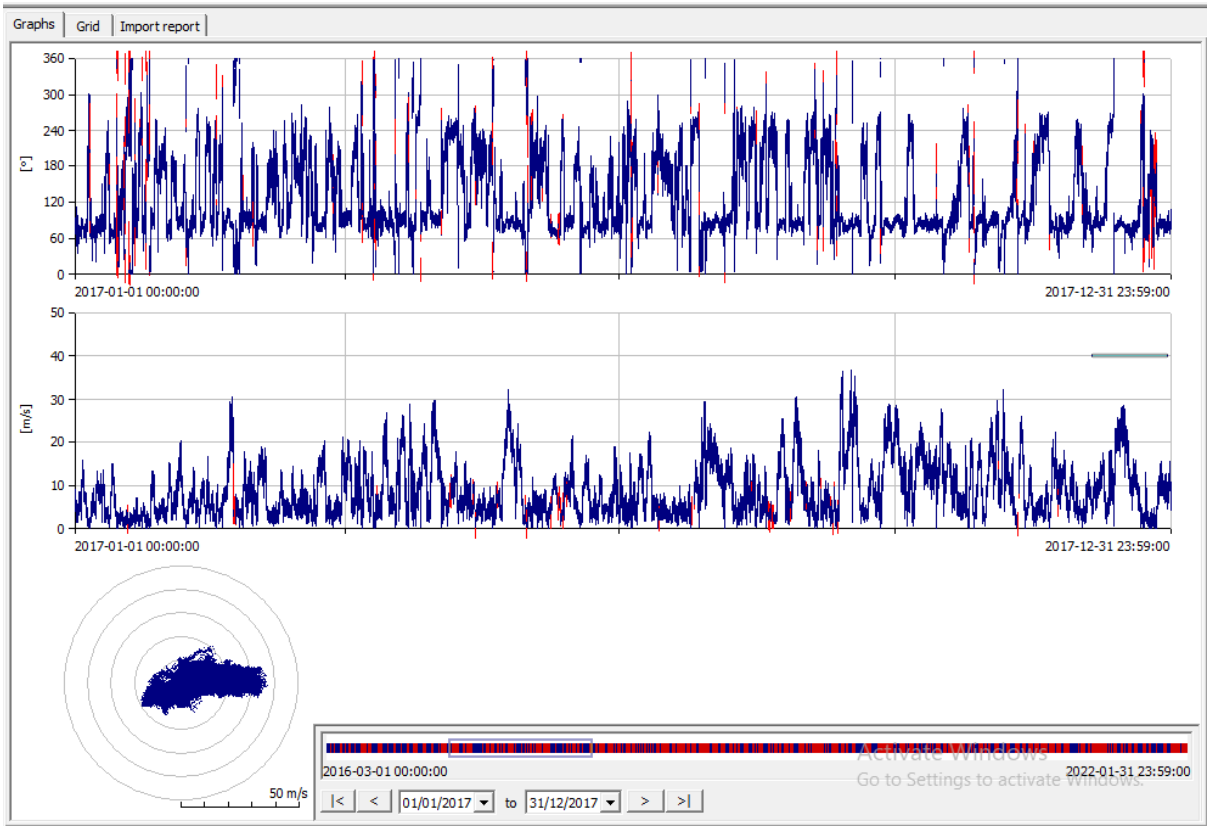

Figure A.2: WAsP Climate Analyst Data Plot - 2017

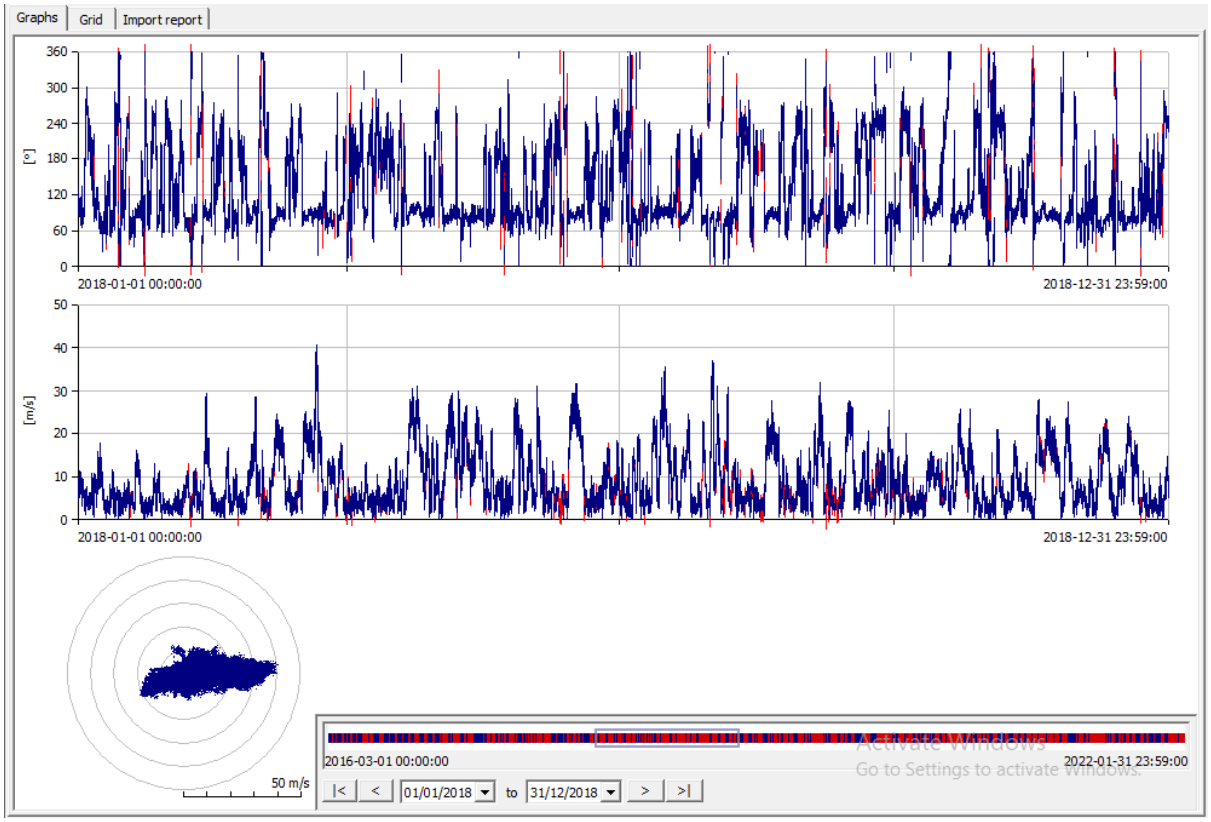

Figure A.3: WAsP Climate Analyst Data Plot - 2018

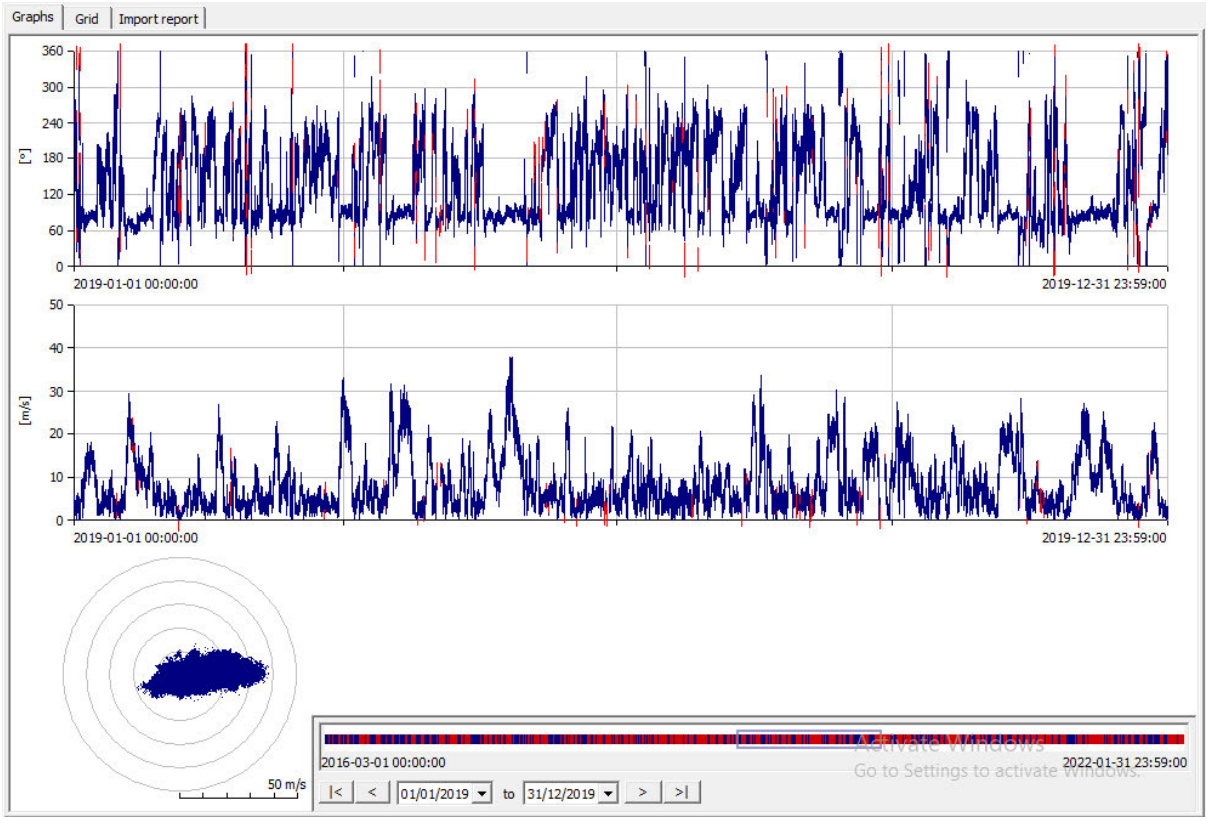

Figure A.4: WAsP Climate Analyst Data Plot - 2019

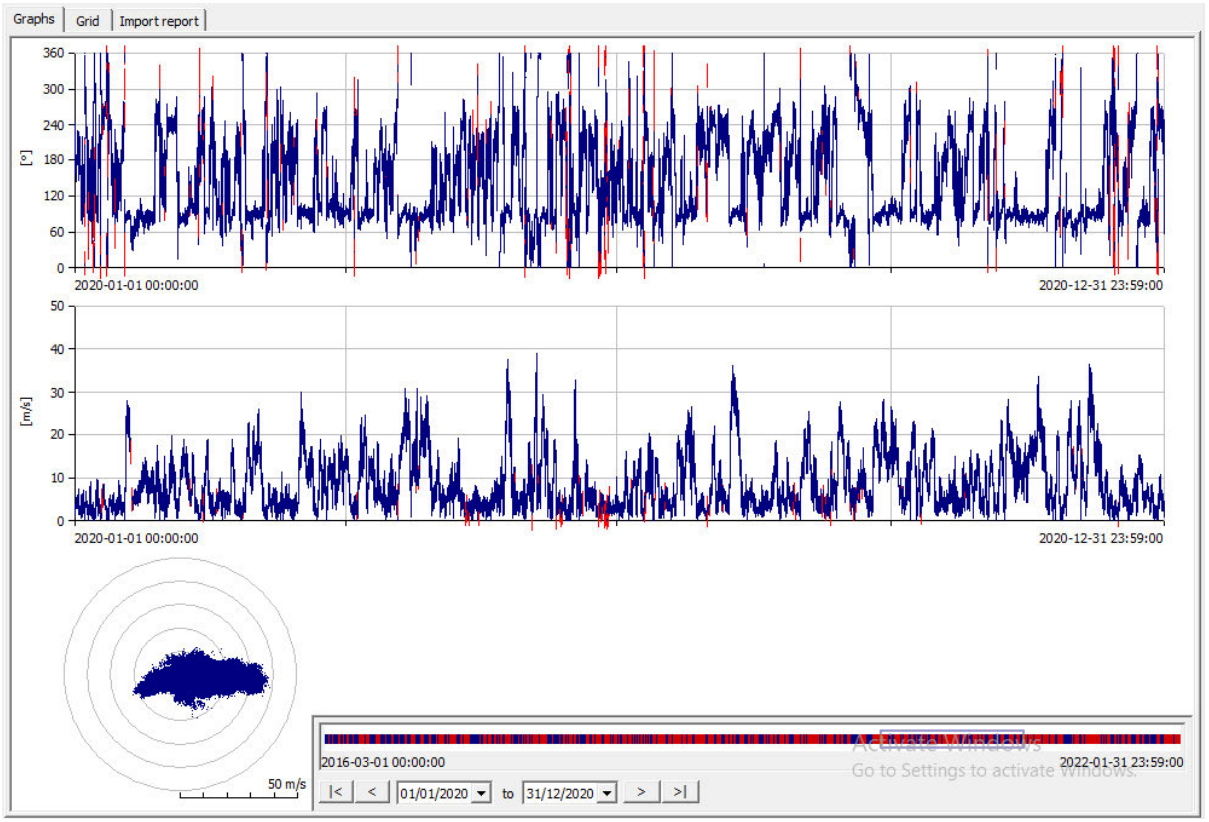

Figure A.5: WAsP Climate Analyst Data Plot - 2020

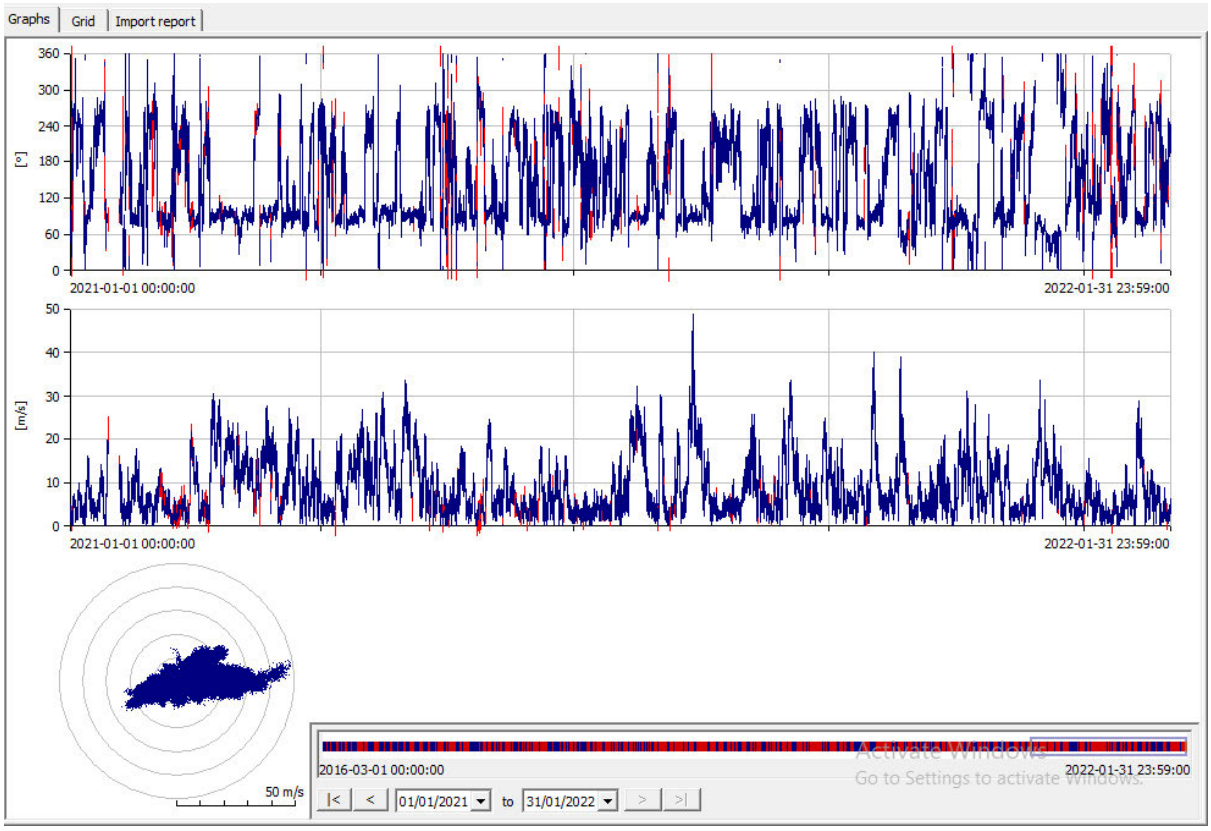

Figure A.6: WAsP Climate Analyst Data Plot - 2021 and 01/2022

F OWC Statistics Report

All-sectors statistics

	Weibull-A	Weibull-k	Mean speed	Power density
Source data (3063333)	-	-	8,72 m/s	1239 W/m²
Fitted	9,1 m/s	1,30	8,38 m/s	1240 W/m²
Emergent	-	-	8,72 m/s	1239 W/m²
Combined	9,6 m/s	1,39	8,72 m/s	1239 W/m²

Mean wind speeds (hourly, by month)

Hour	Jan	Feb	Mar	Apr	May	Jun	Jul	Aug	Sep	Oct	Nov	Dec	Year
0	5.63	6.76	8.69	10.32	10.12	7.05	8.21	9.12	10.39	8.93	9.12	7.34	8.47
1	5.70	6.75	8.74	10.33	10.06	7.17	8.12	9.05	10.37	8.91	9.02	7.41	8.47
2	5.89	6.80	8.67	10.33	9.98	7.12	8.16	9.02	10.33	8.89	9.18	7.56	8.49
3	5.84	6.83	8.76	10.41	10.09	7.14	8.12	9.03	10.31	8.97	9.30	7.61	8.53
4	5.83	7.04	8.85	10.25	10.16	7.00	8.13	9.03	10.25	9.04	9.38	7.64	8.55
5	5.94	6.88	8.95	10.35	9.99	7.06	8.07	8.97	10.26	9.05	9.42	7.71	8.55
6	5.94	7.09	9.06	10.51	10.06	7.12	8.16	9.04	10.36	9.25	9.47	7.65	8.64
7	5.91	7.23	8.95	10.53	10.30	7.06	8.11	9.02	10.47	9.36	9.63	7.70	8.69
8	5.84	7.19	8.98	10.59	10.28	7.06	7.98	9.09	10.46	9.44	9.75	7.93	8.72
9	6.00	7.14	9.13	10.58	10.28	6.88	7.89	9.14	10.34	9.51	9.99	8.17	8.75
10	5.97	7.29	9.13	10.55	10.32	6.88	8.11	9.31	10.58	9.53	10.17	8.29	8.84
11	6.04	7.37	9.18	10.63	10.46	7.00	8.23	9.33	10.57	9.69	10.07	8.29	8.90
12	6.19	7.43	9.18	10.66	10.32	7.20	8.18	9.15	10.49	9.83	10.07	8.31	8.92
13	6.25	7.47	9.23	10.53	10.25	7.29	8.27	9.10	10.45	9.82	10.15	8.28	8.93
14	6.30	7.29	9.15	10.56	10.26	7.25	8.20	9.08	10.38	9.84	9.97	8.26	8.88
15	6.16	7.18	9.02	10.55	10.23	7.15	8.12	9.10	10.23	9.66	9.92	8.21	8.79
16	5.95	7.10	8.89	10.44	10.22	7.12	8.13	9.02	10.25	9.59	9.71	8.02	8.70
17	5.87	7.05	8.97	10.39	10.13	7.12	8.15	9.08	10.40	9.48	9.54	7.87	8.67
18	5.63	7.11	8.96	10.26	10.02	7.13	8.12	9.15	10.52	9.18	9.36	7.74	8.60
19	5.47	7.13	8.91	10.22	10.01	7.01	8.10	9.10	10.40	8.90	9.18	7.58	8.50
20	5.53	7.07	8.80	10.22	10.15	6.96	8.10	9.07	10.33	8.73	9.12	7.53	8.47
21	5.59	7.05	8.69	10.26	10.13	6.92	8.20	9.12	10.42	8.71	9.14	7.53	8.48
22	5.69	7.08	8.61	10.28	10.16	6.83	8.35	8.98	10.56	8.65	9.18	7.48	8.49
23	5.64	7.01	8.67	10.16	10.06	6.84	8.42	9.00	10.52	8.67	9.19	7.41	8.47
Average	5.87	7.10	8.92	10.41	10.17	7.06	8.15	9.09	10.40	9.23	9.54	7.81	8.65

Mean wind speeds (yearly, by month)

Year	Jan	Feb	Mar	Apr	May	Jun	Jul	Aug	Sep	Oct	Nov	Dec	Year
2016	---	---	9.51	10.11	13.62	6.46	10.11	9.93	10.71	9.68	9.14	4.40	9.37
2017	4.52	7.47	6.87	10.46	9.06	6.50	7.44	9.87	11.40	11.55	10.06	9.22	8.70
2018	5.29	6.07	11.10	8.33	11.81	9.53	9.91	9.29	9.81	7.90	9.59	7.71	8.86
2019	7.91	5.12	6.24	11.02	10.91	6.26	6.27	7.92	10.03	8.68	8.09	9.52	8.16
2020	5.87	7.25	8.52	11.55	6.62	7.51	7.30	7.90	10.68	8.78	11.57	8.42	8.50
2021	5.78	9.57	11.35	11.01	8.95	6.08	7.83	9.60	9.76	8.81	8.80	7.65	8.77
2022	5.82	---	---	---	---	---	---	---	---	---	---	---	5.82
Average	5.87	7.10	8.93	10.41	10.16	7.06	8.14	9.08	10.40	9.23	9.54	7.82	8.31

G OWC Generation Report

Climate generation

Generated at:	2024-12-19T14:01:44
Generated using:	WAsP Climate Analyst (using Rvea0100) version 3.1
Generated by:	yazen on DESKTOP-0EC4SNG
Number of data sets:	5
Source file path:	C:\Users\yazen\Desktop\New folder (3)

	Selected Data Summary	All Data Summary	Data set 1	Data set 2	Data set 3	Data set 4	Data set 5
File information:							
Source file name:			Main-2016.txt	5 - 2.txt	S.txt	9 - Copy.txt	6.txt
Last modified (UTC):			2024-09-16T21:49:58	2024-09-15T20:19:07	2024-09-15T20:53:57	2024-09-15T21:01:48	2024-09-10T22:00:44
Time selections							
2016-03-01T00:00:00 to 2022-01-31T23:59:00							
Recordings in file/selections							
Start time	-	2016-03-01T00:00:00	2016-03-01T00:00:00	2017-01-01T00:00:00	2018-01-01T00:00:00	2019-01-01T00:00:00	2020-01-01T00:00:00
End time	-	2022-01-31T23:59:00	2016-12-31T23:59:00	2017-12-31T23:59:00	2018-12-31T23:59:00	2019-12-31T23:59:00	2022-01-31T23:59:00
Count	3111667	3111667	440639	525121	525502	525511	1094894
Recording interval	60 s	60 s	60 s	60 s	60 s	60 s	60 s
Mean wind speed data (' Speed 3 ')							
Data column no. in source file	3	3	3	3	3	3	3
Discretisation width	0.1	0.1	0.1	0.1	0.1	0.1	0.1
Multiplier	1	1	1	1	1	1	1
Offset	0	0	0	0	0	0	0
Averaging time (s)	60	60	60	60	60	60	60
Maximum value	48.8	48.8	35.6	36.7	40.7	37.9	48.8
Minimum value	0.0	0.0	0.1	0.0	0.0	0.0	0.0
Lower limit	0 m/s	0 m/s	0 m/s	0 m/s	0 m/s	0 m/s	0 m/s
Readings below lower limit	0 (0.00 %)	0 (0.00 %)	0 (0.00 %)	0 (0.00 %)	0 (0.00 %)	0 (0.00 %)	0 (0.00 %)
Upper limit	90 m/s	90 m/s	90 m/s	90 m/s	90 m/s	90 m/s	90 m/s
Readings above upper limit	0 (0.00 %)	0 (0.00 %)	0 (0.00 %)	0 (0.00 %)	0 (0.00 %)	0 (0.00 %)	0 (0.00 %)
Calm threshold	0,1 m/s	0.1 m/s	0,1 m/s	0,1 m/s	0,1 m/s	0,1 m/s	0,1 m/s
Calms	1705 (0.05 %)	1705 (0.05 %)	213 (0.05 %)	463 (0.09 %)	95 (0.02 %)	155 (0.03 %)	779 (0.07 %)
Valid readings accepted	3111667 (99.90 %)	3111667 (99.90 %)	440639 (100.00 %)	525121 (99.91 %)	525502 (99.98 %)	525511 (99.98 %)	1094894 (99.78 %)
Accepted values range	0.0 m/s to 48.8 m/s	0.0 m/s to 48.8 m/s	0.1 m/s to 35.6 m/s	0.0 m/s to 36.7 m/s	0.0 m/s to 40.7 m/s	0.0 m/s to 37.9 m/s	0.0 m/s to 48.8 m/s
Mean wind direction data (' Direction 2')							
Data column no. in source file	2	2	2	2	2	2	2
Discretisation width	0.1	0.1	0.1	0.1	0.1	0.1	0.1
Multiplier	1	1	1	1	1	1	1
Offset	0	0	0	0	0	0	0
Averaging time (s)	60	60	60	60	60	60	60
Maximum value	360.0	360.0	360.0	360.0	360.0	360.0	360.0
Minimum value	0.0	0.0	0.6	0.0	0.0	0.0	0.0
Lower limit	0°	0°	0°	0°	0°	0°	0°
Readings below lower limit	0 (0.00 %)	0 (0.00 %)	0 (0.00 %)	0 (0.00 %)	0 (0.00 %)	0 (0.00 %)	0 (0.00 %)
Upper limit	360°	360°	360°	360°	360°	360°	360°
Readings above upper limit	0 (0.00 %)	0 (0.00 %)	0 (0.00 %)	0 (0.00 %)	0 (0.00 %)	0 (0.00 %)	0 (0.00 %)
Calm threshold	0 m/s	0 m/s	0 m/s	0 m/s	0 m/s	0 m/s	0 m/s
Calms	20 (0.00 %)	20 (0.00 %)	0 (0.00 %)	3 (0.00 %)	3 (0.00 %)	4 (0.00 %)	10 (0.00 %)
Valid readings accepted	3111667 (99.90 %)	3111667 (99.90 %)	440639 (100.00 %)	525121 (99.91 %)	525502 (99.98 %)	525511 (99.98 %)	1094894 (99.78 %)
Accepted values range	0.0° to 360.0°	0.0° to 360.0°	0.6° to 360.0°	0.0° to 360.0°	0.0° to 360.0°	0.0° to 360.0°	0.0° to 360.0°
Data recovery:							
Expected recordings count	3114720	3114720	440640	525600	525600	525600	1097280

Expected meas. duration	6 y 0 d	6 y 0 d	1 y 0 d	1 y 0 d	1 y 0 d	1 y 0 d	2 y 32 d
Count of records	3111667 (99.90 %)	3111667 (99.90 %)	440639 (100.00 %)	525121 (99.91 %)	525502 (99.98 %)	525511 (99.98 %)	1094894 (99.78 %)
Missing records	3053	3053	1	479	98	89	2386
Recordings with invalid values in one or more fields	48354 (1.55 %)	48354 (1.55 %)	1268 (0.29 %)	6760 (1.29 %)	6907 (1.31 %)	15820 (3.01 %)	17599 (1.60 %)
Accepted recordings	3063313 (98.35 %)	3063313 (98.35 %)	439371 (99.71 %)	518361 (98.62 %)	518595 (98.67 %)	509691 (96.97 %)	1077295 (98.18 %)
Recovery percentage (vs. expected)	98.35%	99.90%	100.00%	99.91%	99.98%	99.98%	99.78%

H WAsP Climate Analysis: OWC Fitted Distribution for each Section

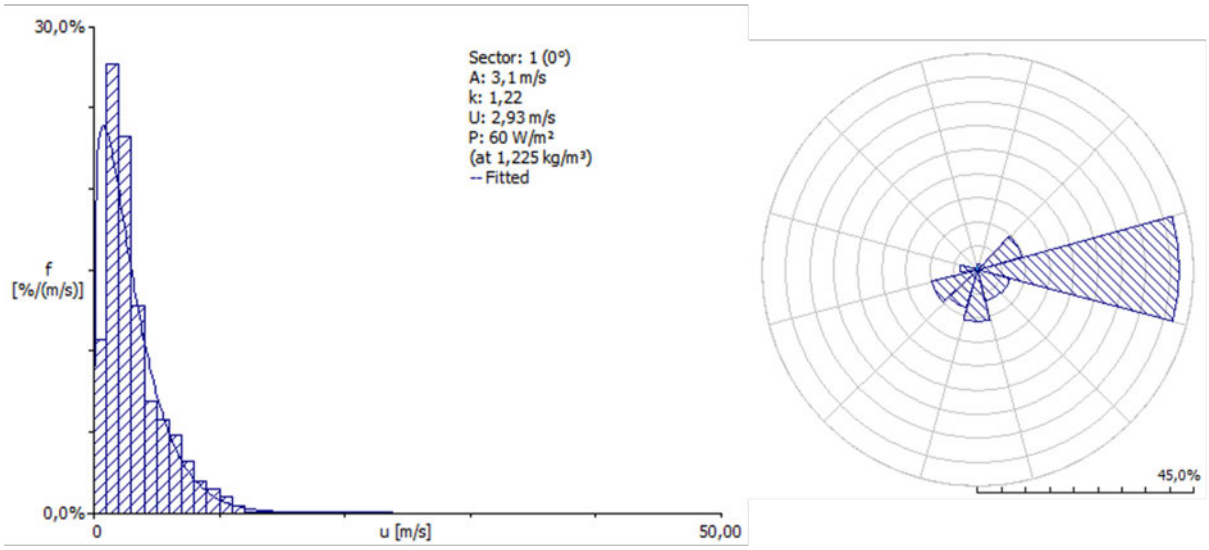

Figure A.7: OWC Fitted Distribution for Section 1

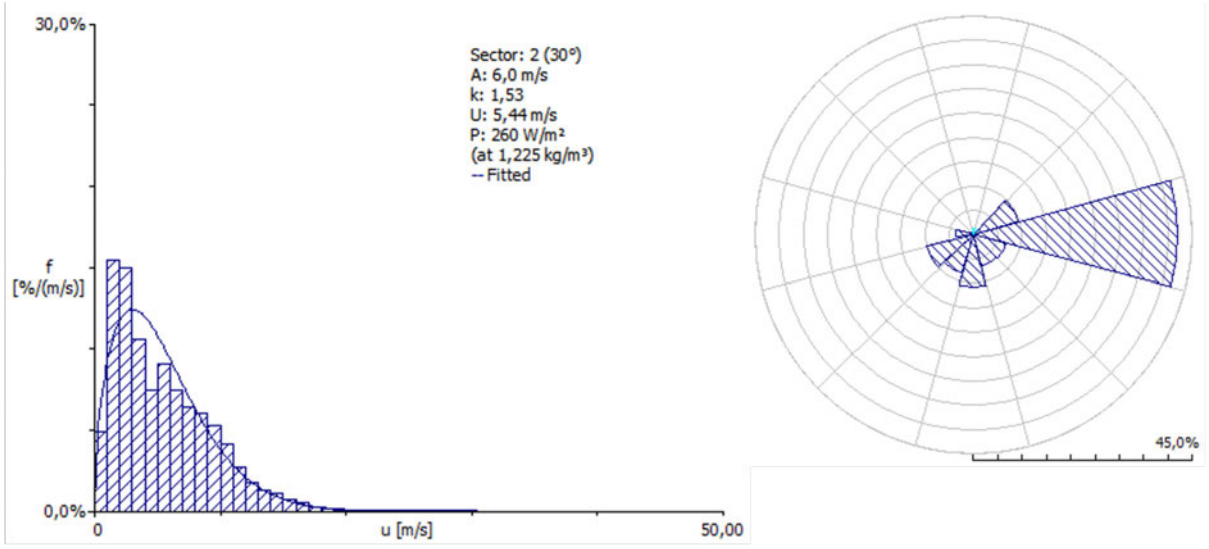

Figure A.8: OWC Fitted Distribution for Section 2

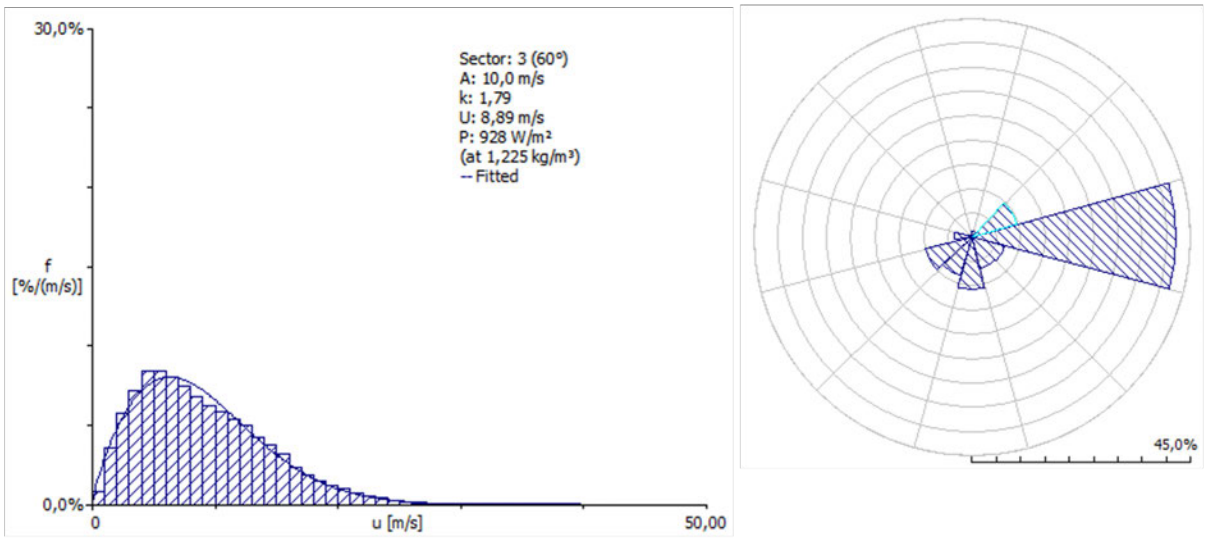

Figure A.9: OWC Fitted Distribution for Section 3

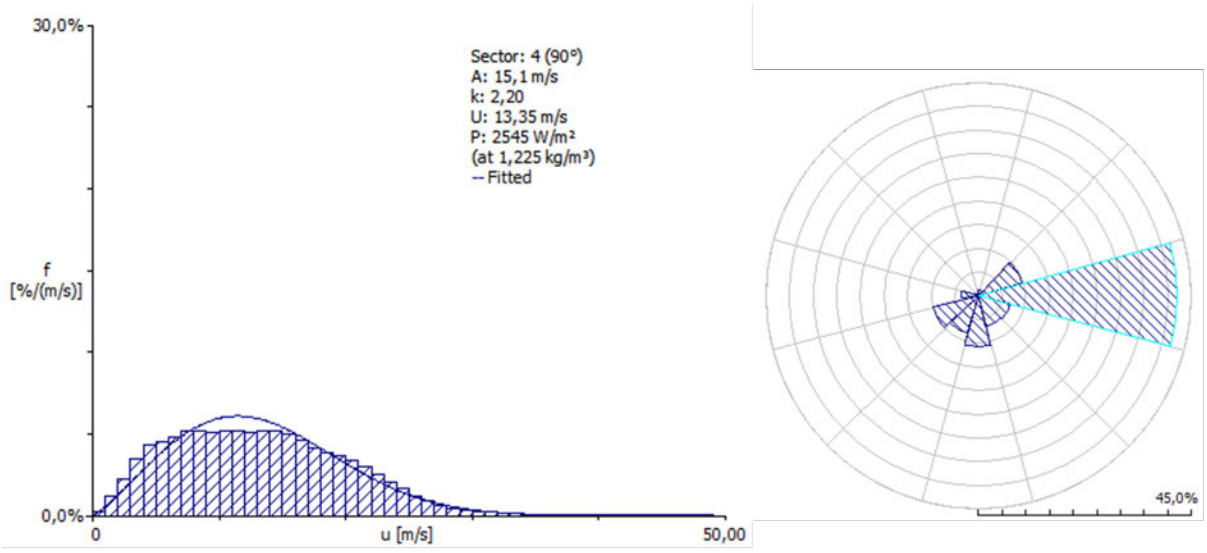

Figure A.10: OWC Fitted Distribution for Section 4

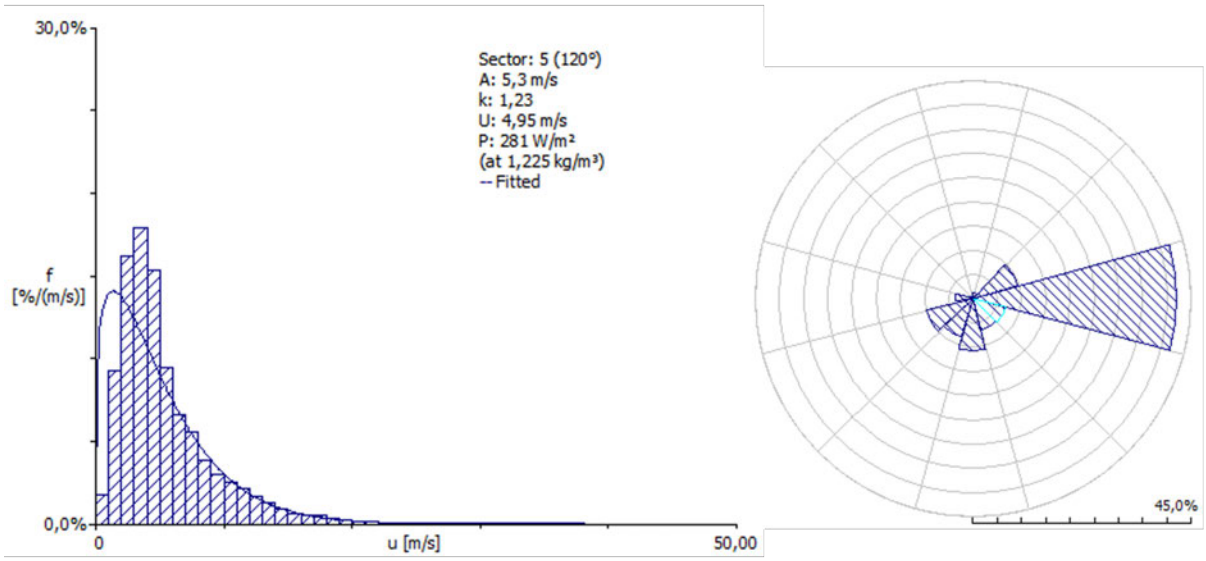

Figure A.11: OWC Fitted Distribution for Section 5

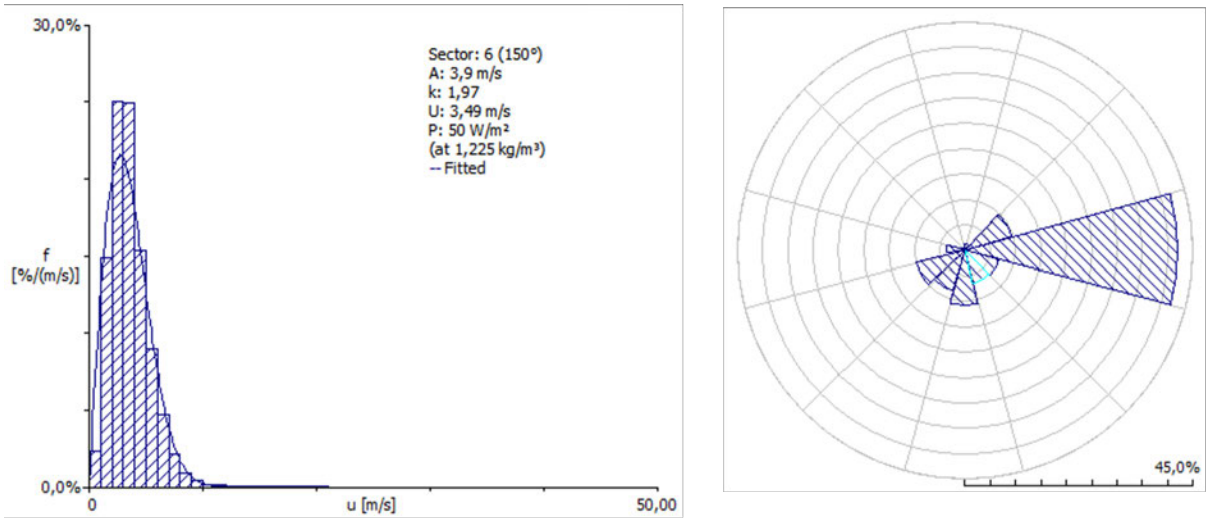

Figure A.12: OWC Fitted Distribution for Section 6

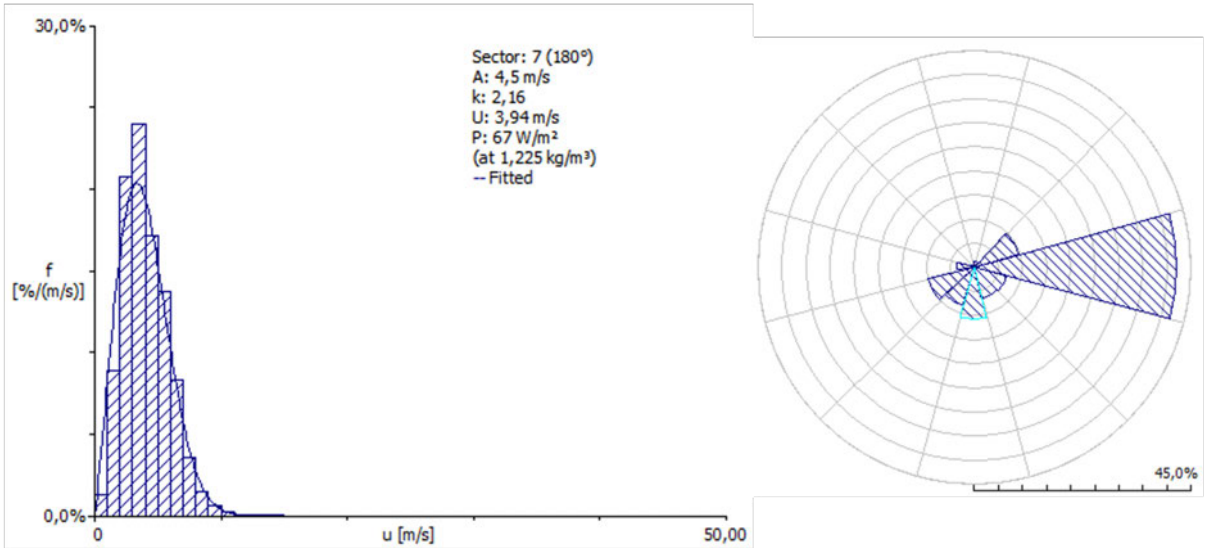

Figure A.13: OWC Fitted Distribution for Section 7

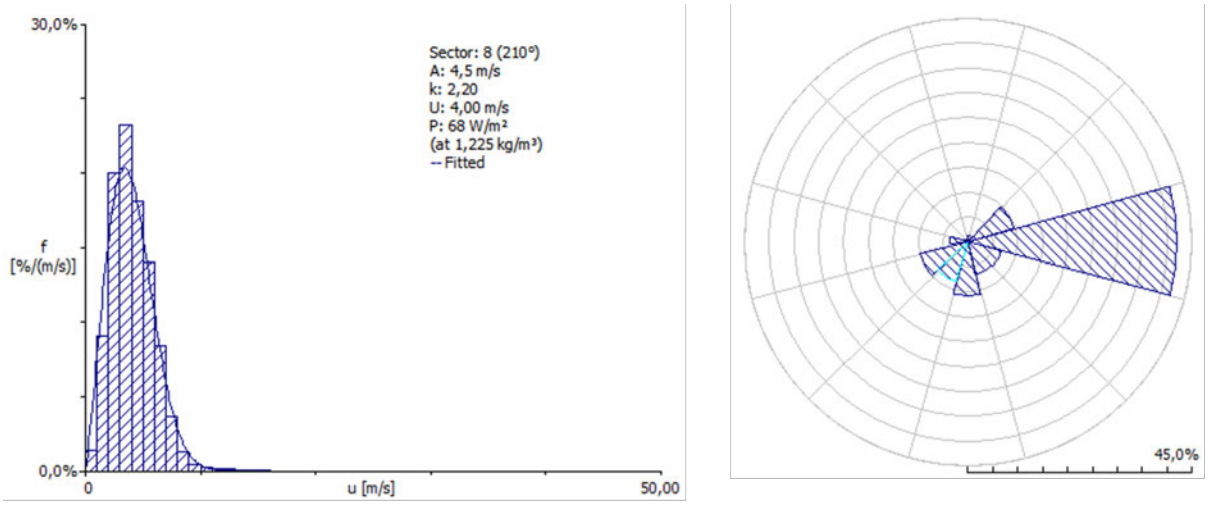

Figure A.14: OWC Fitted Distribution for Section 8

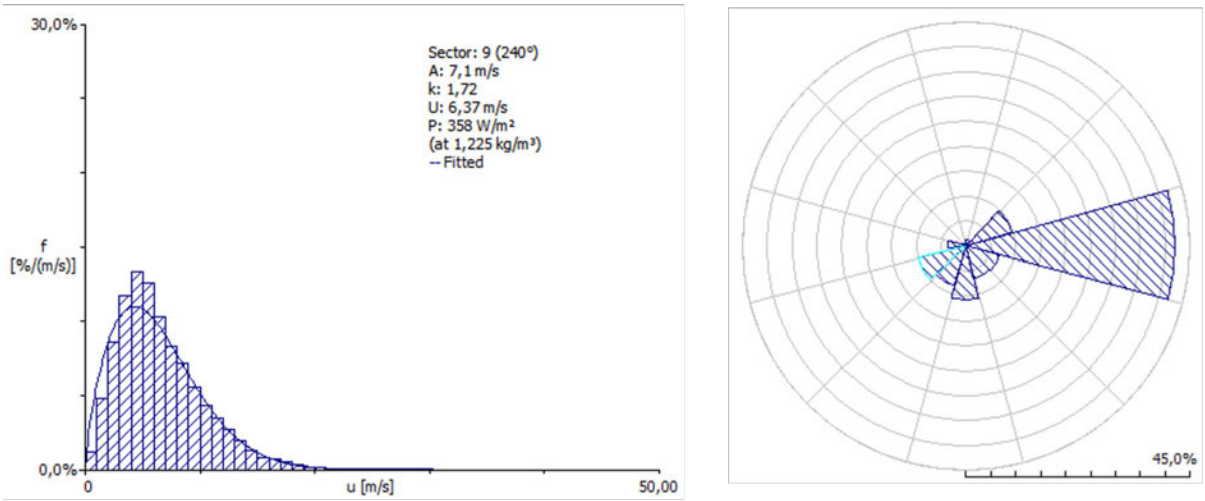

Figure A.15: OWC Fitted Distribution for Section 9

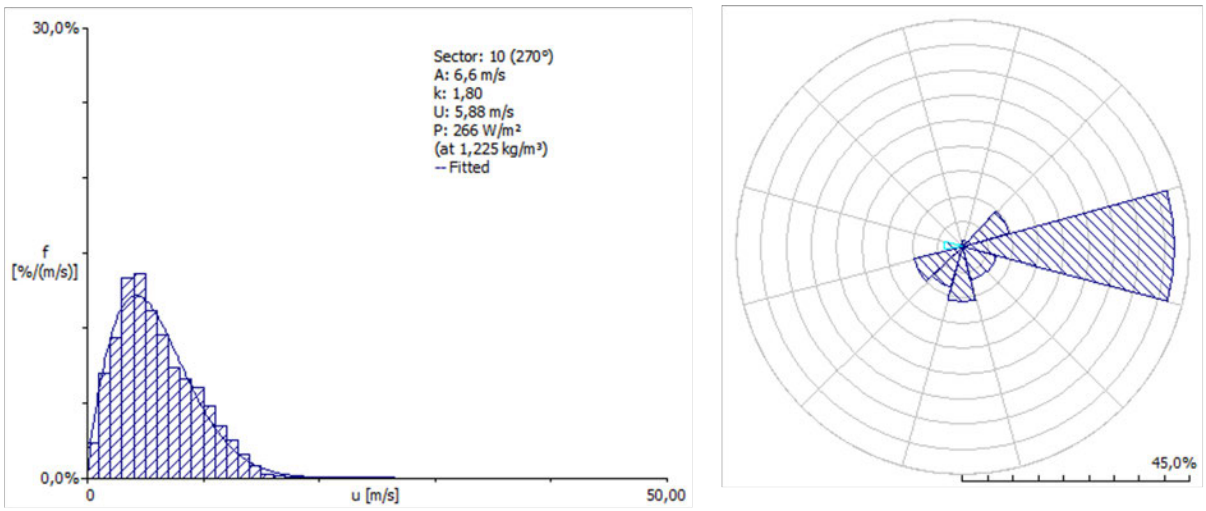

Figure A.16: OWC Fitted Distribution for Section 10

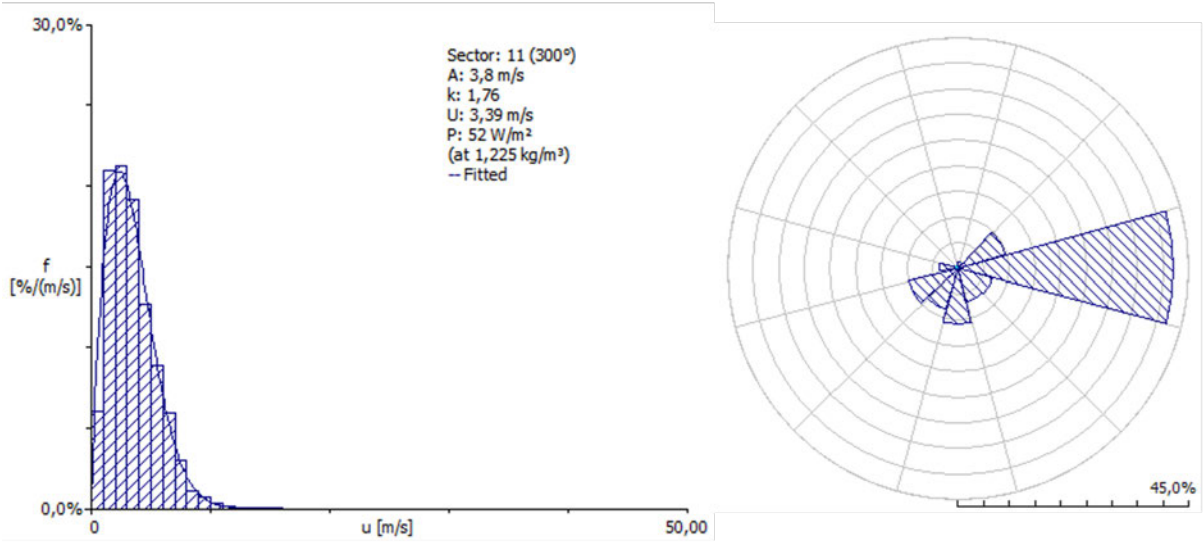

Figure A.17: OWC Fitted Distribution for Section 11

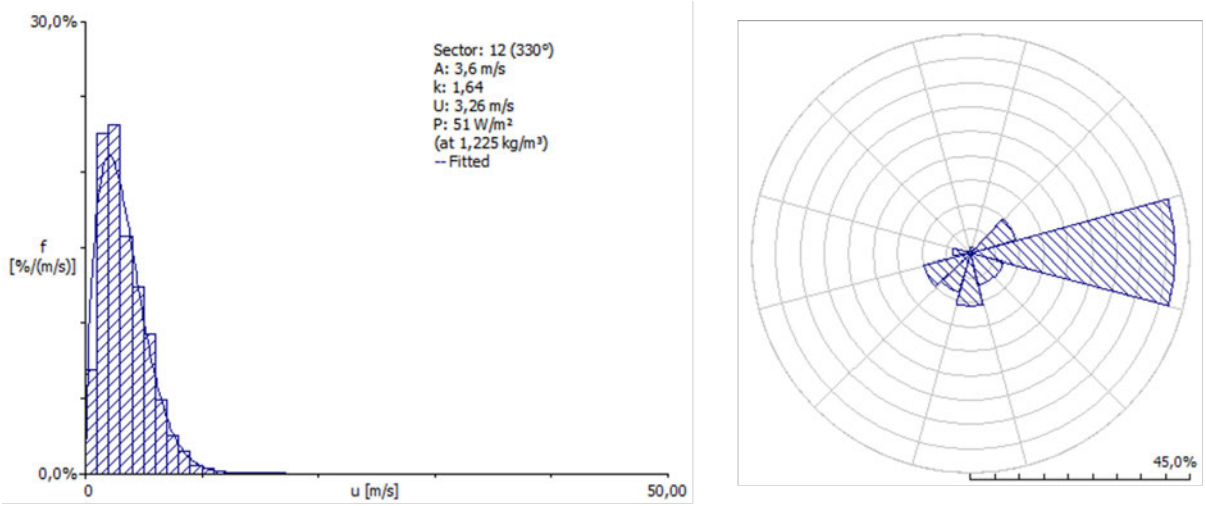

Figure A.18: OWC Fitted Distribution for Section 12

I Wind Turbine Data Table - WAsP Turbine Editor

ρ [kg/m^3]	A [m^2]	v [m/s]	P_{Wind} [kW]	P_{Output} [kW]	C_p	a	C_t
1.225	24.600	0.450	0.001	0.000	0.000	0.000	0.000
		0.890	0.011	0.000	0.000	0.000	0.000
		1.340	0.036	0.000	0.000	0.000	0.000
		1.790	0.086	0.000	0.000	0.000	0.000
		2.240	0.169	0.000	0.000	0.000	0.000
		2.680	0.290	0.010	0.034	0.018	0.069
		3.130	0.462	0.050	0.108	0.057	0.216
		3.580	0.691	0.170	0.246	0.144	0.492
		4.020	0.979	0.170	0.174	0.096	0.347
		4.470	1.346	0.300	0.223	0.128	0.446
		4.920	1.794	0.480	0.267	0.159	0.535
		5.360	2.320	0.510	0.220	0.126	0.440
		5.810	2.955	0.620	0.210	0.119	0.420
		6.260	3.696	1.030	0.279	0.167	0.557
		6.710	4.552	1.450	0.319	0.199	0.637
		7.150	5.508	1.670	0.303	0.186	0.606
		7.600	6.614	1.880	0.284	0.172	0.568
		8.050	7.860	2.680	0.341	0.218	0.682
		8.490	9.221	2.980	0.323	0.203	0.646
		8.490	9.221	3.600	0.390	0.266	0.781
		9.390	12.475	4.500	0.361	0.236	0.721
		9.830	14.312	4.900	0.342	0.219	0.685
		10.280	16.369	5.500	0.336	0.214	0.672
		10.730	18.614	6.000	0.322	0.202	0.645
		11.180	21.056	6.300	0.299	0.183	0.598
		11.620	23.641	6.600	0.279	0.168	0.558
		12.070	26.495	6.900	0.260	0.154	0.521
		12.520	29.570	7.100	0.240	0.140	0.480
		12.960	32.799	7.300	0.223	0.128	0.445
		13.410	36.335	7.600	0.209	0.119	0.418
		17.880	86.128	7.900	0.092	0.048	0.183
		22.350	168.219	8.100	0.048	0.025	0.096
		26.820	290.682	8.300	0.029	0.014	0.057
		31.290	461.592	8.600	0.019	0.009	0.037
		35.760	689.023	8.900	0.013	0.007	0.026
		40.230	981.050	9.000	0.009	0.005	0.018
		44.700	1345.748	9.000	0.007	0.003	0.013
		49.170	1791.191	9.000	0.005	0.003	0.010
		53.640	2325.453	9.000	0.004	0.002	0.008

Table A.1: Detailed Wind Turbine Data

J MATLAB Code to prepare data for the WAsP Climate Analysis tool

```
% MATLAB Function to extract wind data from NMS-III Meteorological Data

function extractColumnsFromFolder(folder_path, output_file)
    files = dir(fullfile(folder_path, '*.tab'));
    if isempty(files)
        disp('No .tab files found in the specified folder.');
        return;
    end
    combinedData = [];
    for k = 1:length(files)
        file_path = fullfile(folder_path, files(k).name);
        % Read the .tab file
        opts = detectImportOptions(file_path, 'FileType', 'text', 'Delimiter',
            '\t');
        % The three columns to extract
        targetColumns = {'Date_Time','DD10_deg__average_Anemometer_',...
            'FF10_m_s__average_Anemometer_'};
        % Find the closest matches
        colMatches = cell(1, length(targetColumns));
        for i = 1:length(targetColumns)
            colMatches{i} = find(contains(opts.VariableNames,
                targetColumns{i}, 'IgnoreCase', true));
        end
        % Check if all target columns are found
        if all(cellfun(@(x) ~isempty(x), colMatches))
            % If all columns are found, read only the required columns
            selectedCols = [colMatches{:}];
            opts.SelectedVariableNames = opts.VariableNames(selectedCols);
            data = readtable(file_path, opts);

            % Ensure the Date_Time column is treated as text (string)
            data.Date_Time = string(data.Date_Time);
            data.FF10_m_s__average_Anemometer_ =
                string(data.FF10_m_s__average_Anemometer_);
            data.DD10_deg__average_Anemometer_ =
                string(data.DD10_deg__average_Anemometer_);

            % Append the data from this file to the combinedData
            if isempty(combinedData)
                combinedData = data;
            else
                combinedData = [combinedData; data];
            end

            disp(['Extracted columns from: ', file_path]);
        else
            disp(['One or more of the required columns were not found in: ',
                file_path]);
        end
    end
    % Save the combined data to a new file
    if ~isempty(combinedData)
        writetable(combinedData, output_file);
    else
        disp('No data to save');
    end
end
```

K MATLAB Code to create a vertical wind profile from radiosonde data

```
% MATLAB Script to Plot Vertical Profiles from Radiosonde Data
% Load the consolidated data
file_path = 'consolidated_data.tab';
data = readtable(file_path, 'Delimiter', '\t', 'FileType', 'text');

% Extract the necessary columns
Altitude = data.Altitude;
WindSpeed = data.WindSpeed;

% Define altitude bins
binSize = 100; % Bin size in meters
altitudeBins = 0:binSize:max(Altitude);

% Initialize arrays
medianWindSpeed = zeros(length(altitudeBins)-1, 1);
percentiles = zeros(length(altitudeBins)-1, 9); % 10th to 90th percentiles

% Calculate statistics for each altitude bin
for i = 1:length(altitudeBins)-1
    % Get indices for the current altitude bin
    binIndices = Altitude >= altitudeBins(i) & Altitude < altitudeBins(i+1);

    % Get wind speeds for the current bin
    binWindSpeeds = WindSpeed(binIndices);
    binWindSpeeds = binWindSpeeds(~isnan(binWindSpeeds)); % Remove NaN values

    if ~isempty(binWindSpeeds)
        % Calculate median and percentiles
        medianWindSpeed(i) = median(binWindSpeeds);
        percentiles(i, :) = prctile(binWindSpeeds, 10:10:90); % 10th to 90th
            percentiles
    else
        % Handle empty bins
        medianWindSpeed(i) = NaN;
        percentiles(i, :) = NaN(1, 9);
    end
end

% Smooth the median line (for visual clarity)
medianWindSpeed = smoothdata(medianWindSpeed, 'movmean', 3); % Moving average
    smoothing

%% Full Altitude Range
figure;
hold on;

% Plot percentile lines
colors = jet(9);
for p = 1:9
    plot(percentiles(:, p), altitudeBins(1:end-1), 'Color', colors(p, :),
        'LineWidth', 1.5);
end

% Plot median wind speed
plot(medianWindSpeed, altitudeBins(1:end-1), 'k-', 'LineWidth', 2);

xlabel('Wind Speed (m/s)', 'Interpreter', 'latex', 'FontSize', 14);
ylabel('Altitude (m)', 'Interpreter', 'latex', 'FontSize', 14);
```

```
title('Vertical Profile of Wind Speed (Full Altitude)', 'Interpreter', 'latex', 'FontSize', 16);
grid on;

percentileLabels = strcat(string(10:10:90), '\% Percentile');
legend([percentileLabels, 'Median'], 'Location', 'eastoutside', 'Interpreter', 'latex', 'FontSize', 12);
set(gca, 'TickLabelInterpreter', 'latex', 'FontSize', 12);
hold off;

%% Zoomed-In to 500 m
% Find indices for altitude below 500 m
zoomIndices = altitudeBins(1:end-1) <= 500;

figure;
hold on;

% Plot percentile lines (zoomed-in)
for p = 1:9
    plot(percentiles(zoomIndices, p), altitudeBins(zoomIndices), 'Color', colors(p, :), 'LineWidth', 1.5);
end

% Plot median wind speed (zoomed-in)
plot(medianWindSpeed(zoomIndices), altitudeBins(zoomIndices), 'k-', 'LineWidth', 2);

xlabel('Wind Speed (m/s)', 'Interpreter', 'latex', 'FontSize', 14);
ylabel('Altitude (m)', 'Interpreter', 'latex', 'FontSize', 14);
title('Vertical Profile of Wind Speed (Below 500 m)', 'Interpreter', 'latex', 'FontSize', 16);
grid on;

legend([percentileLabels, 'Median'], 'Location', 'eastoutside', 'Interpreter', 'latex', 'FontSize', 12);
set(gca, 'TickLabelInterpreter', 'latex', 'FontSize', 12);
hold off;
```

L MATLAB Code to Calculate AEP for AWES

```
% MATLAB Script to Calculate AEP of AWES
% Load data
file_path = 'consolidated_data.tab';
data = readtable(file_path, 'Delimiter', '\t', 'FileType', 'text');

% Extract necessary columns
DateTime = data.DateTime;
Altitude = data.Altitude;
WindDirection = data.WindDirection;
WindSpeed = data.WindSpeed;

% Define constants
target_altitude = 350; % Target altitude in meters
tolerance = 280; % Range: 70-350 m

% Filter data for the target altitude
valid_indices = Altitude >= target_altitude - tolerance & Altitude <=
    target_altitude  & ...
                ~isnan(WindSpeed);
valid_wind_speeds = WindSpeed(valid_indices);

% Ensure all wind speeds are positive
valid_wind_speeds = valid_wind_speeds(valid_wind_speeds > 0);

% Check for valid data
if isempty(valid_wind_speeds)
    error('No positive wind speed data available for analysis.');
end

% Debugging information
fprintf('Number of valid wind speeds: %d\n', length(valid_wind_speeds));
fprintf('Range of valid wind speeds: %.2f to %.2f m/s\n',
    min(valid_wind_speeds), max(valid_wind_speeds));

% Weibull Distribution Fitting
weibull_params = fitdist(valid_wind_speeds, 'Weibull');
k = weibull_params.B;
c = weibull_params.A;

% Weibull PDF
f_weibull = @(v) (k / c) .* ((v / c).^(k - 1)) .* exp(-(v / c).^k);

% Power curve - Kitepower Falcon
power_curve = [-5, -2.5, 2, 7, 15, 33, 55, 75, 90, 95, 99, 100, 100, 99, 98,
    97, 96]; % Power in kW
wind_speed_curve = [0, 1, 2, 3, 4, 5, 6, 7, 8, 9, 10, 11, 12, 13, 14, 15, 16];
    % Wind speed in m/s
P_c = @(v) interp1(wind_speed_curve, power_curve, v, 'linear', 0);

% Cut-in and cut-out wind speeds
v_cut_in = 5; % Minimum operational wind speed (m/s)
v_cut_out = 15; % Maximum operational wind speed (m/s)

% Calculate average power using Weibull distribution
P_av = integral(@(v) P_c(v) .* f_weibull(v), v_cut_in, v_cut_out);

% Total AEP
hours_per_year = 8760 ; % Hours in a year
AEP = 0.8 * P_av * hours_per_year; %Account for retraction phase at 20%

% Display results
```

```
fprintf('Average Power (P_av): %.2f kW\n', P_av);
fprintf('Total Annual Energy Production (AEP): %.2f kWh/year\n', AEP);

% Weibull PDF Plot
figure;
v_range = 0:0.1:max(valid_wind_speeds); % Adjust range for Weibull curve
plot(v_range, f_weibull(v_range), 'r-', 'LineWidth', 2);
xlabel('Wind Speed (m/s)', 'Interpreter', 'latex', 'FontSize', 14);
ylabel('Probability Density', 'Interpreter', 'latex', 'FontSize', 14);
title('Weibull Probability Density Function', 'Interpreter', 'latex',
    'FontSize', 16);
grid on;

% Wind Speed Histogram and Weibull Fit
figure;
histogram(valid_wind_speeds, 'Normalization', 'pdf', 'FaceColor', [0.2 0.6
    0.8]);
hold on;
plot(v_range, f_weibull(v_range), 'r-', 'LineWidth', 2);
xlabel('Wind Speed (m/s)', 'Interpreter', 'latex', 'FontSize', 14);
ylabel('Probability Density', 'Interpreter', 'latex', 'FontSize', 14);
title('Wind Speed Histogram and Weibull Fit', 'Interpreter', 'latex',
    'FontSize', 16);
legend('Histogram', 'Weibull Fit', 'Interpreter', 'latex');
grid on;
hold off;
```

M MATLAB Code for the Calculation of Wind Farm COE

```
% MATLAB Script to Calculate COE for a Wind Turbine Project including Diesel
    Replacement

% Inputs
% Project lifetime (in years)
N = 25;

% Capital cost of the wind turbine system (in Euro) - including Transport
C_c = 1478375;

% Annual operation and maintenance cost (in Euro)
C_OandM = (0.9*C_c)/N;

% Energy replaced by the wind turbine (in MWh/year)
diesel_replaced_MWh = 809.953; % From AEP

% Price of diesel (per liter, in $)
diesel_price_per_liter = 15;

% Diesel generator efficiency (fraction)
diesel_efficiency = 0.40; % Assumed 40%

% Energy content of diesel (in kWh/liter)
diesel_energy_content = 10; % 1 liter of diesel = 10 kWh thermal energy

% Annual energy output of the wind turbine (in kWh/year)
annual_energy_output = 809953;



% Discount rate (set to 0)
r = 0;

% Calculations
% Savings
% Diesel liters needed to generate the replaced MWh
diesel_needed_liters = (diesel_replaced_MWh * 1000) / (diesel_energy_content *
    diesel_efficiency);

% Annual savings from replacing diesel with wind energy
savings_per_year = diesel_needed_liters * diesel_price_per_liter;

% NPV
NPV = 0;
for j = 1:N
    NPV = NPV + (savings_per_year / (1 + r)^j);
end

% CRF
CRF = 1 / N;

% FCR
TPI = C_c; % Total Plant Investment equals the capital cost
FCR = CRF * (NPV / TPI);

% COE
COE = ((C_c * FCR) + C_OandM) / annual_energy_output;
```

N MATLAB Input Data Code for the Reference Economic Model for AWES - From the Reference Economic Model, only edited

```
function inp = eco_system_inputs_example
  %ECO_SYSTEM_INPUTS_EXAMPLE Generate example input parameters for the economic model.
  %   This function generates example input parameters for the economic model based on the
  %   selected configuration in eco_settings. It provides values for wind conditions,
  %   business-related quantities, and topology-specific parameters.
  %
  %   Outputs:
  %   - inp: Structure containing input parameters.

  global eco_settings

  eco_settings.name             = 'example_system';
  eco_settings.input_cost_file  = 'eco_cost_inputs_GG_soft'; % eco_cost_inputs_GG_fixed || eco_cost_inputs_FG || eco_cost_inputs_GG_soft ||
        set the input file
  eco_settings.input_model_file = 'code'; % code || eco_system_inputs_GG_fixed_example || eco_system_inputs_FG_example ||
        eco_system_inputs_GG_soft_example || set the input file
  eco_settings.power            = 'GG';  % FG || GG
  eco_settings.wing             = 'soft';  % fixed || soft

  %% Common parameters
  % Wind conditions
  atm.k = 1.46;
  atm.A = 12.33;

  % Business related quantities
  inp.business.N_y     = 25; % project years
  inp.business.r_d     = 0.08; % cost of debt
  inp.business.r_e     = 0.12; % cost of equity
  inp.business.TaxRate = 0.30; % Tax rate (25%) ...
  % https://www.oecd.org/content/dam/oecd/en/topics/policy-sub-issues/corporate-taxation/etrs-rd-modelling-notes.pdf
  inp.business.DtoE    = 0.9; % Debt-Equity-ratio %https://eqvista.com/debt-to-equity-ratio-by-industry/

  %% Topology specific parameters
  switch eco_settings.input_model_file
      case 'code'

          switch eco_settings.power
              case 'FG'

                  % Wind resources
                  inp.atm.wind_range = [3:1/3:10, 15, 20]; % m/s
                  inp.atm.gw         = atm.k/atm.A *(inp.atm.wind_range/atm.A).^(atm.k-1).*...
                      exp(-(inp.atm.wind_range/atm.A).^atm.k); % - Wind distribution

                  % Kite
                  inp.kite.structure.m            = 122.5; % kg
                  inp.kite.structure.b            = 10;    % m
                  inp.kite.structure.AR           = 6; % -
                  inp.kite.structure.f_repl       = 0; % 1/year

                  % Tether
                  inp.tether.d      = 1.6 *1e-3 * inp.kite.structure.b; % m
                  inp.tether.L      = 100; % m
                  inp.tether.rho    = 970; % kg/m^3
                  inp.tether.f_repl = -1;

                  % System
                  inp.system.F_t       = inp.tether.d^2/4*pi* [0.124572136342289,0.151797436838344,...
                      0.181460994246145,0.214172304028360,0.250094485666586,0.289217262316979,0.331480668302760,...
                      0.376825094990467,0.425204519064134,0.476587107759039,0.530951609064390,0.588284030406247,...
                      0.648575480469101,0.711819900342773,...
                      0.667172308938198,0.538286443708873,0.479418546822401,0.440125256353379,0.410771458547833,...
                      0.387467590011167,0.368260306087034,0.352050875661555,0.3,0.25]*1e9; % N
                  inp.system.P_e_rated = 100e3; % W
                  inp.system.P_e_avg   = inp.system.P_e_rated * [0.0514836036930580,0.0740924523303653,...
                      0.101398515897930,0.133916653105838,0.172155839837058,0.216618610982057,0.267802451082606,...
                      0.326201238110832,0.392306298442283,0.466607150752925,0.549592018061346,0.641748164098206,...
                      0.743562144341504,0.855519973731538,0.978107215387062,0.999997934928179,0.999999974273665,...
                      0.999999480541176,0.999999330603523,0.999999355894903,0.999999280365251,0.999996057827535, 1,1]; % W
                  inp.system.lambda    = 7; % wing speed ratio
                  inp.system.R0        = 5*inp.kite.structure.b; % turbing radius

                  % Ground station
                  inp.gStation.ultracap.E_rated = inp.kite.structure.m * 9.81*inp.kite.structure.b*5/3.6e6; % kWh
                  inp.gStation.ultracap.f_repl  = -1;
                  inp.gStation.batt.E_rated     = inp.system.P_e_rated/1e3; % kWh
                  inp.gStation.batt.f_repl      = -1; % /year

              case  'GG'
                  switch eco_settings.wing
                      case 'fixed'

                          % Wind resources
                          inp.atm.wind_range = [1:1:25]; % m/s
                          inp.atm.gw         = atm.k/atm.A *(inp.atm.wind_range/atm.A).^(atm.k-1).*...
                              exp(-(inp.atm.wind_range/atm.A).^atm.k); % Wind distribution

                          % Kite
                          inp.kite.structure.m            = 5543; % kg
                          inp.kite.structure.A            = 100; % m^2
                          inp.kite.structure.f_repl       = 0; % /year
                          inp.kite.obGen.P                = 1e3; % W
                          inp.kite.obBatt.E                = 1; % kWh

                          % Tether
                          inp.tether.d      = 0.0273; % m
                          inp.tether.L      = 2600; %m
                          inp.tether.rho    = 970; % kg/m^3
                          inp.tether.f_repl = -1; % /year

                          % System
                          inp.system.F_t       = [0   0     0     0     0     176218.741942466  247326.729934132...
                              335309.738279319  349999.999905368  349999.999983002  349999.999999204...
                              349983.541245218  348784.001594628  345425.348864681  349095.793762565...
                              346191.685571336  341260.264393564  340281.862240894  340333.765419009...
                              340876.771496480  341638.231403760  342493.800708096  343392.451059166...
                              344311.108894388  345237.030244762]; % N
                          inp.system.P_m_peak  = 1.87e+06; % W
                          inp.system.P_e_avg   = [0   0     0     0     0     145524.730974731  288495.257975699...
```

```
                            488571.542997977  727335.279338411  953941.843495889  1000000.00000461...
                            999999.999798969  1000000.00001413  1000000.00000000  1000000.00000046...
                            1000000.00000080  1000000.00000000  1000000.00000017  1000000.00000000...
                            999999.999732790  999999.999965783  999999.999995972  999999.999999559...
                            999999.999999956  1000000.00000000]; % W
                        inp.system.P_e_rated = 100000; % W
                        inp.system.Dt_cycle  = [0   0     0     0     0     0     130.388949196501  132.125896939284...
                            130.302239127635  135.689613751230  132.500820465091  124.515660439110...
                            123.350051661913  122.919611216260  122.626866710798  122.754436421934...
                            122.745072840010  122.773588271380  122.901681745870  123.093919941459...
                            123.315575577003  123.547269528843  123.778584819469  124.003535889111...
                            124.218500332100  124.421040233482]; % s

                        % Ground station
                        inp.gStation.ultracap.E_rated = 11.25; % kWh
                        inp.gStation.ultracap.E_ex    = [0      0     0     0     0     0.794997961209469 1.91620710592149
                              3.66340782590143  7.00053194254757  10.6616297528835  11.1890647627290  11.2279405187141  11.2277213125461
                              11.1934366085895  11.2473922571621  11.2098142616423  11.1438062076693  11.1273616907102  11.1228424486107
                              11.1240295153377  11.1278176039227  11.1328371206444  11.1385755705485  11.1448282168896  11.1514961274243];
                              % kWh
                        inp.gStation.ultracap.f_repl  = -1; % /year
                        inp.gStation.batt.E_rated     = inp.system.P_e_rated/1e3; % kWh
                        inp.gStation.batt.E_ex        = [0      0     0     0     0     0.794997961209469 1.91620710592149
                              3.66340782590143  7.00053194254757  10.6616297528835  11.1890647627290  11.2279405187141  11.2277213125461
                              11.1934366085895  11.2473922571621  11.2098142616423  11.1438062076693  11.1273616907102  11.1228424486107
                              11.1240295153377  11.1278176039227  11.1328371206444  11.1385755705485  11.1448282168896  11.1514961274243];
                              % kWh
                        inp.gStation.batt.f_repl      = -1; % /year
                        inp.gStation.hydAccum.E_rated = inp.gStation.ultracap.E_rated ;  % kWh
                        inp.gStation.hydAccum.E_ex    = inp.gStation.ultracap.E_ex; % kWh
                        inp.gStation.hydAccum.f_repl  = -1; % /year
                        inp.gStation.hydMotor.f_repl  = 0; % /year
                        inp.gStation.pumpMotor.f_repl = 0; % /year

                    case 'soft'

                        % Wind resources
                        inp.atm.wind_range = [5,6,7,8,9,10,11,12,13,14,14.5,15];
                        inp.atm.gw         = atm.k/atm.A *(inp.atm.wind_range/atm.A).^(atm.k-1)...
                            *exp(-(inp.atm.wind_range/atm.A).^atm.k); % Wind distributio

                        % Kite
                        inp.kite.structure.A           = 80; % m
                        inp.kite.structure.f_repl      = 1; % /year
                        inp.kite.obGen.P               = 1000; % W
                        inp.kite.obBatt.E              = 0; % kWh

                        % Tether
                        inp.tether.d      = 0.04; % m;
                        inp.tether.L      = 350; % m
                        inp.tether.rho    = 970; % kg/m^3
                        inp.tether.f_repl = -1; % /year

                        % System
                        inp.system.F_t       = [4083, 32667, 36750, 32667, 36458, 49000, 57167, 65333, 73500,...
                            77583, 82793, 87500]; % N
                        inp.system.P_m_peak  = 130000; % W
                        inp.system.P_e_avg   = 1e3.*[10, 20, 30, 40, 50, 60, 70, 80, 90, 95, 98, 100]; % W
                        inp.system.P_e_rated = max(inp.system.P_e_avg); % W
                        inp.system.Dt_cycle  = 100; % s

                        % Ground station
                        inp.gStation.ultracap.E_rated = (inp.system.P_m_peak+10e3) * 20/3600/1e3; % kWh
                        inp.gStation.ultracap.E_ex    = inp.gStation.ultracap.E_rated/2; % kWh
                        inp.gStation.ultracap.f_repl  = -1; % /year
                        inp.gStation.batt.E_rated     = inp.system.P_e_rated/1e3; % kWh
                        inp.gStation.batt.E_ex        = inp.gStation.ultracap.E_rated/2; % kWh
                        inp.gStation.batt.f_repl      = -1; % /year
                        inp.gStation.hydAccum.E_rated = inp.gStation.ultracap.E_rated ;  % kWh
                        inp.gStation.hydAccum.E_ex    = inp.gStation.ultracap.E_ex; % kWh
                        inp.gStation.hydAccum.f_repl  = 0.1; % /year
                        inp.gStation.hydMotor.f_repl  = 0.083; % /year
                        inp.gStation.pumpMotor.f_repl =  0.125; % /year

                end
            end
        otherwise
            inp = eco_import_model(inp);
            inp.atm.gw  = atm.k/atm.A *(inp.atm.wind_range/atm.A)....
                ^(atm.k-1).*exp(-(inp.atm.wind_range/atm.A).^atm.k); % Wind distribution

    end
end
```

O SD6+ Product Leaflet

PERFORMANCE. EXPERTISE. RELIABILITY

SD WIND ENERGY

WORLD LEADERS IN SMALL SCALE WIND

+44 (0) 1560 486 570
www.sd-windenergy.com

PERFORMANCE . EXPERTISE . RELIABILITY

SD6 +

Product Specification

Rated Power	6.0kW @ 11m/s
Applications	Agricultural, Domestic, Remote Islands, Utility, Telco
Solutions	Grid Tied & Battery Charge, 48V, 300V
Architecture	Downwind, 3 Bladed, Self Regulating
Rotor	5.6m Diameter
Swept area (m2)	24.6m2
Blade Material	Glass Thermoplastic Composite
Head Weight	550kg
Generator	Brushless Direct Drive Permanent Magnet
Tower Height Options	9m / 15m / 20m Taperfit Monopole – Hydraulic or Gin Pole
Tower Specification	Class 1 Rated / Galvanised Steel
Foundation Options	Pad / Root / Rock Anchor
Cut In Speed	2.5m/s
Cut Out Speed	None - Continuous Operation
Survival Wind Speed	Designed to Class 1 (70m/s)
Warranty	5 Years
Cold Climate Options	Available on Request
Colour Options	Light Grey (RAL7035) Black (RAL9005)

The SD6 is regarded by many as the turbine of choice and has been one of the World's Best Selling Small Wind Turbines for over 25 years.

Renowned for quality and durability, the SD6 is internationally recognised as a market leader in Small Wind.

Continuous Operation is guaranteed due to the innovative downwind design, incorporating the delta rotor. This unique system uses the latest advances in composite technology, allowing the blades to flex and regulate their speed. This ensures the turbine can continue operating and producing energy during extreme wind conditions when alternative wind turbines need to stop to protect themselves.

Utilising hydraulic towers ensures minimum downtime for service inspections, which are only required at 25,000kWh intervals. This offers customers a low cost of ownership compared to alternative wind turbines on the market.

SD Wind Energy delivers affordable energy security to a wide range of customers. The SD6 is fully certified under the MCS & SWCC schemes, ensuring eligibility for incentive programs.

Our SD6+ turbine is a 6KW turbine that can reach 9kW in high wind speeds, mounted onto either a 9m, 15m or 20m gin pole or hydraulic tower which can be set in either a fixed concrete base, or above ground base. The SD6+ turbine follows the SD6 power curve up to a point, then exponentially increases in high wind speeds. This is due to additional copper winding included in the generator. The design of the SD6+ is otherwise the same as the SD6 wind turbine.

SD WIND ENERGY

+44(0) 1560 486 570
info@sd-windenergy.com
sd-windenergy.com

SECURE YOUR ENERGY FUTURE TODAY WITH SD WIND ENERGY

APPROVED PRODUCT

MCS

SWCC CERTIFIED

SD WIND ENERGY

SD6 + Power Curve

SD6+ Power Curve		
MPH	M/S	Power (kW)
1	0.45	0
2	0.89	0
3	1.34	0
4	1.79	0
5	2.24	0
6	2.68	0.01
7	3.13	0.05
8	3.58	0.17
9	4.02	0.17
10	4.47	0.3
11	4.92	0.48
12	5.36	0.51
13	5.81	0.62
14	6.26	1.03
15	6.71	1.45
16	7.15	1.67
17	7.60	1.88
18	8.05	2.68
19	8.49	2.98
20	8.94	3.6

SD6+ Power Curve		
MPH	M/S	Power (kW)
21	9.39	4.5
22	9.83	4.9
23	10.28	5.5
24	10.73	6.0
25	11.18	6.3
26	11.62	6.6
27	12.07	6.9
28	12.52	7.1
29	12.96	7.3
30	13.41	7.6
40	17.88	7.9
50	22.35	8.1
60	26.82	8.3
70	31.29	8.6
80	35.76	8.9
90	40.23	9
100	44.70	9
110	49.17	9
120	53.64	9

The power curve values tabled above are representative of the wind power output produced using an SD6+ turbine with a specific inverter set up. Actual output is dependent on several factors including turbine siting and inverter type and setup.

+44 (0) 1560 486 570
www.sd-windenergy.com

P Falcon Product Leaflet

Discover the Great Advantages of Kitepower

Integrate Kitepower into your micro-grid with solar PV and batteries to reap the benefits of smart hybrid energy generation.

Avoid idle generators & save diesel off-the-grid

When integrating Kitepower in combination with batteries, diesel generators can be switched off completely. Hybridizing with Kitepower results in less diesel consumption for more clean energy, culminating in considerable financial savings even for areas that don't experience consistent high wind speeds.

Find out more about Kitepower's competitive advantages when compared to solar PV or traditional wind turbines:

	Mass t	Area m^2	Energy throughout 24 hrs		Hurricane Proof	Installation Time
	220	50	✓	✓	✗	weeks
	70	2000	✓	✗	✗	days
KITEPOWER	15	50	✓	✓	✓	hours

Learn more about the energy perks of Kitepower at *thekitepower.com/products/*

Electricity Generation 24/7
Produce electricity during day, night, on cloudy and rainy days

High Energy Production
Higher capacity factor than solar PV and wind turbines

Easy to Transport
All equipment fits in one 20ft container

Deployable in Harsh Environments
Ideal for remote locations

Plug & Play
Install it in less than 24hrs and operate it out-of-the-box

Why Kitepower?

Taking Only the Best from Wind Turbines

Problem

Conventional wind energy systems rely on electricity generation by means of wind turbines installed on the ground. Wind turbines, therefore, require resource -intensive towers and heavy foundations thus imply a demanding transportation and installation process.

Difficult logistics limit the geographical versatility of wind turbines while their constrained height limit their efficiency. This results in unsustainable diesel supplies needed for most of the remote off- and micro-grid applications across the globe.

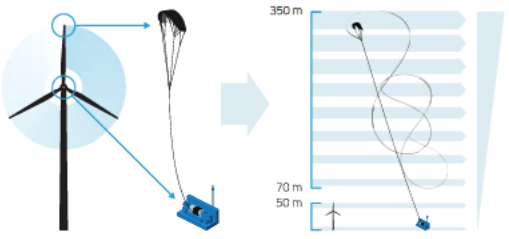

Solution

Kitepower develops cost-effective alternatives to existing wind turbines by using kites to generate electricity.

Kitepower systems do not require resource-intensive towers nor heavy foundations and is thus easy to transport and deploy. The system is able to harness stronger and more persistent winds at higher altitudes, allowing for higher capacity factors than traditional wind turbines and solar PV while being easier to transport, install and maintain. Moreover a Kitepower system is also able to start generating electricity with lower winds speeds than the ones required by windmills.

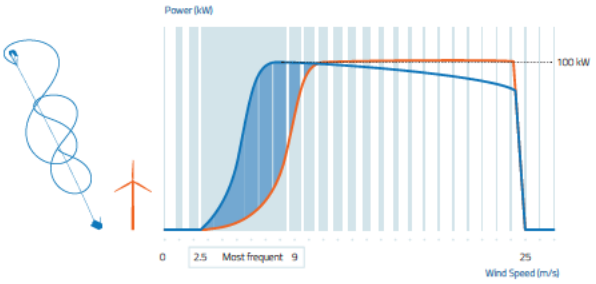

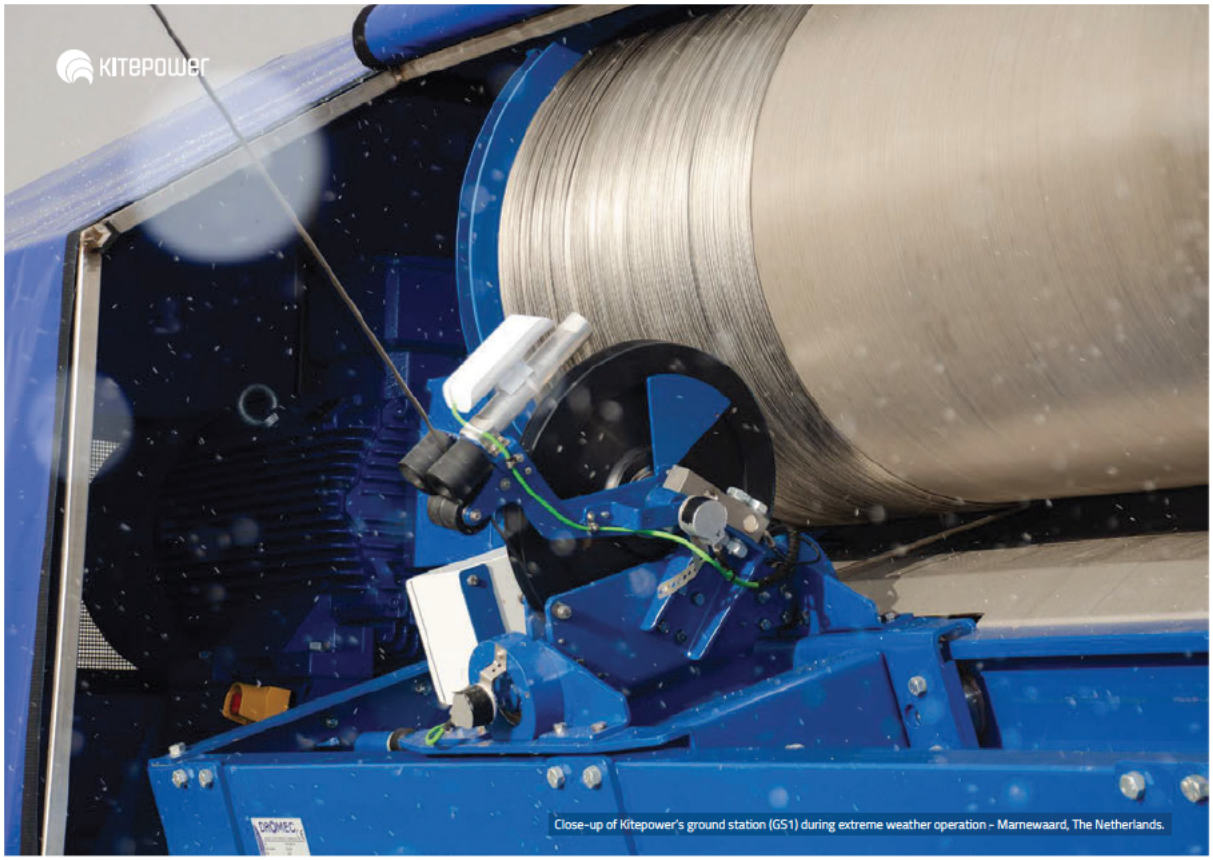

Close-up of Kitepower's ground station (GS1) during extreme weather operation - Marnewaard, The Netherlands.

The Power Output

Continuous Pumping Cycle Operation

The electricity generation works in two phases, which repeated in continuous cycles result in positive net energy output.

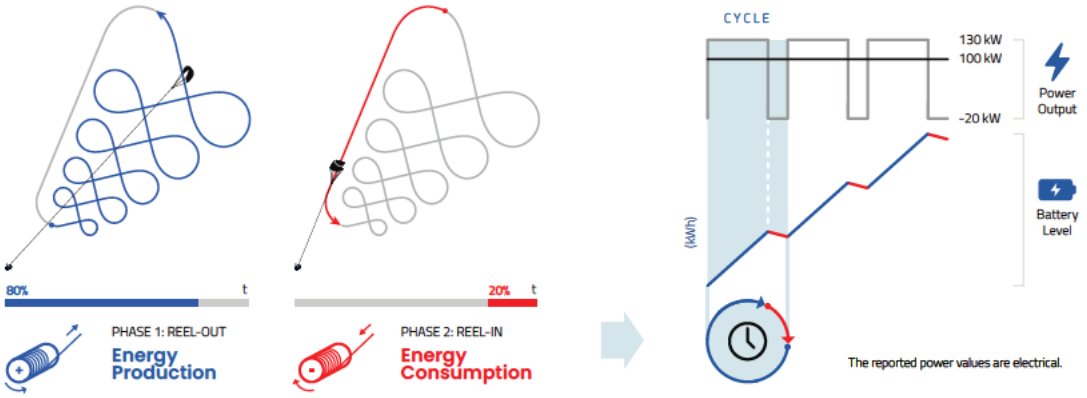

During the first energy production phase the kite is flown in a cross-wind figure of eight pattern to achieve a high pulling force and reel out the tether from the winch in the ground station.

When the max tether length is reached, the kite's profile is adjusted in order to reel-in the tether with low force, using a small fraction of the energy produced in the previous phase.

The Kitepower Falcon:

- Has a single cycle duration of 100 seconds
- Produces 130 kW 80% of the cycle's time when in Reel-out
- Consumes 20 kW 20% of the cycle's time when in Reel-in

Kitepower Falcon's system operation - Marnewaard, The Netherlands.

Introducing The Kitepower Falcon

System Components & Space Requirements

4. Kite

Consists of a hybrid between an inflatable and a fixed fibre-glass skeleton, forming the best combination for a strong and lightweight wing.

3. Kite Control Unit (KCU)

Controls the roll, pitch, and yaw of the kite and takes care of the communications between the sensor unit placed on the kite and the GS.

2. Tether

A Dyneema® line is used for a lightweight and strong connection between the kite and the GS.

1. Ground Station (GS)

Converts the mechanical energy of the kite into electrical power and reels the kite in by using the generator as a motor.

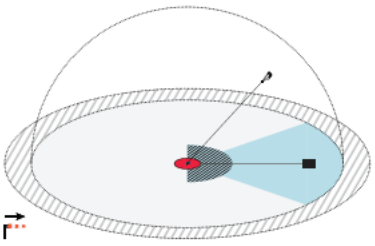

Zone	Dimensions	Dual Land-use[1]
Restricted Zone	30 m (r)	
Flight Zone	350 m (r)	
Potential Flight Zone	350 m (r)	√
Safety Buffer	425 m (r)	√
Landing Zone	100 m (r)	
Launching Corridor	280x1 m	
Launch Pad	20x20 m	

Obstacles' height within operational envelope:
1m allowance every 10m of distance from the GS

[1] Land can be used for alternative activities while Kitepower is deployed.
(r) = Radius

Kitepower's 25-40-60 m² kites - Delft, The Netherlands.

The Kitepower Falcon

Technical Summary

KITEPOWER

General Information

Nominal Power Output[1]	100 kW
Yearly Power Output	450 MWh/year
Rated Wind Speed	7 m/s
Cut-in wind Speed	2 m/s
Max Operating Wind Speed	15 m/s
Min Launching Speed	5 m/s
Airborne Wind Range	0-25 m/s
Max Flight Altitude	350 m
Ground Space Required[2] (radius)	350 m

[1] Power output potential might differ depending on the kite variant
[2] The ground space must be free of obstacles

Kite

Variant	V9
Size flat (m²)	60-80 m²
Size projected (m²)	47-62 m²
Force (t)	3,5 t
Lifetime (hours)	4000h
Avg. Flight Speed (km/h)	110 km/h
Air Traffic Lights	√
Airborne Pump	√
Field Pump	√
Sensor Unit	√
Kite Bags	√
Safety Line	√
Landing Protection	√
Safety Attachment Points	√
Parachute Landing	√

KCU

Weight	23 kg
IP Rating	IP65
Wireless communication link	2 km
Airborne Power Supply	√
Protective Cover	√
Air Traffic Lights	√
Airborne Wind Turbine	√
Protection Cover	√
Safety Release	√
Health Supervisor	√

Tether

Type	UHMWPE Dyneema®
Length (default)	350 m
Passive Safety Release	√

Power Curves

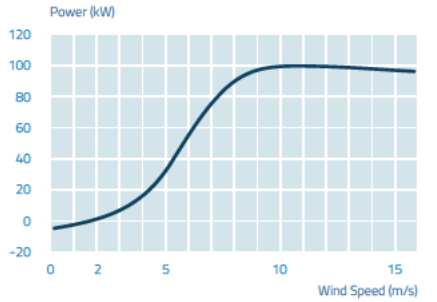

Ground Station

Main Dimensions	W: 2,44 m H: 2,60 m L: 6,06 m
Weight	9.6 t
IP Rating	IP64
Lifetime	25 years
AC Power output	400V AC 3 phase
DC power output	550-700 V
Nominal Power	100kW
Peak Power	120 kW AC / 250 kW DC
Connection mode	Power lock or screw terminals
Launch Unit	√
Safety Emergency Stop	√
Health Supervisor	√

+ More information can be found within *The Kitepower Falcon 100kW Technical Specification Document.*

▲ Long exposure shot of the Falcon's system operation - Valkenburg, The Netherlands.

Hochschule für Angewandte Wissenschaften Hamburg
Hamburg University of Applied Sciences

Erklärung zur selbstständigen Bearbeitung einer Abschlussarbeit

Gemäß der Allgemeinen Prüfungs- und Studienordnung ist zusammen mit der Abschlussarbeit eine schriftliche Erklärung abzugeben, in der der Studierende bestätigt, dass die Abschlussarbeit „– bei einer Gruppenarbeit die entsprechend gekennzeichneten Teile der Arbeit [(§ 18 Abs. 1 APSO-TI-BM bzw. § 21 Abs. 1 APSO-INGI)] – ohne fremde Hilfe selbständig verfasst und nur die angegebenen Quellen und Hilfsmittel benutzt wurden. Wörtlich oder dem Sinn nach aus anderen Werken entnommene Stellen sind unter Angabe der Quellen kenntlich zu machen."

Quelle: § 16 Abs. 5 APSO-TI-BM bzw. § 15 Abs. 6 APSO-INGI

Dieses Blatt, mit der folgenden Erklärung, ist nach Fertigstellung der Abschlussarbeit durch den Studierenden auszufüllen und jeweils mit Originalunterschrift als letztes Blatt in das Prüfungsexemplar der Abschlussarbeit einzubinden.
Eine unrichtig abgegebene Erklärung kann -auch nachträglich- zur Ungültigkeit des Studienabschlusses führen.

Erklärung zur selbstständigen Bearbeitung der Arbeit

Hiermit versichere ich,

Name: _____

Vorname: _____

dass ich die vorliegende – bzw. bei einer Gruppenarbeit die entsprechend gekennzeichneten Teile der Arbeit – mit dem Thema:

ohne fremde Hilfe selbständig verfasst und nur die angegebenen Quellen und Hilfsmittel benutzt habe. Wörtlich oder dem Sinn nach aus anderen Werken entnommene Stellen sind unter Angabe der Quellen kenntlich gemacht.

- die folgende Aussage ist bei Gruppenarbeiten auszufüllen und entfällt bei Einzelarbeiten -

Die Kennzeichnung der von mir erstellten und verantworteten Teile der ist erfolgt durch:

Ort _____ Datum _____ Unterschrift im Original